Structural Evaluation and Life Cycle Assessment of a Transparent Composite Facade System Using Biofiber Composites and Recyclable Polymers

by

Kyoung-Hee Kim

A dissertation submitted in partial fulfillment
of the requirements for the degree of
Doctor of Philosophy
(Architecture)
in The University of Michigan
2009

Doctoral Committee:

Professor Harry Giles, Co-Chair
Professor Richard E. Robertson, Co-Chair
Professor Jean D. Wineman
Associate Professor Gregory A. Keoleian

This dissertation is dedicated to my mom,

Byung-Im Choi,

who has instilled in me academic passion and emotional strength.

Acknowledgements

I would like to take this opportunity to express my thanks to everyone who contributed directly and indirectly to my thesis. First and foremost, I would like to thank my committee members, especially Professor Harry Giles for his support, patience, and tremendous counsel as my academic advisor and for sharing his knowledge of the field with me; Professor Richard Robertson for his constant guidance and critical encouragement; Gregory Keoleian for his theoretical insight and constructive advice on my research and Professor Jean Wineman for her steadfast support and infinite wisdom throughout my graduate studies.

There are several individuals I wish to thank for helping me complete my doctoral training: Dr. Jong Jin Kim for his powerful words of encouragement and advice about research methodology; Mark Krecic and Gerald Weston who provided valuable technical advice and physical assistance when constructing the testing platforms and testing samples; Dr. Theodore Provder and Sarjak Amin at the Coatings Research Institute at Eastern Michigan University, who lent their equipment and shared their technical expertise; Julianna Lieu for her assistance with the metal work; Jeremy Freeman, Stephanie Driver, Josh Bard, Steve Jelinek, and Erin Putalik at the architecture department, Eric Heininger and Carrie Bayer at the department of Materials Science and Engineering, Michelle Cho, Katie Kerfoot, Brandon Cox, John Stepowski, and Shangchao Lin at the department of Mechanical Engineering, and Han Zhang, Thomas DiCorcia, Sarah Ann Popp, and Mitsuyo Yamamoto at the School of Natural Resources and Environment for their support and inspirational work with the 2006 EPA-P3 research; Jong-Kuk Kim for his invaluable help with conducting final experiments.

I am thankful to the architecture department at the University of Michigan to provide me continuous financial support and teaching opportunity. I would also like to thank the faculty, staff, and my colleagues at the architecture department for their advice, assistance, and encouragement.

Finally, I would like to express my heartfelt gratitude to my beloved family: my parents and parents-in-laws, who have supported me while I worked to accomplish my goal, my husband, Yau Shun Hui, and our two sons, Anthony and Henry, who have tolerated my absence and distraction for many years and who have given me joy and rest when it was needed. Without you, I would not be here. Thank you.

TABLE OF CONTENTS

Dedication ..... **ii**
Acknowledgements ..... **iii**
List of Figures ..... **ix**
List of Tables ..... **xii**
List of Appendices ..... **xiv**
Abstract ..... **xv**

Chapter 1 ..... **1**
Introduction **1**
1.1 Background of the Study 1
1.2 Statement of the Problem 2
1.3 Research Objectives 4
1.4 Significance of the Research 5

Chapter 2 ..... **7**
Literature Review **7**
2.1 Previous Studies on Composite Panel Systems for Building Applications 8
2.2 Transparent Composite Façade System 11
2.2.1 Recyclable Polymers as Skin Materials 12
2.2.2 Biofiber Composites as Core Materials 21
2.1.3 Bio-Coatings 27
2.2.3 Existing System Review 27
2.3 Structural Evaluation Framework 30
2.3.1 Strength and Stiffness 30

2.3.2 Impact Performance 36
2.4 Environmental Performance Evaluation Framework 40
2.4.1 Framework of the Life Cycle Assessment (LCA) 40
2.4.2 LCA Application to a Building Window System 44
2.5 Conclusions 45

Chapter 3 48
Structural Performance Evaluation of a TCFS 48
3.1 Structural Design of a TCFS 48
3.1.1 Strength and Deflection Requirements of a TCFS 48
3.1.2 Design Load Verification 49
3.1.3 Structural Properties of a TCFS 51
3.1.4 Bending Stress and Deflection Check of a TCFS Panel 54
3.1.5 Structural Design Conclusions 55
3.2 Installation of a New Testing Facility 56
3.2.1 Overview of Testing Facility Design 56
3.2.2 Structural Analysis of Testing Frame 58
3.2.3 Fabrication of Testing Frame 62
3.2.4 Frame Installation Conclusions 63
3.3 Static Performance 64
3.3.1 Static Testing Apparatus and Specimens 64
3.3.2 Static Testing Procedure 66
3.3.3 Static Testing Result 67
3.3.4 Finite Element Analysis 79
3.3.5 Static Performance Evaluation Conclusion 84
3.4 Impact Performance Evaluation 85
3.4.1 Impact Testing Apparatus and Specimens 85
3.4.2 Impact Testing Procedure 87
3.4.3 Impact Testing Results 89
3.4.4 Impact Testing Conclusions 98
3.5 Charpy Impact Performance 99

3.5.1 Charpy Impact Tester and Specimens 99
3.5.2 Charpy Impact Testing Procedure 101
3.5.3 Charpy Impact Testing Result 101
3.5.4 Charpy Impact Testing Conclusion 102
3.6 Conclusions 103

Chapter 4 105
Life Cycle Assessment (LCA) 105
4.1 Goal and Scope Definition 105
4.1.1 Goal and Scope 105
4.1.2 System Boundaries 106
4.1.3 Functional Unit 107
4.1.4 Assumptions and Limitations 110
4.2 Life Cycle Inventory (LCI) 113
4.2.1 Energy Inputs 114
4.2.3 Environmental Emissions 120
4.3 Life Cycle Impact Assessment (LCIA) 121
4.4 Sensitivity Analysis 123
4.4.1 Pre-use Phase: Improved life expectancy 124
4.4.2 Post-Use Phase: Recycling as an Alternative to Incineration 125
4.5 LCA Conclusions 127

Chapter 5 132
Conclusions and Future Work 132
5.1 Structural Conclusions 132
5.1.1 Problem Statement 132
5.1.2 Summary of Research Activities 132
5.1.2 Structure Conclusions and Recommendations 134
5.1.4 Study Limitations and Future Work 137
5.2 LCA Conclusions 137
5.2.1 Problem Statement 137

5.2.2 Summary of Research Activities 138
5.2.3 LCA Conclusions and Recommendation..... 139
5.2.4 Study Limitations and Future Work 140

APPENDICES 142
BIBLIOGRAPHY 171

List of Figures

Figure 1.2.1 Simplified Sectional View of TCFS 4
Figure 1.3.1 Overview of Research Areas 6
Figure 2.1.1 Composite Construction of Spacecraft (a) 9
Figure 2.2.1.1 Impact Resistance of PC, PMMA, and Glass 14
Figure 2.2.1.2 Creep Modulus of SAN at Various Time and Stress Levels 15
Figure 2.2.1.3 Yellowness Index (a) and Haze of PC and PMMA 16
Figure 2.2.2.1 Overview of Biofiber Composite Material Components 22
Figure 2.2.2.2 E-modulus Comparison of Biofiber Composites 23
Figure 2.2.2.3 Discoloration of Jute Composites after Outdoor Exposure 24
Figure 2.2.2.4 Pictorial Ratings of Microbial Degradation: 26
Figure 2.2.3.1 ClearShade IGU Assembly and Application in Mexico City 28
Figure 2.2.3.2 ClearShade IGU Energy Performance Values 29
Figure 2.2.3.3 Louvers-Integrated IGU: Summer (left) and Winter (right) 30
Figure 2.3.1.1 Transformed Section for Equivalent Moment 32
Figure 2.3.1.1 An Effective Thickness Calculation Diagram 36
Figure 2.3.2.1 Shot Bag Impactor for Simulating Human Body Impacts 37
Figure 2.3.2.2 Shot-Bag Impact Modes 38
Figure 2.3.2.3 Human Engineering Data 38
Figure 2.3.2.4 Charpy Impact Machine and Specimen Set-Up 39
Figure 2.3.2.5 Fracture Patterns of Laminated Glass (a) and Tempered Glass (b) 40
Figure 2.4.1.1 LCA Procedure in accordance with ISO 14040 41
Figure 2.4.1.3 System Boundary Example of an LCA for a Plastic Sheet 42
Figure 2.4.1.3 Flow Diagram of Life Cycle Inventory Analysis 43
Figure 3.1.2.1 An Office Building Enclosed with TCFSs Located in Detroit, MI 50
Figure 3.1.2.2 Varying Wind Loads across the Building Façade 51

Figure 3.1.3.1 Transformed Section Using the E-modulus of PMMA 52
Figure 3.1.3.2 Plan (a) and Section (b) Details of a TCFS 53
Figure 3.2.1.1 Overview of Testing Frames 57
Figure 3.2.2.1 Sectional Properties of Testing Frames 59
Figure 3.2.2.2 Impact Load (34 kN) Set-Up in STAAD.Pro 60
Figure 3.2.2.3 Bending Moment Diagram Under Impact Load 61
Figure 3.2.2.4 Axial Fore Diagram Under Impact Load 61
Figure 3.2.2.5 Displacement Diagram Under Impact Load 62
Figure 3.2.3.1 Fabrication Process of Testing Frames 63
Figure 3.3.1.1 Static Test Set-Up 64
Figure 3.3.1.2 Installation Position of Loading Jack and Displacement Gauges 65
Figure 3.3.1.3 Two-edge (a) and Four-edge (b) Supported Conditions 65
Figure 3.3.2.1 TCFS (a) and Laminated Glass (b) Test Set-Up 66
Figure 3.3.3.1 Bending Stresses Comparison of a TCFS 68
Figure 3.3.3.2 Radius of Curvature (ρ) and Displacement (δ) 69
Figure 3.3.3.3 Displacement Comparison of a TCFS 70
Figure 3.3.3.4 Bending Stress Comparison of Laminated Glass 71
Figure 3.3.3.5 Displacement Comparison of Laminated Glass 72
Figure 3.3.3.6 Bending Stress Comparison of Fully Tempered Glass 73
Figure 3.3.3.7 Displacement Comparison of Fully Tempered Glass 74
Figure 3.3.3.8 Structural Properties of TCFS that Affects Bending Stiffnesss 76
Figure 3.3.3.9 Bending Stress Comparisons of a TCFS 77
Figure 3.3.3.10 Displacement Comparisons of a TCFS 78
Figure 3.3.4.1 Model Set-Up in STAAD.Pro 80
Figure 3.3.4.2 STAAD.Pro Results of a Two-Edge Supported TCFS 81
Figure 3.3.4.3 STAAD.Pro Results of a Four-Edge Supported TCFS 82
Figure 3.4.1.1 Overview of Impact Test Frames (a) and Drop Height (b) 86
Figure 3.4.1.2 Overview of Impact Test Instrumentation 87
Figure 3.4.2.1 Impact Test Set-Up: Fully Tempered Glass (a) and TCFS (b) 88
Figure 3.4.3.1 Breakage Modes of Laminated Glass 90
Figure 3.4.3.2 Displacement (a) and Strain (b) Output of Laminated Glass 91

Figure 3.4.3.3 Breakage Modes of Fully Tempered Glass 92
Figure 3.4.3.4 Displacement and Strain Outputs of Fully Tempered Glass 93
Figure 3.4.3.5 Fracture Patterns (a) of PMMA Skin at 457 mm Drop Height 95
Figure 3.4.3.6 Post Breakage Modes of TCFS at 457 mm Drop Height 96
Figure 3.4.3.7 Displacement (a) and Strain (b) Output of TCFS..... 97
Figure 3.4.3.8 Displacement Comparisons between Glass and TCFS 98
Figure 3.5.1.1 Charpy Impact Tester (a) and Specimen Set-Up Plan View (b) 100
Figure 3.5.2.1 Broken PMMA After Calibrating the Charpy Impact Tester..... 101
Figure 3.5.3.1 Charpy Impact Strength as a Fuction of Time 102
Figure 4.1.2.1 Overview of the System Boundaries of the LCA..... 107
Figure 4.1.3.1 Functional Unit (FU) of TCFS and GCWS..... 108
Figure 4.1.3.2 Material Mass Per TCFS and GCWS..... 109
Figure 4.1.3.3 Material Mass Input Composition Per Functional Unit 110
Figure 4.1.4.1 Travelling Distance Between Builidng Site and Suppliers 111
Figure 4.2.1.1 Embodied Energy Distributions of TCFS and GCWS Per FU 114
Figure 4.2.1.2 An Office Building Set-Up in eQUEST..... 116
Figure 4.2.1.3 Use Phase Energy of TCFS and GCWS Per FU 118
Figure 4.2.1.4 Total Life Cycle Energy Input of TCFS and GCWS Per FU..... 120
Figure 4.2.3.1 CO2 Emissions of TCFS and GCWS Per FU 121
Figure 4.3.1 Global Warming Potential of TCFS and GCWS Per FU 122
Figure 4.4.1.1 Sensitivity Analysis Results for Pre-Use Phase 125
Figure 4.4.2.1 Sensitivity Analysis Results for Post-Use Phase..... 126
Figure 4.5.1 LCA and Sensitivity Analysis Comparisons..... 130

List of Tables

Table 2.2.1.1 Material Density of PC, PMMA, and Glass 13
Table 2.2.1.2 E-modulus of PC, PMMA, and Glass based on Tensile Test 13
Table 2.2.1.3 Coefficient of Thermal Expansion of PC, PMMA, and Glass 17
Table 2.2.1.5 Water Absorption of PC, PMMA, and Glass 18
Table 2.2.1.6 Flammability of PC, PMMA, and Glass 18
Table 2.2.1.7 U-factor of PC, PMMA, and Glass 19
Table 2.2.1.8 SHGC of PC, PMMA, and Glass 20
Table 2.2.1.9 VLT of PC, PMMA, and Glass 20
Table 2.2.1.10 Embodied Energy of PC, PMMA, and Glass 21
Table 2.2.2.1 Mechanical Properties of Biofiber Composites 23
Table 2.2.2.2 Weathering of Biofiber Composites 24
Table 2.2.2.3 Water Absorption of Different Biofiber composites 25
Table 2.3.1.1 Tabulated Values for Four-Edge Supported Plates 34
Table 2.3.1.2 Formulas for Four-Edge Supported Plates 35
Table 3.1.3.1 Sectional Properties of a TCFS Panel 52
Table 3.1.4.1 Material Properties of TCFS Components 54
Table 3.1.4.2 Summary of Stress and Deflection of a TCFS 55
Table 3.3.3.1 Bending Stress Comparison of a TCFS 68
Table 3.3.3.2 Displacement Comparison of a TCFS 69
Table 3.3.3.3 Bending Stress Comparison of Laminated Glass 71
Table 3.3.3.4 Displacement Comparison of Laminated Glass 72
Table 3.3.3.5 Bending Stress Comparison of Fully Tempered Glass 73
Table 3.3.3.6 Displacement Comparison of Fully Tempered Glass 74
Table 3.3.3.7 Bending Stress Comparisons of a TCFS 77
Table 3.3.3.8 Displacement Comparisons of a TCFS 78

Table 3.3.4.1 Material Properties of PMMA Skin and Cardboard Core 80
Table 3.3.4.2 Stress and Displacement Comparisons 81
Table 3.3.4.3 Stress and Displacement Comparisons 83
Table 3.5.3.1 Measured and Charpy Impact Strength of PMMA 102
Table 4.1.3.1 Functional Unit (FU) of TCFS and GCWS for Baseline LCA 107
Table 4.1.3.2 Material Inputs of TCFS and GCWS Per Functional Unit (FU) 109
Table 4.1.4.1 Major Assumptions and Limitations of the LCA study 112
Table 4.2.1 Life Cycle Inventory Data for Energy Inputs and GHG Emissions 113
Table 4.2.1.1 Pre-Use Phase Energy of TCFS and GCWS per FU 115
Table 4.2.1.2 Office Building Information for eQUEST Simulation 116
Table 4.2.1.3 Site Energy Consumed by End Uses of TCFS and GCWS Per FU 117
Table 4.2.1.4 Primary Energy Conumption of TCFS and GCWS Per FU 118
Table 4.2.1.5 Post-Use Energy Consumption of TCFS and GCWS per FU 119
Table 4.2.1.6 Total Life Cycle Energy Input of TCFS and GCWS Per FU 119
Table 4.2.3.1 Pollutant Emissions of TCFS and GCWS Per FU 121
Table 4.3.1 Global Warming Potential for 100-Year Time Horizon 121
Table 4.3.2 Global Warming Potential of TCFS and GCWS Per FU 123
Table 4.4.1 Key Factors for Sensitivity Analysis 123
Table 4.4.1.1 Sensitivity Analysis Results for Pre-Use Phase 124
Table 4.4.2.1 Sensitivity Analysis Results for Post-Use Phase 126
Table 4.5.1 LCA and Sensitivity Analysis Comparisions 129
Table 4.5.2 Summarized Comparisions of LCA and Sensitivity Analysis 131

List of Appendices

Appendix A Material Properties 143
Appendix B Characteristics of Polymers and Glass 144
Appendix C Biofiber Composites vs. Synthetic Fiber Composites 145
Appendix D Wind Load Calculation in accordance with ASCE 7-02 146
Appendix E Joint Shear Testing 148
Appendix F LRFD for Testing Frame Members 150
Appendix G Charpy Impact Testing Report Provided By Bodycote Testing Group ... 154
Appendix H Energy Use and Environmental Emission Inventory Data 163
Appendix I Energy Performance Value Verification Process 166

Abstract

Structural Evaluation and Life Cycle Assessment
of a Transparent Composite Facade System
Using Biofiber Composites and Recyclable Polymers

By

Kyoung-Hee Kim

Co-Chairs: Harry Giles and Richard E. Robertson

A composite façade system concept was developed at the University of Michigan by Professor Harry Giles that considered the use of various transparent and composite materials in building construction. Particular aspects of this transparent composite façade system (TCFS) were investigated in this dissertation and involved the use of recyclable polymers and biofiber composites. This dissertation addresses research questions related to structural and environmental performance of the transparent composite façade system (TCFS) compared to a glass curtain wall system (GCWS). In order to better understand the context for the TCFS and establish performance evaluation methods, an extensive literature review was conducted focusing on material performance, structural

performance requirements, life cycle assessment (LCA) techniques, composite panel principles, product surveys and building codes. Structural design criteria were established for the TCFS with respect to the strength and stiffness requirements of the International Building Code (IBC). A new testing frame was fabricated and installed at the architectural department of the University of Michigan to conduct static and impact tests in accordance with Safety Performance Specifications and Methods of Test (ANSI Z97.1). Initial static tests were carried out to measure bending stiffness of TCFS specimens in order to compare the results with theoretical predictions. Impact tests were also carried out to examine whether TCFS specimens conformed to the safety glazing criteria specified in ANSI Z97.1. In addition, a comparative LCA of a TCFS and a GCWS was performed on each system to assess their respective environmental implications.

Structural testing results indicated that the bending stiffness according to simple beam theory is in agreement with measured stiffness under two-edge supported conditions. Impact tests demonstrated that TCFS specimens satisfy the Class B of the safety glazing requirements of ANSI Z97.1. Comparative LCA results showed that the total life cycle energy of the TCFS was estimated to be 93% of that of the uncoated GCWS and the total emission of kg CO2 equivalent for the TCFS was determined as 89% of the uncoated GCWS. The impact associated with transportation and the end-of-life management was estimated to be insignificant in this study.

Chapter 1

Introduction

1.1 Background of the Study

At present, the US has only 5% of the world's population but is responsible for a quarter of the total world energy consumption and CO2 emissions (EIA, 2007, p. 5-6). Buildings in the residential and commercial sectors in the US consume 40% of total energy, 72% of total electricity, and 40% of raw materials while generating 39% of the US's CO2 emissions (DOE, 2007, p. 5). 136 tons of construction and demolition (C and D) waste were generated in the US in 1996 which accounted for more than 40% of total municipal solid waste in US landfills (Franklin Associates Prairie Village, 1998, p. 2-11, 3-1, 3-10). Further, depending on building type and design life, energy consumption associated with fabricating building materials vary from 10% for typical office buildings (Scheuer, Keoleian, & Reppe, 2003) up to 40% for medium density housing over their total life cycle (Thormark, 2006). Buildings are, therefore, prime candidates for reducing energy and materials consumption, as well as lowering the environmental impact associated with building material production, operation, and disposal. Possible opportunities for improving the current situation include enhanced building energy performance, on-site energy generation using renewable energy resources, sustainable construction methods and waste management, and the use of recycled materials.

There is increasing interest in the application of new materials in contemporary buildings in the pursuit of more creative forms and lightweight materials. Polymers, which offer great potential applications for buildings, have been used in manufacturing industries for some time. However, the long term durability of polymers in outdoor applications still needs to be improved. With advances in polymer technology, new

applications are opening up where polymers are used in conjunction with various reinforcements and coatings. TCFS were originally developed with the intention of creating new possibilities for building enclosures and at the same time addressing improvements in building use energy, recyclability and use of renewable sources as a means by which to reduce the energy and landfill waste noted above. TCFS incorporate recyclable polymers and biofiber composites made out of renewable fiber reinforcements, as an alternative to conventional glazing systems for buildings. It is recognized that since polymers are recyclable, and their thermal conductivity (0.2 W/m-K) is five times less than that of glass (1 W/m-K), they offer great potential to be used in buildings to reduce waste and energy use. This researcher investigated the performance of these new materials in a typical TCFS application according to standard assessment methods and compared its performance with that of a typical glass façade system.

1.2 Statement of the Problem

The building envelope as a mediator between dynamic external climates and static indoor conditions is subjected to various factors depending on the region in which the building is located, including heat, ultraviolet (UV) radiation, moisture, sound, wind, and seismic situations. While the use of opaque walls primarily focuses on security, privacy, and energy conservation, glazing walls provide daylighting, natural ventilation, and visual transparency. Glass is the most commonly used material in glazing systems, and various structural, thermal, acoustic, visual, and detailing issues have been continuously challenged in order to achieve high performance buildings.

The structural attributes of glass material are of concern because of impact resistance. Glass fails catastrophically when it is subjected to excessive bending stress, thermal shock, or imposed strain (Institution of Structural Engineers (ISE), 1999, p. 22). Further, when fully tempered glass is used in a glazing wall to provide higher strength, the inclusion of nickel sulphide can cause spontaneous breakage long after installation due to its slow growth within the glass over time (Loughran, 1999, p. 15). This continues to be a problem unless the glass is subjected to a heat soaking process prior to installation. The use of extra-large windows is still challenging due to handling and installation issues,

and requires more metal frames to hold the glass, adding more material and weight to the building.

In addition to these structural challenges, the environmental impact of using a glass façade system is of increasing concern. Glass windows are responsible for $40 billion in energy loss in US buildings annually (Selkowitch, 2008, p. 6). Various coating such as low-e and reflective coatings, solar control films, surface treatment (frit), and/or laminated glass with high performance interlayer are widely available to create energy efficient windows. However, these methods are beginning to limit the benefit of winter sun and daylight for buildings in cold climates, adding energy consumption during heating seasons (Carmody, Selkowitz, Lee, Arasteh, & Willmert, 2004, p. 14). Certain reflective coatings can cause glare for occupants of other buildings (Carmody, Selkowitz, Lee, Arasteh, & Willmert, 2004, p. 88). Therefore, glazing systems need to be more carefully considered for location, use, and solar orientation, the studies of which are not addressed in this research.

Glazing systems are structurally and environmentally challenging, and therefore, research on alternative glazing systems is essential to increase the knowledge base of structural and energy performance of the building envelope. The research investigation focused on studying the performance characteristics of recyclable polymers, which also possess greater impact resistance compared to glass. A transparent composite façade system (TCFS) incorporates a stiff layered panel system through composite interaction between a core and skin configuration, similar to most composite honeycomb panel systems used in lightweight construction. In this instance, a biofiber composites core is bonded between two polymer skins, and offers ecological advantages due to its renewability, recyclability, and biodegradability. The TCFS referred to here, uses a transparent recyclable polymer skin and opaque biofiber composites core, and was investigated for its structural integrity and environmental impact. Figure 1.2.1 illustrates a simplified sectional view of a TCFS showing heat transfer characteristics depending on the sun's position.

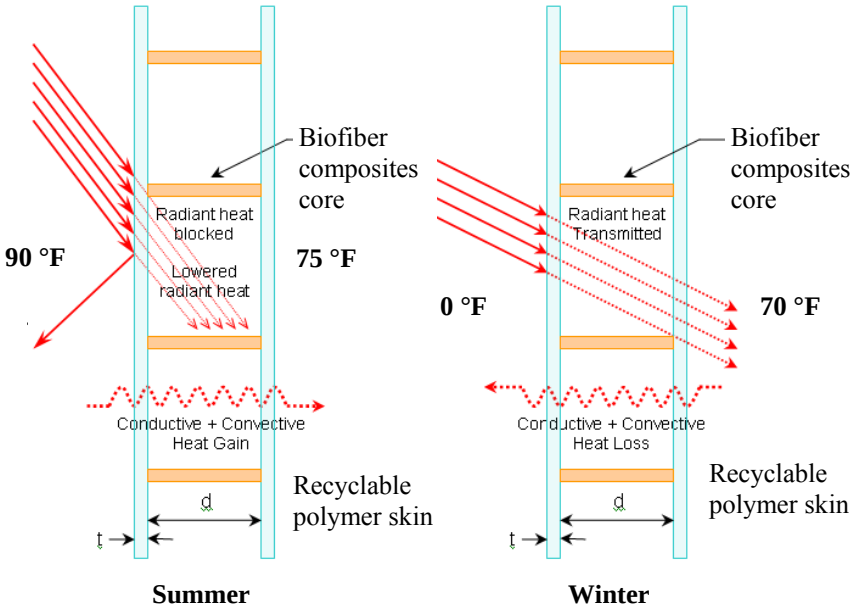

Figure 1.2.1 Simplified Sectional View of TCFS

1.3 Research Objectives

The primary objectives of this research are to explore the influence of recyclable polymer and biofiber composites material properties on the performance of TCFS and to establish a simple structural design procedure for building applications. The structural investigations also include static and impact load testing. Life Cycle Assessments (LCA) are carried out on a TCFS and a glass curtain wall system (GCWS) to compare their relative environmental impact

This study specifically addresses the following research questions:

1) Building Materials Investigation
    a. How do polymers differ from glass with respect to their material properties? What are the pros and cons of each?
    b. What are the mechanical properties of polymers and biofiber composites?
2) Structural Design of Transparent Composite Façade System (TCFS)
    a. What are the structural principles of a composite panel system?
    b. What are the structural design criteria and design procedures for a TCFS?
3) Structural Performance Evaluation of TCFS

a. What is the stiffness of TCFS and are theoretical predictions consistent with experimental results?
b. What is the impact behavior of a TCFS system?

4) Comparative Life Cycle Assessment (LCA)
   a. What is the life cycle energy consumption and corresponding CO2 emissions of TCFS compared to GCWS?
   b. To what extent does the prediction of product life influence the overall life cycle assessment?

Figure 1.3.1 shows the outline of a research method and procedure to achieve the discussed research objectives.

1.4 Significance of the Research

This research investigates some of the key performance characteristics of emerging materials in buildings and carries out baseline comparisons with a typical glass wall system towards assessing any advantages provided by an alternative polymer- and biofiber composites-based glazing system. The primary assessment criteria for this research are related to renewable, recyclable and biodegradable materials that will contribute to reducing energy consumption, waste generation, and environmental pollution. In particular, biofiber composites have the potential to contribute towards greater agricultural diversity, as a non-crop based renewable material, through their extensive use in future building products.

In addition, research on the structural and environmental attributes of TCFS will enhance the knowledge base for building envelope and green building practice including the use of lightweight sustainable materials. The LCA methodology used in this research will also contribute towards a better understanding of how the LCA method can better quantify the overall energy performance of a building envelope by considering the entire life cycle.

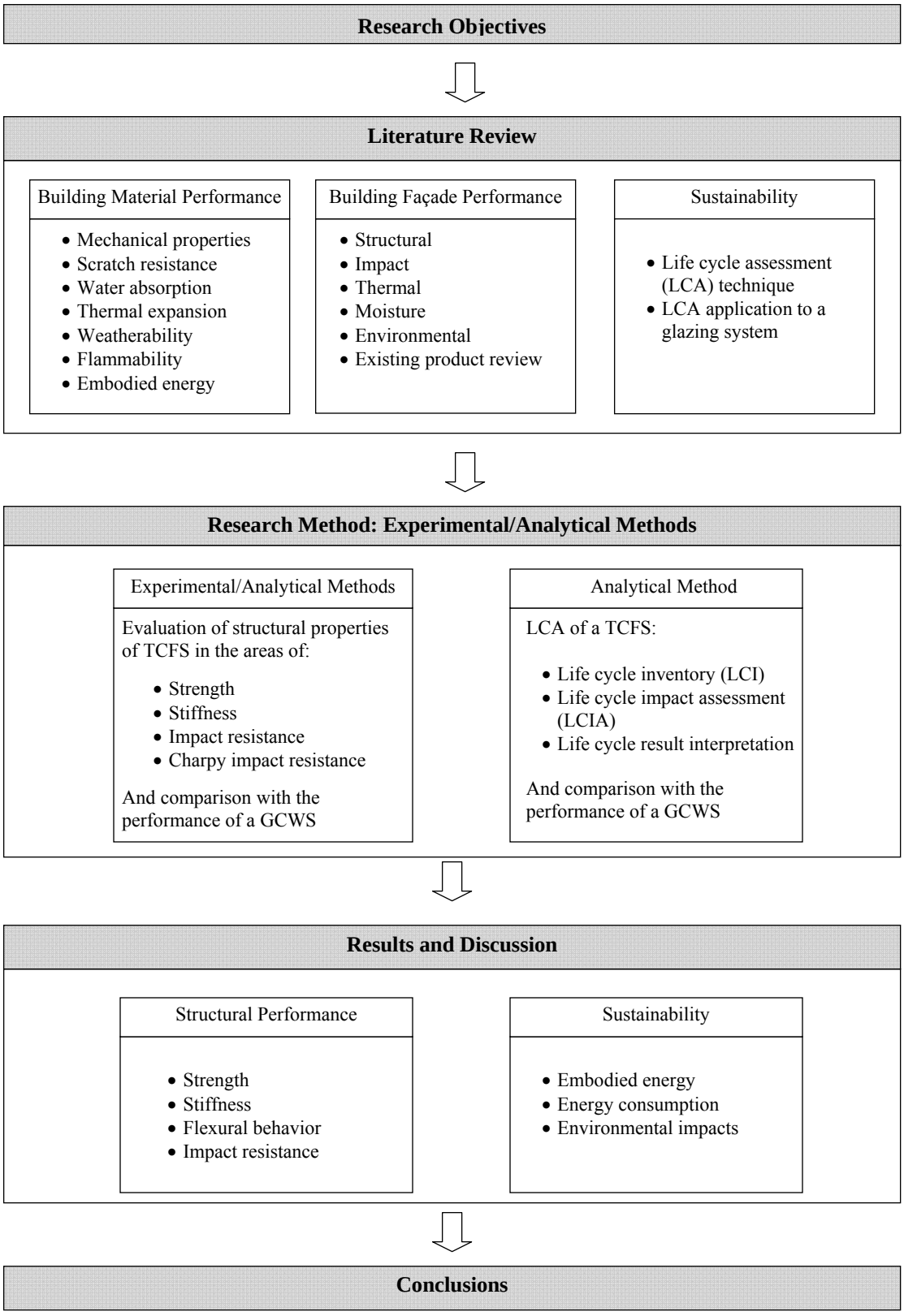

Figure 1.3.1 Overview of Research Areas

Chapter 2

Literature Review

Glass has been used as a load bearing material in building façades since the mid-20th century (ISE, 1999, p. 145). As the popularity of a glass façade in buildings continues to rise (Sutherland, 2008, p. 122), the structural safety and the environmental performance of a glass façade system increase in importance. Two major structural challenges of a glass façade system are its low impact resistance and brittleness, while heat loss and gain through a glass wall is another challenge from an environmental perspective.

In the past, the opaque parts of a building—such as the walls and roofing members—were made of composite panel construction. These panels composed of various skin and core materials are favored in the architecture industry due to their beneficial structural and thermal properties (Hough, 1980; Chong & Hartsock, 1993; Pokharel & Mahendran, 2003; Boni, Franscino, & Almeida, 2003). Many studies have been focused on investigating the structural behaviors of composite panels under static and dynamic loads using analytical, numerical, and experimental methods. The extensive research conducted on opaque composite panels is beneficial to the research of a transparent composite façade system (TCFS) because it helps understanding inherent structural and thermal potentials of a TCFS and similar research methodologies can be employed to measure the performance metrics of a TCFS.

A less stiff transparent polymer has been configured to a very stiff material by sandwiching with a biofiber composites core, which formed a transparent composite façade system (TCFS). A TCFS was designed as a stiffer, safer, energy-efficient and lightweight alternative to glass for building façade applications. To measure whether these goals were met, it is necessary to understand the performance of existing glass

systems. The three structural performance metrics that are examined in this research are strength, stiffness and impact behavior. The sustainability metrics specifically focus on energy consumption and CO2 emissions and are analytically investigated using the life cycle assessment technique. The final two sections of this chapter establish a theoretical framework to measure the aforementioned façade performance.

2.1 Previous Studies on Composite Panel Systems for Building Application

The first practical application of composite panels was for World War II aircrafts, and later, these same types of panels were used on the Apollo spacecraft (Davis (Ed.), 2001, p. 1). The double sandwich shell in the Apollo spacecraft was primarily used for weight reduction and strong and stiff construction (Davis (Ed.), 2001, p. 1). The shell of the Apollo spacecraft, as shown in Figure 2.1.1, consisted of two layers of thin composite panels that were connected by spacers. The outer layer was composed of a 0.038 mm thick plastic honeycomb core sandwiched between two 0.021~0.51 mm thick steel facing sheets. The construction of the inner layer was similar, except the skin was made of a thin aluminum panel rather than a sheet of steel facing. Since the 1960s, composite panels have been widely used in industrial and commercial buildings, with the first architectural application in the Sainsbury Centre for Visual Arts in Norwich, UK, which was designed by Foster Associates in 1977 (Davis (Ed.), 2001, p. 45). The size of each panel was 1.8 m x 1.2 m and 55 mm thick, and all four sides of the panel were prefinished with extruded frames in order to provide fixing mechanisms and a weatherproofing membrane against an aluminum back-up carrier system (Brookes, 1990, p. 161).

Composite panels have been proven to offer a high strength- and stiffness-to-weight ratio. Many researchers have studied the structural behaviors of composite panels used for building applications. The majority of the research that has been conducted has focused on defining simplified design equations or numerical simulation methods to provide time efficient, accurate tools that were validated through experimental results. The studies also have focused on the global and local buckling behaviors of a composite panel system. For building applications, the skin material, which must be relatively strong and durable, is often made of such products as a concrete panel, a piece of cold-formed steel or sheet metal, medium density fiber board, or glass fiber reinforced gypsum

board. The core material in composite panels, which is relatively less strong and stiff than the skin material, ranges in content from a low-density rigid foam core to corrugated metal.

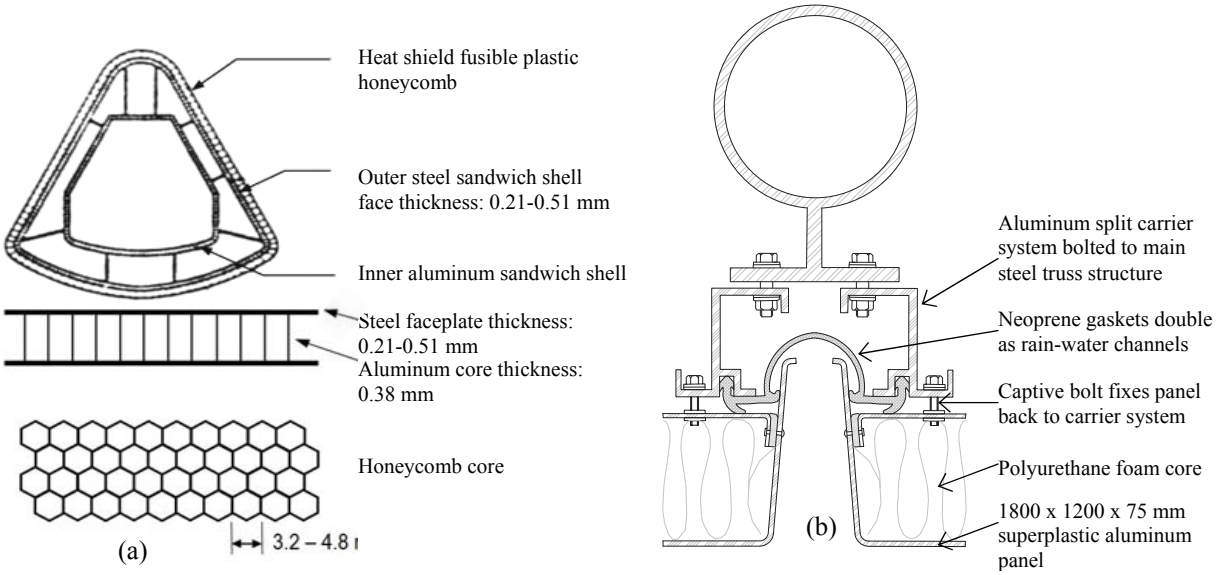

Figure 2.1.1 Composite Construction of Spacecraft (a) and Sainsbury Centre for Visual Art (b)

From "Lightweight Sandwich Construction," by Davies (Ed.), 2001, p. 1 & 186. "Cladding of Buildings," by Brookes, 1990, p. 161.

Hough (1980) investigated the structural attributes of a composite panel used for floor and wall applications. The panels were made out of recycled metal cans that were bonded to steel sheets with epoxy. He compared the theoretical deflections resulting from both bending and shear stiffness by using the simple bending experiment and adjusting the theoretical equations based on the experimental results. The study concluded that the metal can composite panel provided greater span capability with a lower self-weight compared to a typical floor system. Despite these favorable results, economic and fabrication challenges arose due to the high cost of epoxy at the time of the study.

Gentle and Lacey (1990) studied the structural and insulating properties of a composite panel designed as an emergency shelter application and which consisted of a medium density board (MDF) skin and a core made of expanded polystyrene (PS) cups. The expanded polystyrene cups were glued to the MDF skins with a PVA adhesive, and then the cavity between the cups was injected with polyurethane (PU) foam. The simple bending test conduced on the PU foam composite panel revealed that the 100 mm thick composite panel provided a higher strength-to-weight ratio compared to a 38 mm thick

solid board. The thermal test showed that the panel's thermal conductivity (0.15 W/m-K) was comparable to a double brick wall with a PU foam-filled cavity. In order to enhance the economical and ecological performance of the composite panel, the researchers proposed future studies regarding the automated manufacturing process and methods to reduce the amount of PU foam used.

Similarly, Chong and Hartsock (1993) used theoretical and experimental methods to research the flexural behaviors of a composite panel made of cold-formed steel facings with a rigid insulation core. The simplified design equations were validated through experiments that could be used in the design and optimization phases of a corrugated steel composite panel.

Pokharel and Mahendran (2003) examined the local buckling problems of steel facings and the effects of a rigid foam core under axial loadings. The researchers investigated a buckling coefficient which varied depending on the composite panel's width-to-thickness ratio and its material properties. The researchers proposed simplified buckling formulae that were validated through the experimental results. Due to these favorable results, the researchers recommended that the formulae be adopted during the design stage of the load-bearing wall application.

Benayoune et al. (2006) examined the structural behaviors of precast concrete sandwich panels (PCSP) under eccentric axial loads. A PCSP is composed of a concrete panel facing joined with shear connectors, and the space surrounding the shear connectors is infilled with insulated board. The researchers carried out experiments focusing on the load bearing capacity of the PCSP by investigating load vs. displacement, load vs. strain, cracking patterns on the concrete skin and other breaking modes. The study concluded that the experimental results were in agreement with the finite element method (FEM) analysis, thus recommending FEM as an efficient tool for use during the design phase of a PCSP.

In addition to studies focusing on composite panels with rigid foam cores, a number of researchers have studied composite panels with open cell cores. Open cell geometric cores such as honeycomb, corrugated, truss type (pyramidal truss or tetrahedral truss) and textile cellular type have been widely adopted in the aeronautics field due to high strength- and stiffness-to-weight ratios and excellent energy absorption. The studies

on open cell core composite panels are highly academic, mostly dealing with FEM validation through experiments. Except for the panels with a honeycomb core, those open cell composite panels are not practical for building applications due to the complex fabrication process.

Boni and Almeida (2003) utilized experimental and FEM methods to examine the flexural behaviors of a panel made out of glass reinforced epoxy skins and a honeycomb core. To carry out the FEM analyses, the researchers studied two methods of computer simulation; one was to use 2D plate elements for both the facings and the honeycomb core, and the other was to use 3D solid elements for the core and 2D elements for the facing. The FEM simulations were compared with the experimental measurements, and the results of both the FEM simulations using the 2D plate and 3D solid elements agreed with the experimental measurements. For the global behavior assessment of a composite panel, the researchers recommended the simplified FEM method using 2D elements because it provides simpler computations and takes less time compared to the FEM method using 3D elements.

Valdevit, Wei, Mercer, Zok, and Evans (2005) studied the buckling behaviors of a steel composite panel and correlated the experimental measurements with the FEM simulations under transverse and longitudinal loads. The composite panel was made out of stainless steel facings welded to a corrugated core. The experimental results showed agreement with the FEM analysis for the composite panel which behaved linear-elastically without buckling both the steel facing and the core.

2.2 Transparent Composite Façade System

In the aerospace and automobile industries where weight reduction and a streamlined design are the primary design criteria, polymers have become more widely used than glass as a glazing material due to its ease of formability, lighter weight and higher impact resistance (Katsamberis, Browall, Iacovangelo, Neumann & Morgner, 1997). Durability in buildings, however, is one of the major criteria for building material selection, and glass has been the preferred transparent material for a building façade despite its low impact resistance and brittleness. The advancement of polymer and coating technologies has led to the development of a polymer that is significantly more

durable and scratch resistant, thus making it suitable for outdoor use for building façade applications (Sheffield Plastics, 2008; Cyro Industries, 2001). As a result, a composite construction consisting of a polymer skin and biofiber composite core—transparent composite façade system (TCFS)—was configured to provide a stiffer, safer, energy efficient and lightweight alterative to a glass façade system. This new glazing system spurred studies that evaluated the material performance of polymer and biofiber composites as a cladding material. The polymer skin has a sustainable characteristic due to its recyclability, which can help to reduce the environmental impact associated with raw material depletion and disposal. To further promote sustainable practices, a TCFS panel's core material consists of lightweight biofiber composites made of renewable and recycled materials.

Recyclable polymers, a class of thermoplastics, were selected as a facing material for the TCFS for their aforementioned benefits of being impact resistant, lightweight and sustainable. Transparent polymers were reviewed with respect to their mechanical properties, weatherability, thermal movement, scratch resistance, vapor permeability, flammability, energy performance and embodied energy. The results of material performance of polymers were then compared with those of glass. Biofiber composites consisting of natural fibers and polyester resin were chosen for the core of the TCFS due to their sustainability and aesthetic quality. The core materials were examined for their mechanical properties, weatherability, water absorption, resistance to microbial attack, and embodied energy. The aforementioned material characteristics of biofiber composites were compared with glass reinforced composites. Bio-based coatings made out of renewable resources were also briefly reviewed as a sustainable coating material used to enhance the long-term durability of biofiber composites.

2.2.1 Recyclable Polymers as Skin Materials

Advancements in polymer and coating technology led to the development of an outdoor use glazing grade that indicates suitable UV and scratch resistance. Four potential recyclable polymers, commonly called thermoplastics, were reviewed for building applications: polycarbonate (PC), polyethylene terephthalate (PET or nylon), polymethylmethacrylate (PMMA, acrylic, or Plexiglas), and polypropylene (PP).

Appendix A summarizes each material's mechanical properties, durability, energy performance, and environmental attributes in comparison with glass. Mechanical properties, which determine the strength and stiffness of materials, include E-modulus, yield and ultimate strength and Poison's ratio. Durability, which identifies a product's service life, includes weatherability, scratch resistance, and vapor permeability. Energy performance, which contributes to determining a building's energy consumption, includes heat transmittance (U-factor), solar heat gain coefficient (SHGC), and visual light transmittance (VLT). Environmental attributes are defined by the embodied energy and recyclability of materials. Appendix B explains the advantages and disadvantages of the four polymers used as glazing materials when compared to glass. The following section explores PCs and PMMAs in greater detail in order to verify their material performance compared to glass when used as a glazing application. Most of the data gathered about material performance was based on published product data and scholarly work.

(1) Mechanical Properties

A. Density: Density is determined by the mass of a material divided by its volume. As shown in Table 2.2.1.1, the density of PC and PMMA is less than half the density of glass.

Table 2.2.1.1 Material Density of PC, PMMA, and Glass

E-modulus	g/cm3
PC (Makrolon GP)	1.19
PMMA (Acrylite FF)	1.19
Glass	2.44 – 2.5

From "Makrolon GP Product Data," by Sheffield Plastics Inc., 2003, p. 1. "Physical Properties of Acrylite FF," by Cyro Industries, 2001, p. 6. "Materials and Design," by Ashby and Johnson, 2005, p. 228.

B. E-modulus: E-modulus (E) is the ratio of tensile stress to strain established in a uni-axial tension test (i.e., $E = \sigma/\varepsilon$). Stress (σ) is the ratio of the applied load to the cross sectional area of a specimen ($\sigma = F/A$) and strain (ε) is the ratio of the deformation to the original length of a specimen ($\varepsilon = \Delta L/L$). Table 2.2.1.2 shows that glass is approximately 25 times stiffer than PMMA.

Table 2.2.1.2 E-modulus of PC, PMMA, and Glass based on Tensile Test

E-modulus	MPa
PC (Makrolon GP)	2344
PMMA (Acrylite FF)	2800
Glass	68000 - 72000

From "Makrolon GP Product Data," by Sheffield Plastics Inc., 2003, p. 1. "Physical Properties of Acrylite FF," by Cyro Industries, 2001, p. 6. "Materials and Design," by Ashby and Johnson, 2005, p. 228.

C. Impact resistance: Impact resistance is the ability of a material to resist fracture under an impact load. In accordance with ASTM D 4272 Standard Test Method for Total Energy Impact of Plastic Films by Dart Drop, 6 mm thick PMMA can resist 9.5 N-m of impact energy, and 6 mm thick tempered glass can resist 4.1 N-m. Because of its higher impact resistance and lighter weight, PMMA windows are preferred over glass windows in the aircraft industry. Figure 2.2.1.1 compares the impact resistance between PC, PMMA, and glass.

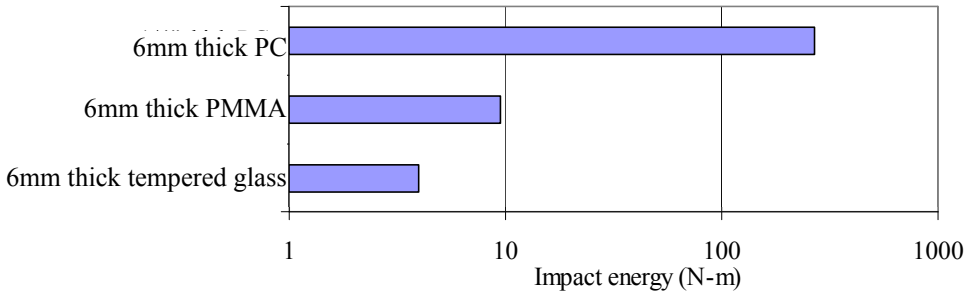

Figure 2.2.1.1 Impact Resistance of PC, PMMA, and Glass
From "Makrolon AR product data," by Sheffield Plastics Inc., 2003, p. 2.

D. Tensile creep modulus: One disadvantage of using polymer materials is the effect of long term creep deformation. Creep is the long-term deformation of a material as a function of stress intensity and the duration of time that the material is subjected to a given level of stress. The tensile creep modulus, which is measured in accordance with ASTM D 2990 Standard Test Methods for Tensile, Compressive, and Flexural Creep and Creep-Rupture of Plastics, is the ratio of applied tensile stress to total creep strain over a given period of time. Typical published tensile creep modulus values for PC (extrusion grade) and PMMA (extrusion grade) when subjected to 1000 hours of constant loading are between 1430 MPa and 1580 MPa respectively. This results in a reduction of the E-modulus to approximately 40%. However, it is important to note that building façade are less susceptible to creep since the stress created by their self weight is relatively small for a vertical façade application. Therefore, it is postulated that the creep modulus of polymers in a façade application will likely be similar to that of the original tensile modulus. Figure 2.2.1.2 shows an example of the creep characteristics for styrene acrylonitrile (SAN) as a function of time and stress levels.

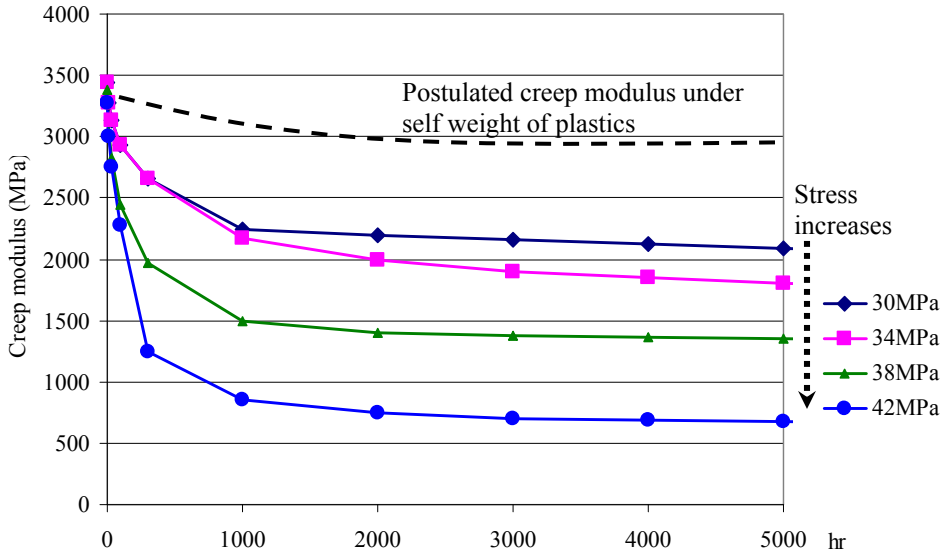

Figure 2.2.1.2 Creep Modulus of SAN at Various Time and Stress Levels

From "ASTM D 2990 Standard Test Methods for Tensile, Compressive, and Flexural Creep and Creep-Rupture of Plastics," by ASTM, 2001, p. 10.

(2) Weatherability

Polymers offer relatively low durability and weatherability under exposure to the natural environment compared to glass (Schmauder, Nauenburg, Kruse & Ickes, 2006). UV radiation, temperature, water, air contaminants and biological factors all play roles in determining the durability and weatherability of plastics (Wypych (Ed.), 1999, p. 60). UV radiation causes the deterioration of mechanical toughness and optical clarity − Yellowness Index (YI) and % Haze (Wypych (Ed.), 1999, p. 60; Plastics Institutes of America, 2001, p. 1356). In order to prevent UV degradation, UV-resistant additives and fillers as well as UV-protective coatings and films are applied to plastic materials (Margolis, 2006, p. 354; Plastics Institutes of America, 2001, p. 1355). The weathering performance of an uncoated PMMA and a coated PC undergoes significantly less change in color (YI) and optical properties (% Haze) after 10 years of UV exposure, as opposed to uncoated plastics (Altuglas, 2001, p. 8; Hayes and Bonadies, 2007, p.25). ASTM D 1925 Standard Test Method for Yellowness Index of Plastics is used in the plastics industry to measure discoloration levels under UV exposure. The yellowness becomes visibly detectable when the YI is greater than YI-8 (Altuglas, 2005). The light-transmitting properties of plastics are measured in accordance to ASTM D 1003 Haze and Luminous Transmittance of Transparent Plastics, and materials with greater than

30% haze are considered diffusing materials (ASTM, 2007). Figure 2.2.1.3 demonstrates that coated plastics provide greater light transmission over time compared to uncoated PCs.

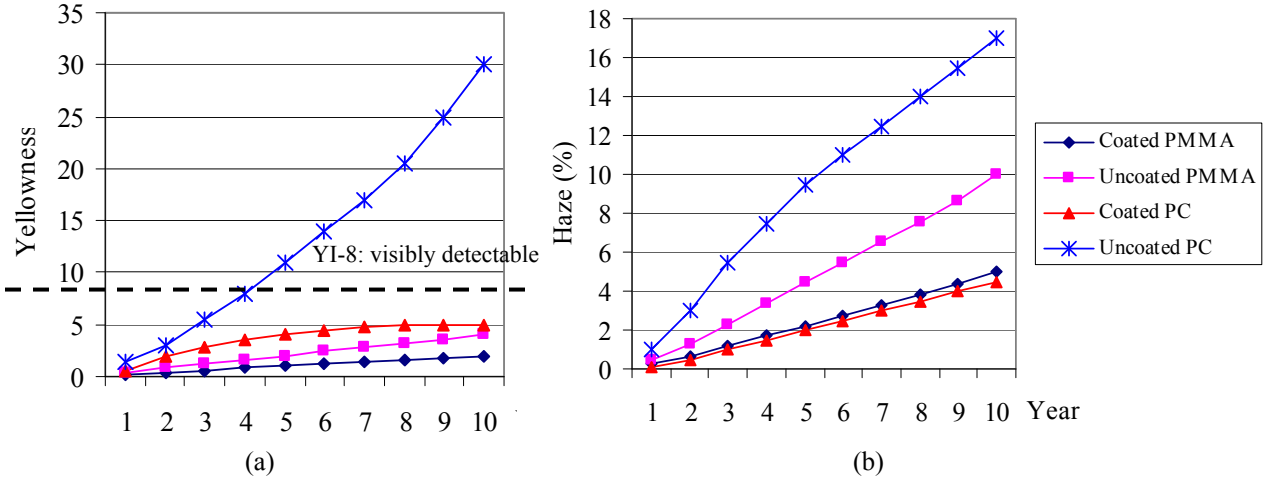

Figure 2.2.1.3 Yellowness Index (a) and Haze of PC and PMMA under UV Exposures
From "Cast and Extruded Sheet Technical Brochure," by Altuglas International, 2001, p. 8. "A New Hard Coat for Automotive Plastics," by Hayes and Bonadies, 2007, p. 25.

(3) Thermal Movement

Differential movement due to temperature changes in a material is an important consideration for façade applications. The coefficient of thermal expansion (α) is a measure of the linear expansion or contraction per unit of length divided by the difference in temperature, as shown in the equation below. The standard for measuring the thermal expansion of materials is ASTM D 228 Standard Test Method for Linear Thermal Expansion of Solid Materials with a Push-Rod Dilatometer.

$$\alpha = (L_2-L_1) / [L_0 (T_2-T_1)] \qquad \text{Equation (2.2.1.1)}$$

Where, L_1 = Specimen length at the temperature T_1

L_2 = Specimen length at the temperature T_2

L_0 = Original length at the reference temperature

Table 2.2.1.3 displays the coefficient of thermal expansion of PC and PMMA in comparison to glass. The coefficient for PMMA (6.8 x 10-5/K) is seven times greater than that of glass (average 0.1 x 10-5/K).

Table 2.2.1.3 Coefficient of Thermal Expansion of PC, PMMA, and Glass

	/K x10-5
PC (Makrolon GP)	6.75
PMMA (Acrylite FF)	6.8
Glass	0.7-1.3

From "Makrolon GP Product Data," by Sheffield Plastics Inc., 2003, p. 1. "Physical Properties of Acrylite FF," by Cyro Industries, 2001, p. 6. "Materials and Design," by Ashby and Johnson, 2005, p. 228.

(4) Scratch Resistance

The scratch resistance of plastics is measured by the amount of abrasive damage in accordance with ASTM D 1044 Standard Test Method for Resistance of Transparent Plastics to Surface Abrasions. Abrasive damage is judged by the percent of haze per cycles abraded. Table 2.2.1.4 shows the Taber abrasion resistance of a PC and a PMMA at 100 cycles abraded in comparison with glass. A coated PMMA (2% haze) performs better than an uncoated PMMA (40% haze), but it is still not as good as glass (0.5% haze).

Table 2.2.1.4 Taber Abrasion Resistance of PC, PMMA, and Glass

Products	% haze
Coated PC (Makrolon AR)	1-2
Coated PMMA (Acrylite AR)	2
PC (Makrolon GP)	35
PMMA (Acrylite FF)	40
Glass	0.5

From "Makrolon AR Product Data," by Sheffield Plastics Inc., 2003, p. 1. "Acrylite AR Technical Data," by Cyro Industries, 1998, p. 2.

(5) Water Absorption

Water vapor permeability indicates a polymer's ability to transmit vapor or gas through its thickness, which is usually measured according to ASTM E 96 Standard Test Method for Water Vapor Transmission of Materials. The water absorption of plastics is measured by ASTM D 570 Standard Test Method for Absorption of Plastic. In a water absorption test, specimens are immersed in water for a prescribed period of time, and the water absorption is determined by measuring the change in mass. Table 2.2.1.5 illustrates the water absorption rate after 24 hours for a PMMA, a PC and glass. Glass allows no water absorption, whereas PC and PMMA absorb 0.15% and 0.2 % respectively.

Table 2.2.1.5 Water Absorption of PC, PMMA, and Glass

Products	Water absorption (%)
PC (Makrolon GP)	0.15
PMMA (Acrylite FF)	0.2
Glass	0

From "Makrolon GP Product Data," by Sheffield Plastics Inc., 2003, p. 1. "Physical Properties of Acrylite FF," by Cyro Industries, 2001, p. 6. "Materials and Design," by Ashby and Johnson, 2005, p. 228.

(6) Flammability

For a glazing application, plastics are required to meet a self-ignition temperature of 343ºC or greater when tested according to ASTM D 1929 Standard Test Method for Determining Ignition Temperature of Plastics (IBC, 2003, p. 538). In addition, plastic glazing must provide a smoke density rating of less than 75% according to ASTM D 2843 Standard Test Method for Density of Smoke from the Burning or Decomposition of Plastics (IBC, 2003, p. 538). At the same time, plastic glazing must also conform to the combustibility classification of either class CC1 or class CC2 when tested according to ASTM D 635 Standard Test Method for Rate of Burning and/or Extent and Time of Burning of Plastics in a Horizontal Position (IBC, 2003, p. 538). In order to be in class CC1, plastics must limit the burning extent to 25 mm or less for the intended thickness to be used, and in order to qualify for the CC2 classification, plastics must provide a burning rate of 25 mm/min or less. Table 2.2.1.6 shows that, for the specific tests carried out, PC, PMMA, and Glass all conform to the flammability requirements of the ASTM codes. However, full compliance with the International Building Code (IBC) will need to be checked on a case-by-case basis, depending on the location, application and fire rating classification by occupancy group. The IBC further limits the installation of plastic glazing to a maximum area of 50% of a building's façade and with special provisions for different applications which is beyond the scope of this review (IBC, 2003, p. 540).

Table 2.2.1.6 Flammability of PC, PMMA, and Glass

	Thickness	Self-Ignition Temp. ASTM D 1929	Smoke Density Rating (%) ASTM D 2843	Burning Rate ASTM D 635
PC (Makrolon GP)	6 mm	554 ºC	62.8%	Class CC1
PMMA (Acrylite FF)	6 mm	455 ºC	6.4%	Class CC2
Glass (Clear)	6 mm	incombustible	incombustible	incombustible

From "Wisconsin Building Products Evaluation," by Wisconsin Department of Commerce, 2000, p. 4. "Physical Properties of Acrylite FF," by Cyro Industries, 2001, p. 6. "Materials and Design," by Ashby and Johnson, 2005, p. 228.

(7) Energy Performance (Heat Transmittance [U-factor], Solar Heat Gain Coefficient [SGHC] and Visible Light Transmittance [VLT])

A building's energy performance is related to the heat transmittance (U-factor), solar heat gain coefficient (SHGC) and visible light transmittance (VLT) of a glazing system. The thermal performance of a glazing system is attributable to the heat transfer caused by temperature differences and the amount of solar energy that is able to penetrate through the glazing. Generally, polymer materials have a better U-factor and a higher SHGC and VLT compared to glass.

A. U-factor: Heat transmittance (U-factor) is the combined effect of heat transfer consisting of conduction, convection, and radiation. Thermal conductivity (k) is a unique material property that is measured by the amount of energy flowing through a unit area, in unit time, where there is a unit temperature difference between the two sides of the surface (W/m2-K). Convection coefficients, often referred to as air film coefficients, are determined by the effects of temperatures and wind speeds on glazing surfaces. The American Society of Heating, Refrigerating and Air-conditioning Engineers (ASHRAE) defines an inside convection coefficient to be 1.35 W/m2-K based on a stagnant air condition with an indoor temperature of 21 ºC and an outside convection coefficient of 26 W/m2-K based on an outside wind speed of 5.5 m/s with a temperature of -18 ºC. The radiation effect is determined by indoor and outdoor temperatures and material emissivity. The U-factor of PMMA (5.16 W/M2-K) is slightly better than that of glass (5.81 W/m2-K). Table 2.2.1.7 summarizes the U-factor of PC, PMMA, and Glass with a thickness of 6 mm.

Table 2.2.1.7 U-factor of PC, PMMA, and Glass

Product	Thickness mm	W/m^2-K
PC (Lexan XL)	6	5.185
PMMA (Plexiglass)	6	5.167
Glass (clear)	6	5.818

From "Window (version 5.2) [Computer software]," by Lawrence Berkeley National Laboratory, 2001.

B. SHGC: The solar heat gain coefficient (SHGC) is the fraction of heat from the sun that a window admits. It is expressed as a number between 0 and 1. The lower a window's SHGC, the less heat it transmits. SHGC combines transmitted, absorbed, and reemitted solar energy. Equation 2.2.1.2 includes the directly transmitted portion τ_s and the absorbed and reemitted portion $N_i\alpha_s$.

$$SHGC = \tau_s + N_i\alpha_s \qquad (2.2.1.2)$$

Where, τ_s = the solar transmittance

N_i = the inward-flowing fraction of absorbed radiation

α_s = the solar absorptance of a single-pane fenestration system

PMMA (SHGC-0.85) transmits slightly higher solar energy compared to glass (SHGC-0.81). Table 2.2.1.8 shows the SHGC of a PC, a PMMA and clear glass with a thickness of 6 mm.

Table 2.2.1.8 SHGC of PC, PMMA, and Glass

Product	Thickness mm	SHGC
PC (Lexan)	6	0.813
PMMA (Plexiglas)	6	0.858
Glass (clear)	6	0.816

From "Window (version 5.2) [Computer software]," by Lawrence Berkeley National Laboratory, 2001.

C. VLT: Visible light transmittance (VLT) is a measure of the fraction of visible light transmitted through a window. It is expressed as a number between 0 and 1. The higher a window's VLT, the more visible light it transmits. A PMMA transmits slightly more visible light (92%) than clear glass (84%) due to its optical clarity. Table 2.2.1.9 compares the VLT of a PC, a PMMA and clear glass with a 6 mm thickness.

Table 2.2.1.9 VLT of PC, PMMA, and Glass

Product	Thickness inch (mm)	% VLT
PC (Lexan)	6	81
PMMA (Plexiglas)	6	92
Glass (clear)	6	84

From "Window (version 5.2) [Computer software]," by Lawrence Berkeley National Laboratory, 2001.

(8) Embodied Energy

Embodied energy is a measure of the energy used to manufacture a product, including raw material extraction, manufacturing, fabrication and transportation. Typically, a 1 kg PMMA sheet consumes 135 MJ of embodied energy whereas 1 kg of float glass consumes approximately 15 MJ (Huberman & Pearlmutter 2008; Yasantha Abeysundraa, Babela, Gheewalab & Sharpa, 2007; Chen, Burnett & Chau, 2000; SimaPro 7.1 database). PMMA and PC consume approximately nine times more embodied energy compared to glass of the same weight. However, when the volumes are the same for all three materials, PMMA and PC consume only about four times more embodied energy than that of glass due to their lighter density. Table 2.2.1.10 compares the embodied energy of these glazing materials.

Table 2.2.1.10 Embodied Energy of PC, PMMA, and Glass

Product	Embodied energy per unit weight	Embodied energy per unit volume
PC (extrusion grade)	130 MJ/kg	156,000 MJ/m^3
PMMA (extrusion grade)	135 MJ/kg	160,650 MJ/m^3
Float glass	15 MJ/kg	38,400 MJ/m^3

From "A Life Cycle Energy Analysis of Building Materials in the Negev Desert," by Huberman and Pearlmutter, 2008. p. 842. "Environmental, Economic and Social Analysis of Materials for Doors and Windows in Sri Lanka," by Abeysundra, Babela, Gheewalab & Sharpa, 2007, p. 2145. "Analysis of Embodied Energy Use in the Residential Building of Hong Kong," by Chen, Burnett, and Chau, 2000, p. 328. "SimaPro (version 7.1) [computer software]," by Pre Consultants.

2.2.2 Biofiber Composites as Core Materials

Biofiber composites are composed of a synthetic or bio-based polymer matrix reinforced with natural fibers (Mohanty, Misra, & Drzal [eds.], 2005, p. 4-5). Examples of the natural fibers typically used are: bamboo, china reed, cotton lint, jute, kenaf, flax, sisal, hemp and coir (Mohanty, Misra, & Drzal [eds.], 2005, p. 7). Synthetic polymers include polypropylene, polyester and epoxy, whereas bio-based polymers include cellulose plastic, starch-based polymer and polylactic acid (PLLA) (Mohanty, Misra, & Drzal [eds.], 2005, p. 251-253). Figure 2.2.2.1 shows an overview of biofiber composites. Studies showed that bio-based polymer composites are more susceptible to heat and moisture compared to synthetic-based polymer composites, resulting in the degradation of mechanical properties that are not suitable for long-term structural application (Ram, 1997 as cited in Ballie [ed.], 2004, p. 102). Therefore, this section focuses on the material

properties of biofiber composites that use synthetic-based polymer matrices with natural fiber reinforcements. Appendix C compares the general characteristics of biofiber composites to those of synthetic fiber composites.

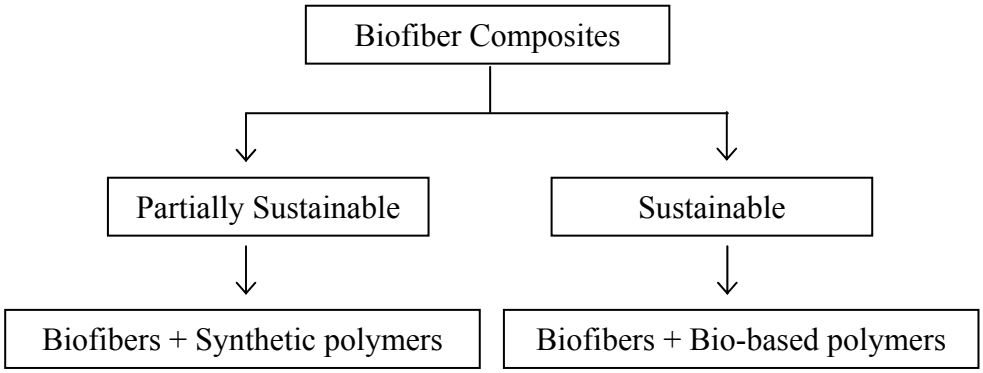

Figure 2.2.2.1 Overview of Biofiber Composite Material Components
From "Natural fibers, Biopolymers, and Biocomposites," by Mohanty, Misra, and Drzal (eds.), 2005, p. 5.

(1) Mechanical Properties

The mechanical properties of biofiber composites are influenced by different factors such as the fiber volume fraction, the fiber aspect ratio, the elastic modulus and fiber strength as well as the types of adhesions and toughness of matrices (Mohanty, Misra, & Drzal [eds], 2005, p. 272). The mechanical properties of a biofiber composite with a polyester matrix are comparable to those of a medium density fiberboard and weaker and less stiff than a glass fiber reinforced composite (Mohanty, Misra, & Drzal, 2005, p. 275). As can be seen from Figure 2.2.2.2, the overall mechanical properties of composite materials are reduced as the temperature increases (Baillie [ed.], 2004, p. 172). The E-modulus of a kenaf fiber composite at 100° C, for example, is 450 MPa, resulting in a 30% reduction of the original E-modulus (1250 MPa) at 30° C. Table 2.2.2.1 shows the mechanical properties of a biofiber composite with a polyester matrix compared to a glass fiber reinforced polyester composite.

Table 2.2.2.1 Mechanical Properties of Biofiber Composites

Composites	Density g/cm^3	Tensile strength MPa	Flexural strength MPa	E-modulus MPa
Sisal + Polyester	1.051	40	77	2130
Jute + Polyester	1.218	66	94	4420
Coir + Polyester	1.412	41	41	1600
Glass fiber + Polyester	1.60	163	362	26000

From "Natural fibers, Biopolymers, and Biocomposites," by Mohanty, Misra, and Drzal (eds.), 2005, p. 272 & 275.

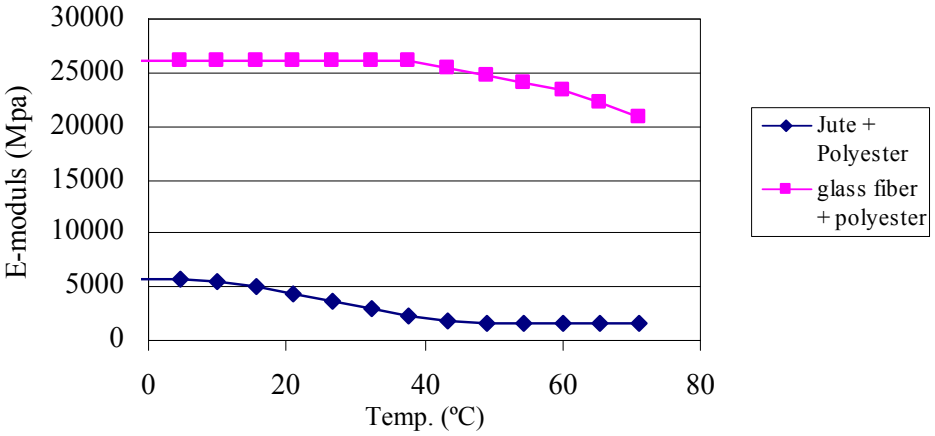

Figure 2.2.2.2 E-modulus Comparison of Biofiber Composites and Glass Fiber Composites at Varying Temperatures

From "Green Composites," by Caroline Baillie (ed.), 2004, p. 175.

(2) Weatherability

Weathering effects on biofiber composites exposed to outdoor environments include discoloration, surface deterioration and reduction in strength (Mohanty, Misra, & Drzal [eds.], 2005, p. 273). The exposed surface of the biofiber composite is subject to color fading while the unexposed surface develops black spots with hyphae-like structures (Mohanty, Misra, & Drzal [eds.], 2005, p. 273). The combined effects of biofiber fibrillation and lignin degradation reduce the tensile and flexural strength by 50% (Mohanty, Misra, & Drzal [eds.], 2005, p. 273). Glass fiber composites, on the other hand, undergo less change in color and strength compared to biofiber composites (Mohanty, Misra, & Drzal [eds.], 2005, p. 273). Polyurethane-coating and/or UV-stabilized resin can be applied to biofiber composites in order to minimize discoloration and strength reduction (Mohanty, Misra, & Drzal [eds.], 2005, p. 273). Table 2.2.2.2 summarizes the weathering effects of biofiber composites and glass fiber composites

after 2 years of exposure to an outdoor environment in Roorkee, India. Discoloration of biofiber composites due to exposure to the outdoors is shown in Figure 2.2.2.3.

Table 2.2.2.2 Weathering of Biofiber Composites

	Jute fiber composites	Glass fiber composites
2 years of natural exposure in Roorkee-India	• Color fading on the exposed surface • Black spots on the edge and black color on the unexposed surface • Reduction of tensile and flexural strength by >50%	• Less color change on both exposed and unexposed surfaces • Reduction of tensile and flexural strength by ~5-15%

From "Natural fibers, Biopolymers, and Biocomposites," by Mohanty, Misra, & Drzal (eds.), 2005, p. 273.

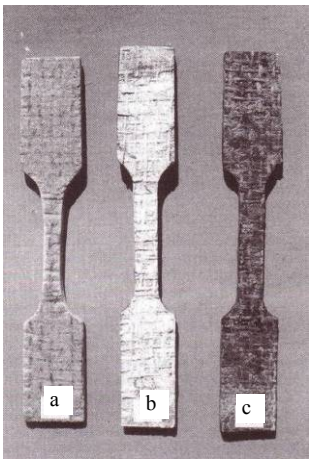

Figure 2.2.2.3 Discoloration of Jute Composites after Two Years of Outdoor Exposure;

Fresh (a), exposed side after two years outdoors (b) and unexposed side after two years outdoors(c).
From "Natural fibers, Biopolymers, and Biocomposites," by Mohanty, Misra, and Drzal (eds.), 2005, p. 274.

(3) Water Absorption

The amount of water absorption in biofiber composites is greater than that of synthetic fiber composites because there is a substantial number of voids present in laminates between natural fibers and polymer matrices, resulting in dimensional changes (Mohanty, Misra, & Drzal, 2005, p. 272-273). When immersed in water, the strength of a biofiber composite is reduced to 11~38% (Mohanty, Misra, & Drzal, 2005, p. 273). Interfacial voids between the natural fibers and matrix are due to the irregular surface characteristics and morphology of the fibers, but they can be minimized by chemically treating the surface of the biofibers during the fabrication process (Mohanty, Misra, & Drzal, 2005, p. 229). Table 2.2.2.3 describes the dimensional changes of various biofiber composites after being immersed in water for 24 hours at room temperature. Since

polymers tend to absorb more water as the temperature rises (Shah, 2007, p. 264), it is presumed that biofiber composites will admit more water as the water temperature goes up.

Table 2.2.2.3 Water Absorption of Different Biofiber composites

	Water absorption 24 hrs. (%)	Swelling in thickness 24 hrs. (%)
Sisal + Polyester	3-4	5
Jute + Polyester	1.09	Negligible
Coir + Polyester	3-4	5-6
Glass fiber + Polyester	1.03	Negligible

From "Constr. Buiod. Master., Singh, B. et al., 9, 39, 1995 Cited in Natural fibers, Biopolymers, and Biocomposites," by Mohanty, Misra, and Drzal (eds.), 2005, p. 272 & 275.

(4) Microbial Attack

A building material's durability can also be negatively affected by microorganisms, eventually leading to structural failure. Considerable research has been conducted on how wood preservatives and wood products provide microbial resistance, but little data is available about biofiber composites. The test method used for determining the microbial resistance of coated biofiber composites is ASTM D 3273 Standard Test Method for Resistance to Growth of Mold on the Surface of Interior Coatings in an Environmental Chamber. The major detrimental effects of microbial attack on biofiber composites include the degradation of mechanical properties and a change in aesthetic quality (Shah, 2007, p. 140). The microbial resistance is measured based on the degree of discoloration and disfiguration of a material's surface (ASTM D 3274, 2007. p. 1). The Federation Society of Coating Technology provides pictorial standards with ratings from 0 (minor degradation) to 10 (100% disfigurement), depending upon the surface defects (ASTM D 3274, 2007, p. 1 & 3). Figure 2.2.2.4 shows examples of different levels of disfigurement and their ratings.

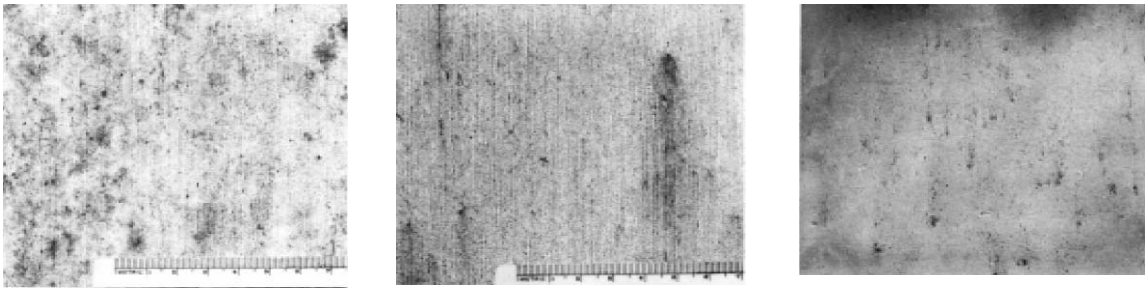

(a) (b) (c)

Figure 2.2.2.4 Pictorial Ratings of Microbial Degradation:
Rating-0 (a), Rating-2 (b), and Rating-4 (c)

From "ASTM D3274 Standard Test Method for Evaluating Degree of Surface Disfigurement of Paint Films by Fungal or Algal Growth, or Soil and Dirt Accumulation," by ASTM, 2007, p. 3.

(5) Embodied Energy

The embodied energy of biofiber composites varies according to the fiber types and weights. Biofiber composites typically have a lower embodied energy value and less CO2 emissions, which can make their environmental impact 20% less than that of synthetic fiber composites (Mohanty, Misra, & Drzal [eds], 2005, p. 851). Considerable research has been conducted in quantifying the embodied energy of biofibers compared to synthetic fibers, but little data is available about biofiber composites with a polymer-based matrix. In order to quantify the embodied energy of biofiber composites, a certain assumption was made with respect to a fiber-to-polyester composition ratio. As a result, a biofiber composite (74 MJ/kg) based on 0.2 kg of Chinese reed with 0.8 kg of a polyester matrix consumes 15% less embodied energy than a glass fiber composite (84 MJ/kg) made of 0.2 kg of glass fiber and 0.8 kg of a polyester matrix. However, the embodied energy of a biofiber composite is expected to be higher than the calculated value of 75 MJ/kg since the embodied energy is strongly related to the mass of the biofiber composite's polymer matrix.

Table 2.2.2.4 Embodied Energy of a Biofiber Composite and Glass Fibers Composite

Product	Mass (kg)	Embodied energy (MJ)
Chinese reed mat	1	3.64
Glass fiber mat	1	54.7
Polyester	1	92
Biofiber composite (reed : polyester = 0.2 kg : 0.8 kg)	1	74
Glass fiber composite (glass fiber : polyester = 0.2 kg : 0.8 kg)	1	84

From "Natural fibers, Biopolymers, and Biocomposites," by Mohanty, Misra, and Drzal (eds.), 2005, p. 851. "Materials and Design," by Ashby and Johnson, 2005, p. 204.

2.1.3 Bio-Coatings

The packaging and food industries have carried out considerable research on bio-coatings to establish more environmentally sustainable practices. Bio-coatings can include shellac, zein, corn protein, wheat gluten, soy protein, cottonseed protein, whey protein, casein, fish myofibrillar protein, egg whites and wool keratin (Gennadios, 2002, p. iii-x). These bio-coatings are widely available as renewable resources and byproducts of the food processing industry (Gennadios, 2002, p. xi). The following section references preliminary findings for shellac and zein as possible bio-coatings applied to protect biofiber composites. More research is needed to assess the long-term durability of shellac and zein when exposed to outdoor conditions and microbial attack.

(1) Shellac: Shellac is a natural polymer made from renewable resources. It is a resin excreted onto trees in India and Thailand by the female lac bug (Limmatvapirat et al., 2004). It is chemically similar to synthetic polymers and is commonly used in the food and paint industries (Limmatvapirat et al., 2004).

(2) Zein: Zein is a water-insoluble protein (prolamins) made from corn gluten and is essentially a byproduct of the corn wet-milling industry (Gennadios (Ed.), 2002, p. 43). Zein-based coatings are biodegradable, tough, glossy, hydrophobic greaseproof and resistant to microbial attack (Gennadios (Ed.), 2002, p. 44). Zein is typically used as a barrier against oxygen, lipids and moisture. It is also used in coatings for pharmaceuticals (Gennadios (Ed.), 2002, p. 47; Dong, Sun, & J-Y, 2004). Zein is mostly used in the food and packaging industries because when it is combined with a plasticizer it makes a film that is stretchable (Gennadios (Ed.), 2002, p. 49).

2.2.3 Existing System Review

In this section, composite façade panels available on the market are reviewed with regard to materials, structural attributes, thermal performance and their architectural applications. The integrated core materials between the glazing panels efficiently control solar heat gain and serve an aesthetic purpose, but the amount of visual transparency is limited due to the core materials. The core materials do not add any stiffness to the glazing system because they are independently installed in the air cavity without being bonded to the glazing panels. Therefore, like typical IGUs, glass make-ups need to be

calculated according to the ASTM E1300 Standard Practice for Determining Load Resistance of Glass in Buildings (ASTM, 2006). The embodied energy was estimated using the material components of the glazing panel of 1.2 m by 3.0 m. ClearShade IGU, manufactured by a Panelite Inc., and Okasolar by Okalux Inc. were used to understand their fundamental façade performance.

(1) Panelite: Panelite is a translucent honeycomb panel developed by New York-based architects. ClearShade IGU (insulated glass unit), which was developed for outdoor use, is made out of glass skins with an independent honeycomb polycarbonate core in the air cavity. The glass skin offers long-term durability and the polycarbonate honeycomb core acts as a shading device by limiting solar heat gain and daylight transmittance. A typical ClearShade IGU consists of a 6 mm outboard, a 12 mm thick honeycomb core and a 6 mm inboard, and the polycarbonate honeycomb core is normally 6 mm diameter and 12 mm thick. The glass skin can be available with up to 15 mm thickness depending on the wind load and panel size, and reinforced glass is also available for use in hurricane-prone regions. The span capability of the panel is determined according to ASTM E1300 depending on the design load, glass thickness, number of supported edges and deflection requirements. The maximum panel size available is 1346 mm wide by 3048 mm high. The embodied energy of a 1.2 m wide by 3.0 m high panel consisting of a 6 mm glass inboard, a 12 mm polycarbonate honeycomb core and a 6 mm glass outboard, for example, is estimated to be 1500 MJ based on the material mass (kg) input to fabricate the unit (SimaPro, 2007). The polycarbonate honeycomb core accounts for a minimum amount of impact on the embodied energy due to its small mass input. Figure 2.2.3.1 shows the layered construction for ClearShade IGU and its application to an external building envelope in Mexico.

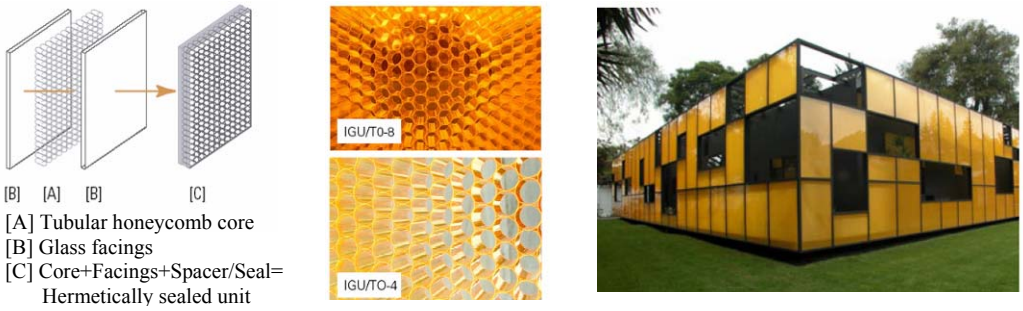

Figure 2.2.3.1 ClearShade IGU Assembly and Application in Mexico City, Mexico
From "Panelite Brochure," by Panelite, 2008, p. 9.

To illustrate its thermal performance which influences the operation energy of a building during its use phase, a ClearShade IGU consisting of a 6mm-thick glass skin and a 12mm-thick clear tubular core provides a U-factor of 2.67 W/m2-K and a variable SHGC of 0.17 to 0.5 depending on the sun's angle (Panelite, 2001, p. 12). Figure 2.2.3.2 shows the U-factor and dynamic solar shading coefficients of a ClearSharde IGU without low-e coating and with low-e coating respectivelv.

Performance Value	ClearShade IGU without low-e coating	ClearShade IGU with low-e coating
VLT	0.48	0.48
SHGC	Variable values	Variable values
U-value (W/m2-K)	2.67	1.65

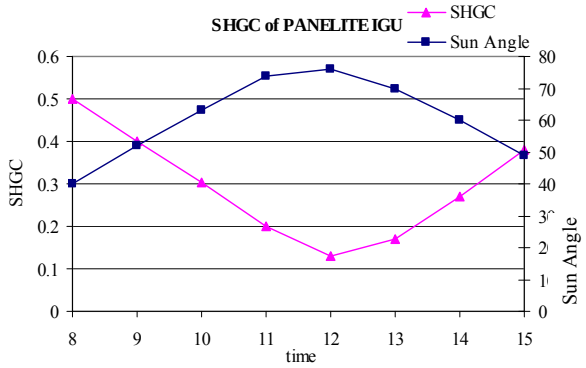

Figure 2.2.3.2 ClearShade IGU Energy Performance Values
From "Panelite Brochure," by Panelite, 2008, p. 12.

(2) Okalux

Okalux products consist of a glass skin and different shading elements such as wood strips, wire mesh, capillary tubes and Venetian blinds installed in the air cavity. According to their product performance description, Okalux products offer good light diffusion, solar heat gain reduction, and thermal insulation. In particular, Okasolar, as shown in Figure 2.2.3.3, has sun shading louvers in the glass cavity that offers both light transmission and shading coefficients as high as SHGC- of 0.32 in winter and SHGC-0.16 in summer. The aluminum louvers are suspended in a 22 mm thick glass cavity, and typically span 1000 mm. Like a ClearShade IGU, an Okalux panel's glass thickness is determined in accordance with ASTM E1300, depending on the design load, size of the panel and number of supported edges (ASTM, 2007). The maximum available panel size is 3000 mm wide by 4500 mm high. The estimated embodied energy of a 1.2 m x 3.0 m panel with aluminum louvers is approximately 3000 MJ, which is higher than the ClearShade IGU due to the greater mass input of energy-intensive aluminum louvers.

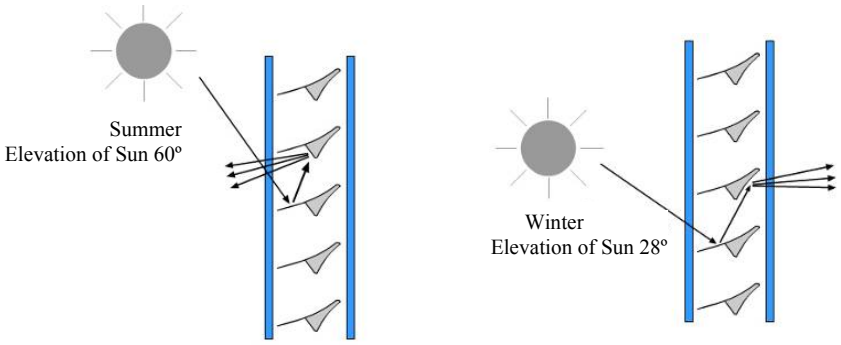

Figure 2.2.3.3 Louvers-Integrated IGU: Summer (left) and Winter (right) Conditions
From "Okasolar W: Glazing with Integral Sun Control Louvers," by Okalux, 2008, p. 1.

2.3 Structural Evaluation Framework

This section discusses a theoretical framework to measure façade performance with respect to strength, stiffness and impact resistance under static and impact loads. The fundamental structural requirements for a façade system involve its strength and stiffness. Both strength and stiffness are a function of material properties, sectional geometry, span length, type of support and loading types. Flexural strength refers to the ability of a member to resist internal stresses without rupturing or being crushed under an external bending force, whereas stiffness refers to the ability of a member to resist excessive deformation. In addition to strength and stiffness, understanding the impact behaviors is also important because impact performance is directly related to the structural integrity and safety requirements of a façade system. Therefore, this section reviews the theoretical framework used to determine the strength, stiffness and safety performance of a façade system.

2.3.1 Strength and Stiffness

(1) Simply Supported Beam

Simple beam theory, in accordance to Roark's formulas (Young & Budynas, 2002, p. 190 & 192), was reviewed to calculate the maximum bending stress and deflection of a composite beam with a two-edge support within the elastic range. The transformed section method (Gere, 2006, p. 403) was used to compute the sectional properties of a composite beam. Depending on the span and depth ratio, the deflection of a composite beam would consist of bending deflection and shear deflection, and the shear deflection

of a composite beam in a typical application (i.e., relatively long spans with thin sections) contributes to less than 2% of the total deflection (Bitzer, 1997, p. 49). Therefore, this section focuses on defining the flexural deflection of a composite beam. Equations 2.3.1.1 through 2.3.1.4 show the formulas used to calculate the bending stress and deflection of a simple beam with a point load (P) and a uniformly distributed load (w) respectively. Equations 2.3.1.5 and 2.3.1.6 provide the equations to calculate the sectional properties (I [moment of inertia] and S [sectional modulus]) of a composite section using a transformed section method.

A. A simple beam with a point load (P)

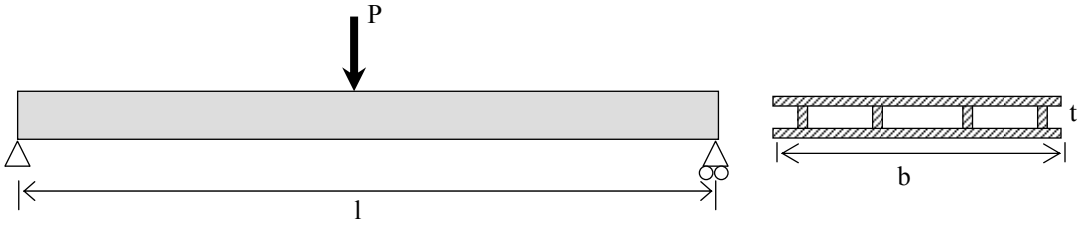

$$\text{Bending stress: } \sigma = \frac{My}{I} \qquad (2.3.1.1)$$

$$\text{Deflection: } \delta = \frac{Pl^3}{48EI} \qquad (2.3.1.2)$$

Where, M = bending moment (= Pl/4)

P = point load

y = distance from the neutral axis to the extreme fiber of a section (= t/2)

l = span

E = E-modulus

I = moment of inertia (= $bt^3/12$)

b = width of a composite panel

t = thickness of a composite panel

B. A simple beam with a uniformly distributed load (w)

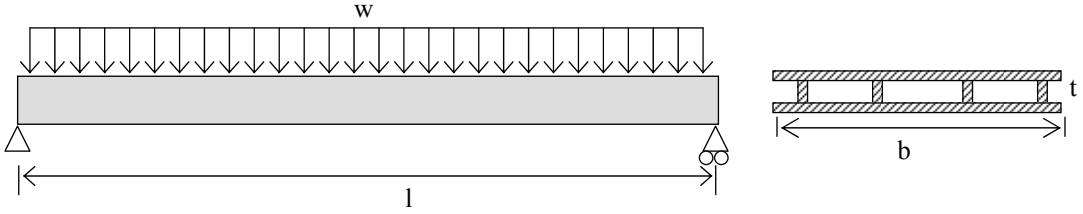

Bending Stress: $\sigma = \frac{My}{I}$ (2.3.1.3)

Deflection: $\delta = \frac{5wl^4}{384EI}$ (2.3.1.4)

Where, M = bending moment (= $wl^2/8$)

w = uniformly distributed load

y = distance from the neutral axis to the extreme fiber of a section (= t/2)

l = span

E = E-modulus

I = moment of inertia (refer to Equation 2.1.1.5)

b = width of a composite panel

t = thickness of a composite panel

C. Transformed Section Method

The moment of inertia (I_{total}) of the composite section is computed by converting the width of the core into the width of the skin material using the modular ratio (n) as shown in Figure 2.3.1.1. The modular ratio (n) is the ratio of the E-modulus of the core to the E-modulus of the skin. Equation 2.3.1.5 shows the moment of inertia calculation of the transformed section.

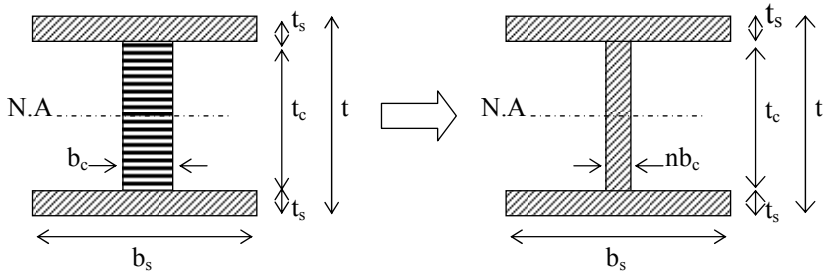

Figure 2.3.1.1 Transformed Section for Equivalent Moment of Inertia Calculation; Original Section (a) and Transformed Section (b)

$$I_{total} = I_{skin} + I_{core} = 2 \times Ad^2 + I_{core}$$

$$= 2 \times \left((b_s \times t_s) \times \left(\frac{(t_s + t_c)}{2} \right)^2 \right) + \left(\frac{nb_c \times t_c^3}{12} \right) \quad (2.3.1.5)$$

Where, b_s = width of skin

t_s = thickness of skin

b_c = width of core

t_c = thickness of core

t = total thickness of a composite section

E_s = E-modulus of skin material

E_c = E-modulus of skin material

n = modular ratio (= E_c/E_s)

(2) Simply Supported Plate

Simple plate theory, according to Roark's formulas (Young & Budynas, 2002, p. 502), was reviewed to calculate the bending stress and deflection of a plate with a composite section. Because Roark's plate theory is only applicable to a plate with uniform thickness and homogeneous materials (Young & Budynas, 2002, p. 427), the theory was modified by using effective thickness. The effective thickness is essentially computed by transforming a composite section with varied thicknesses and/or made of different materials into a single plate's thickness asserting the plate's thickness were of uniform thickness and made of homogeneous materials as shown in Figure 2.3.1.1. Equations 2.3.1.6 and 2.3.1.7 show the maximum deflection and bending stress of a four-edge supported plate with a composite section, and Table 2.3.1.1 provides the tabulated values used in Equations 2.3.1.6 and 2.3.1.7.

A. A simple plate under a uniformly distributed load over an entire plate

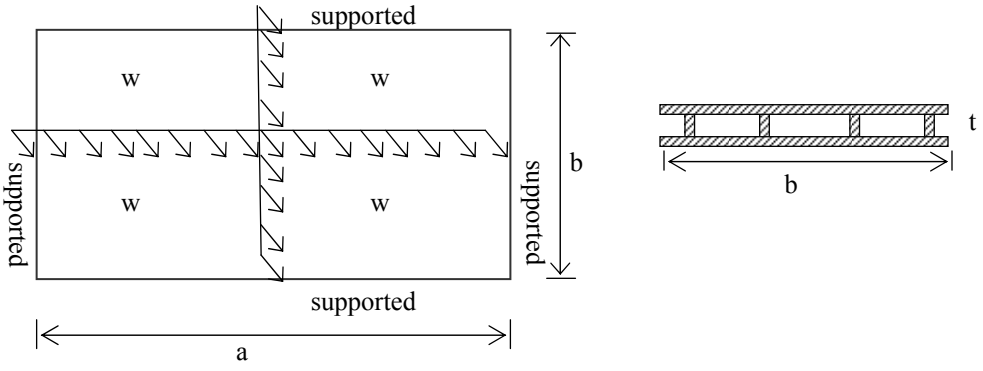

$$\text{Bending Stress } \sigma_{\max} = \frac{\beta w b^2}{t_{eff}^{\ 2}} \qquad (2.3.1.6)$$

$$\text{Deflection } y_{\max} = \frac{-\alpha w b^4}{E t_{eff}^{\ 3}} \qquad (2.3.1.7)$$

Where,

α, β, γ = tabulated value as a function of the aspect ratio of the plate

a = width of a composite panel

b = height of a composite panel

w = uniformly distributed load

E = E-modulus

t = thickness of a composite panel

t_{eff} = effective thickness (refer to Equation 2.3.1.5)

Table 2.3.1.1 Tabulated Values for Four-Edge Supported Plates under a Uniformly Distributed Load over an Entire Area

a/b	1.0	1.2	1.4	1.6	1.8	2.0	3.0	4.0	5.0	unlimited
B	0.2874	0.3762	0.4530	0.5172	0.5688	0.6102	0.7134	0.7410	0.7476	0.7500
A	0.0444	0.0616	0.0770	0.0906	0.1017	0.1110	0.1335	0.1400	0.1417	0.1421
Γ	0.420	0.455	0.478	0.491	0.499	0.503	0.505	0.502	0.501	0.500

From "Roark's Formulas for Stress and Strain," by Young & Budynas, 2003, p. 502

B. A simple plate under a uniformly distributed load over a central area

Under a uniformly distributed load over a local area, the maximum bending stress and the deflection at the center of the plate are calculated using the following equations (2.3.1.8 & 2.3.1.9) and the tabulated values are provided in Table 2.3.1.2.

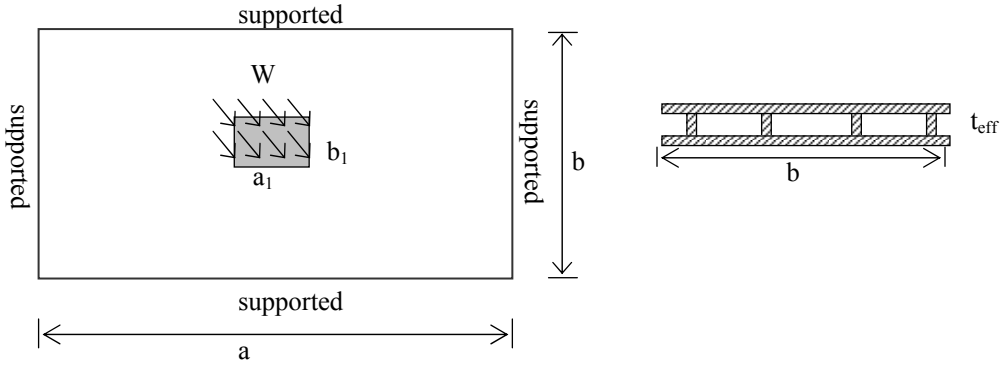

Bending stress: $$\sigma_{\max} = \frac{3P}{2\pi t_{eff}^{\ 2}}\left[(1+\nu)\ln\frac{2b}{\pi r'_0} + \beta\right] \qquad (2.3.1.8)$$

Deflection: $$y_{\max} = \frac{-\alpha P b^2}{E t_{eff}^{\ 3}} \qquad (2.3.1.9)$$

where, α,β,γ = tabulated value as a function of the aspect ratio of the plate

a = width of a composite panel

b = height of a composite panel

a_1 = width of a loaded area

b_2 = height of a loaded area

W = uniformly distributed load over a rectangular area

E = E-modulus

t_{eff} = effective thickness (refer to Equation 2.3.1.10)

v = Poisson's ratio

$r'_0 = \sqrt{(1.6r_0^2 + t_{eff}^2)} - 0.675t_{eff}$ if $r_0 < 0.5t_{eff}$, and $r'_0 = r_0$ if $r_0 \geq 0.5t_{eff}$

Table 2.3.1.2 Formulas for Four-Edge Supported Plates under a Uniformly Distributed Load over a Central Area

a/b	1.0	1.2	1.4	1.6	1.8	2.0	3.0	4.0	5.0	unlimited
B	0.2874	0.3762	0.4530	0.5172	0.5688	0.6102	0.7134	0.7410	0.7476	0.7500
A	0.0444	0.0616	0.0770	0.0906	0.1017	0.1110	0.1335	0.1400	0.1417	0.1421
Γ	0.420	0.455	0.478	0.491	0.499	0.503	0.505	0.502	0.501	0.500

From "Roark's Formulas for Stress and Strain," by Young & Budynas, 2003, p. 502.

C. Effective Thickness (t_{eff}) Calculation

The effective thickness of a composite section is computed using a section of a monolithic plate, assuming that the moment of inertia (I) of a composite (a) and transformed section (b) is the same as that of the monolithic plate (c) as shown in Figure 2.3.1.1. Equation 2.3.1.10 shows an effective thickness calculation based on the same width (bs) of the facing material.

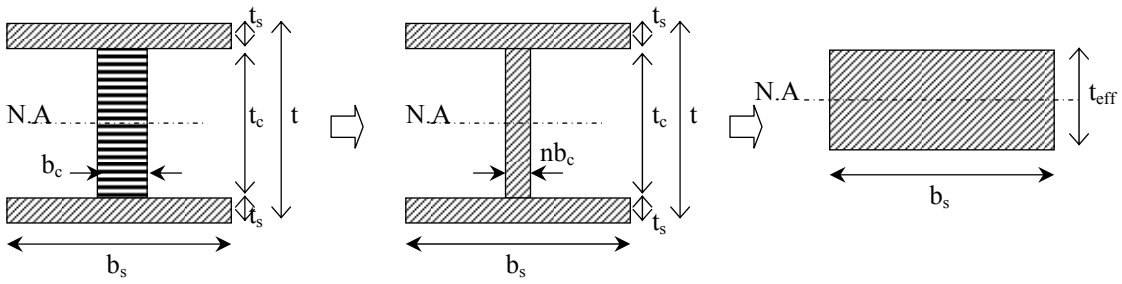

Original section (a) Transformed section (b) Monolithic section (c)

Figure 2.3.1.1 An Effective Thickness Calculation Diagram
from Transformed Sections to a Monolithic Section

$$I = 2 \times \left((b_s \times t_s) \times \left(\frac{(t_s + t_c)}{2} \right)^2 \right) + \left(\frac{nb_c \times t_c^{\,3}}{12} \right) = \frac{b_s t_{eff}^{\,3}}{12}$$

$$t_{eff} = \sqrt[3]{24 t_s \left(\frac{(t_s + t_c)}{2} \right)^2 + \left(\frac{nb_c t_c^{\,3}}{b_x} \right)} \qquad (2.3.1.10)$$

2.3.2 Impact Performance

A glass window is typically the most vulnerable building material due to its low impact resistance. In order to provide adequate safety against human body impact, a performance-based safety glazing standard, ANSI Z97.1, is used in the United States to comply with the various safety standard categories for glazing products. This section provides a theoretical framework of experiments under impact loads to determine the impact behaviors of a TCFS, which is discussed in Chapter 3.

(1) Impact Testing Apparatus and Specimen

ANSI Z97.1-2004 – the American National Standard for Safety Glazing Materials Used in Buildings – specifies impact testing procedures. The testing apparatus in ANSI Z97.1 consists of a metal frame, an impactor and a traction and release system. ANSI Z97.1 specifies that testing frames must use 76 mm x 127 mm x 6 mm steel angles (or other sections and materials of equal or greater rigidity) with either welded or bolted connections to minimize the deflection, racking and twisting of the testing frames. The impactor is a leather bag filled with number 7-1/2 lead shot weighing 45 kg, which is

connected from the upper swivel-fixture to the lower swivel by a steel cable. Testing specimens are 609 mm x 762 mm for the limited size or 863 mm x 1930 mm for the unlimited size, depending on the panel size intended for its final application.

(2) Human Impact Simulator and Impact Energy

Two types of impactors are internationally prescribed for a safety glazing test: a shot bag and a weighted double tire. Foss (1999) explains that the shot bag simulates a human head and body more accurately than does a weighted double tire. Figure 2.3.2.1 illustrates how a shot bag is analogous to human body impact.

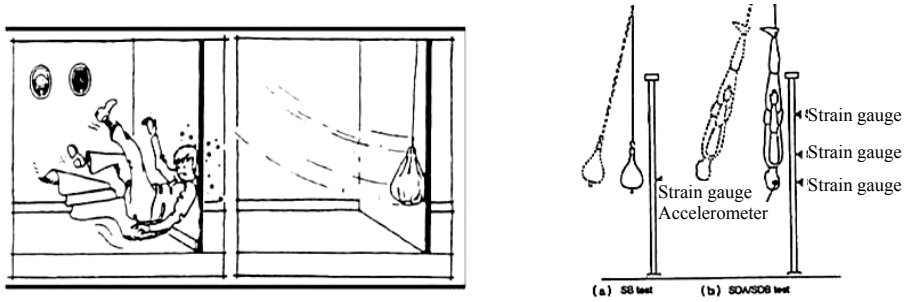

Figure 2.3.2.1 Shot Bag Impactor for Simulating Human Body Impacts
From "Safety Glass Testing: Human Head Impactor Simulation by Dynamic Transient Analysis," by Foss, 1999, p. 446.

In an accidental impact situation, the human body undergoes inelastic impact, resulting in a loss of kinetic energy (Toakley, 1966). The shot bag impactor specified by ANSI Z97.1 rebounds to about 50% of the original arc (Jacob, 2001), resulting in an inelastic collision in which part of the kinetic energy is transferred into the deformation of the impactor and another part is absorbed by the specimen. Figure 2.3.2.2 depicts the impact modes of shot-bags with perfectly elastic, inelastic and perfectly inelastic behaviors. The shaded impactors in Figure 2.3.2.2 indicate the impactor's final positions after striking the vertical specimen. A maximum potential energy of 1,355 N-m is specified in ANSI Z97.1 based on a drop height of 1.2 m and a 45 kg impactor, which is the equivalent amount of impact energy created by a 45 kg boy running at 6.7 m/s. Figure 2.3.2.3 shows different impact energies depending on the velocity and weight of the impactor.

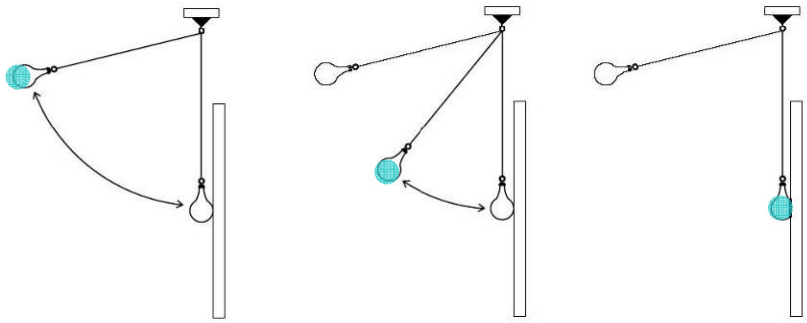

(a) Perfectly elastic (b) Inelastic (c) Perfectly inelastic

Figure 2.3.2.2 Shot-Bag Impact Modes
● indicates the final position of the impactor.

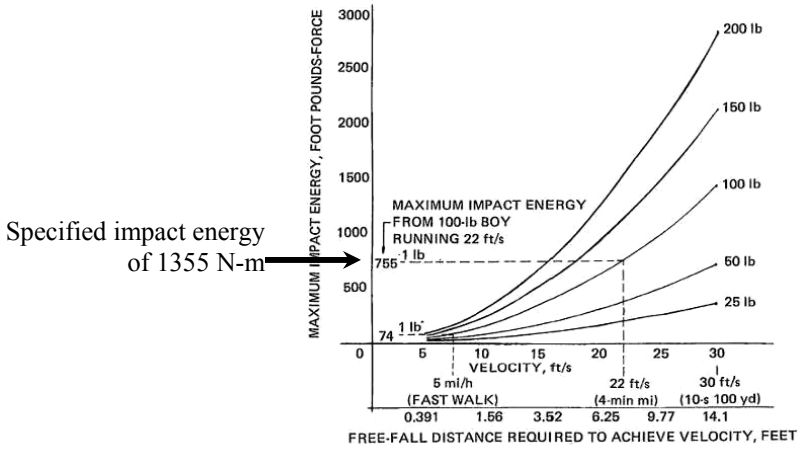

Figure 2.3.2.3 Human Engineering Data
From "ANSI Z97.1 American National Standard for Safety Glazing Materials Used in Buildings - Safety Performance Specifications and Methods of Test," by American National Standard, 2004, p. 37.

(3) Safety Glazing Classifications

ANSI Z97.1 specifies three classifications for safety glazing related to an impactor's drop height and the post-breakage modes of a specimen: Class A for a 1,219 mm-drop height, Class B for a 457 mm-drop height and Class C for a 304 mm-drop height. Six types of glazing materials are referred to as safety glazing in ANSI Z97.1: laminated glass, fully tempered glass, wired glass, polymer safety glazing, organic coated glass and a safety insulating unit. In order to pass the safety requirements of ANSI Z97.1, a sheet of laminated glass must either not fracture when dropped from a specified drop height, or if it does fracture, the broken pieces must adhere to an interlayer, and there

should be no opening large enough for a 76 mm diameter sphere to freely pass through. Fully tempered glass must either not fracture when dropped from a specified class drop height, or if it cracks, the ten largest pieces should not be heavier than the weight of 64.5 cm^2 of the specimen. In accordance with ANSI Z97.1, polymer with an E-modulus of less than 5,171 MPa and a Rockwell hardness of less than M are specified as safety glazing materials regardless of post-breakage modes. The Charpy impact test specifications stipulate that the test must be conducted after 2000 hours of UV exposure and that the weathered surfaces of the specimens should be placed on the opposite side of the impact hammer to avoid direct contact with the hammer's striking edge. The impact strength of aged polymers must maintain more than 75% of the Charpy impact strength of the original specimen to meet the safety requirements of ANSI Z97.1. Figure 2.3.2.4 demonstrates a Charpy impact machine and specimen set-up as per ASTM D 6110 Standard Test Methods for Determining the Charpy Impact Resistance of Notched Specimens of Plastics.

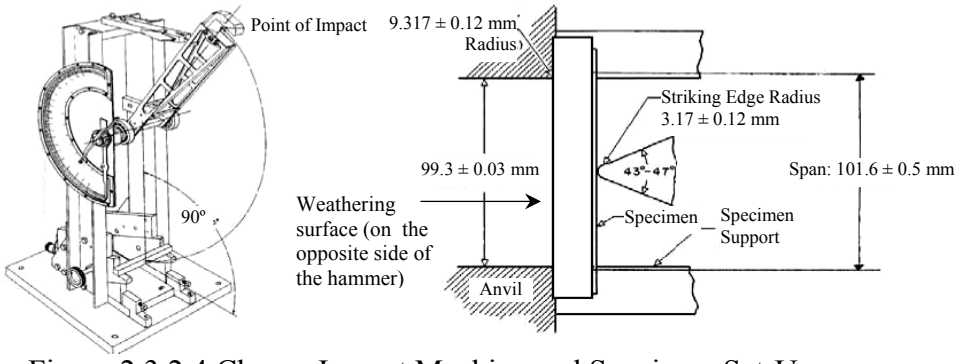

Figure 2.3.2.4 Charpy Impact Machine and Specimen Set-Up

From "ASTM D 6110 Standard Test Methods for Determining the Charpy Impact Resistance of Notched Specimens of Plastics," by ASTM, 2006, p. 3 & 4.

Figure 2.3.2.5 demonstrates the post-breakage patterns of a 6 mm-thick sheet of laminated glass and tempered glass. While broken laminated glass is shown to adhere to an interlayer, tempered glass breaks into granules. Many of the fractured clumps of tempered glass tend to break into sharp, dagger-like shapes rather than rounded clusters, as shown in the figure below (Jacob, 2001). Therefore, further study is required to more accurately assess the safety of the post-breakage patterns of fully tempered glass.

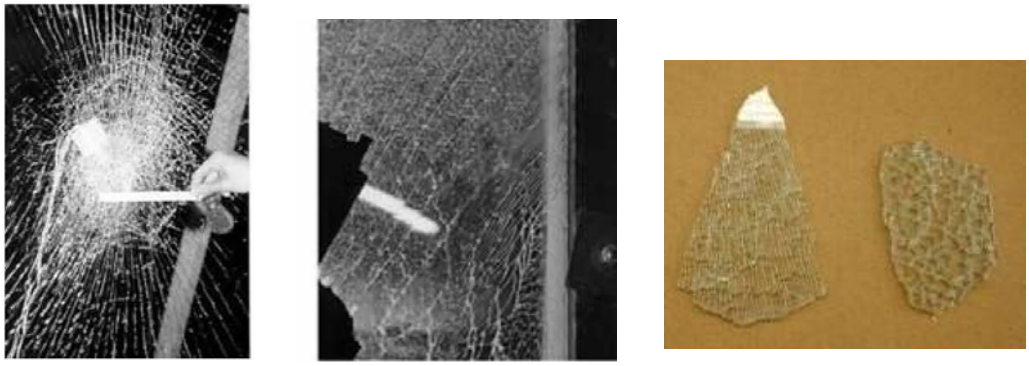

(a) (b) (c)

Figure 2.3.2.5 Fracture Patterns of Laminated Glass (a), Tempered Glass (b), and Shards of Tempered Glass (c)
From "Investigation of Repeatability and Reproducibility of the Shot Bag Impactor," by Oketani, Kikuta, and Aratani, 2001, p. 679 & 680.

2.4 Environmental Performance Evaluation Framework

Buildings are responsible for 40% of the US's total energy use and CO2 emissions (DOE, 2007, p. 5). Due to their high energy consumption, there is a growing effort to promote environmentally sustainable buildings, which has led to the development of a number of assessment tools such as the Life Cycle Assessment (LCA) and Leadership in Energy and Environmental Design (LEED). The LCA measures environmental impacts resulting from all stages of the life cycle of products or activities in a holistic way (Baillie, 2004, p. 23), and LEED evaluates environmental performance from a whole-building perspective by awarding points for satisfying the performance criteria (USGBC, 2003, p. 3). For this study, the researcher chose to use the LCA technique to measure the environmental performance of a glazing system because this method offers a comprehensive examination of the environmental impacts associated with each stage of a building's life cycle, from material production to the end-of-life management.

2.4.1 Framework of the Life Cycle Assessment (LCA)

In essence, an LCA focuses on the examination, identification and evaluation of the environmental implications of a product and its assembly process "from cradle to grave" (Graedel, 1998, p. 18). Various terminologies have been used to represent environmental impact assessments that are synonymous with what LCA accomplishes,

such as "cradle-to-grave analysis," "ecobalance," "ecoprofile," "life cycle balance," "resource and environmental profile analysis," "product line analysis," and "integrated substance chain analysis" (Baillie, 2004, p. 23). However, in 1997, the ISO 14040 series of standards was introduced, which led to the consistent use of LCA terminology in various fields (Baillie, 2004, p. 23). An LCA procedure starts with the goal and scope definition and continues to inventory analysis, impact assessment, and finally, interpretation of the results. Figure 2.4.1.1 depicts the LCA framework in accordance with the ISO 14040 guidelines.

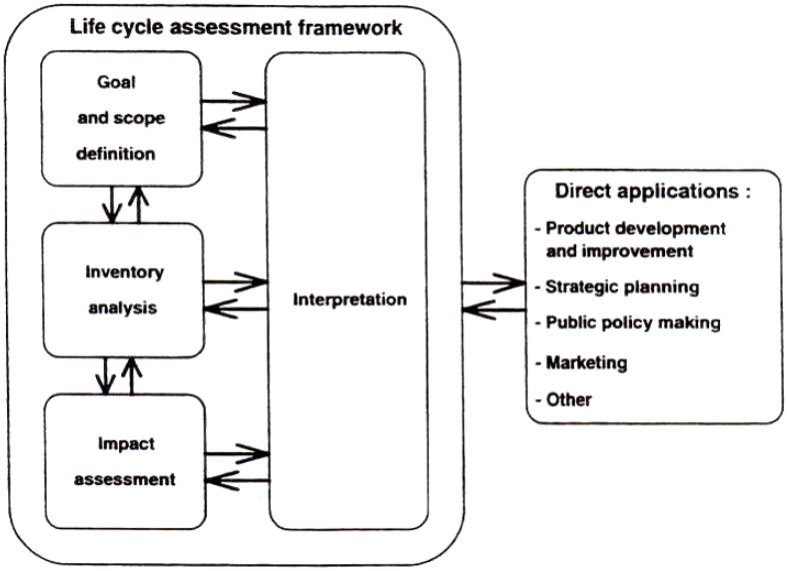

Figure 2.4.1.1 LCA Procedure in accordance with ISO 14040
From "Environmental Management− Life Cycle Assessment− Principles and Framework," by ISO, 2006, p. 4.

(1) Goal and Scope Definition

The first phase of the LCA framework under ISO 14040 is to describe the reasons for carrying out the study and to define the scope of work with respect to the functional unit, system boundaries, assumptions and limitations of the study and the data quality to ensure accurate and reliable results. A functional unit is defined by the functional requirements of a product system for a certain period of time. For example, the functional unit for a glass window can be defined as the area covered by a glass window for a specified service period. System boundaries are usually defined by whether an LCA study constitutes a complete analysis (e.g., cradle-to-grave) or partial analysis (e.g., gate-

to-grave) (Baillie, 2004, p. 28). Figure 2.4.1.2 illustrates a general material and process flow diagram that demonstrates a cradle-to-grave system boundary.

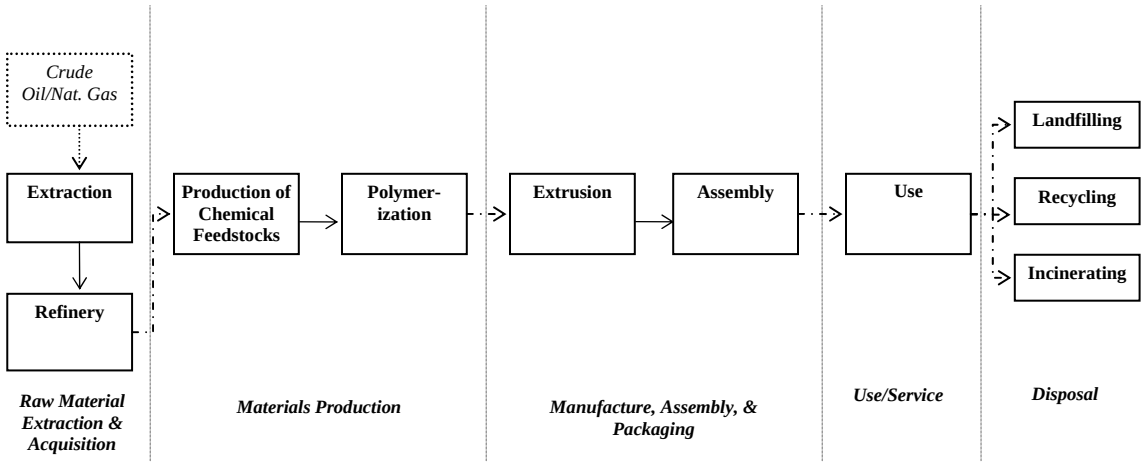

Figure 2.4.1.3 System Boundary Example of an LCA for a Plastic Sheet used for a Glazing Application; Material and Process Flow Diagram (Cradle-to-Grave)

(2) Life Cycle Inventory Analysis

The second phase of the LCA framework under ISO 14040 is the life cycle inventory analysis, which involves data collection to calculate material use, energy input and pollutant emissions during the entire life cycle of a product or process. These data can be obtained from companies engaged in product fabrication and processing activities as well as from published databases. Material use and primary energy consumption are calculated as a form of kg/functional unit and MJ/functional unit respectively, and pollutant emissions are expressed in terms of kg/functional unit. Figure 2.4.1.3 shows a life cycle inventory flow diagram published by the Society of Environmental Toxicology and Chemistry (SETAC).

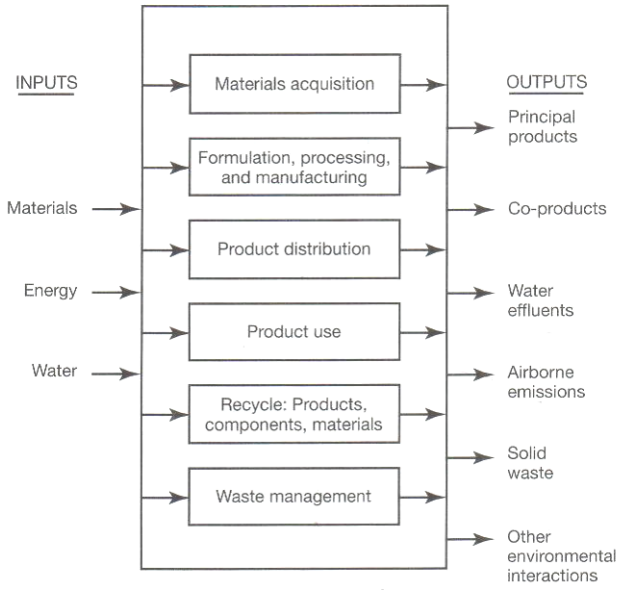

Figure 2.4.1.3 Flow Diagram of Life Cycle Inventory Analysis

From "Society of Environmental Toxicology and Chemistry [SETAC] by SETAC, 1999 Cited in Streamlined Life-Cycle Assessment," by Graedel, 1998, p. 23.

(3) Life Cycle Impact Assessment

The third phase of the LCA framework is the life cycle impact assessment, which focuses on evaluating and understanding the environmental impacts determined by the life cycle inventory analysis. ISO 14040 defines the impact assessment phase as consisting of the following elements:

(1) Classification: assigning inventory results to impact categories,

(2) Characterization: modeling inventory data within impact categories,

(3) Weighting: aggregating inventory data in very specific cases.

Examples of specific impact categories include: (1) resource depletion (i.e., depletion of abiotic/biotic resources), (2) pollution substances causing global warming, ozone depletion, eutrophication, acidification, and human toxicity, and (3) degradation of ecosystems and landscapes (i.e., land use). The characterization process involves defining characterization factors to convert each pollutant emission into equivalent potentials represented by a reference substance (e.g., CO2 equivalent). Weighting is used to combine the impact categories into a single score (e.g., ecopoint, SimaPro eco indicator method).

(4) Life Cycle Result Interpretation

The fourth phase of an LCA is the interpretation of the results, where the findings from the inventory analysis and the impact assessment are combined in order to reach conclusions and make recommendations. A sensitivity analysis can be carried out in order to understand how model parameters influence the LCA results or how critical uncertain parameters help to reduce environmental impacts.

2.4.2 LCA Application to a Building Window System

An LCA technique has been used to assess the life cycles of various industrial products, but there are a limited number of studies that focused on a building's window system. Weir and Muneer (1996) performed a comparative LCA of a window system using different inert gasses. They investigated the embodied energy and CO2 emissions associated with fabricating a window system that consists of an insulated glass unit (IGU), inert gas (air, argon, krypton and xenon), a timber frame and aluminum components. The LCA study showed that the xenon-filled IGU consumed the most embodied energy, followed by the argon-filled IGU and finally the krypton-filled IGU. These results were mainly attributed to the energy-intensive process of producing inert gasses. The environmental impact of these IGUs, however, will change when their use phase is included, because building are designed for long-term durability and an inert gas-filled IGU will consume less building operational energy due to its superior U-factor.

Citherlet, Di Guglielmo, and Gay's (2000) study took all stages of a window's life cycle into consideration. They conducted a comparative LCA by combing four variables: window types, building types (office, school and dwelling), façade orientation (East/West, South and North) and different climates zones. Eight different window systems were configured with and/or without incorporating hard low-e coating and inert argon gas to create different U-values so that their energy efficiency could be examined depending on building type, orientation and site location. The study concluded that the high performance window (hard coating with an argon gas-filled cavity) consumes more energy during its pre-use phase (from extraction to product fabrication), but this difference is reduced when it saves energy during the use phase because of its superior U-value compared to a typical window (without coating and argon gas). The study results,

however, somewhat are limited in that most of environmental impacts typically takes place in the use phase and the design life of the buildings and service span of the window system were not specified. The researchers speculated that the high performance window would consume more lighting energy than a typical window due to its relatively low visible light transmittance (VLT). Although higher VLT allows more sunlight and saves lighting energy consumption, this may require operable blinds for glare controls, which add environmental impact associated with production, maintenance and disposal of the blinds.

Whereas the aforementioned studies focused on the environmental impacts of window systems, Abeysundra, Gheewala, and Sharp's (2007) study considered the environmental impacts of two types of window frames—one made from wood, and the other from aluminum. Results indicated that, compared to the wood-framed window, the aluminum-framed window created higher environmental impacts due to the energy-intensive process involved in aluminum fabrication. However, this study was not conclusive because only the energy associated with material production was considered.

2.5 Conclusions

The first part of this chapter reviewed studies on composite panel systems for building applications and research methodologies. The second part involved assessing the material performance of recyclable polymers and biofiber composites in a transparent composite façade system (TCFS) in order to establish whether they are feasible materials to be used in outdoor environments. The final part of the study considered the structural framework to measure the performance metrics of stiffness, strength and impact resistance. An LCA technique to measure energy consumption and CO2 emission was discussed, and previous studies conducting an LCA for building glazing systems were also explained.

Section 2.1 discussed previous studies of composite panels made of various skin and core materials for building applications. Research focused on defining the structural behaviors of a composite panel through experimental and theoretical methods. Cores that are adhered to a strong skin material are made of wide range of less stiff and lightweight materials and configurations, and provide flexural and shear stiffness, impact resistance

and buckling resistance of the skin material. Composite panels can have either solid cores or open cell cores, depending on their structural and thermal requirements. Most studies on the composite panel focused on validating the analytical calculations and numerical simulations through experiments to provide a time-efficient and accurate tool that can be used during the design phase. The products available in the markets using a composite panel concept were also discussed in section 2.2. The glass panels integrated with shading louvers in the air cavity provides long-term durability for outdoor application while at the same time optimizing building energy performance. However, the cavity-installed core does not offer complete visual transparency and there are still challenges associated with the glass panel size and span capability of the products. The embodied energy of the façade system greatly depended on the types and the mass amount of the core material.

A transparent composite façade system (TCFS) made out of a polymer skin and biofiber composite core was newly configured, and the material performance of polymer and biofiber composites for outdoor use was verified as discussed in Section 2.2. The use of polymers in a glazing application has certain advantages over glass in the areas of weight reduction, impact resistance, thermal conductivity, optical clarity and design flexibility. For the construction of a composite panel system, biofiber composites provide sufficient mechanical properties and environmental benefits as a core material. The use of a polymer skin and biofiber composite core is expected to show lower weatherability when exposed to outdoor environments compared to glass. Due to the vapor permeability of polymers, moisture can migrate into the cavity of a composite panel through the polymer skin, which potentially produces mold growth on the biofiber composite core and condensation in the cavity. Possible ways to improve the current materials' performance is to seal both the polymer skins and the biofiber composite core with a protective coating in order to prevent vapor permeation, water contact and discoloration. At present, silicon hard coat technology is available for use on polymer materials, which provides UV, abrasion and vapor resistance. Bio-based coatings made from renewable organic resources provide the necessary durability for a biofiber composite core, but further research regarding this specific application should be carried out to access the long-term performance of the bio-based coatings when exposed to UV, heat and moisture.

In order to avoid stresses induced by thermal movement, a façade system joint configuration will need to be carefully designed to accommodate thermal movements. Long-term stress levels in plastics significantly affect long-term creep strain, but this may not be a major issue for a vertical façade application since the long term gravity stress is low and the higher wind loads are transient. The PCs and PMMAs meet the flammability requirements of the International Building Code, but future research is needed to verify the overall fire performance of both the polymer skins and the biofiber composite core of a TCFS.

Elastic simple beam and plate theories were reviewed in section 2.3 to compute the strength and stiffness of a composite panel construction. The transformed section method and effective thickness calculation was reviewed to estimate the sectional properties (e.g. moment of inertia [I] and sectional modulus [b]) of a composite section. The ANSI Z97.1 was also reviewed to verify safety glazing requirements and impact test specifications and used as a basis on which to fabricate a new test frame and carry out impact tests, as is described in Chapter 3.

The Life cycle assessment (LCA) method was reviewed in accordance with ISO 14040 in section 2.4 in order to measure the environmental performance of glazing façade systems during their life cycles. The first phase of an LCA—goal and scope definition—requires defining the functional unit, system boundary, study assumptions, and data quality. The life cycle inventory analysis, which is the second phase of an LCA, involves extensive data collection in order to calculate the total resource and energy consumption and the environmental emissions for a defined functional unit. The last phase of an LCA—life cycle impact assessment—consists of classifying impact categories and relating various types of pollutant emissions to a single substance. The previous studies concerning the LCA application for window systems provided limited information on their environmental impacts from the whole life cycle perspective because most studies did not explicitly discuss the impacts associated with the use phase and the end-of-life management.

Chapter 3

Structural Performance Evaluation of a TCFS

Chapter 3 focuses on establishing a structural design method for a transparent composite façade system (TCFS) and conducting structural static and impact testing in order to evaluate a TCFS safety classification in relation to ANSI Z97.1. This chapter also provides recommendations for the design of a TCFS, based on the results of the above analysis and tests and compares this with the design criteria of the International Building Code (IBC 2003). A new test frame was designed and fabricated in accordance with the requirements of ANSI Z97.1 for purposes of conducting both static and impact tests.

3.1 Structural Design of a TCFS

3.1.1 Strength and Deflection Requirements of a TCFS

A building façade system must resist design loads without material failure and without excessive deformation. Due to the lack of any structural performance design criteria for TCFSs, similar deflection and strength criteria were set, based on equivalent parameters specified in IBC 2003. According to IBC strength requirements, structural systems must provide adequate safety by not exceeding their strength limit under factored loads (Load and Resistance Factor Design [LRFD]) or they must not exceed allowable stress levels under working or service loads (Allowable Stress Design [ASD]). With regard to deflection requirements, current US building codes provide limited guidance on allowable deflections for a glazing system. For example, IBC 2003 limits the lateral deflection of glazing framing members and the edges of a glass panel to the lesser of 1/175 times the shorter span or 19 mm while ASTM E 1300-2007 limits the edge of glass to be 1/175 times the shorter span. The rationale for the deflection of a frame being

limited to 19 mm is likely to ensure a suitable support connection between a frame and the edge of a glazing panel (IBC, p. 515) and as such will be a suitable criterion for a TCFS panel. Therefore, the researcher uses 19 mm as a maximum allowable deflection of a TCFS panel. For the allowable bending stress criteria of a TCFS, the researcher used an ASD approach to verify the bending stress of a TCFS panel and examine a suitable safety factor for the TCFS design. Safety factor (N) is characterized as the ratio of allowable stress to working stress (N = allowable stress/working stress). A tensile member of steel, for example, uses a safety factor of 1.67 to calculate allowable stress (ASIC ASD, 2006, p. 16.1-46) whereas the allowable stress of glass is determined based on statistical analysis (ASTM E 1300, 2007, p. 3). A safety factor of concrete for flexural design is approximately 1.77 based on a ratio of load factor to load resistance factor (Nawy, 2005, p. 81). Plastic, however, has no guidance on safety factors for glazing application due to the lack of long term established practical experience. Therefore, the research uses a factor of 2 according to the Baker's weighted safety factor to estimate the allowable stress of plastics (Baker, 1956, p. 91 cited in Nawy, 2005, p. 78).

3.1.2 Design Load Verification

A façade system is subject to dead and various types of live load such wind, seismic, thermal expansion induced forces and impact. For the purposes of this research the scope of applicable loads were limited to the dead load, wind loads and impact forces to establish a design method for initial sizing and the evaluation of the performance of a TCFS that would satisfy the performance criteria of IBC 2003. Thermal and seismic forces can be accommodated through suitable connection details, similar to glazing systems design practice. Dead load is determined from the self weight of the façade system components, and wind load is established from code values, and in some specialized cases from the results of wind tunnel measurements. A typical 10-story office building located in Detroit, Michigan was used as a baseline model to establish suitable wind loads on a TCFS. The building configuration and dimensions are as shown in Figure 3.1.2.1. The size of each TCFS is 4.8 m wide by 4 m high and consists of a vision

and a spandrel panel. The structural span of the panel is 4 m, which is taken over its height and assumed to be fixed at each floor level.

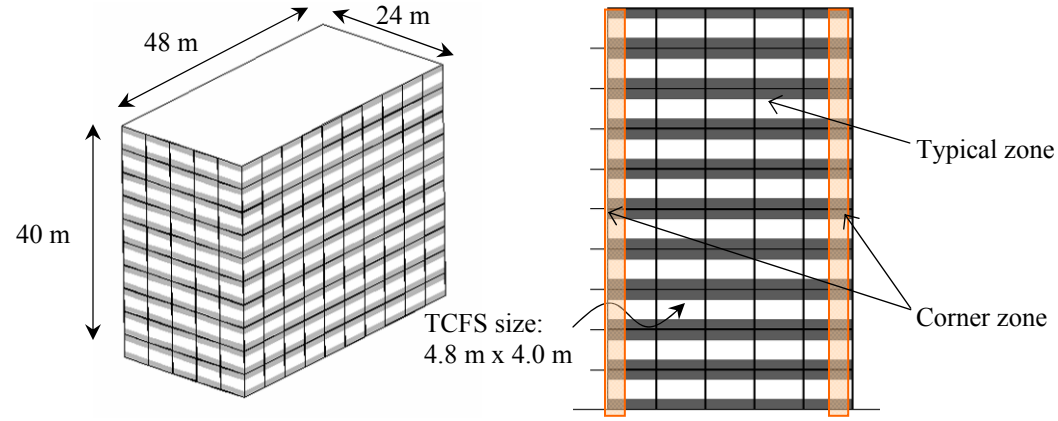

Figure 3.1.2.1 An Office Building Enclosed with TCFSs Located in Detroit, MI
Highlighted areas indicate the corner zones, each width of which is equivalent to 10% of the total façade width. The rest 80% represents the typical zone.

IBC requires that for this location (Detroit, MI) a basic wind speed of 40.2 m/s, exposure category B, and an importance factor of 1 is used. Generally a façade will experience positive and negative pressures, resulting from external and internal pressures. Depending on the location of the surface area of the façade, the sum of these pressures can result in a net pressure or suction on the wall. Wind loads also vary with increasing magnitude over the height of a building according to defined Velocity and Pressure Coefficients (kz) in the IBC. The detailed wind load calculation and the parameters used are documented in Appendix D. High local pressure areas occur at the corner of the building as defined by IBC and shown in Figure 3.1.2.1. The maximum positive and negative pressures are 0.87 kPa and -0.9 kPa on the general façade area and 0.87 kPa and -1.49 kPa on the corner areas. Figure 3.1.2.2 shows the wind loads that vary along the building façade. Since the corner area pressures are significantly higher than the general façade area, two different considerations might need to be taken into account in the recommendations for design. That is, corner TCFS panels may need to be further strengthened compared to the general areas, in order to optimize the design for the general areas which represents 80% of the total façade area.

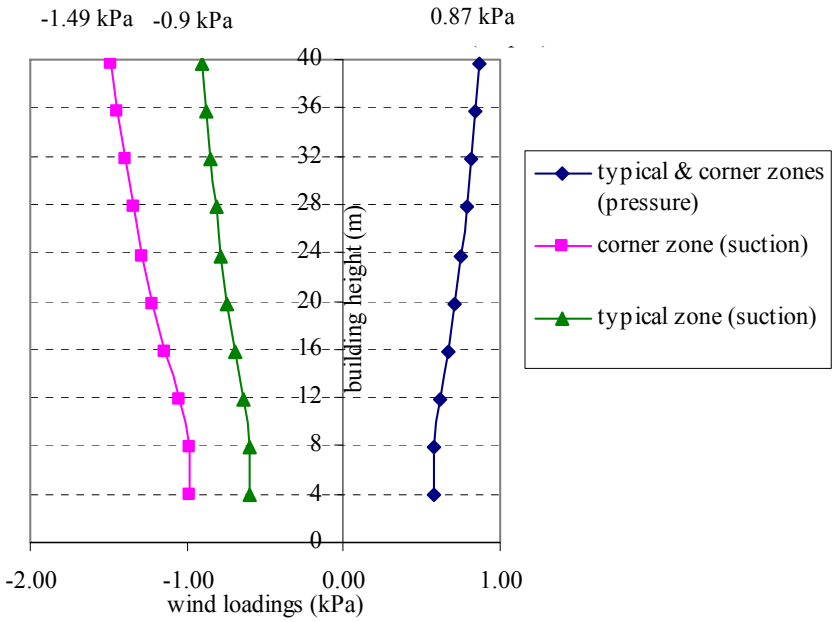

Figure 3.1.2.2 Varying Wind Loads across the Building Façade

3.1.3 Structural Properties of a TCFS

This section focuses on verifying the sectional properties of a TCFS to confirm whether the current design of the TCFS specimens meets the structural requirements established in Section 3.1.1. A TCFS panel is composed of a cardboard core that is sandwiched between two PMMA skins and connected by epoxy adhesives. Transformed section method (Gere, 2006, p. 403) was employed to verify the sectional properties of a TCFS panel with respect to its moment of inertia (I) and sectional modulus (S), assuming that the joint completely transfers the shear load to the cardboard core. Since the E-modulus of cardboard is different from that of PMMA, the thickness of the core is reduced by the E-modulus ratio of cardboard (800 MPa) to PMMA (3300 MPa), which results in a modular ratio (n) of 0.25 (800 MPa/3300 MPa). Figures 3.1.3.1 shows how the transformed section is obtained based on the transformed section method using the E-modulus of PMMA.

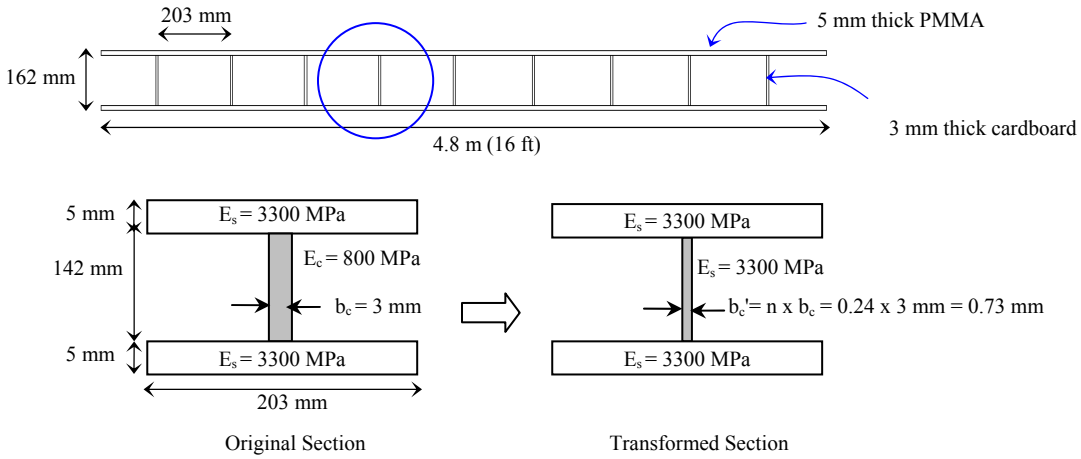

Figure 3.1.3.1 Transformed Section Using the E-modulus of PMMA

Based on the transformed section defined in Figure 3.1.3.1, the sectional properties of a full TCFS panel are determined as shown in Table 3.1.3.1. Figure 3.1.3.2 shows schematic details of a TCFS.

Table 3.1.3.1 Sectional Properties of a TCFS Panel

Centroid	X: 0 mm, Y: 0 mm
Distance from neutral axis to the extreme fiber, y_c	X: -76 mm, 76 mm
Moment of inertia	X: 254,895,070 mm^4
Section modulus	X: 3,345,079 mm^3

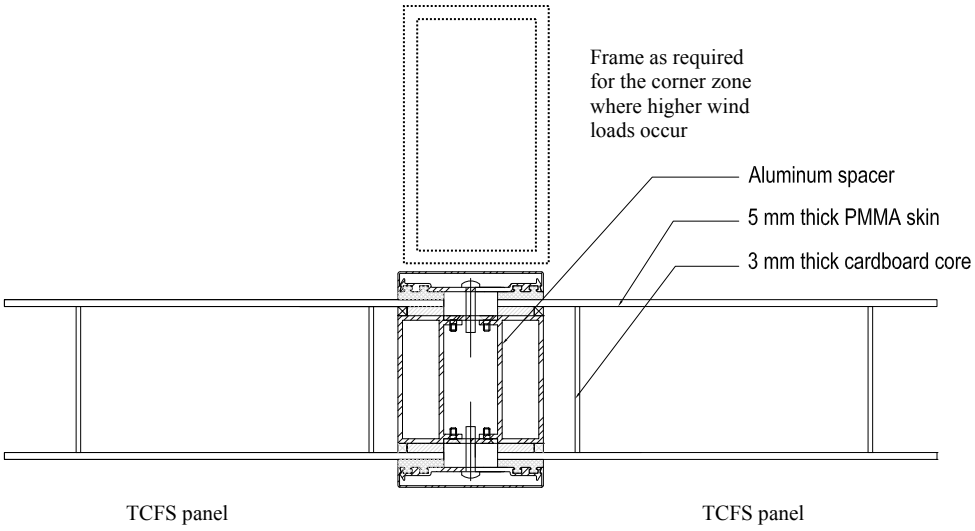

(a)

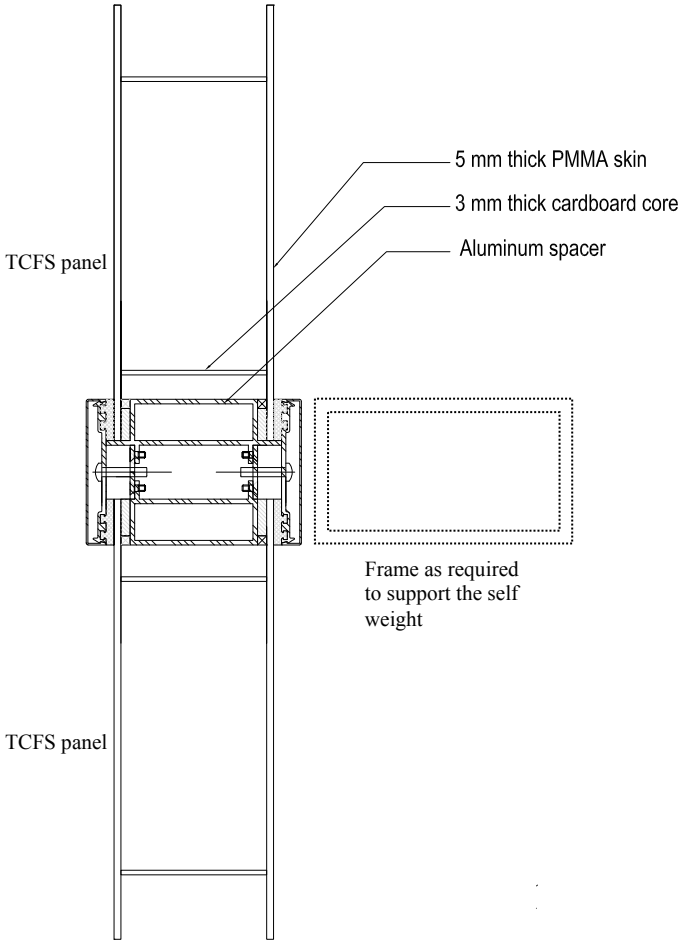

(b)

Figure 3.1.3.2 Plan (a) and Section (b) Details of a TCFS

3.1.4 Bending Stress and Deflection Check of a TCFS Panel

Based on the sectional properties as defined in section 3.1.3, the actual defections and bending stresses of a TCFS panel were calculated and compared with the structural design criteria established in section 3.1.1. As shown in Table 3.1.4.1, the material properties of PMMA (Acrylite FF) were referenced from the published product data. The yield strength is 117 MPa, thus resulting in allowable stress of 58.5 MPa (allowable stress = yield strength / safety factor of 2) as established in section 3.1.1.

Table 3.1.4.1 Material Properties of TCFS Components

	Density g/ cm^3	Flexural E-modulus, MPa	Ultimate Tensile Strength, MPa	Yield Flexural Strength, MPa
PMMA (Acrylite FF)	1.19	3300	124	117

From "Physical Properties of Acrylite FF," by Cyro Industries, 2001, p. 6.

(1) A TCFS Panel

The stress of a TCFS panel located at the typical zone (Figure 3.1.2.1) is 2.4 MPa with a deflection of 16 mm, and the panel located at the corner zone (Figure 3.1.2.1) has a bending stress of 4.0 MPa and a deflection of 26 mm respectively using the following equations. Equations 3.1.4.1(a) through (4) describe the stress and deflection calculation of a TCFS panel at the typical and corner zone.

A. Stress and deflection of a TCFS panel at the typical zone:

$$\sigma = \frac{M}{S} = 2.4 \text{ MPa} < 58.5 \text{ MPa} \qquad \text{Equation 3.1.4.1 (a)}$$

$$\delta = \frac{5wl^4}{384EI} = 16 \text{ mm} < 19 \text{ mm} \qquad \text{Equation 3.1.4.1 (b)}$$

B. Stress and deflection of a TCFS panel at the corner zone:

$$\sigma = \frac{M}{S} = 4.0 \text{ MPa} < 58.5 \text{ MPa} \qquad \text{Equation 3.1.4.1 (c)}$$

(safety factor of 17 based on the ultimate stress 69 MPa)

$$\delta = \frac{5wl^4}{384EI} = 26 \text{ mm} \approx L/165 \qquad \text{Equation 3.1.4.1 (d)}$$

Where,

M = bending moment calculated by $wl^2/8$

(typical zone- 9,568575 N-m; corner zone- 15,841,308 N-mm)

S = sectional modulus as noted in Table 3.1.3.1 (= 3,954,661 mm^3)

w = uniformly distributed load at typical zone calculated by

wind load (0.9 kPa) multiplied by the width of the TCFS panel

(typical zone- 4.14 N/mm; corner zone: 6.16 N/mm)

l = shorter span of the TCFS panel (= 4300 mm)

E = E-modulus of PMMA (= 3300 MPa)

I = moment of inertia as given in Table 3.1.3.1(= 351,569,448 mm^4)

The TCFS panel located at the typical zone meets structural criteria of allowable stress and deflection. The panel at corner zone resulted in higher deflection (23 mm) than the established value (19 mm) while the bending stress maintained an allowable stress level. Table 3.1.4.2 summarizes the comparison of calculated values and established requirements. Under The horizontal shear stresses at the contact area where the cardboard core meets the PMMA skin were calculated to be minimal. Shear stress calculations and experimental results of the shear testing are presented in Appendix E.

Table 3.1.4.2 Summary of Stress and Deflection of a TCFS

	Typical zone		Corner zone		Requirements	
	Stress	Deflection	Stress	Deflection	Stress	Deflection
TCFS panel	2.4 MPa	16 mm	4.0 MPa	23 mm	58.5 MPa	19 mm

3.1.5 Structural Design Conclusions

A façade system must meet strength and stiffness requirements in order to resist design loads and provide serviceability. This chapter reviewed the IBC 2003 to establish the structural design criteria for a TCFS. The design wind loads were determined by the analytical process described in IBC 2003 and a model of a 10-story office building enclosed with TCFSs was used to establish the structural design criteria for a TCFS. As a result, the maximum deflection of a TCFS panel under the wind load is limited to be 19 mm to provide a rigid connection between the edge of a TCFS and the edge spacer frame. Allowable bending stress of a PMMA skin is estimated to be 58.5 MPa calculated from

the allowable stress (119 MPa) divided by the safety factor of 2 according to Baker's weighted safety factor. The expected maximum bending stress under wind, however, was calculated to be $1/17^{th}$ of the allowable stress (or safety factor of 17) as the deflection criterion limits the sectional properties of the façade panel rather than the strength requirement. The deflection of the TCFS at the corner zone, however, deflects slightly more than the requirements, but it is presumed to be acceptable for visual perception due to the greater depth to deflection ratio (152 mm: 19 mm).

3.2 Installation of a New Testing Facility

3.2.1 Overview of Testing Facility Design

A new testing facility was designed, fabricated, and installed at the architecture department of the University of Michigan to evaluate the structural performance of a TCFS. The primary design intent of the testing frame is to provide two test platforms to conduct both static and impact tests. The testing frames should also be able to carry out bending tests for two-edge supported and four-edge supported specimens under static loads. The design must also consider the rigidity of the testing frame to avoid any vibration or racking during impact testing. ANSI Z97.1 standards were adopted for the design of the testing facility.

The vertical static testing apparatus, as shown in Figure 3.2.1.1.(a) consists of two vertical main frames(A), a specimen holder frame (B), and a loading frame (C). The vertical main frames (A) have holes along their length to adjust the height of the loading frame (C). The static loading jack (D) is installed in the middle of the loading frame (C). The rectangular specimen holder frame (B) can be demounted from the main vertical frames (A) so it can be placed horizontally for static tests as noted in Figure 3.2.1.1 (a). The two-edge and four-edge supported specimens can be tested by adding or removing the shims (E) underneath panels in the specimen holder. The impact testing apparatus as shown in Figure 3.2.1.1 (b) consists of a main vertical frame (A), a specimen holder (B), an impactor (F), a traction and release system (G), and a safety screen (H). The specimen holder (B) is vertically installed within the vertical frames (A), and the impactor (F) is mounted from the loading frame (C) to simulate a pendulum impact. The traction and release system (G) is used to precisely operate the impactor at specified drop heights. A

removable safety screen (H) made of polycarbonate limit the dispersion of the specimens under impact testing. Figure 3.2.1.1 illustrates the testing facility used for both static and impact tests.

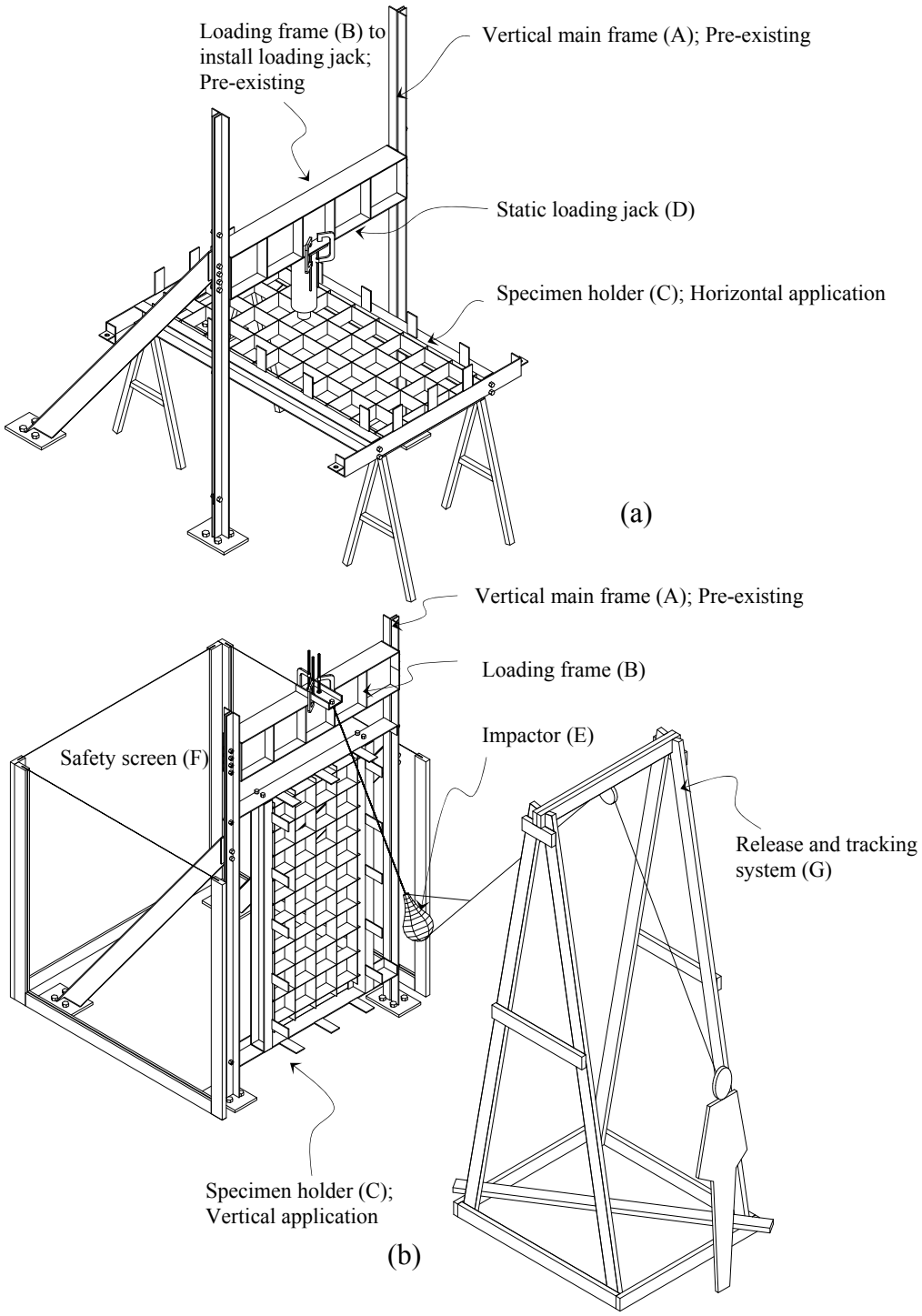

Figure 3.2.1.1 Overview of Testing Frames:
Static Test Set-Up (a) and Impact Test Set-Up (b)

3.2.2 Structural Analysis of Testing Frame

The strengths of each steel member was verified in accordance with the AISC ASD (allowable strength design) specification and analyzed for force distribution and deformation through computer simulations using STAAD.Pro (Bentley, version 2007). In order to quantify the likely maximum impact load that is transferred to the testing frames from the impactor through the specimen, the maximum impact force was determined by calculating the energy transfer between components during impact. A maximum impact energy value of 1024 N-m was obtained from ANSI Z97.1 and stiffness (*k*) of 350 kN/m was computed for the TCFS panel based on the experimental results of the static test from load-deflection relationship as shown in Table 3.3.3.1 and Figure 3.3.3.1 assuming that the TCFS panel behaves elastically. Displacement term (δ) in Equation 3.2.2.1 can be expressed as Equation 3.2.2.2 , which resulted in 76 mm using the specified PE (1024 N-m) and stiffness (350 kN/m) values in Equation 3.2.2.2. By combining the displacement value (73 mm) in Equation 3.2.2.3, the resultant maximum impact force (P) of 34 kN was calculated as being transferred to the testing frame.

$$\text{PE} = \frac{1}{2}k\delta^2 = 1024 \text{ N-m} \qquad \text{Equation 3.2.2.1}$$

$$\delta = \sqrt{\frac{2PE}{k}} = 73 \text{ mm} \qquad \text{Equation 3.2.2.2}$$

$$P = \frac{48EI\delta}{l^3} \approx 34 \text{ kN} \qquad \text{Equation 3.2.2.3}$$

Where,

PE = 1024 N-m in accordance with ANSI Z97.1

k = 387 kN/m measured from load-displacement graph
(P/ δ = 1148 N/2.1 mm where δ is the theoretical displacement (2.1 mm) in order to calculate the largest load (P))

E = 3,200 MPa (Table 3.1.4.1)

I = 24,724,620 mm^4 (calculated value using transform section method as shown in Figure 3.1.3.1)

l = 1930 mm (Figure 3.3.1.3)

(1) Analytical Method using AISC Specification

According to the AISC specification the testing frames are either categorized as flexural or compressive members depending on their structural behavior. The specimen holder frames were fabricated from C (channel) and L (angle) shapes. Based on the width- and height-to-thickness ratios, the flexural members are classified as compact sections and the compressive members are classified as non-compact sections. Critical yielding and buckling stresses were calculated in accordance with AISC specification, and the results indicated that all frame members have no risk of yielding or buckling under the impact load. The details of the calculation process are presented in Appendix F. Figure 3.2.2.1 shows the member size of the testing frames.

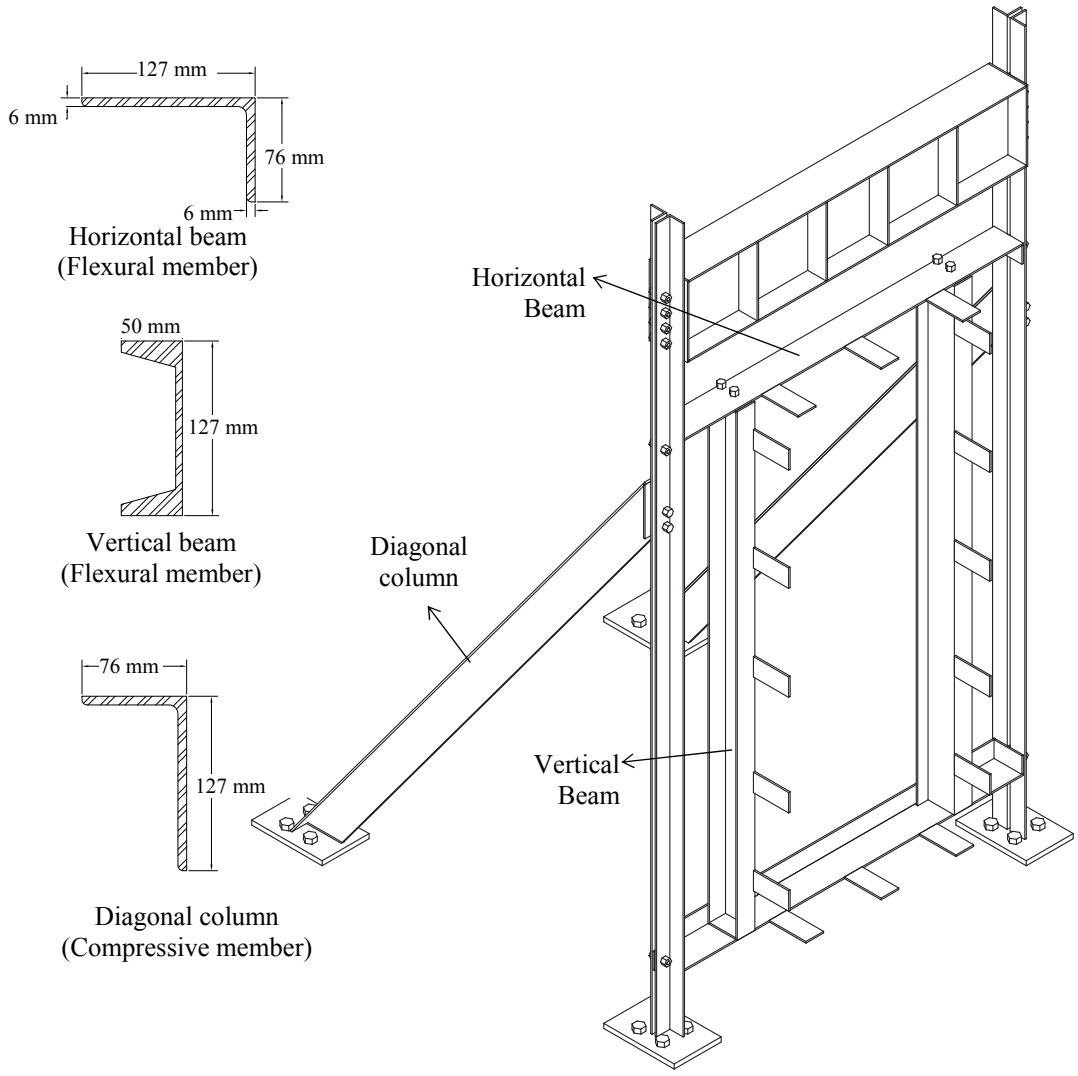

Figure 3.2.2.1 Sectional Properties of Testing Frames

(2) STAAD.Pro Simulation

A finite element model was created in STAAD.Pro (Bentley, 2007 version) to carry out an elastic analysis to determine overall forces and deflections in members. The testing frame and the specimen panel were modeled together in a combined analysis using both beam and plate elements. Pin supports were assigned at the bottom of the vertical and diagonal frames, and an impact load of 34 kN (Equation 3.2.2.3) was applied to the middle of the panel as shown in Figure 3.2.2.2. The analysis results show that the greatest bending stress occurs on the vertical members of the specimen holder, followed by the horizontal member of the specimen holder. The diagonal member and vertical main frame were mostly subjected to axial force, which remains within the buckling stress level. The maximum deflection of 3 mm occurred at the vertical members of the specimen holder frame under 34 kN. The analysis results with respect to bending moments, axial force, and deflection of each member are shown in Figure 3.2.2.3 through 3.2.2.5.

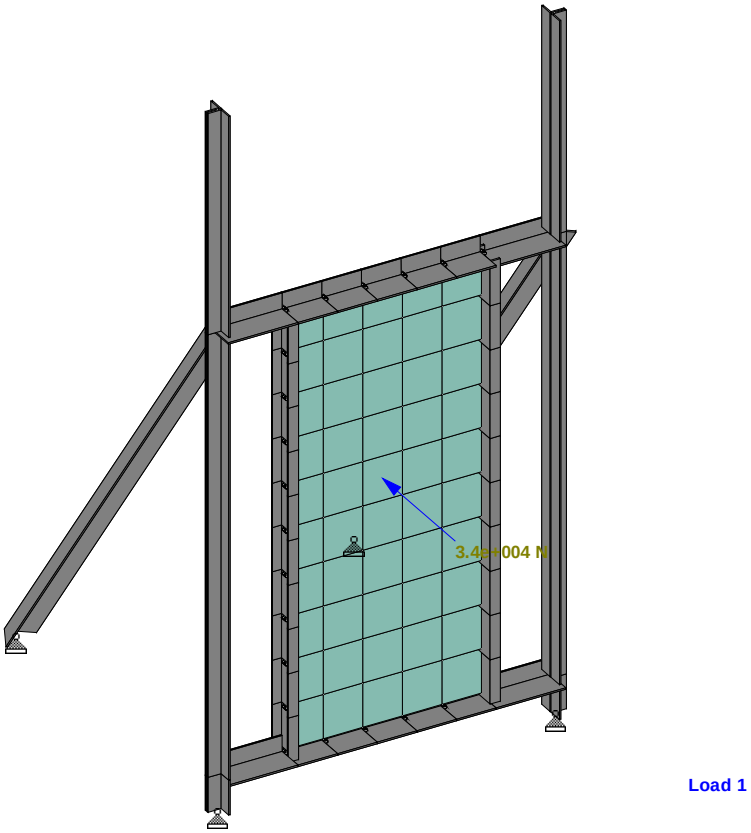

Figure 3.2.2.2 Impact Load (34 kN) Set-Up in STAAD.Pro

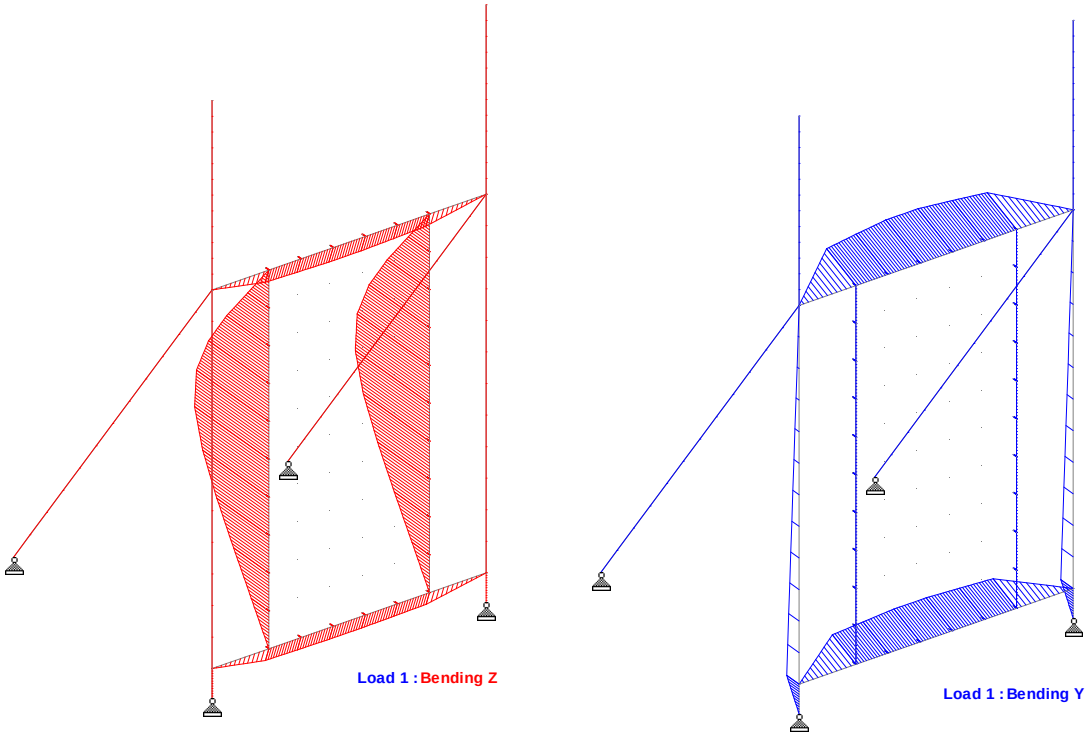

Figure 3.2.2.3 Bending Moment Diagram Under Impact Load

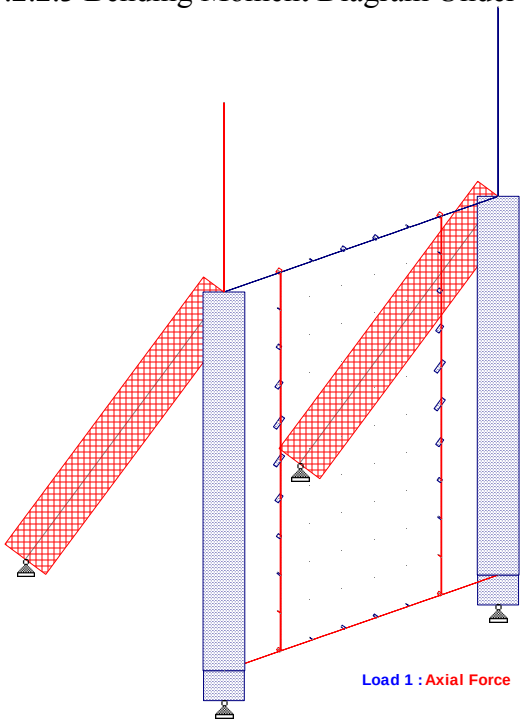

Figure 3.2.2.4 Axial Fore Diagram Under Impact Load

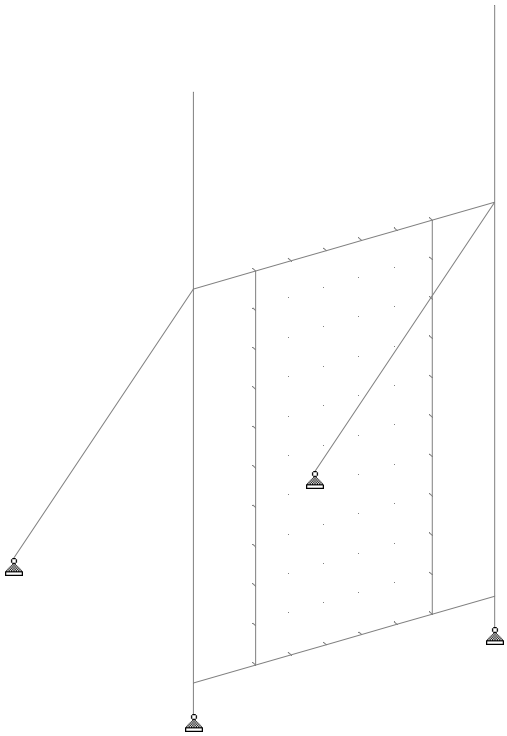

Figure 3.2.2.5 Displacement Diagram Under Impact Load

3.2.3 Fabrication of Testing Frame

After an analytical calculation of the testing frames was completed, fabrication drawings were prepared for the manufacture of the frame members. The fabrication process included steel procurement, material preparation (cutting, grinding, and welding of steel), surface protection of steel members (primer and paint application of steel), and final assembly of the steel frames using bolting. Figure 3.2.3.1 illustrates the fabrication process of the testing frames.

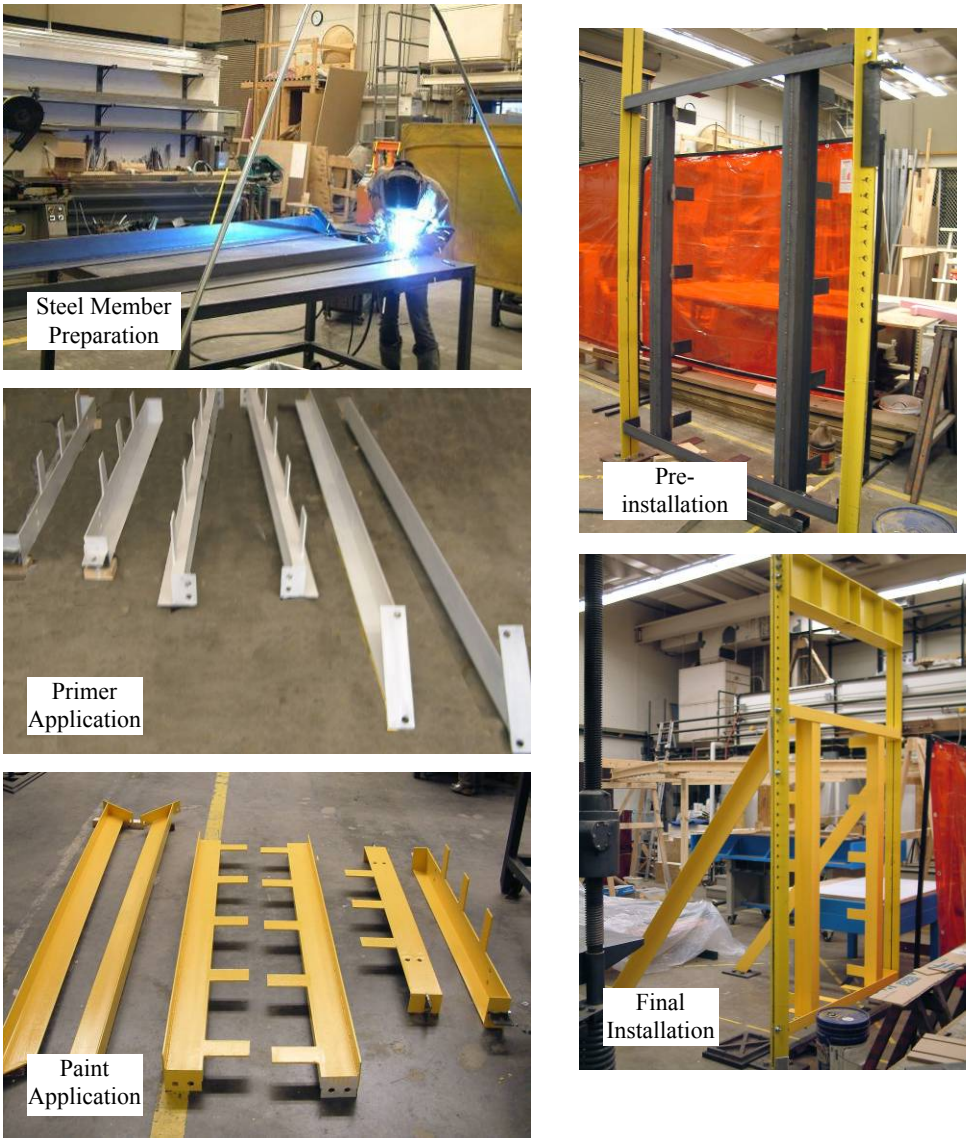

Figure 3.2.3.1 Fabrication Process of Testing Frames

3.2.4 Frame Installation Conclusions

A new testing frame was fabricated and installed in order to carry out static and impact testing. Prior to fabrication of the frames, ANSI Z97.1 standards were reviewed to understand the structural requirements of the impact testing frames. Analytical calculations of the testing frame were performed to access the stresses and displacements of each member. Analysis results confirmed that the testing frames would withstand the impact forces during the impact testing with minimum deflections.

3.3 Static Performance

The primary goals of conducting the static test were to measure the flexural stress and stiffness of a TCFS panel, to compare the experimental results with the theoretical values, and to recommend a structural design method that can be employed at the early design stage of a TCFS. Simple bending theories and a finite element method (FEM) were compared to the testing measurements in order to provide a better understanding of their applicability to the design of a TCFS. The flexural stiffness obtained from the static test was used to determine the maximum impact load in order to design the impact testing frames as discussed in section 3.3.

3.3.1 Static Testing Apparatus and Specimens

The static test was set up to conduct flexural testing of the two- and four-edge supported specimens. As shown in Figure 3.3.1.1, the static test apparatus consists of a main frame (A), loading frame (B), and specimen holder (C). Loading and measuring device includes hydraulic loading jack (1), wood block (2), displacement dial gauge (3), and strain gauges (4). Wood shims (5) were placed between the specimen and specimen holder frame (C) to simulate a simply supported condition. Figure 3.3.1.2 shows the installation position of loading jack, displacement, and strain gauges.

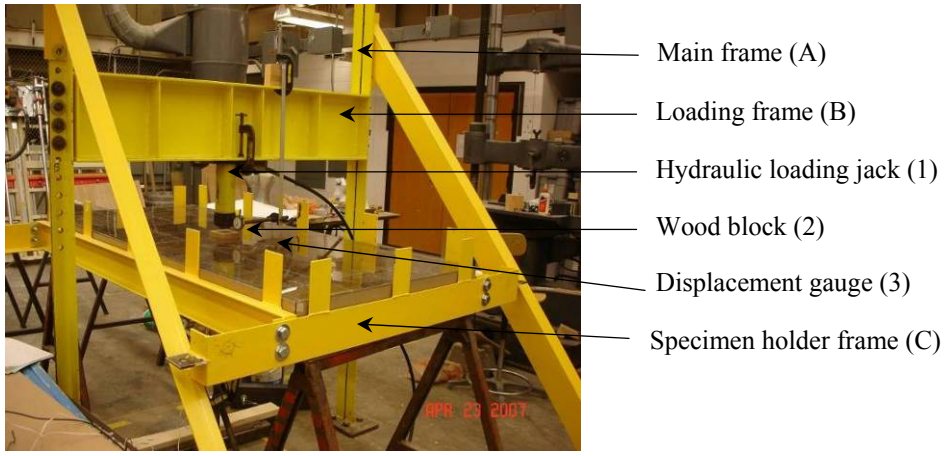

Figure 3.3.1.1 Static Test Set-Up

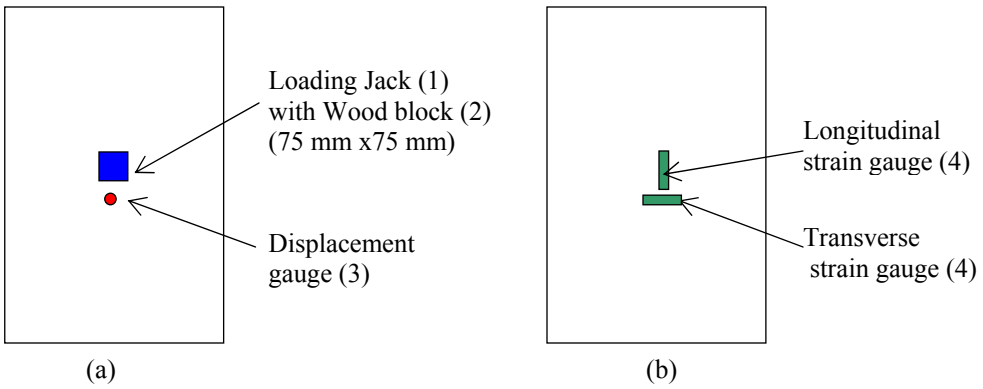

Figure 3.3.1.2 Installation Position of Loading Jack and Displacement and Strain Gauges: Top view (a) and bottom view (b)

The size of the specimen was 863 mm x 1930 mm, and they were panels of 6 mm -thick laminated glass, 6 mm-thick fully tempered glass, and 111 mm-thick TCFS. Wood shims were used to create different two- or four-edge support variations. Figure 3.3.1.3 shows diagrams of simply supported two- and four-edge conditions and section of edge details of the specimens.

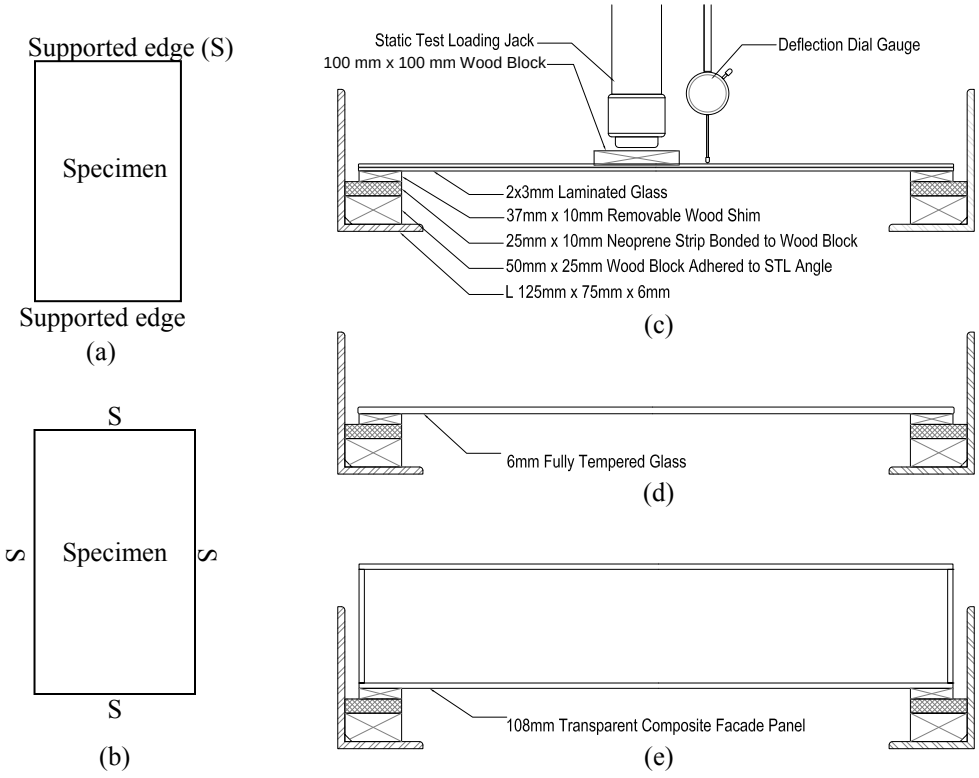

Figure 3.3.1.3 Two-edge (a) and Four-edge (b) Supported Conditions and Edge Support Details: Laminated Glass, Fully Tempered Glass (d), and Transparent Composite Façade Panel (e)

3.3.2 Static Testing Procedure

Preparation for the test began with placing the specimen horizontally in the specimen holder. Wooden shims were placed between the specimen holder frame and the edges of the specimen in order to create different boundary conditions as shown in Figure 3.3.1.3. A hydraulic jack was clamped to the horizontal loading frame above the specimen (Figure 3.3.1.2 (a)), and deflection gauge was positioned at the mid span of the specimen to measure the flexural deflection at the center of the specimen (Figure 3.3.1.2 (b)). Two strain gauges were vertically and horizontally attached to the center of a specimen on the tension side to measure longitudinal and transverse strains. A wooden block (100 mm x 100 mm) was located at the middle of the specimen as a point load and placed between the hydraulic jack and the specimen to distribute a point load across the width of the specimen (Figure 3.3.1.3 (c)).

The hydraulic jack applied concentrated loads increments of 0.24 kPa. The magnitudes of the loads as well as their corresponding deflections and strains were recorded at each incremental increase in load. The TCFS specimen was first tested with two- and then with four-edge supported conditions. Next, a sheet of laminated glass was tested, and then a sheet of tempered glass was tested. The static test on the glass specimens was limited to a maximum load of 1.7 kN to avoid specimen breakage. Figure 3.3.2.1 shows the static test set-up for the (a) TCFS and (b) laminated glass.

(a) (b)

Figure 3.3.2.1 TCFS (a) and Laminated Glass (b) Test Set-Up with Four-Edge Supported Condition

3.3.3 Static Testing Results

(1) TCFS panel with two-edge supported

A flexural test of the two-edge supported TCFS panel was carried out according to the procedure described in the previous section. Loads of 0.11 kN were applied incrementally until a maximum load of 1.11 kN was reached. The flexural strains were recorded at the same intervals and multiplied by the E-modulus of PMMA. The bending stresses were estimated based on the strain and displacement measurements and compared with the simple beam theory. The maximum bending stress of the PMMA skin was measured to be 1.3 MPa based on a longitudinal strain of 400 μm/m using Equation 3.3.3.1. The maximum bending stress using Equation 3.3.3.2 by substituting the measured displacements resulted in 1.7 MPa. As can be seen from Table 3.3.3.1 and Figure 3.3.3.1 shows, the measurements and simple beam theory yielded similar bending stresses.

$$\sigma = E_f \times \varepsilon \qquad \text{Equation 3.3.3.1}$$

Where, σ = bending stress (MPa)

E_f = flexural modulus according to the product data (= 3300 MPa)

ε = longitudinal strain from measurements

$$\sigma = \frac{My}{I} \qquad \text{Equation 3.3.3.2}$$

Where, $I = \frac{Pl^3}{48E\delta}$ (substituting δ with the displacement measurements)

Where, P = point load (N)

l = unsupported span of specimen (1930 mm)

E = E-modulus (3300 MPa)

δ = measured displacement

M = bending moment ($M = Pl^2/4$)

y = distance from neural axis to the extreme fiber of a section (55 mm)

Table 3.3.3.1 Bending Stress Comparison
between Experiment and Simple Beam Theory for a TCFS

Load (N)	Measurements		Bending Stress (kPa)		
	Longitudinal Strain (mm/mm)	Displacement (mm)	Based on the strain gauge measurements using Eq. 3.3.3.1	Based on the displacement measurements using Eq. 3.3.3.2	Simple beam theory using Eq. 3.1.4.1.(c)
115	0.000038	0.20	124	120	117
230	0.000077	0.51	255	300	235
345	0.000115	0.81	381	480	352
460	0.000253	1.12	836	659	470
575	0.000200	1.45	662	854	587
690	0.000235	1.75	778	1034	704
805	0.000275	2.06	910	1214	822
920	0.000318	2.34	1051	1379	939
1035	0.000357	2.59	1182	1529	1057
1150	0.000400	2.95	1324	1744	1174

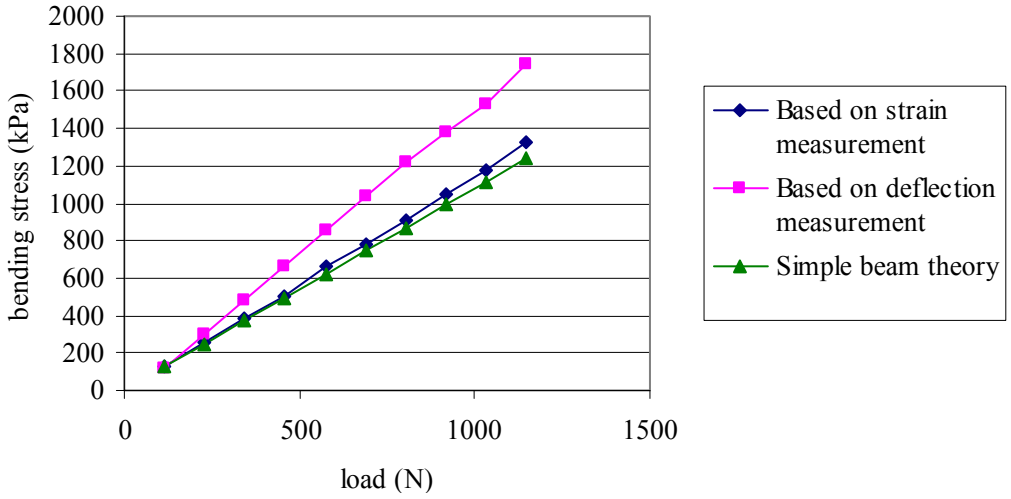

Figure 3.3.3.1 Bending Stresses Comparison
between Experiment and Simple Beam Theory for a TCFS

Displacements were calculated using the curvature of radius (ρ) and displacement (δ) relationship in a simple beam using Equation 3.3.3.3 by substituting the measured strains (Gere, 2007, p. 308). The corresponding maximum deflection by the measurements and simple beam theory was approximately 3 mm respectively. As noted in Table 3.3.3.2 and Figure 3.3.3.3, the measured and calculated displacements show agreement. The flexural stiffness of the TCFS panel was 350 N/mm, which was obtained

from the linear load-deflection relationship based on experiment results (third column in Table 3.3.3.2).

$$\delta = \rho (1-\cos \theta) \qquad \text{Equation 3.3.3.3}$$

Where, δ = displacement (mm)

ρ = radius of curvature = y/ε (substituting ε with the strain measurements)

$\sin \theta = L/2/ \rho$ (where L = 1930 mm)

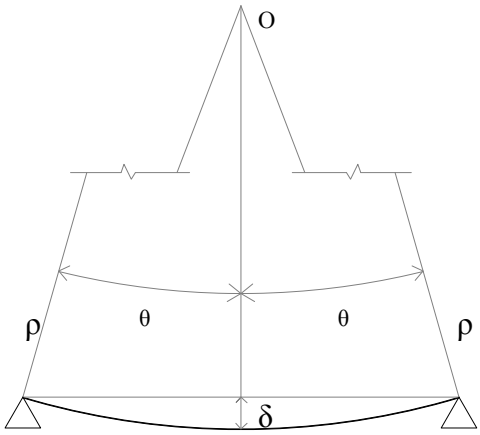

Figure 3.3.3.2 Radius of Curvature (ρ) and Displacement (δ) in Pure Bending of a Simple Beam
From "Mechanics of Materials," by Gere, 2006, p. 308.

Table 3.3.3.2 Displacement Comparison between Experiment and Simple Beam Theory for a TCFS

Load (N)	Measurements		Displacement (mm)		
	Longitudinal Strain (mm/mm)	Displacement (mm)	Based on the strain gauge measurements using Eq. 3.3.3.1.(c)	Based on the displacement measurements	Simple beam theory using Eq. 3.1.4.1.(d)
115	0.000038	0.20	0.32	0.20	0.21
230	0.000077	0.51	0.62	0.51	0.42
345	0.000115	0.81	0.93	0.81	0.63
460	0.000253	1.12	0.75	1.12	0.84
575	0.000200	1.45	1.48	1.45	1.05
690	0.000235	1.75	1.82	1.75	1.26
805	0.000275	2.06	2.12	2.06	1.47
920	0.000318	2.34	2.398	2.34	1.68
1035	0.000357	2.59	2.698	2.59	1.89
1150	0.000400	2.95	2.98	2.95	2.10

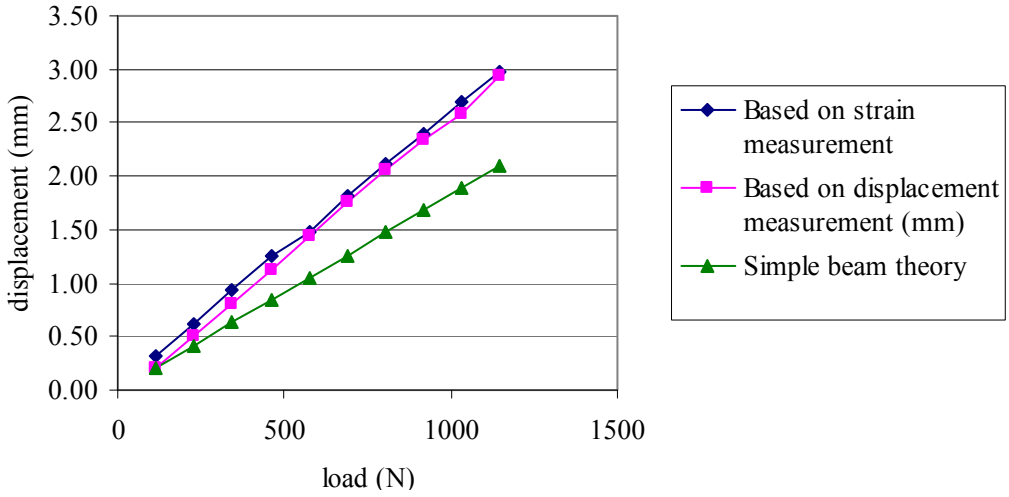

Figure 3.3.3.3 Displacement Comparison
between Experiment and Simple Beam Theory for a TCFS

(2) Glass specimens with four-edge supported

Under the flexural test of the four-edge supported specimens, 0.11 kN (25 lb) load increments were applied until the maximum load of 2.1 kN was reached. The test on the laminated glass was stopped at a safety factor of 2 to keep stress below the allowable stress level to avoid breakage and weakening of the glass. Bending stress and displacement of laminated glass are compared between the experimental measurement and theoretical prediction using simple plate theory (Young & Budynas, 2002, p.502). As noted in Table 3.3.3.3 and Figure 3.3.3.4, the bending stress determined based on the strain measurements (using Equation 3.3.3.1) showed agreement with the calculated stress using Equation 3.3.3.3. Both measured and calculated displacement (using Equation 3.3.3.4) yielded similar results (Table 3.3.3.4 and Figure 3.3.3.5). The maximum bending stress under the applied load of 445 N was 20 MPa, which is below the specified allowable stress (ASTM E1300, 2007, p. 2), and the corresponding displacement was 5 mm.

$$\sigma = \frac{\beta W}{t^2} \qquad \text{Equation 3.3.3.3}$$

$$\delta = \frac{\alpha W b^2}{E t^3} \qquad \text{Equation 3.3.3.4}$$

Where, β = 1.59 from Table 26.1c (Young & Budynas, 2002, p.502)

α = 0.18 from Table 26.1b (Young & Budynas, 2002, p.502)

W = applied load as shown in Table 3.3.3.3

E = 70,000 MPa (glass); 3,200 MPa (PMMA) as given in Table 2.2.1.1

b = shorter span of 864 mm

t = 5.9 mm for laminated glass due to the semi-composite action due to laminated interlayer; 6.4 mm for fully tempered glass; 70 mm for a TCFS calculated based on moment of inertia given in Table 3.1.3.1 ($I = bt^3/12$)

Table 3.3.3.3 Bending Stress Comparison
between Experiment and Simple Plate Theory for Laminated Glass

Load (N)	Measurements		Bending Stress (MPa)		
	Longitudinal Strain (mm/mm)	Transverse Strain (mm/mm)	Based on the strain gauge measurements using Eq. 3.3.3.1	Based on simple plate theory using Eq. 3.3.3.2	Allowable stress of heat strengthened glass according to ASTM E 1300
44	0.000020	0.000041	1	2	
89	0.000050	0.000057	4	4	
133	0.000075	0.000073	5	6	
178	0.000100	0.000089	7	8	
222	0.000126	0.000105	9	10	52
267	0.000153	0.000123	11	12	
311	0.000180	0.000143	13	14	
356	0.000203	0.000160	14	16	
400	0.000228	0.000175	16	18	
445	0.000253	0.000193	18	20	

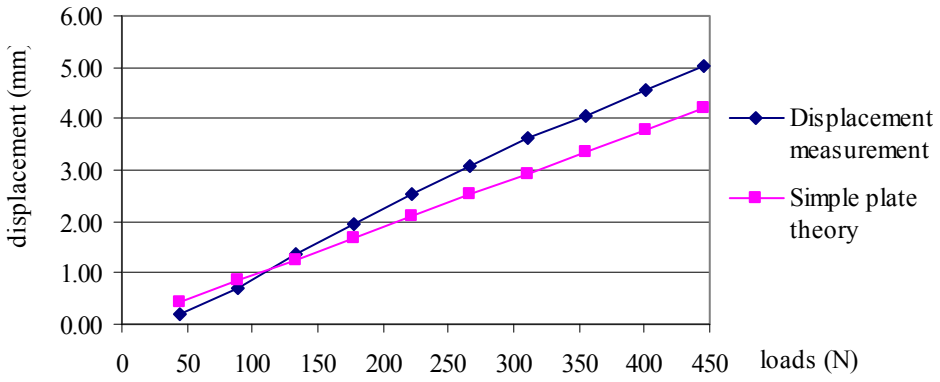

Figure 3.3.3.4 Bending Stress Comparison
between Experiment and Simple Plate Theory for Laminated Glass

Table 3.3.3.4 Displacement Comparison
between Experiment and Simple Beam Theory for Laminated Glass

Load (N)	Displacements (mm)	
	Measurement	Simple plate theory
44	0.20	0.42
89	0.71	0.84
133	1.37	1.26
178	1.93	1.68
222	2.54	2.10
267	3.07	2.52
311	3.63	2.94
356	4.06	3.36
400	4.55	3.78
445	5.03	4.20

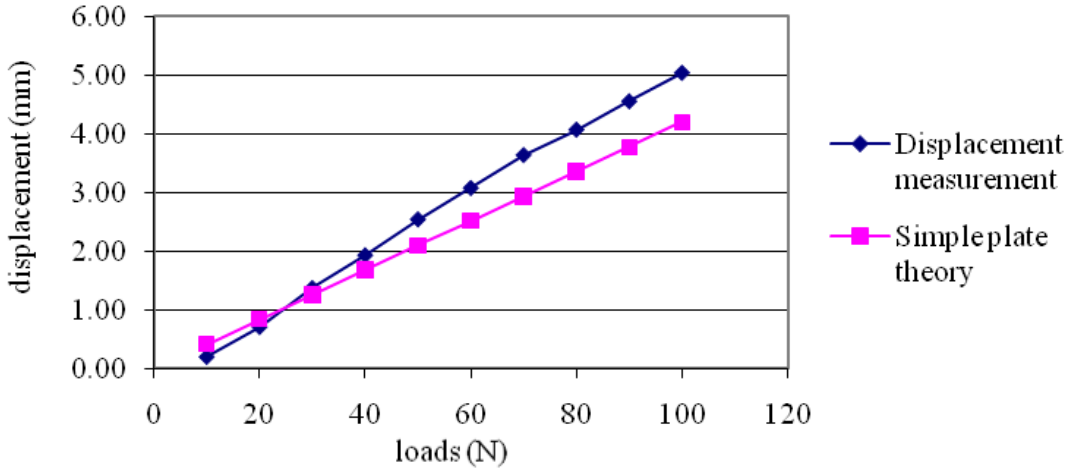

Figure 3.3.3.5 Displacement Comparison
between Experiment and Simple Plate Theory for Laminated Glass

Since the higher bending stress occurred along the shorter span, only transverse strains of fully tempered glass were measured as shown in Table 3.3.3.5. As indicated in Tables 3.3.3.5 and 3.3.3.6 and Figures 3.3.3.6 and 3.3.3.7, both the bending stress and displacement yielded similar results between experiment and theoretical calculation. The maximum bending stress of fully tempered glass under the final load was 18 MPa with the corresponding deflection of 4 mm.

Table 3.3.3.5 Bending Stress Comparison
between Experiment and Simple Plate Theory for Fully Tempered Glass

Load (N)	Measurements		Bending Stress (MPa)		
	Longitudinal Strain (mm/mm)	Transverse Strain (mm/mm)	Based on the strain gauge measurements using Eq. 3.3.3.1	Based on simple plate theory using Eq. 3.3.3.2	Allowable stress of fully tempered glass according to ASTM E 1300
44	-	0.000020	1	2	
89	-	0.000045	3	4	
133	-	0.000065	5	5	
178	-	0.000090	6	7	
222	-	0.000113	8	9	10.4
267	-	0.000138	10	11	
311	-	0.000158	11	12	
356	-	0.000180	13	14	
400	-	0.000203	14	16	
445	-	0.000226	16	18	

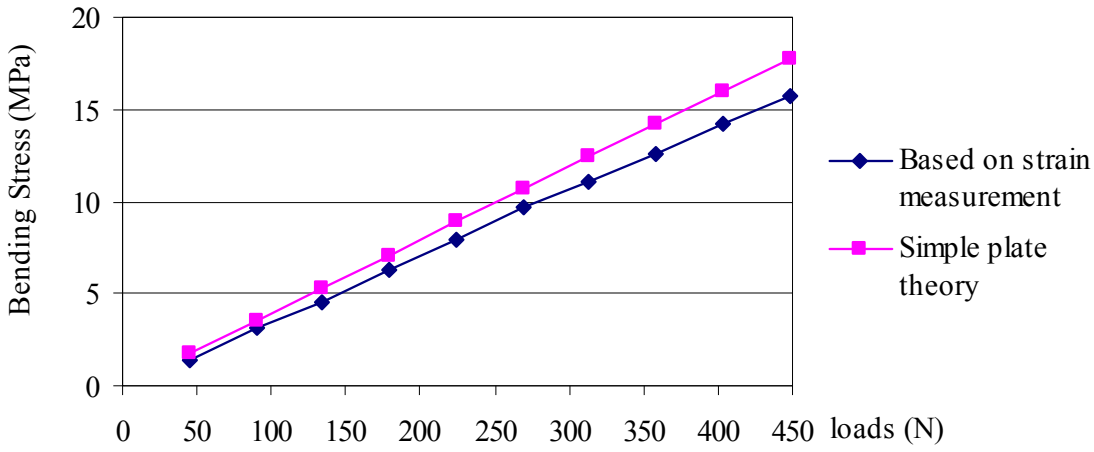

Figure 3.3.3.6 Bending Stress Comparison
between Experiment and Simple Plate Theory for Fully Tempered Glass

Table 3.3.3.6 Displacement Comparison
between Experiment and Simple Beam Theory for Fully Tempered Glass

Load (N)	Displacements (mm)	
	Measurement	Simple plate theory
44	0.38	0.34
89	0.86	0.68
133	1.35	1.03
178	1.75	1.37
222	2.16	1.71
267	2.59	2.05
311	3.02	2.39
356	3.43	2.74
400	3.81	3.08
445	4.27	3.42

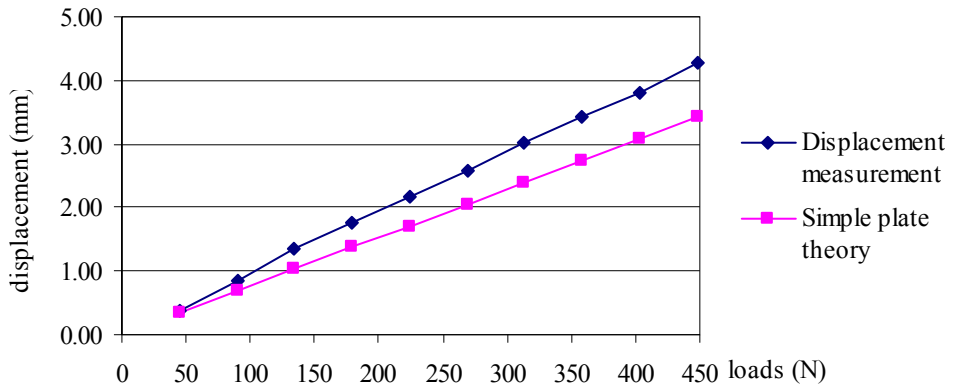

Figure 3.3.3.7 Displacement Comparison
between Experiment and Simple Plate Theory for Fully Tempered Glass

(3) TCFS panel with four-edge supported

The static test of a TCFS panel with four-edge supported showed that the bending stress and deflection of the TCFS panel were far less than of the glass panels at the given load. The four-edge supported TCFS panel yielded much less bending stress and deflection compared to the two-edge supported TCFS. The tests also revealed that the flexural stiffness of the four-edge supported TCFS panel is around 700 kN/m, which is 2.5 times stiffer than the two-side supported TCFS (387 kN/m) as shown in Figure 3.3.3.7. The theoretical predictions using simple plate theory and experimental measurements of the four-edge supported TCFS were compared as shown in Figure 3.3.3.7. Theoretical values of bending stress and deflection of the TCFS panel were computed using simple plate theory, and compared with the experimental measurements.

The comparison indicated that the modified plate theory predicted less bending stress and deflection compared to the measurements. This was due to the fact that the open cell structure of the TCFS core reduced the torsional stiffness that weakened the bending stiffness (Figure 3.3.3.8 (a)). The PMMA skin was likely subjected to the shear lag and the effective widths of the PMMA skin undermined the shear stiffness, resulting in the greater bending deformation (Figure 3.3.3.8 (b)). It is also postulated that the microscopic material failure at bonding area between the cardboard core and PMMA skin may cause semi-composite action that reduces the bending stiffness (Figure 3.3.3.8 (c)). The groove cut on the PMMA skin and notches of the cardboard core may result in reduction in bending stiffness due to the reduced sectional stiffness (Figure 3.3.3.8 (d)).

By considering these factors, a modified simple design equation was derived to estimate the strength and stiffness of the TCFS panel. Adjustment factors were computed by substituting measurement values to theoretical calculations. Equation 3.3.3.5 and 3.3.3.6 shows a modified equation with the adjustment factors of A and B. As can be seen Table 3.3.3.7 and Figure 3.3.3.9 and Figure 3.3.3.10, close agreement was observed between the experimental data and the predicted values using modified equations.

$$\sigma = \frac{B\beta W}{t^2} \qquad \text{Equation 3.3.3.5}$$

$$\delta = \frac{\mathrm{A}\alpha W b^2}{Et^3} \qquad \text{Equation 3.3.3.6}$$

Where, B = stress adjustment factor of 2.7

β = 1.59 from Table 26.1c (Young & Budynas, 2002, p.502)

A = deflection adjustment factor of 7.15

α = 0.18 from Table 26.1b (Young & Budynas, 2002, p.502)

W = applied load as shown in Table 3.3.3.7

E = 3,300 MPa (PMMA) as given in Table 2.2.1.1

b = shorter span of 864 mm

t = 70 mm based on moment of inertia given in Table 3.1.3.1

($I = bt^3/12$, $t = (1/3)\sqrt{}(12I/b)$, where I is given in Table 3.1.3.1)

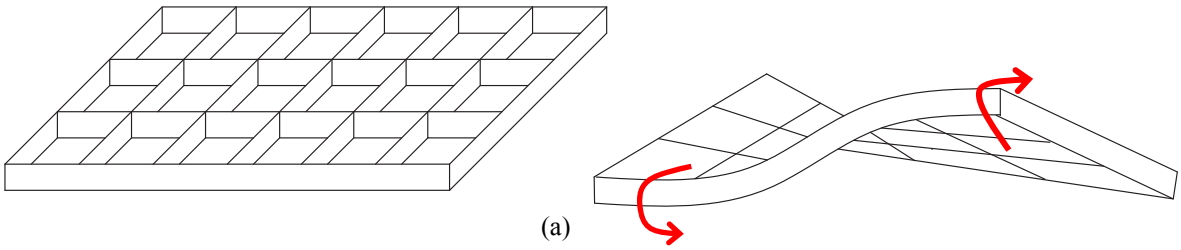

(a)

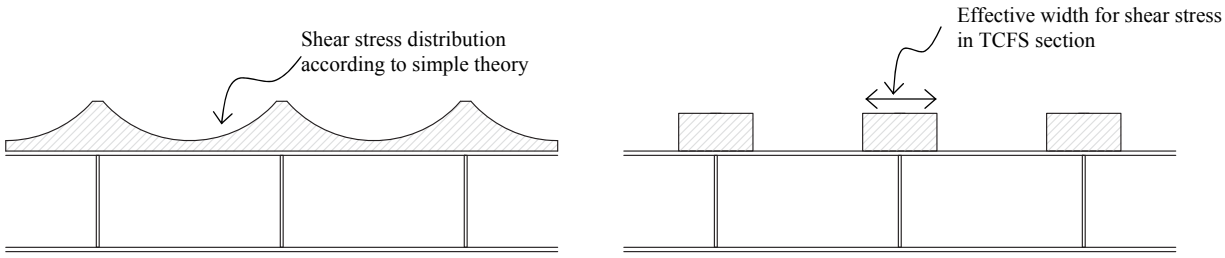

(b)

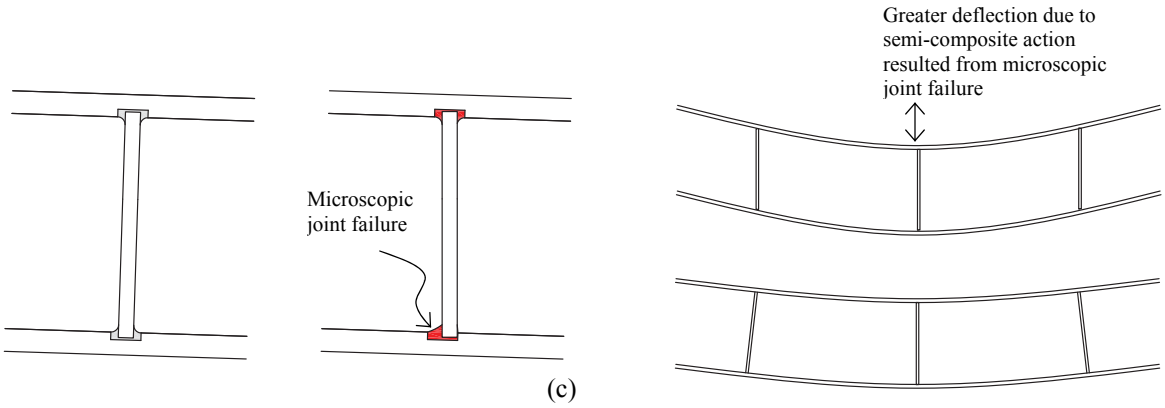

(c)

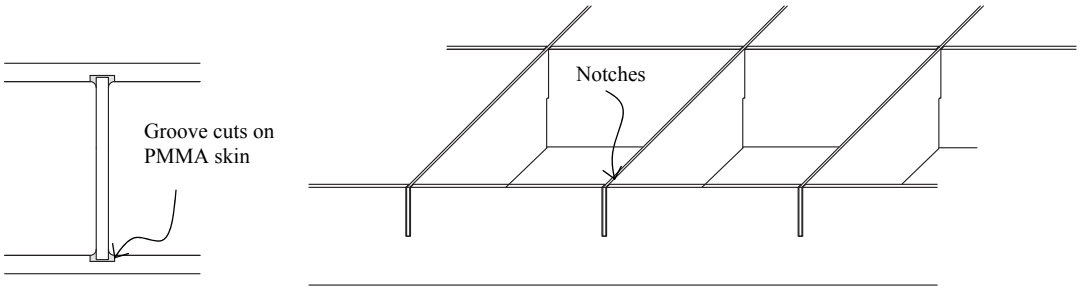

(d)

Figure 3.3.3.8 Structural Properties of TCFS that Affects Bending Stiffnesss: Torsional Stiffness (a), Shear Lag (b), Non-Composite Action (c), and Reduced Sectional Stiffness (d)

Table 3.3.3.7 Bending Stress Comparisons
between Experiment and Simple Plate Theory for a TCFS Panel

Load (N)	Measurements		Bending Stress (MPa)		
	Longitudinal Strain (mm/mm)	Transverse Strain (mm/mm)	Based on the strain gauge measurements using Eq. 3.3.3.1	Based on adjusted simple plate theory using Eq. 3.3.3.5	Based on simple plate theory using Eq. 3.3.3.3
230	0.0000050	0.0000255	0.08	0.20	0.07
345	0.0000075	0.0000425	0.14	0.30	0.11
460	0.0000175	0.0000900	0.30	0.40	0.15
575	0.0000225	0.0001450	0.48	0.50	0.19
690	0.0000300	0.0001950	0.64	0.60	0.22
805	0.0000400	0.0002370	0.78	0.70	0.26
920	0.0000500	0.0002650	0.87	0.80	0.30
1035	0.0000600	0.0003000	0.99	0.90	0.34
1150	0.0000725	0.0003300	1.09	1.00	0.37
1265	0.0000850	0.0003570	1.18	1.10	0.41
1380	0.0000975	0.0003875	1.28	1.20	0.45
1495	0.0001100	0.0004150	1.37	1.31	0.48
1610	0.0001250	0.0004420	1.46	1.41	0.52
1725	0.0001420	0.0004700	1.55	1.51	0.56
1840	0.0001550	0.0004950	1.63	1.61	0.60
1955	0.0001875	0.0005150	1.70	1.71	0.63
2070	0.0002200	0.0005350	1.77	1.81	0.67

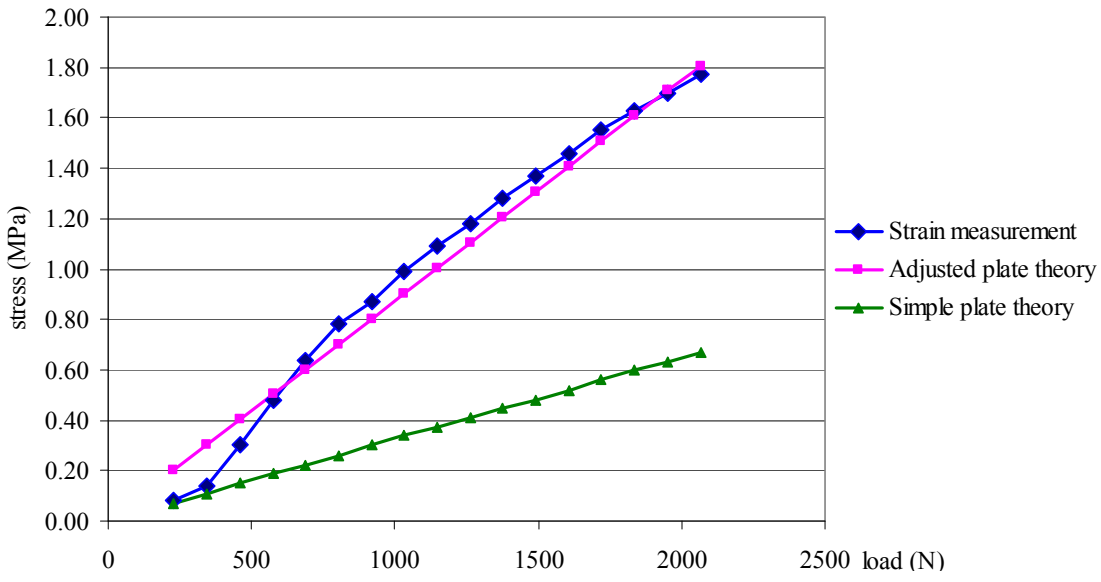

Figure 3.3.3.9 Bending Stress Comparisons
between Experiment and Simple Plate Theory for a TCFS Panel

Table 3.3.3.8 Displacement Comparisons
between Experiment and Simple Beam Theory for a TCFS Panel

Load (N)	Displacements (mm)		
	Measurement	Adjusted simple theory using Eq. 3.3.3.6	Simple plate theory using Eq. 3.3.3.2
230	0.08	0.23	0.03
345	0.13	0.34	0.05
460	0.28	0.46	0.06
575	0.43	0.57	0.08
690	0.56	0.69	0.10
805	0.69	0.80	0.11
920	0.81	0.92	0.13
1035	0.94	1.03	0.14
1150	1.09	1.15	0.16
1265	1.19	1.26	0.18
1380	1.35	1.38	0.19
1495	1.45	1.49	0.21
1610	1.57	1.61	0.22
1725	1.70	1.72	0.24
1840	1.85	1.84	0.26
1955	1.97	1.95	0.27
2070	2.08	2.07	0.29

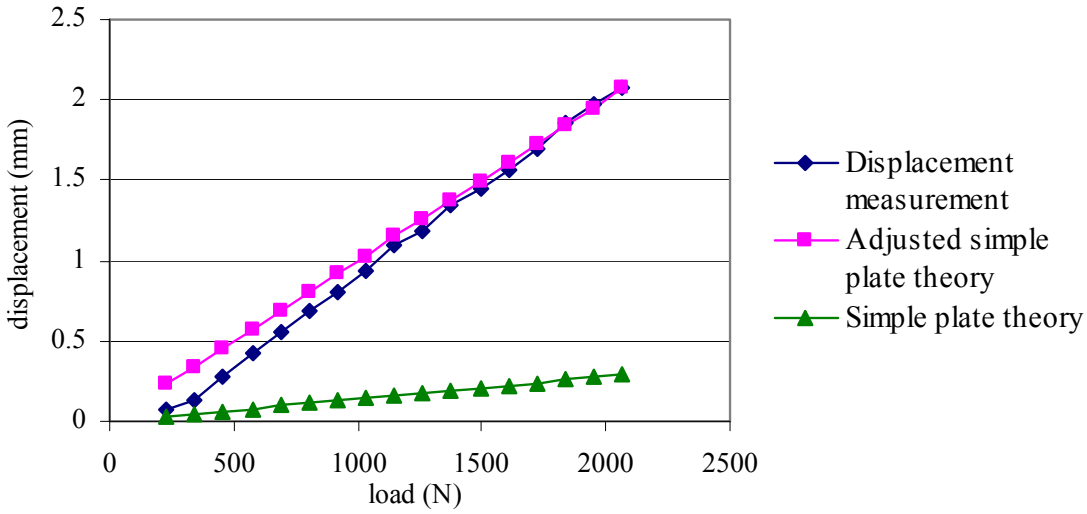

Figure 3.3.3.10 Displacement Comparisons
between Experiment and Simple Plate Theory for a TCFS Panel

3.3.4 Finite Element Analysis

One of the primary goals of this research was to establish a general structural design guideline for a TCFS by analytically and experimentally investigating its structural performance. It has been shown from the experiments in Section 3.3.3 that the simple plate theory requires adjustment to account for the effects of the open cell core structures in a TCFS. Therefore, this section focuses on using a finite element method to define load-deformation behaviors of a TCFS under static loads, which take into account the effects of open cell geometry. These results are then compared with the experimental data. A numerical study was conducted using STAAD.Pro (version 2007), a general purpose finite element method (FEM) software. A simple finite model set-up for both a simple beam and a plate is described in Figure 3.3.4.1. The size of the TCFS is 864 mm x 1930 mm x 106 mm, and the PMMA skin and cardboard core are 5 mm thick and 3 mm thick respectively. The skin and core was modeled with plate elements in STAAD.Pro, and the mesh was sized to approximately 25 mm x 25 mm. The boundary conditions consisted of a pin support and a roller support. The pin support was assigned at one shorter edge of the TCFS, restraining the following degree of freedom (DOF): $U_X = U_Y = U_Z = 0$, where U is the transitional displacement about the respective axis. The roller support was used at the other shorter edge of the pin support, restraining $U_Y = U_Z = 0$. For the four-edge supported TCFS, the roller support restraining $U_Z = 0$ was used along the longer sides of the TCFS. The two-edge and four-edge supported TCFS were loaded at midspan with a magnitude of 1150 N and 2070 N respectively over a patch area of 75 mm by 75 mm, and the load was increased by 115 N to be consistent with the experiments of the two-edge and four-edge supported TCFSs.

The material properties of the PMMA skin were obtained from the product data of Acrylite FF provided by CYRO Industries. The E-modulus of the cardboard core was measured from the tensile tests performed by the researcher. The Poisson's ratio of the cardboard is assumed to be 0.35, and the shear modulus was calculated using the equation: $G = E/2(1+\nu)$. Table 3.3.4.1 shows the material properties used in the FEM analysis.

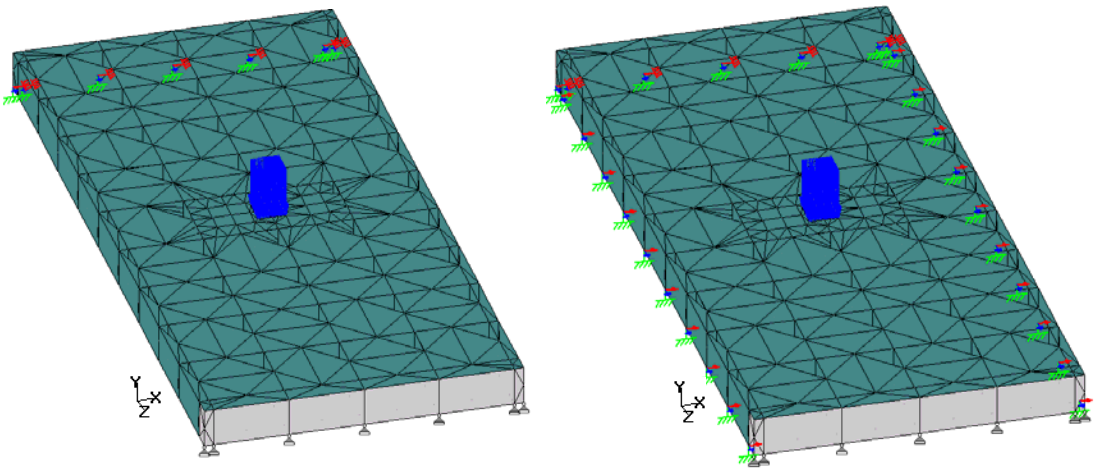

(a) (b)

Figure 3.3.4.1 Model Set-Up in STAAD.Pro:
Two-Edge Supported TCFS (a) and Four-Edge Supported TCFS (b)

Table 3.3.4.1 Material Properties of PMMA Skin and Cardboard Core Used in STAAD.Pro Analysis

	Density (g/c^3)	E-modulus (MPa)	Poisson's Ratio, ν	G-modulus (MPa)
PMMA skin	1.19	3300	0.37	1168
Cardboard core	0.95	800	0.35	296

Comparisons of the experiments and the FE results of a two-edge supported TCFS are presented in Figures 3.3.4.2 and Table 3.3.4.2, and the results of a four-edge supported TCFS are shown in Figure 3.3.4.3 and Table 3.3.4.3. It was observed from the FEM results that, when point loads were applied to both the two-edge supported and four-edge supported TCFS panels, high local stresses appeared at the loading area of the top skin. Therefore, the bending stresses were computed by averaging the stresses of the adjacent plates of the bottom skin, and the midspan deflection was taken to be the maximum value of the center point of the bottom skin. As a result, both the two-edge and four-edge supported TCFS panels yielded agreement between the experiments and the FEM (Table 3.3.4.2 and 3.3.4.3). The shear lag effect under point loads was not visually captured in the FEM analysis, but the effect is assumed to be pronounced under a uniformly distributed load such as wind loads.

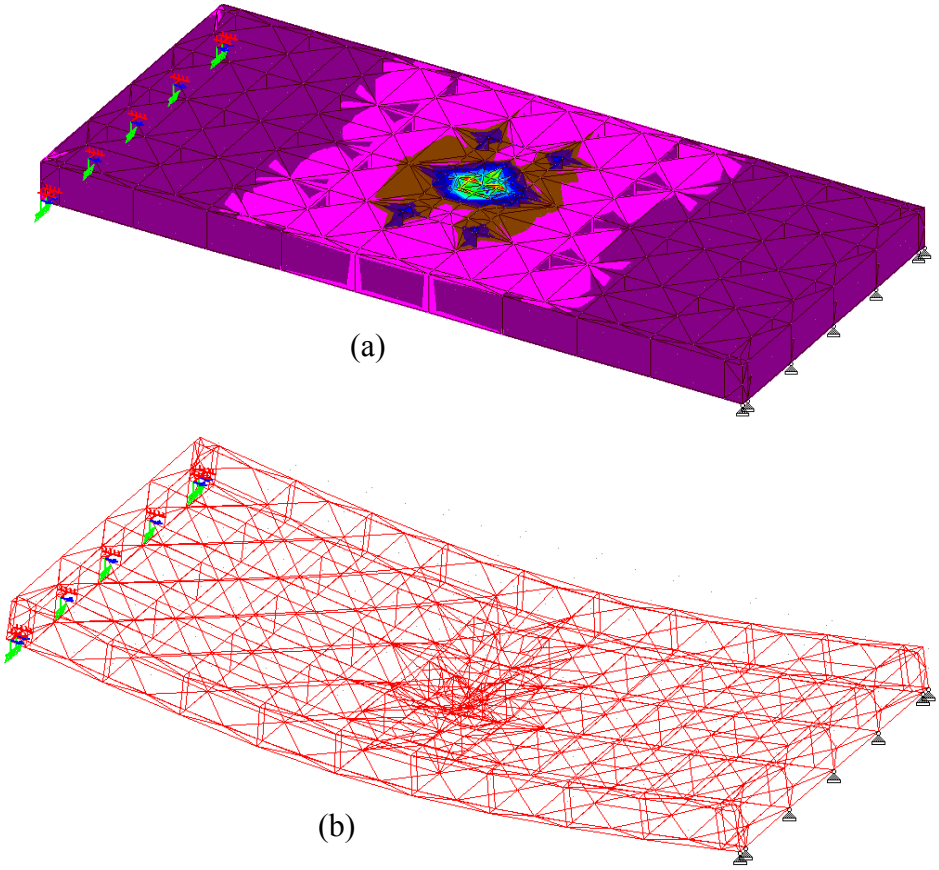

Figure 3.3.4.2 STAAD.Pro Results of a Two-Edge Supported TCFS; Principal Stress Distribution (a) and Displacement (b)

Table 3.3.4.2 Stress and Displacement Comparisons between Experiment and FEM for a Two-Edge Supported TCFS Panel

	Bending Stress (MPa)		Displacement (mm)	
Load (N)	Experiment	STAAD. Pro	Experiment	STAAD. Pro
115	0.25	0.26	0.61	0.61
230	0.38	0.39	0.89	0.91
345	0.50	0.51	1.19	1.22
460	0.66	0.65	1.52	1.52
575	0.78	0.79	1.83	1.83
690	0.91	0.92	2.16	2.13
805	1.05	1.05	2.49	2.41
920	1.18	1.19	2.77	2.72
1035	1.32	1.32	3.12	3.02

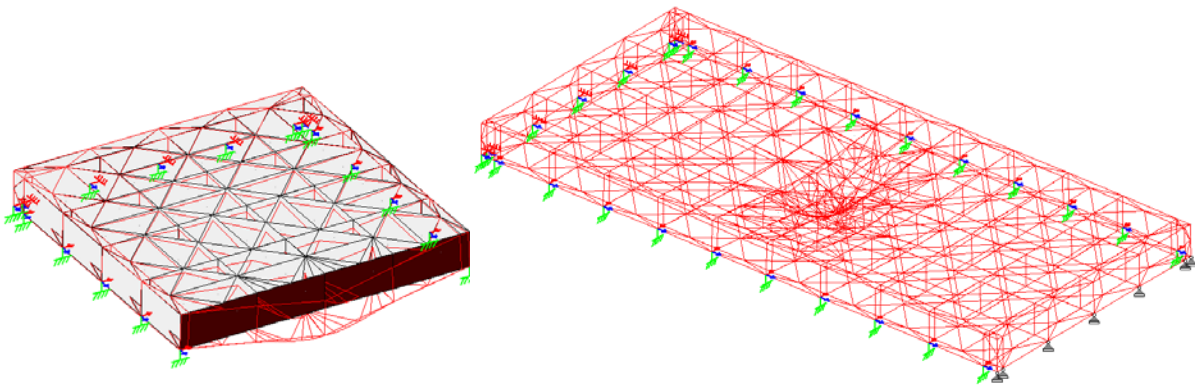

(a)

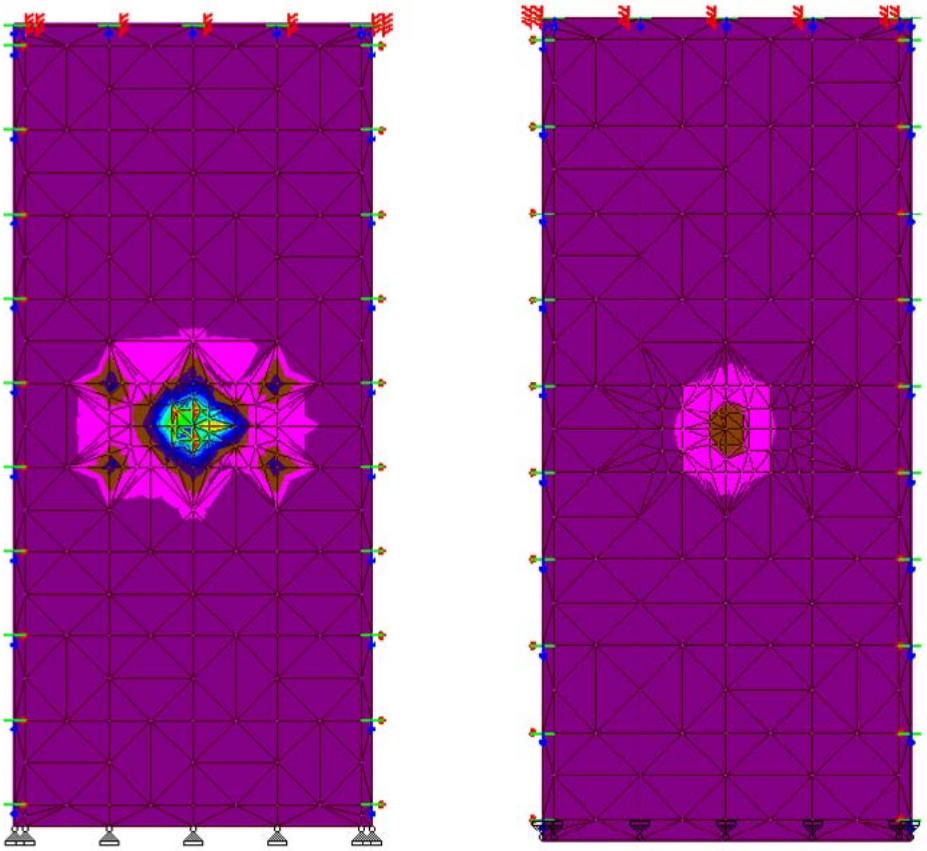

(b) (c)

Figure 3.3.4.3 STAAD.Pro Results of a Four-Edge Supported TCFS; Displacement (a), Principal Stress on the Top Skin (b) and Principal Stress on the Bottom Skin (c)

Table 3.3.4.3 Stress and Displacement Comparisons
between Experiment and FEM for a Four-Edge Supported TCFS Panel

	Bending Stress (MPa)		Displacement (mm)	
Load (N)	Experiment	STAAD. Pro	Experiment	STAAD. Pro
230	0.08	0.20	0.08	0.23
345	0.14	0.31	0.13	0.34
460	0.30	0.41	0.28	0.46
575	0.48	0.51	0.43	0.57
690	0.64	0.62	0.56	0.69
805	0.78	0.72	0.69	0.80
920	0.87	0.82	0.81	0.91
1035	0.99	0.92	0.94	1.03
1150	1.09	1.02	1.09	1.14
1265	1.18	1.13	1.19	1.26
1380	1.28	1.23	1.35	1.37
1495	1.37	1.33	1.45	1.47
1610	1.46	1.43	1.57	1.57
1725	1.55	1.54	1.70	1.69
1840	1.63	1.64	1.85	1.80
1955	1.70	1.74	1.97	1.92
2070	1.77	1.85	2.08	2.03

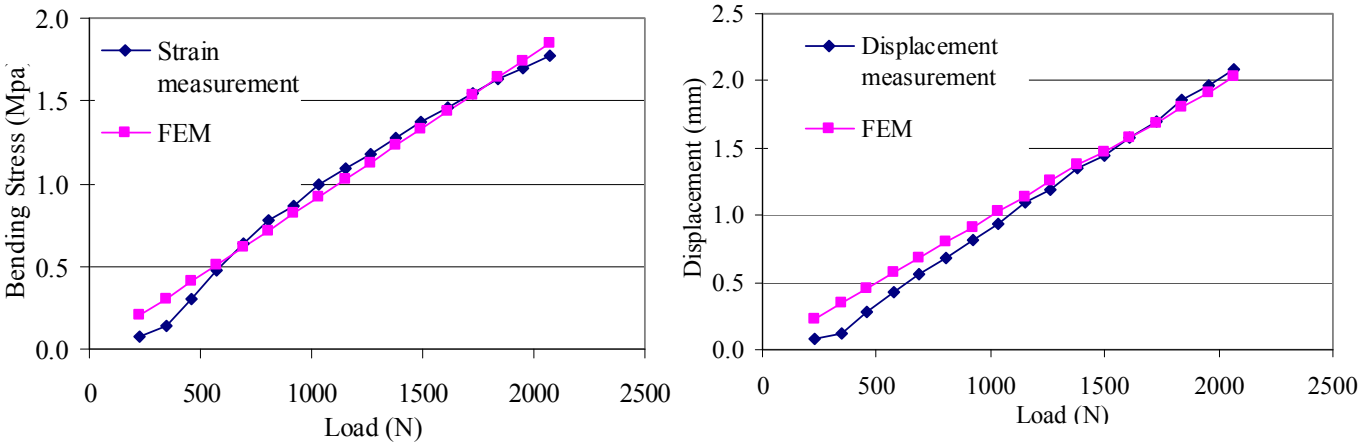

Figure 3.3.4.4 Stress (a) and Displacement (b) Comparisons
between Experiment and FEM for a Four-Edge Supported TCFS Panel

3.3.5 Static Performance Evaluation Conclusion

A simplified analytical method that could be used in the pre-design phase of a TCFS was investigated and compared to the empirical measurements. The two-edge supported bending test revealed the accuracy of simple beam theory, and the composite section method was used to calculate the sectional properties of the TCFS. For the four-edge supported TCFS, the theoretical values calculated from simple plate theory predicted that the panel was stiffer than the empirical measurements showed. Modified simple plate equations were established by taking into consideration the two-way stiffness and open cell geometry of the TCFS panel. It is postulated that the open cell structure of the cardboard core reduces the torsional stiffness and shear lag effect that undermines the overall bending stiffness thus increasing the bending stiffness. The adjustment factors that were applied to the simple plate equations considered these aspects, and their validity was confirmed based on the experimental measurements. As a result, the modified simple plate theory was in agreement with the experimental measurements. However, these modified equations may be applicable to design a TCFS panel that contains similar aspect ratios and open cell geometries of the studied TCFS panel. A FEM was carried out to evaluate its accuracy by validating against the experimental results, and the results showed agreement with the testing data. It can be concluded that simple beam theory and FEM analysis are suitable for the structural design of a TCFS, and further research on extensive tests is recommended to provide a reliable plate theory that can be used for different open cell geometries and types of a TCFS panel.

3.4 Impact Performance Evaluation

According to the ANSI Z97.1 standard, safety glazing materials refer to laminated glass, tempered glass, organic coated glass, plastic glazing, and fire resistant wired glass. Plastic glazing material include single sheets of plastic, laminated plastic, and fiber reinforced plastic. These materials provide safety properties that "reduce or minimize the likelihood of cutting and piercing injuries when the glazing materials are broken by human contact" (ANSI, 2004, p. 11). However, compositions of geometric and material variations within composite panels made from plastic skins and biofiber composite cores are not contained within any ANSI Z97.1 category, therefore this research includes a procedure for testing and evaluating composite panels that aligns with the methods specified in ANSI Z97.1. The purpose of this procedure is to quantify the impact behavior of a TCFS panel, by establishing an equivalent safety glazing classification to ANSI Z97.1, and to provide recommendations for enhanced impact resistance, based on the results of the impact tests.

3.4.1 Impact Testing Apparatus and Specimens

The impact testing apparatus consists of a main frame (A), a loading frame (B), a specimen holder frame (C), an impactor (D), a traction and release system (E), and a safety screen (F) as shown in Figure 3.4.1.1. The testing frame utilized L5 x 3x 1/4 and C5 x 6.7 to provide the required strength and stiffness called for "steel angles 3 inches by 5 inches by 0.25 inches or other sections and materials of equal or greater rigidity" in ANSI Z97.1 specification. The specimen holder frame (C) which was made from steel angles and channels, was installed vertically into the main frame (A). Clamping plates (C_1) were intermittently welded to the specimen holder frame (C) every 457 mm in order to hold the specimen firmly in place against the frame. A 100 lb shot-bag impactor was manufactured according to clause "the leather bag shall be filled with lead shot of 2.4 ± 0.1 mm diameter and the exterior surface shall be completely covered with glass filament reinforced pressure sensitive polyester adhesive tape" of ANSI Z97.1. The impactor was suspended from the loading frame (B) using an 1828 mm long cable (G), which was able to attain a maximum drop height of 1,220 mm. The underside of the impactor was tied to a polyester rope, and the rope was drawn over a pulley at the top of a wood frame. This

served as a traction and release system that could harness the rebound of the impactor after initial impact. A safety screen (F) made with polycarbonate sheets was fabricated and formed to enclose the testing frame to contain any pieces of specimen in the event of breakage.

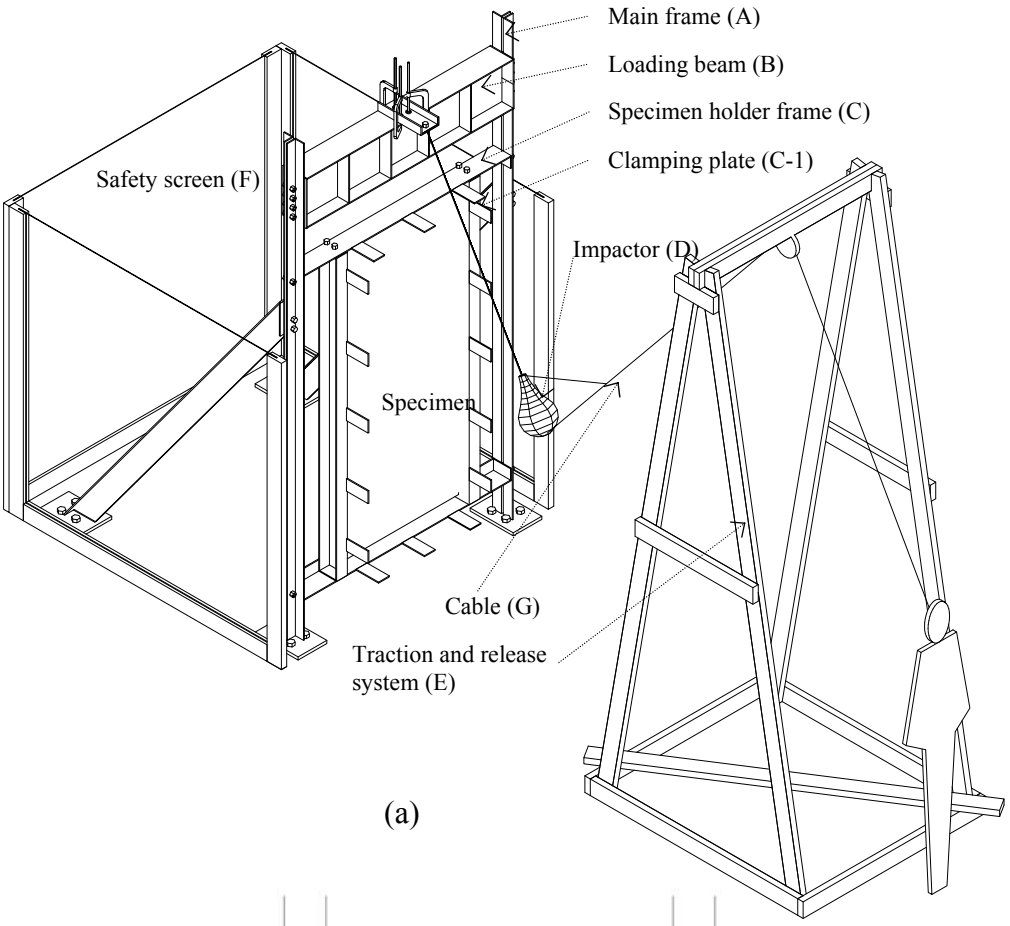

(a)

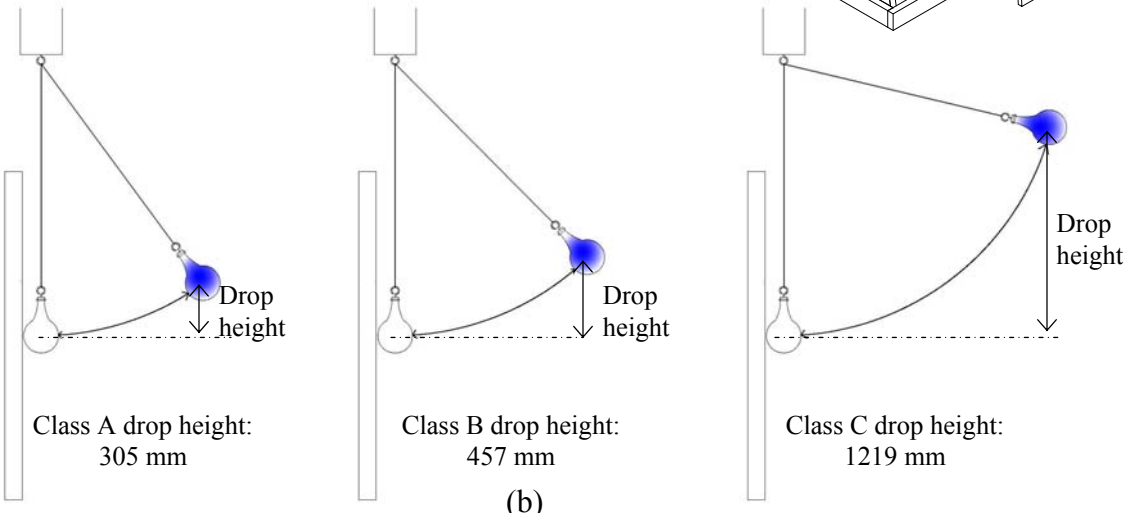

(b)

Figure 3.4.1.1 Overview of Impact Test Frames (a) and Drop Height (b): Colored impactor indicates the final position

Figure 3.4.1.2 shows impact test instrumentations consisting of strain gauges (H), a displacement transducer (I), a data acquisition system (DAS) (J), and a personal computer (PC) (K). The experiment was set up to continuously measure deflection and material strain at very short intervals (5000Hz) during impact. The experimental data was collected through the strain gauges (H), displacement transducer (I), and DAS (J). The displacement transducer (I) was capable of measuring each specimen's deflection up to 102 mm in short intervals of 5000Hz. Two strain gauges (H) were positioned on the tension side of the specimen at the mid point to measure both horizontal and vertical strains. The displacement transducer and strain gauges were connected to the DAS, which was connected to a PC (K). The sampling frequency of the DAS at 5000 Hz, was fast enough to capture all events during impact. High-speed video cameras were set up to record the impact process in order to obtain an accurate visual record and observe the differences in breakage mechanism of each specimen.

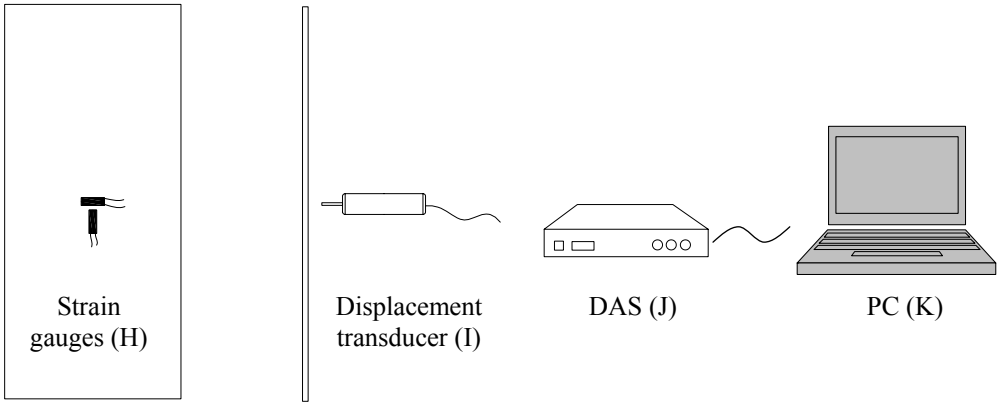

Figure 3.4.1.2 Overview of Impact Test Instrumentation
From "Kyowa PCD-300 brochure," by Kyowa, 2006, p. 2.

3.4.2 Impact Testing Procedure

It was decided to test both laminated and tempered glass panels in order to establish a standard against which to compare the behavior of a TCFS panel. The glass tests would serve to calibrate the test frame and would allow meaningful comparative conclusions to be drawn, since the tests would have been carried out using the same equipment and set up. The laminated glass specimen was placed on the specimen holder (C in Figure 3.4.1.1 (a)) and fastened by portable clamp angle (C-2) and locking clamps (C-3 in Figure 3.4.1.3 (a)). Two strain gauges were bonded to the mid point of the tension

side and the displacement transducer was installed at the mid span of the compression side, which were connected to the DAS and computer (Figure 3.4.1.2). The shot-bag impactor, suspended from the loading frame, was pulled up to the required drop height and locked until the DAS was activated. The impactor was released and at the same time the DAS was activated. After completion of the impact test on the laminated glass, the tempered glass was tested following the same procedure. The breakage modes of the laminated and fully tempered glass panels confirmed that the testing frame yielded accurate impact results, and therefore, the calibration process was completed. The TCFS specimen was then placed in the specimen holder frame and locked with the clamp angles. Two strain gauges and the displacement transducer was installed at the mid point of the TCFS panel and connected to the DAS and computer. The impactor was released from the drop height of 457 mm and strains and displacements were recorded. Photographs and video recordings were taken to document the breakage modes and impact behaviors of the TCFS and glass samples. Figure 3.4.2.1 illustrates the impact test set-up for the tempered glass and TCFS samples.

(a) (b)

Figure 3.4.2.1 Impact Test Set-Up: Fully Tempered Glass (a) and TCFS (b)

3.4.3 Impact Testing Results

Both the laminated and tempered glass failed the impact test at the initial drop height of 457 mm and the breakage modes of the laminated and fully tempered glass were verified according to the ANSI Z97.1 specification.

(1) Glass Specimens

Laminated Glass: A drop height of 305 mm caused small cracks in the laminated glass (Figure 3.4.3.1 (a)). The test was repeated at a drop height of 457 mm and the cracks became more fully extended, although the specimen did not collapse and remained intact because of its polymer interlayer (Figure 3.4.3.1 (b)). The maximum displacement under the drop height of 305 mm was approximately 2.8 mm at 0.04 s and the displacement returned to zero after impact (Figure 3.4.3.2 (a)). The maximum displacement under the drop height of 457 mm was measured to be 55 mm at 0.07 s and the permanent displacement of 4.8 mm was recorded after impact (Figure 3.4.3.2 (a)). The strain gauges on the tension side of the laminated glass were broken by glass cracks upon impact and thus the strain was not accurately recorded (Figure 3.4.3.2 (b)). Figure 3.4.3.1 shows the post breakage mode of the laminated glass at a drop height of 305 mm and 457 mm and Figure 3.4.3.2 shows a displacement versus time history.

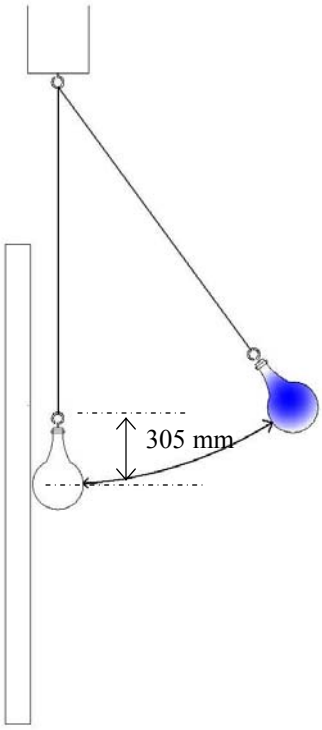

(a)

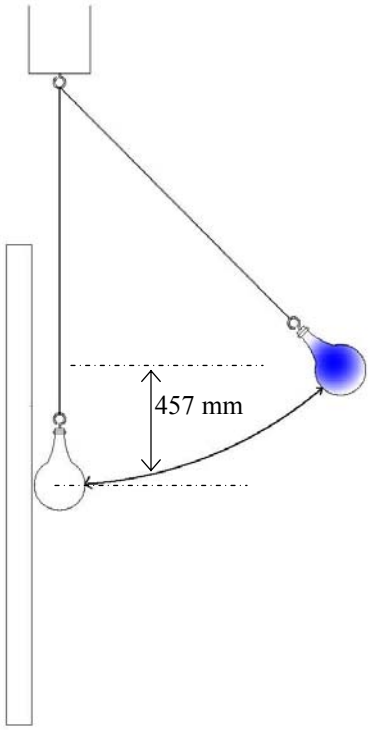

(b)

Figure 3.4.3.1 Breakage Modes of Laminated Glass
at the Drop Height of 305 mm (a) and 457 mm (b)

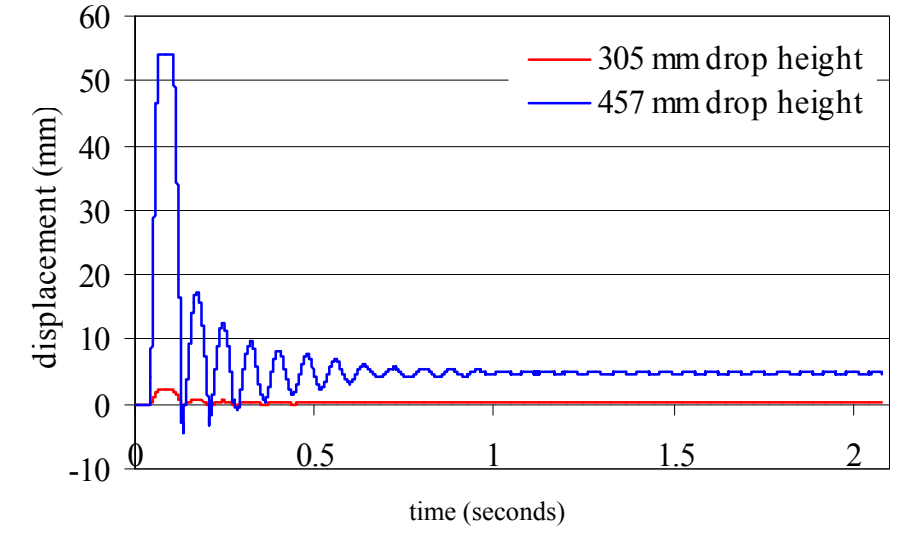

(a)

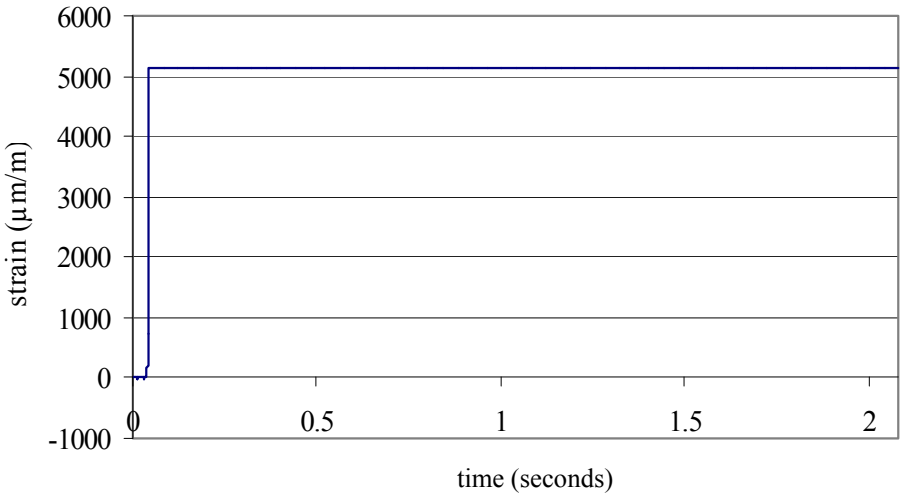

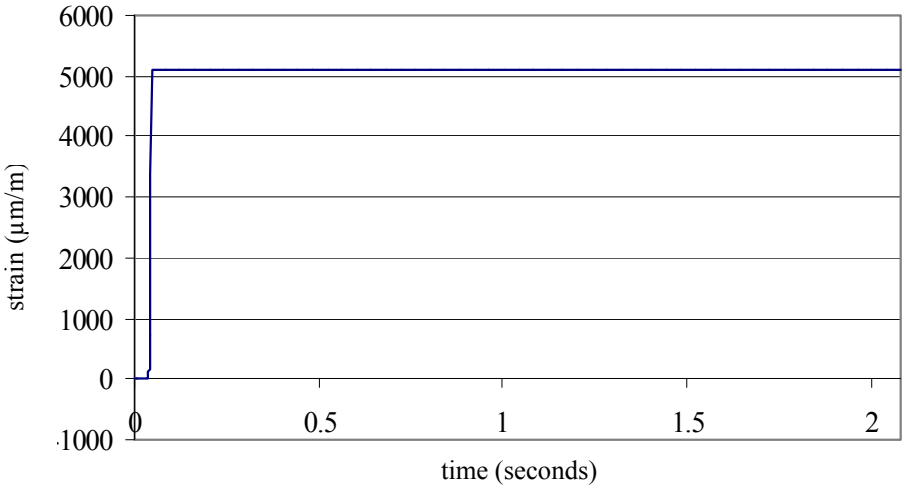

(b)

Figure 3.4.3.2 Displacement (a) and Strain (b) Output of Laminated Glass

B. Tempered Glass

Unlike the laminated glass sample, the tempered glass did not fail under the first impact at a height of 457 mm (Figure 3.4.3.3 (a)), but it failed upon the second impact from a lesser height (Figure 3.4.3.3 (b)). The specimen mostly broke into small granules, but some pieces formed bigger shards (Figure 3.4.3.5). The peak deflection measured was 54 mm (2 1/8 inch) at 0.07 s, and the strain recorded upon first impact and second impact was 2800 μm/m and 5100 μm/m respectively. Figure 3.4.3.3 and 3.4.3.4 depicts the post breakage patterns of the tempered glass and its dynamic displacement and strain outputs.

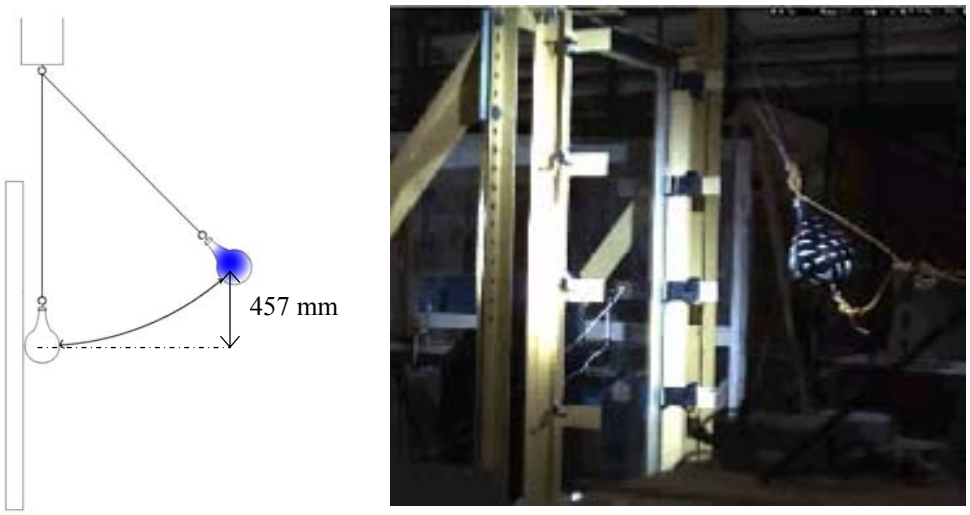

(a)

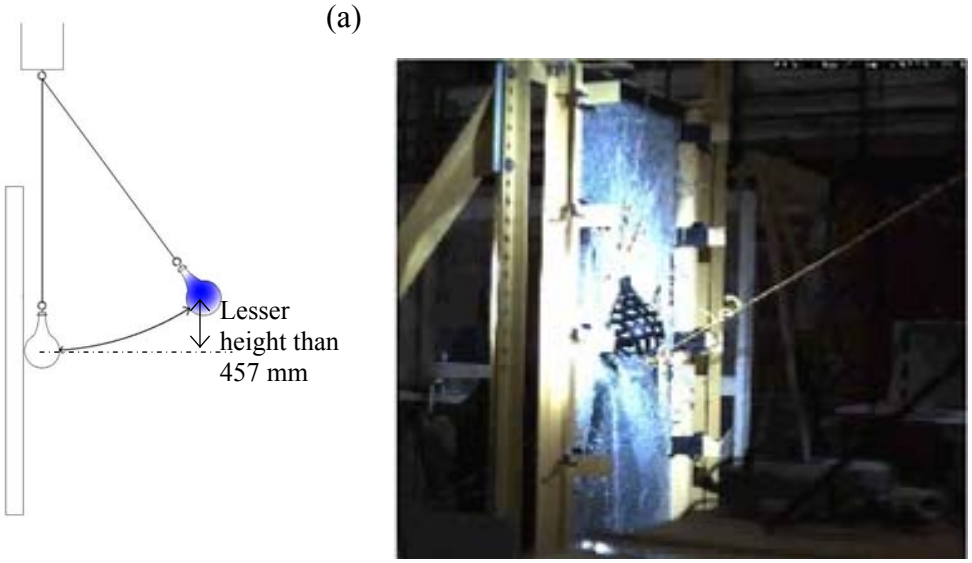

(b)

Figure 3.4.3.3 Breakage Modes of Fully Tempered Glass: First Impact at the Drop Height of 457 mm (a) and Second Impact at the Reduced Drop Height (b)

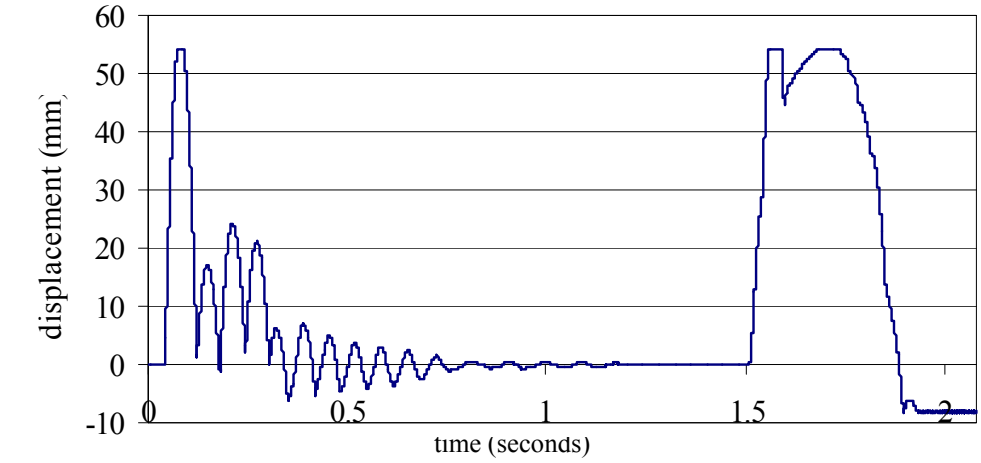

(a)

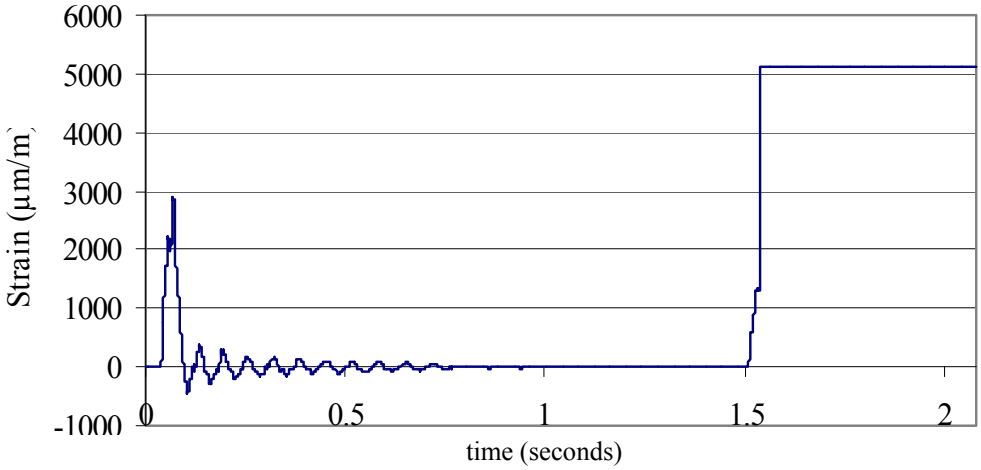

(b)

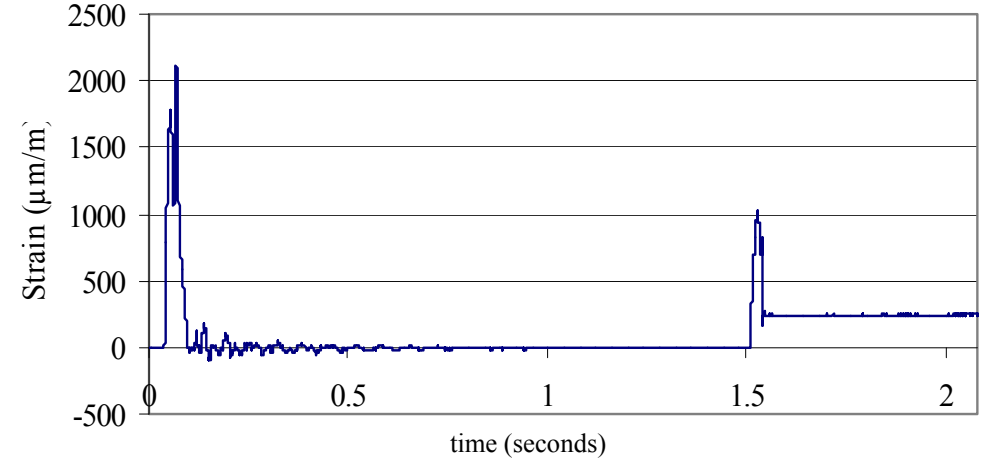

(c)

Figure 3.4.3.4 Displacement and Strain Outputs of Fully Tempered Glass: Displacement (a), Transverse Strain (b) and Longitudinal Strain (c)

(2) TCFS Specimen

The TCFS panel demonstrated different impact behaviors compared to the glass specimens. Most damage occurred local to the impact point, in a type of 'punching' failure which included cracks on the PMMA skins, debonding between the cardboard core and the PMMA skins, as well as material shear failure in the cardboard core. Upon impact, a circular crack with a diameter of 400 mm formed on the facing PMMA skin (Figure 3.4.3.5 (a) and (c)). A diagonal crack measuring 1,200 mm developed on the rear PMMA skin, which originated from the middle of one vertical edge and extended to the top of the other vertical edge (Figure 3.4.3.5 (a) and (b)). The deboning between the skin and core occurred on both sides of the panel near the impact point (Figure 3.4.3.6 (d) and (e)), but the PMMA skins remained intact. The epoxy adhesive attaching the PMMA skin to the cardboard core was subjected to longitudinal shear failure, resulting in deboning between the PMMA and cardboard core. The cardboard core underwent transverse shear failure at the middle and the corner of the core cells (Figure 3.4.3.6 (d) and (e)), accompanying the debonding between the PMMA and cardboard core. The notched cardboard used to create an egg crate core was also presumed to be a weak point, resulting in material failure due to the transverse shear (Figure 3.4.3.6 (d)). Crushing on the cardboard core was also occurred at the impact point (Figure 3.4.3.6 (f)). The fracture patterns of the PMMA skin and post-breakage modes are highlighted in Figure 3.4.3.6 and 3.4.3.6. The top and bottom of the panel showed no structural failure. The TCFS panel overall deformed in the direction of the impact with a permanent deformation of 25 mm. The maximum displacement at the point of impact was approximately 51 mm at 0.07 s and the corresponding strain was 4,900 μm/m as shown in Figure 3.4.3.7.

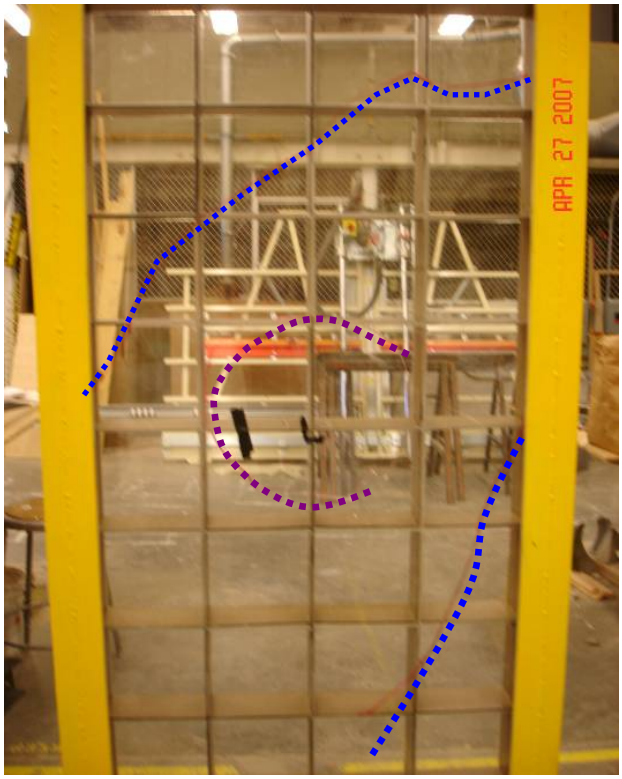

(a)

(b)

(c)

Figure 3.4.3.5 Fracture Patterns (a) of PMMA Skin at 457 mm Drop Height: Diagonal Crack on Back Skin (b) and Circular Crack on Front Skin (c)

(d)

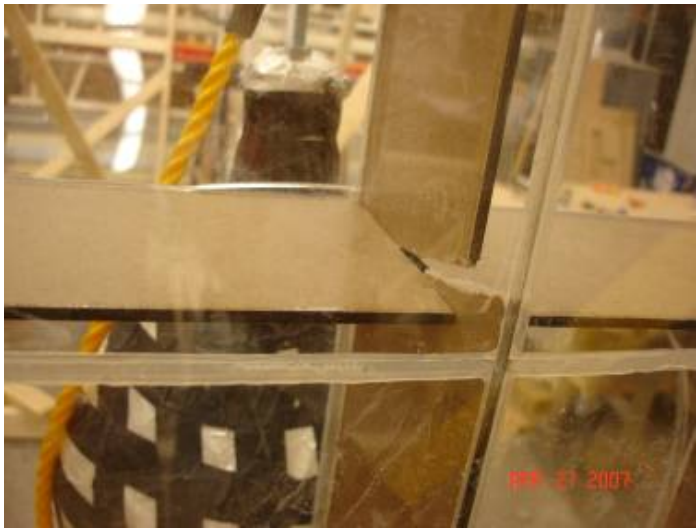

(e)

(f)

Figure 3.4.3.6 Post Breakage Modes of TCFS at 457 mm Drop Height: Transverse Shear Failure at Cardboard Core ((d) and (e), Longitudinal Shear Failure at Adhesive Joint ((d), (e), and (f)) and Crumbling of Cardboard Core (f)

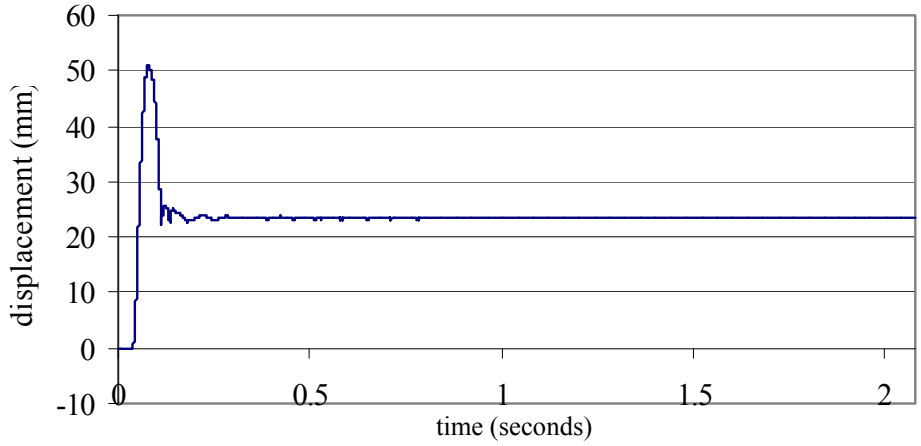

(a)

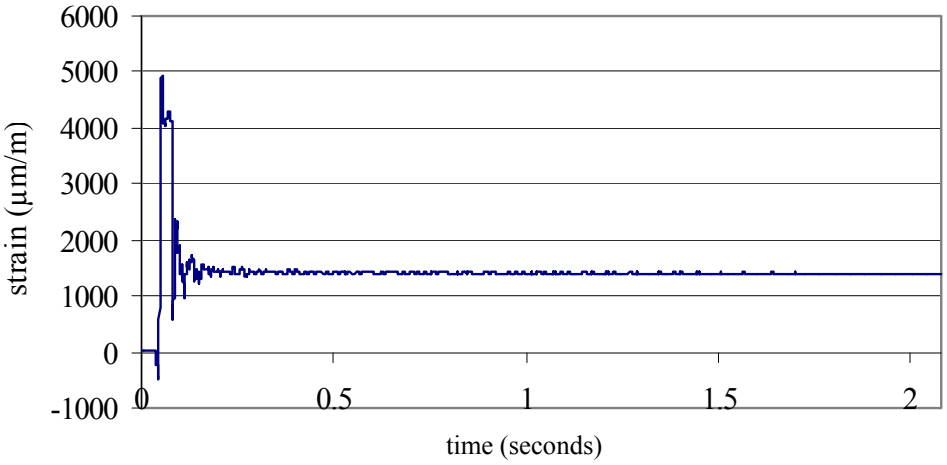

(b)

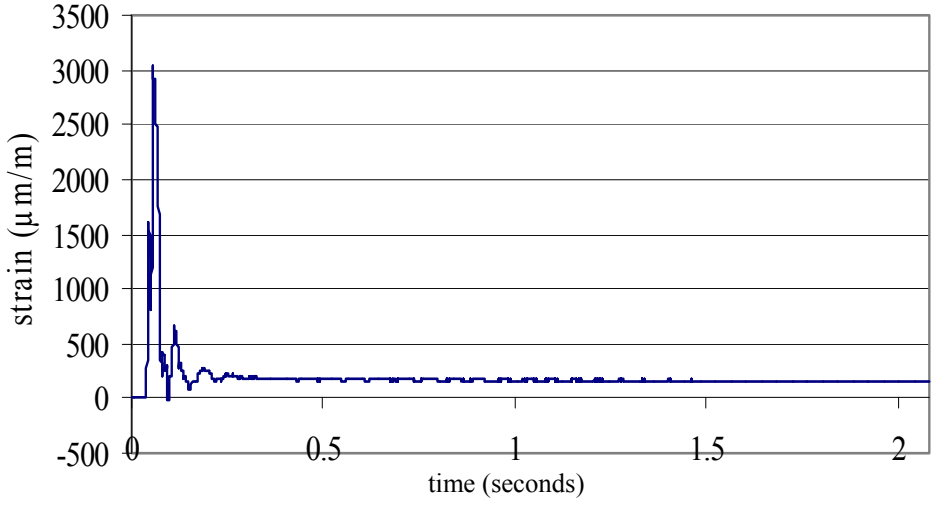

(c)

Figure 3.4.3.7 Displacement (a) and Strain ((b) anc (c)) Output of TCFS: Displacement (a), Transverse Strain (b) and Longitudinal Strain (c)

Figure 3.4.3.8 shows the energy absorbing characteristics of the glass and TCFS panels. The displacement comparisons revealed that the TCFS panel appears to be stiffer than glass under impact and therefore, results in absorbing less impact energy.

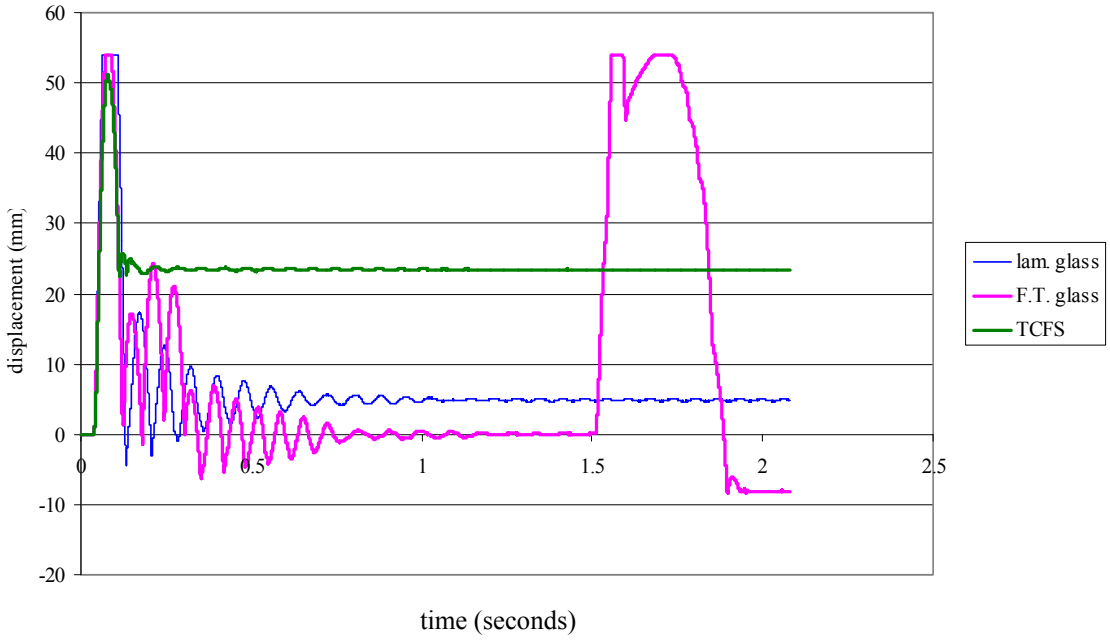

Figure 3.4.3.8 Displacement Comparisons between Glass and TCFS

3.4.4 Impact Testing Conclusions

It was observed that the laminated glass panel (2 x 3 mm heat strengthened glass) complied with the Class B safety standards of ANSI Z97.1, and the tempered glass panel (6 mm thick) was able to withstand the initial drop of 457 mm without failure, and therefore it complied with the Class B safety standards of ANSI Z97.1. However, since it failed upon a second impact from a lesser height than that required for Class B standard, it might be concluded that it in fact should have failed the Class B safety standard. This calls into question the procedure of ANSI Z97.1 which allows for a singular impact force to establish compliance. However, an initial impact may well have caused the panel to weaken without any obvious visual indication of this. It is therefore suggested that test panels should be tested with a second (and perhaps third) impact of the same magnitude (or at least say 50% of the initial magnitude) to ensure adequate continuing strength after initial impact. This is further verified by the ability of the laminated glass to withstand a

greater level of impact without failure and as such tempered glass ought to be subjected to 'secondary' testing to ensure consistent results with laminated glass. The calibration process of the impact testing frame using glass specimens revealed that the newly developed testing facility conformed to the ANSI Z97.1 specification. When dropped from a height of 457 mm, circular and diagonal cracks occurred on both the TCFS panel's front and rear PMMA skins. Despite the cracking, holes large enough for a 76 mm (3 inch) diameter sphere to freely pass though were not formed. Debonding between the PMMA skins and the cardboard core occurred, but the PMMA skins and cardboard core remained intact. The epoxy adhesives underwent longitudinal shear, causing the skin and core to debond. The resultant breakage modes under impact concluded that the TCFS meets the Class B requirements of ANSI Z97.1. Time history and displacement output indicated that the TCFS absorbs less impact energy than glass panels, but it is postulated that the TCFS panel provides greater residual strength, which would make the TCFS more resistant to second and third impacts.

3.5 Charpy Impact Performance

The primary purpose of the Charpy impact testing was to verify whether the PMMA skin of the TCFS maintain their safety characteristics after prolonged exposure to outdoor environment in accordance with ANSI Z97.1, which requires that weathered plastics or glass with an organic coating must maintain an impact strength of more than 75% of their initial strength. To test this, the plastics must undergo an accelerated weathering process followed by impact testing.

3.5.1 Charpy Impact Tester and Specimens

The Charpy impact test on PMMA specimens was carried out in accordance with ASTM D 6110 Standard Test Methods for Determining the Charpy Impact Resistance of Notched Specimens of Plastics. The testing was performed by the Bodycote Testing Group. The Charpy impact test is required to exert a maximum impact energy of 6.78 Nm- from a swing pendulum. Prior to the Charpy impact test, three specimens of PMMA sheet were exposed to an accelerated weatherometer (QUV) for 2,400 hours according to ASTM G154 Standard Practice for Operating Fluorescent Light Apparatus for UV

Exposure of Nonmetallic Materials. The weatherometer (QUV) equipped with fluorescent lamps (UVA-340) was digitally programmed to generate UV for 8 hours illumination at 60°C by light intensity of 0.89 W/m^2/nm followed by 4 hours condensation at 50°C (Cycle 1) repeatedly according to ASTM G154 specification. Three duplicate specimens were stored in a dark, conditioned space to be used to compare with the weathered specimens. The size of each specimen was 12 mm wide by 101 mm long by 3 mm thick without notches on its surface in accordance with ANSI Z97.1. The weathered surface of the specimen was located on the tension side of the swing hammer impact, and was laid flat in the impact tester. Figure 3.5.1.1 shows the Charpy impact tester (a) and the specimen set-up (b).

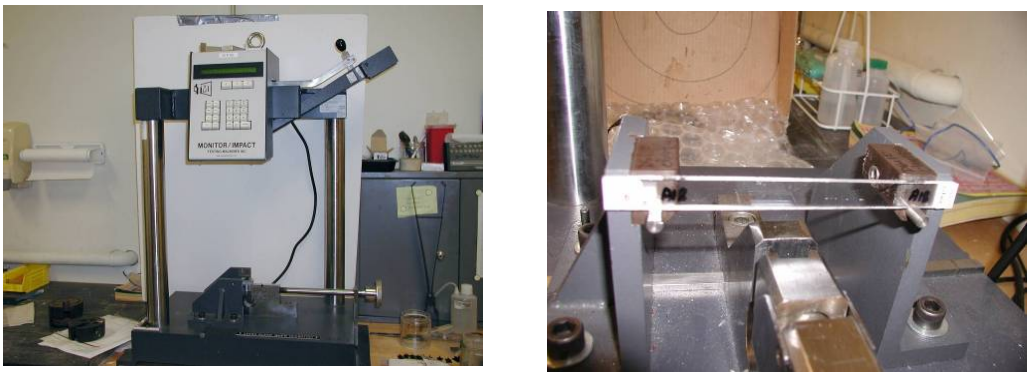

(a)

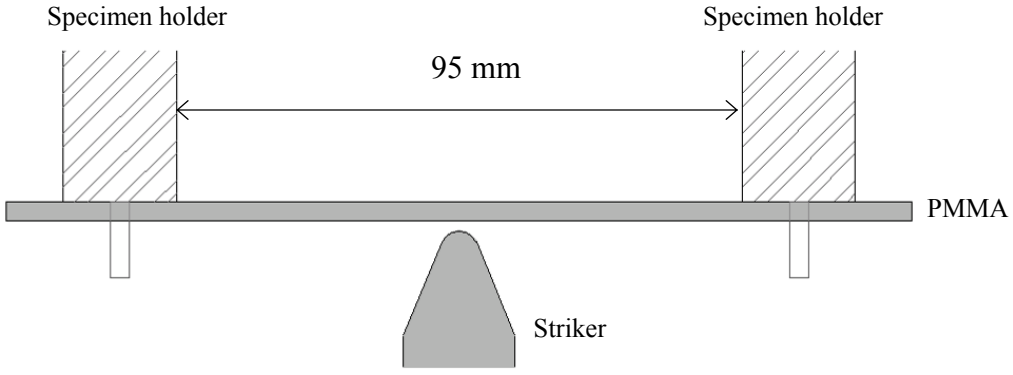

(b)

Figure 3.5.1.1 Charpy Impact Tester (a) and Specimen Set-Up Plan View (b)

3.5.2 Charpy Impact Testing Procedure

The Charpy impact test machine was calibrated using a non-weathered PMMA sample. After the machine was calibrated, each specimen was tested using repeated impacts, with incremental increases in height of the swing hammer until a specimen broke. Each specimen's impact strength was recorded in kg-cm/cm. Prior to testing, all specimens were conditioned to 24°C and 50% RH for 40 hours. Figure 3.5.2.1 shows the broken PMMA after testing.

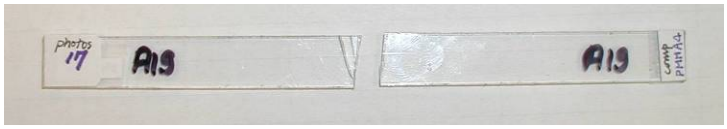

Figure 3.5.2.1 Broken PMMA After Calibrating the Charpy Impact Tester

3.5.3 Charpy Impact Testing Result

The average value of impact strength was determined for the three non-weathered specimens and another average value was determined for the weathered specimens. The average values of the two sets of specimens were then compared and the results are as follows. The average impact strength of the non-weathered PMMA (uncoated) was 6.22 ± 0.0784 kg-cm/cm and the average impact strength of the weathered specimen was 4.14±0.174 kg-cm/cm. The impact strength of the PMMA after 2,400 hours of outdoor exposure was approximately 64% of its original strength. This did not meet the ANSI Z97.1 requirement that a weathered material must have greater than 75% of its original strength to be certified as a safety glazing.

Since the weathered samples were exposed to a greater length of time (2400 hours) compared to the ANSI Z97.1 requirement (2400 hours), the results were more severe than might have been the case at the standard measure. In order to assess the impact strength at 2,000 hours of weathering exposure, the impact resistance at 2,000 hours was interpolated between zero and the impact strength of 4.14 kg-cm/cm at 2,400 hours, assuming that the impact resistance degrades according to a linear distribution over time. On this basis, the estimated impact strength at 2,000 hours was approximately 6.46 kg-cm/cm (1.186 lbs-ft/inch), which equates to 80% of the original strength (4.98 kg-cm/cm). Therefore, a preliminary conclusion might be that PMMA meets the ANSI Z97.1

requirements for Charpy impact resistance. Further tests at the standard measure will need to be conducted in the future to verify this prediction. Table 3.5.3.1 and Figure 3.5.3.1 shows the impact strength of the weathered specimens after 2,000 hours of exposure in relation to the measured strength at 0 hours and 2,400 hours of exposure. A complete report prepared by Bodycote Testing Group is presented in Appendix G.

Table 3.5.3.1 Measured and Charpy Impact Strength of PMMA

	Impact resistance
Non-weathered PMMA	6.22 kg-cm/cm
Weathered PMMA at 2,400 hours	4.14 kg-cm/cm

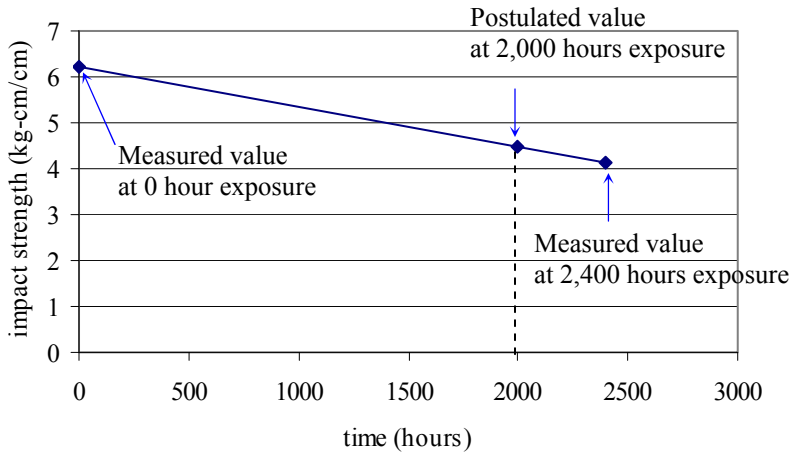

Figure 3.5.3.1 Charpy Impact Strength as a Fuction of Time

3.5.4 Charpy Impact Testing Conclusion

The purpose of the Charpy impact test was to verify the reduction in impact strength of PMMA after 2,000 hours of accelerated weathering conditions. The results show that the weathered PMMA meets the ANSI Z97.1 requirement of maintaining at least 75% of the panel's original strength. Therefore, it is concluded that the particular PMMA material tested conforms to the safety glazing requirements of the ANSI Z97.1 standard. However, additional tests will need to be carried out at the standard measure to validate this prediction.

3.6 Conclusions

Adequate strength and stiffness performance characteristics are important structural requirements for a façade system. The current building codes and standards do not provide strength and stiffness criteria for a TCFS. The International Building Code (IBC 2003) was used as a basis on which to evaluate the structural requirements for a TCFS and from this, the strength and stiffness requirements were established. A new testing frame was fabricated and used to carry out static and impact tests. The objective of the static test was to compare the measured results with theory-based values and provide simple equations that could be used at the initial design phase of a TCFS. As a result, bending tests with a two-edge supported TCFS panel showed good accuracy with the calculated values using simple beam theory. In the case of a four-edge supported TCFS panel, the model needed to be modified to create an 'effective depth' that accounts for the two-way stiffness of the TCFS panel, as well as the open cellular configuration that reduces torsional stiffness. An equivalent 'effective depth' was determined for a typical panel arrangement, by back substituting from two way action plate theory. In order to fully verify the 'effective depth' approach, additional parametric finite element simulations and testing would need to be carried out to test this method in order for it to be applicable to different cellular configurations where 'effective depth' of a TCFS will be a function of panel depth, skin and core thickness, core web spacing, core and skin elastic modulus material properties. This will allow simple beam theory to be comprehensively suitable for the initial design of a TCFS. For simplicity, adjustment factors accounting for the factors that influence the effective depth were calculated based on the experimental results. The adjusted simple plate theory shows agreement with the experimental data, and therefore, can be used to compute the flexural stress and deflection of composite panels that have aspect ratios and open cell geometrics that are similar to the studied TCFS panel. Stress and deflection outputs from the FEM analysis showed agreement with the experimental results for both the two-edge and four-edge supported TCFSs.

In addition to the static test, a pendulum impact test was carried out to investigate the impact behavior of a TCFS panel. Failure modes revealed that the TCFS panel complied with the safety glazing specification for a drop height of 457 mm, which is

equivalent to Class B of ANSI Z97.1. The Charpy impact test results indicate that the TCFS panel tested provides adequate impact strength after exposure to outdoor environments. Following recommendations for improvement in the structural composition and assembly of TCFS panels can be drawn from the impact test results. In order to avoid cracks and enhance the impact resistance of the TCFS panel, grooves should not be made on the PMMA surface. Also, the use of an adhesive that is less brittle than epoxy would likely provide more resilience and thus increase the impact resistance against the longitudinal shear. However, this would reduce overall panel stiffness. Another area that could be improved concerns the core material. The results of the impact test indicated that the cardboard sheared quite easily, and therefore, the use of a core material with greater shear strength is recommended in order to minimize human injury upon impact. Additional impact testing of a TCFS panel at a 1,219 mm ANSI Z97.1 Class A drop height could also be carried out in order to identify whether the panel can resist a greater impact. An impact test on a full-sized TCFS panel with edge connections is recommended to assess both global and local impact behavior.

Chapter 4

Life Cycle Assessment (LCA)

In accordance with ISO 14040 Environmental management – Life cycle assessment – Principles and framework, the LCA study in this chapter consists of four phases: (1) goal and scope definition, (2) life cycle inventory analysis (LCI), (3) life cycle impact assessment (LCIA), (4) life cycle result interpretation. The Semipro 7.1 database serves as the primary source for obtaining the life cycle inventory data.

4.1 Goal and Scope Definition

4.1.1 Goal and Scope

The main goal of the LCA study is to investigate the environmental impact of a TCFS relative to that of a GCWS by conducting a comparative life cycle assessment. The study focuses on identifying both systems' environmental impacts over their service life, determining at which phases contribute the greatest environmental impacts, comparing their overall environmental performance, and identifying methods to reduce the environmental impact caused by facade systems.

In order to accomplish these goals, the scope of this LCA study includes a life cycle inventory analysis (LCI), life cycle impact assessment (LCIA), and life cycle result interpretation for façade systems. The LCA examines environmental impacts during the whole life cycle which is divided into three phases: pre-use, use, and post-use. TCFS and GCWS have a number of important differences in their material composition, system size, and durability. These differences must be considered in order to determine the functional unit, which is discussed in greater detail in section 4.1.3. Inventory data associated with material processing and activities during each life cycle phase is obtained from the SimaPro 7.1 database and the amount of energy consumption associated with the use

phase of each façade system is identified by LBNL software (eQUEST 3.6, THERM 5, and WINDOW 5). However, certain aspects of the system could not be modeled due to data unavailability. A TCFS does not contain energy performance coating (e.g. low-e) and therefore, an uncoated GCWS is used as its counterpart. A coated GCWS is included in LCA study to understand the energy efficiency of a coating compared to the uncoated GCWS. Detailed assumptions and limitations of the LCA study are addressed in section 4.1.4.

4.1.2 System Boundaries

ISO 14040 defines a system boundary as a "set of criteria specifying which unit processes are part of a product system," and a unit process is defined as the "smallest element considered in the life cycle inventory analysis for which input and output data are quantified" (ISO, p.5, 2004). As can be seen in Figure 4.1.2.1, the processes examined in this study consider three life cycle phases: pre-use, use, and post-use.

The processes that typically occur during the pre-use phase of a façade system include raw material extraction, material processing, product assembly, packaging, transportation, and installation. However, due to data unavailability, only raw material extraction, material processing, and transportation are considered in this study. The use phase of a façade system typically involves operating, maintaining and replacing system components over the service life of a building. However, in this study the environmental impacts associated with maintenance and replacement are not inventoried due to a lack of LCA data. The post-use phase investigates the processes of dismantling, transporting, and disposing of a façade system. The study only measures the environmental impacts associated with transportation and the end-of-life disposal. Dismantling is not modeled due to data limitation. Figure 4.1.2.1 shows a summary of the system boundaries for the LCA study.

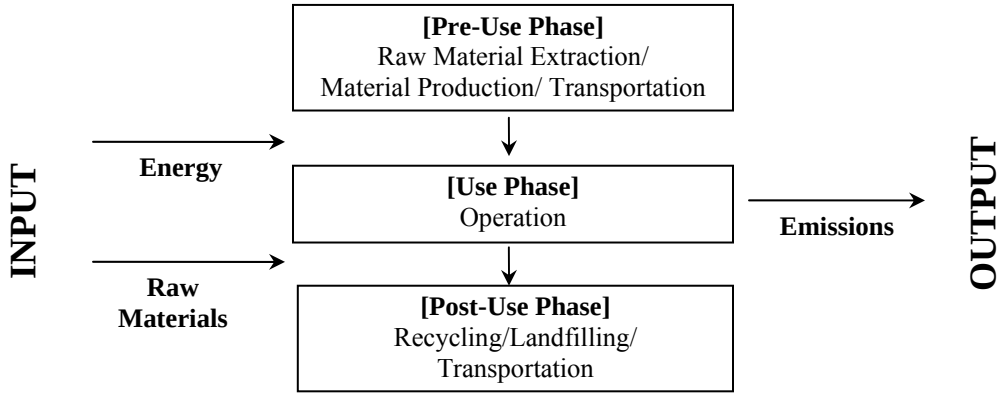

Figure 4.1.2.1 Overview of the System Boundaries of the LCA

4.1.3 Functional Unit

A functional unit is defined as "quantified performance of a product system for use as a reference unit" (ISO, p.4, 2004). Because a TCFS and GCWS each have different sizes and life spans, the functional unit (FU) for the LCA study is determined to be a façade area of 4.0 m high by 4.9 m wide (13 ft x 16 ft), and which encloses a building for a 40-year service life. The expected life spans of TCFS panels and GCWS panels are estimated to be 10 years and 20 years respectively. This indicates that, over a building's 40-year service life, a TCFS panel has to be replaced four times while a GCWS panel has to be replaced only twice. It is also presumed that the metal frames for both façade systems do not require replacement over the 40-year service life of the building. Table 4.1.3.1 summarizes the service life of each façade system for this LCA study. Figure 4.1.3.1 shows how four units of a TCFS and sixteen units of a GCWS enclose the same amount of a building façade area over a 40-year span.

Table 4.1.3.1 Functional Unit (FU) of TCFS and GCWS for Baseline LCA

	Life Span of Façade Systems			Design Life of a Building	Façade Area Covered
	TCFS Panel	GCWS Panel	Metal Frame		
Baseline LCA	10 years	20 years	40 years	40 years	19.11 m^2

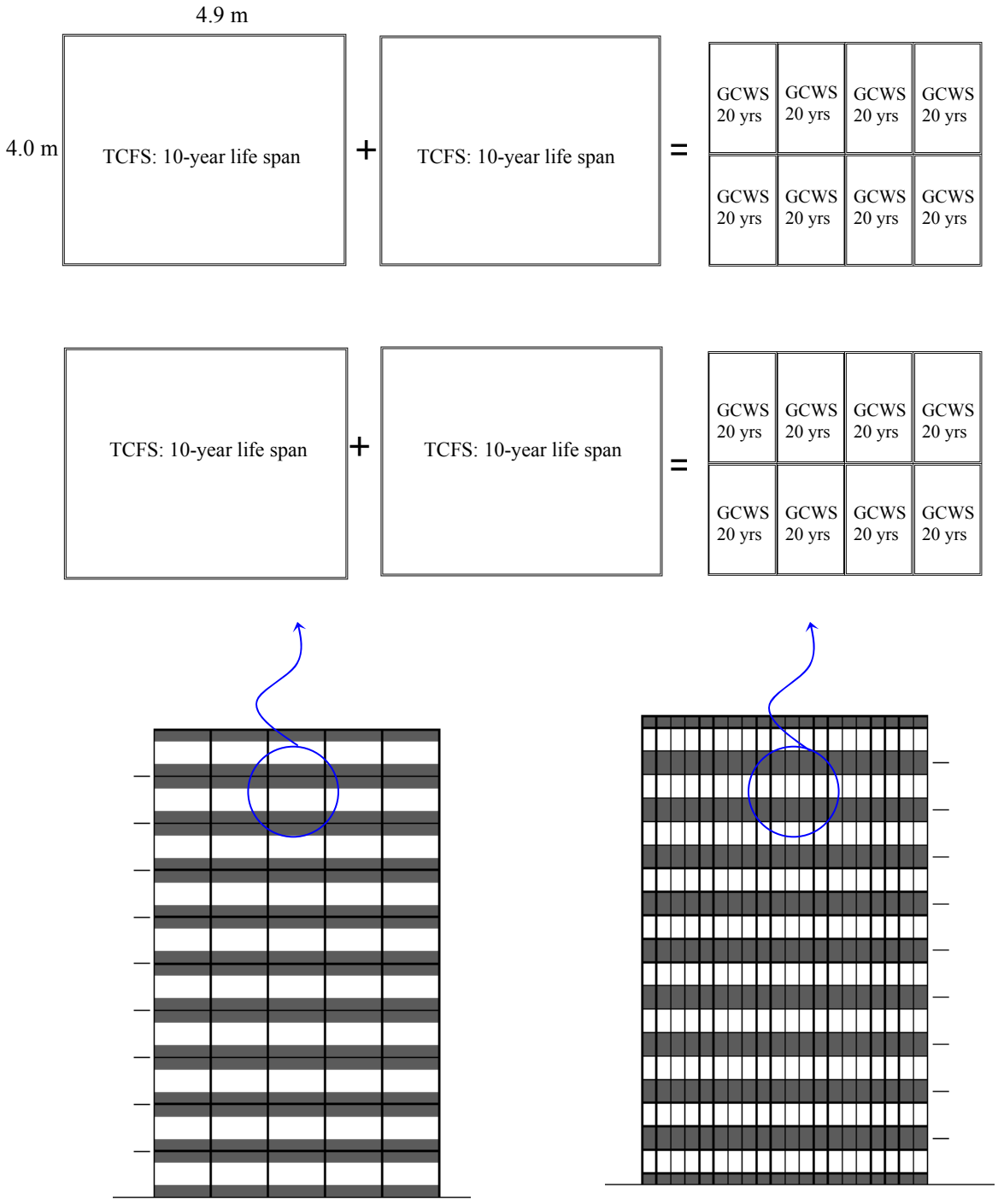

Figure 4.1.3.1 Functional Unit (FU) of TCFS and GCWS
for the 40-Year Service Life of a Building

As shown in Figure 4.1.3.2, the material mass of each façade system is calculated based on the system details that were determined in section 3.1. The material mass per TCFS and GCWS is 300 kg and 980 kg respectively, and the mass input of the GCWS is three times greater than that of the TCFS mainly due to glass weight.

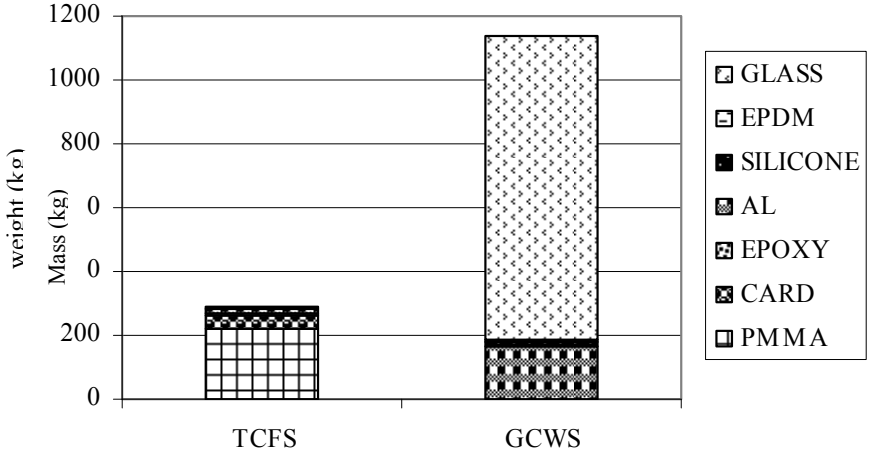

Figure 4.1.3.2 Material Mass Per TCFS and GCWS

The total material input of each façade system for the FU is calculated by multiplying the individual mass (Figure 4.1.3.2) with the required number of replacements over the service life of a building and adding 5% for material wastage estimated in product fabrication. The resulting total material inputs of a TCFS and GCWS per FU are 1,273 kg and 2,217 kg respectively as shown in Table 4.1.3.2. It should be noted that, despite fewer projected replacements of the GCWS over the service life of a building, the mass of a GCWS is still 35% greater than that of a TCFS panel. Figure 4.1.3.3 presents the total material input composition for each system per FU.

Table 4.1.3.2 Material Inputs of TCFS and GCWS Per Functional Unit (FU)

Material Components	TCFS			GCSW		
	Material Mass (kg)	5% Wastage	Total (kg)	Material Mass (kg)	5% Wastage	Total (kg)
PMMA	876	49				-
Biofiber Composites	185	9				-
Epoxy	4	0				-
Aluminum	53	3		164	8	
Silicone	37	2		36	2	
EPDM	15	1		13	1	
Glass	-	-		1,899	95	
Total Input (kg)	1,170	64	1,234	2,112	106	2,217

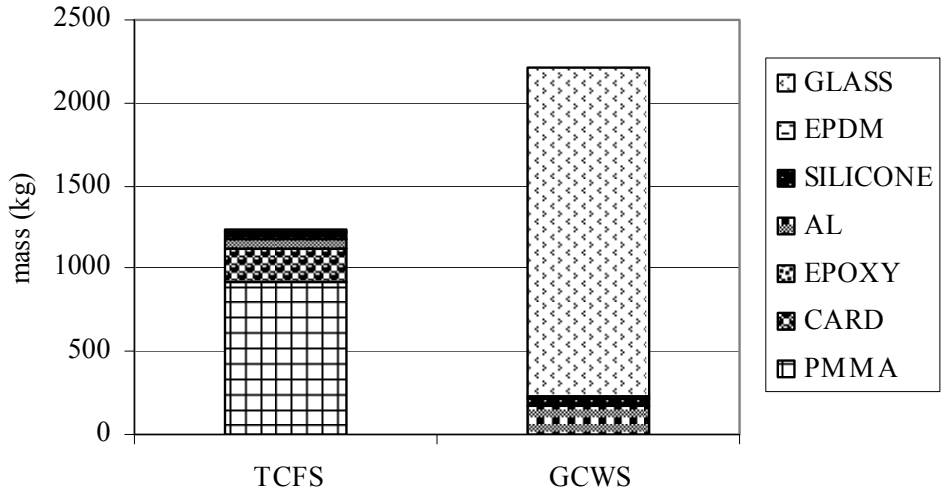

Figure 4.1.3.3 Material Mass Input Composition Per Functional Unit

4.1.4 Assumptions and Limitations

The LCA study makes two assumptions: that a TCFS can fulfill the same tasks as a GCWS and that the lifespan of a TCFS is half that of a GCWS. To facilitate the assessment of environmental burdens and to directly compare the two façade systems, boundary conditions such as building lifespan, building construction type, system installation method, maintenance frequency, and human comfort are assumed to be constant. The origin and production of the materials and the assembly of the product are assumed to occur within a radius of 1600 km from the building site. The transportation distance for the end-of- life disposal is assumed to be 50 km from the building site. Figure 4.1.4.1 shows the estimated traveling distance from the product supplier and building site.

The limitations of the LCA study are related to the system boundaries and the scope of the study. Due to data unavailability, certain fabrication processes such as lamination, tempering, extrusion, surface treatment, and product assembly are not inventoried. The environmental impacts associated with transportation are assessed based on the traveling distance and the weight of the façade system, neglecting the volume of the façade system. Due to the lack of LCA data, certain materials were either excluded or replaced with materials that represent similar characteristics. The polyvinyl butyral (PVB) interlayer of laminated glass, screws, and desiccant are not included due to their negligible weight and data unavailability. Landfilling inventory data of PMMA and cardboard were replaced with that of construction waste to landfill due to data

unavailability. Details of major assumptions and limitations of the LCA study are presented in Table 4.1.4.1.

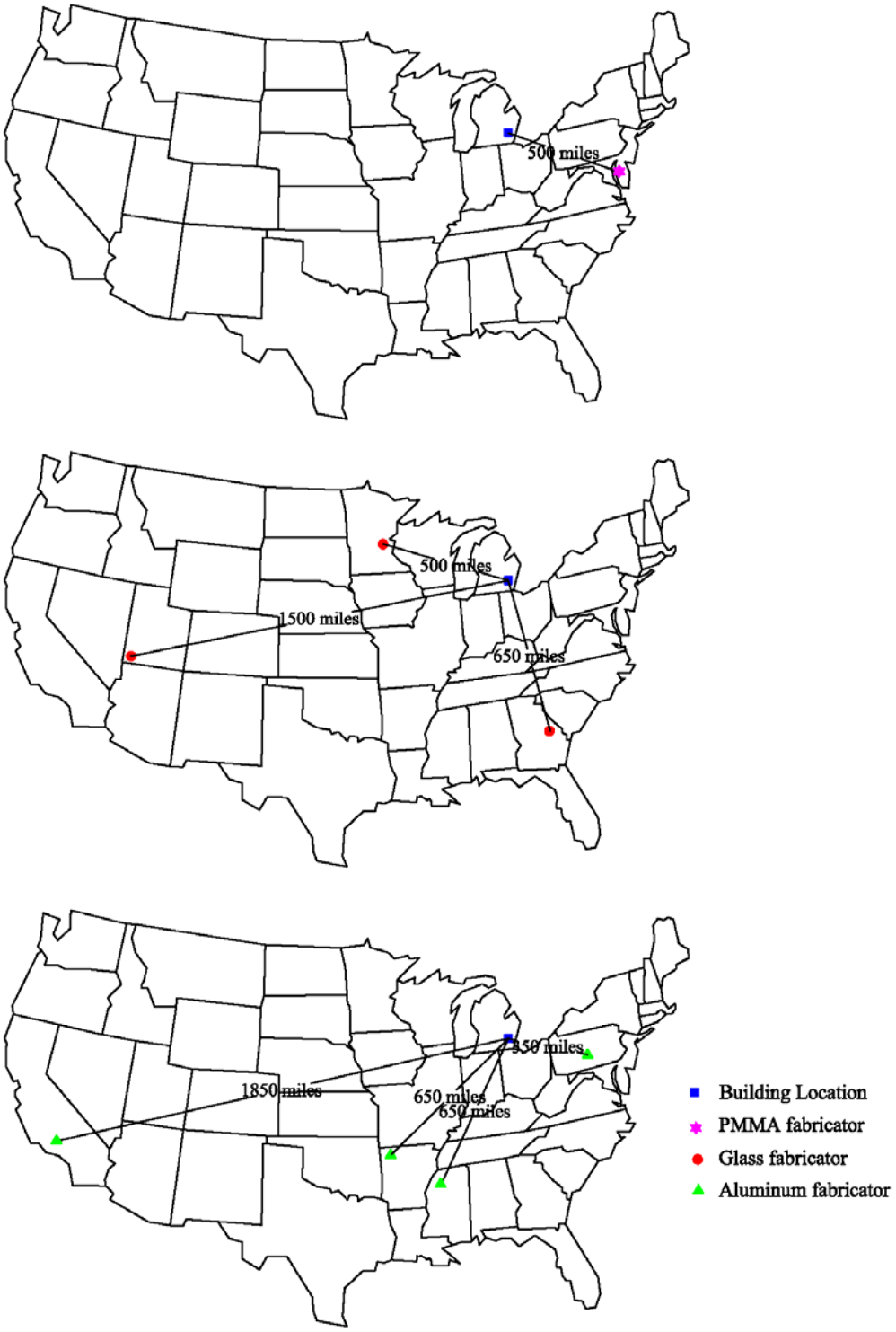

Figure 4.1.4.1 Travelling Distance between Building Site and Suppliers:
(a) Building ~ PMMA fabricator, (b) Building ~ Glass Fabricator and (c) Building ~ Alum.

Table 4.1.4.1 Major Assumptions and Limitations of the LCA study

Life Cycle Phase	TCFS	GCWS
Pre-Use Phase	The inventory data of biofiber composites is represented by the cardboard data; Aluminum without recycled content is inventoried; The aluminum extrusion process is not included; 5% material loss is assumed to occur during product fabrication; None of the environmental burdens associated with product fabrication and assembly are inventoried due to data unavailability; Material finishes such as bio-coatings and paintings are neglected due to data unavailability; The environmental burdens associated with transportation in the pre-use phase are calculated based on a total travel distance of 1600 km.	The data of the heat treated glass are represented by float annealed glass data; The production of coating and PVB interlayer are not included; The PIB primary seal and glazing tape in an IGU is analyzed using silicone data; The desiccant in the aluminum spacer and screws are neglected due to negligible weights; Aluminum without recycled content is considered; The aluminum extrusion process is not included; 5% material loss is assumed to occur during product fabrication; None of the environmental burdens associated with IGU assembly are inventoried due to data unavailability; The environmental burdens associated with transportation in the pre-use phase are calculated based on a total travel distance of 1600 km.
Use Phase	The environmental impacts of the use phase of each façade system are examined based on a building's energy consumption over an operation period of 40 years; A TCFS panel is assumed to be replaced twice as often as a GCWS panel; The environmental attributes associated with maintenance and replacement are not included due to data unavailability.	
Post-Use Phase	Basic end-of-life scenario is 100% landfill of the TCFS panel with 100% recycling of the metal frames; The environmental impact associated with demolition of the façade system is not included due to data unavailability; The transportation distance is assumed to be 50 km.	Basic end-of-life scenario is 100% landfill of the GCWS panel with 100% recycling of the metal frame; The environmental impact associated with demolition of the façade system is not included due to data unavailability; Transportation distance is assumed to be 50 km.
General Notes	The production of capital goods is excluded. The environmental impact associated with transportation is based on ton – km. Thus, the volume of the materials is not considered when calculating the environmental impact of transportation. Returning an empty truck is not included in the inventory analysis. Since the LCIA addresses only the energy and green house gas that are specified in the goal and scope, the LCIA in this chapter is not a complete assessment of all environmental issues of the product systems studied. Inventory data were obtained from the SimaPro 7.1 database.	

4.2 Life Cycle Inventory (LCI)

The environmental burdens associated with unit processes during each life cycle phase of a façade system were inventoried. The required energy input and pollutant emissions associated with production of 1 kg of material of the façade systems, transporting materials for 1 km using a 16-ton truck, generating 1 kWh of electricity and 1 Btu of natural gas (including extraction, production, and delivery), and landfilling and recycling 1 kg of material components are summarized in Table 4.2.1. The LCI data used in the LCA study are obtained from the SimaPro 7.1 database. Detailed inventory data of materials and process is presented in Appendix H.

Table 4.2.1 Life Cycle Inventory Data for Energy Inputs and Green House Gas Emissions

		Energy	Greenhouse Gas Emissions			
		Embodied Energy (MJ)	CO2 (kg)	CH4 (kg)	CF4 (kg)	C2F6 (kg)
Pre-Use Phase	PMMA (1 kg)	135	6.85E+00	2.44E-02	0.00E+00	0.00E+00
	Cardboard (1 kg)	10	7.09E-01	8.92E-04	0.00E+00	0.00E+00
	Epoxy (1 kg)	235	1.10E+00	0.00E+00	0.00E+00	0.00E+00
	Steel (1 kg)	30	9.00E-01	1.63E-04	1.69E-09	2.11E-10
	Aluminum (1 kg)	169	9.96E+00	2.24E-02	3.60E-04	4.20E-05
	Silicone (1 kg)	44	1.16E+00	7.85E-03	0.00E+00	0.00E+00
	EPDM (1 kg)	89	2.96E+00	9.94E-03	8.28E-08	9.20E-08
	Float Glass (1 kg)	14	9.68E-01	2.32E-03	1.69E-07	1.88E-08
	Transportation (1 km)	3	2.28E-01	2.77E-04	0.00E+00	0.00E+00
Use Phase	Electricity (1 MJ)	3.72	2.98E-01	6.49E-03	0.00E+00	0.00E+00
	Natural Gas (1 MJ)	1.15	5.58E-02	1.60E-04	0.00E+00	0.00E+00
Post-Use Phase	Construction Waste (1 kg) Landfilled	0.008	5.32E-04	7.37E-07	1.07E-11	1.19E-12
	PMMA (1 kg) Recycled	-42.92	-3.37E-01	8.28E-05	0.00E+00	0.00E+00
	Cardboard (1 kg) Recycled	-1.25	-5.55E-01	1.31E-03	-6.88E-09	-7.64E-10
	Glass (1 kg) Recycled	-3.15	-3.76E-01	-4.44E-06	0.00E+00	0.00E+00
	Aluminum (1 kg) Recycled	-104.04	-9.33E+00	-1.57E-02	-2.52E-04	-2.80E-05

4.2.1 Energy Inputs

4.2.1.1 Pre-use phase

The pre-use phase energy consists of embodied energy from material processing and transportation energy. The total embodied energy of each façade system is calculated by multiplying the embodied energy required to produce 1 kg of each material by the total mass input per functional unit. The amount of transportation energy is measured by multiplying the functional unit mass times the total traveling distance of 1600 km.

The analysis shows that fabrication of a TCFS panel (148,000 MJ/FU) is two times as energy intensive when compared to a GCWS panel (72,000 MJ/FU) per FU, due to the large amount of PMMA usage (900 kg/FU) and the energy intensity of material production and PMMA sheet fabrication (embodied energy of 135 MJ/kg). The TCFS and product transportation account for 141,000 MJ (95%) and 7,500 MJ (5%) of the total energy usage, whereas the GCWS panel, GCWS frames, and product transportation account for 31, 200MJ (45%), 30,000 MJ (41%), 10,000 MJ (14%) respectively. The GCWS frame is responsible for 41% of the total energy use because of the energy intensive production of the aluminum (169 MJ/kg). The energy associated with transporting the TCFS (7,500 MJ) is lower than that of the GCWS (10,100 MJ) due to its lighter weight. Table 4.2.1.1 and Figure 4.2.1.1 show the embodied energy of 1kg of material and the total pre-use phase energy of each façade system per functional unit.

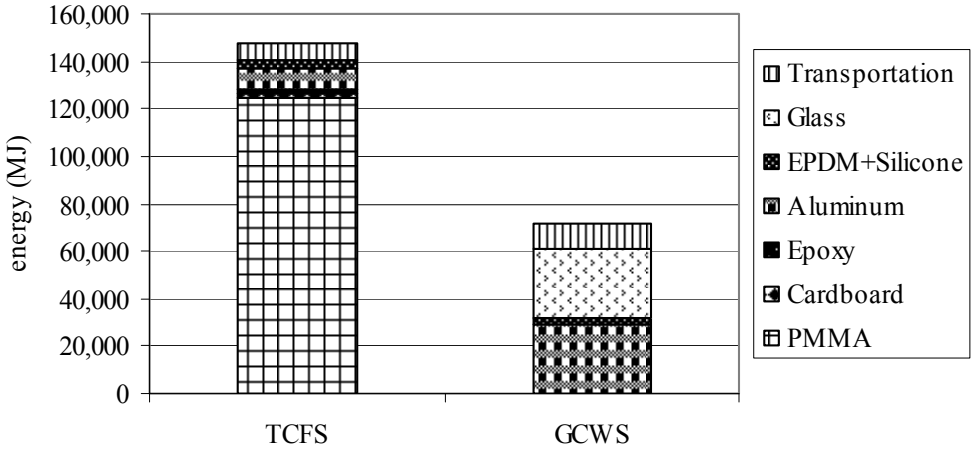

Figure 4.2.1.1 Embodied Energy Distributions of TCFS and GCWS Per FU

Table 4.2.1.1 Pre-Use Phase Energy of TCFS and GCWS per FU

TCFS	Embodied Energy (MJ/kg)	Total Embodied Energy (MJ)
PMMA	135	124,928
Cardboard	10	1,911
Epoxy	235	1,044
Aluminum	169	9,464
Silicone	44	1,727
EPDM	89	1,357
Transportation (4 trips at 1600 km)	3	7,488
Total		147,919

GCWS	Embodied Energy (MJ/kg)	Total Embodied Energy (MJ)
Float glass coated	15	28,950
Aluminum	124	29,241
Silicone	44	1,670
EPDM	89	1,179
Transportation (2 trips at 1600 km)	3	10,138
Total		71,178

4.2.1.2. Use phase

The operational energy of a building is classified as the site energy and primary energy. Site energy refers to the energy consumed by end uses such as space heating and cooling, and primary energy is the site energy combined with the life cycle energy of fuel that accounts for fuel upstream, energy production, and delivery. The primary conversion factor, which is the ratio of the primary energy to the delivered site energy, is obtained from the SimaPro 7.1 database.

The site energy consumed during the use phase of a TCFS and GCWS is determined by performing a building energy simulation. A 10-story office building located in Detroit, Michigan is used as the study's model, and energy simulation software (eQUEST: the QUick Energy Simulation Tool) is used to calculate the site energy associated with cooling, heating, and lighting a building. The site energy consumption is affected by various factors: climate, site orientation, building size, HVAC (heating, ventilation, and air conditioning) system, building operation schedule, building envelope construction, window-to-wall ratio, air infiltration, U-factor (heat transmission), solar heat gain coefficient (SHGC), and visible light transmittance (VLT) (ASHRAE, p. 124,

2001). The energy performance values (U-factor, SHGC, and VLT) are input parameters in the eQUEST simulation to model. The difference in the energy usage between a TCFS and GCWS, Appendix I shows how the U-factor, SHGC, and VLT for each façade system are calculated using WINDOW 5 and THERM 5 software. Table 4.2.1.2 outlines the parameters used in the eQUEST simulation and Figure 4.2.1.2 shows a building set-up in eQUEST.

Table 4.2.1.2 Office Building Information for eQUEST Simulation

Building Parameters	Values
Location	Detroit, MI
Service life	40 years
Building footprint	160 m x 80 m
Number of floor	10
Floor-to-floor height	4 m
Floor-to-ceiling height	2.7 m
Daylighting control	Yes
Building envelope construction	Curtain wall construction with vision and spandrel glazing
Window-to-wall ratio	50%
Wall infiltration rate	0.038 CFM/ft2

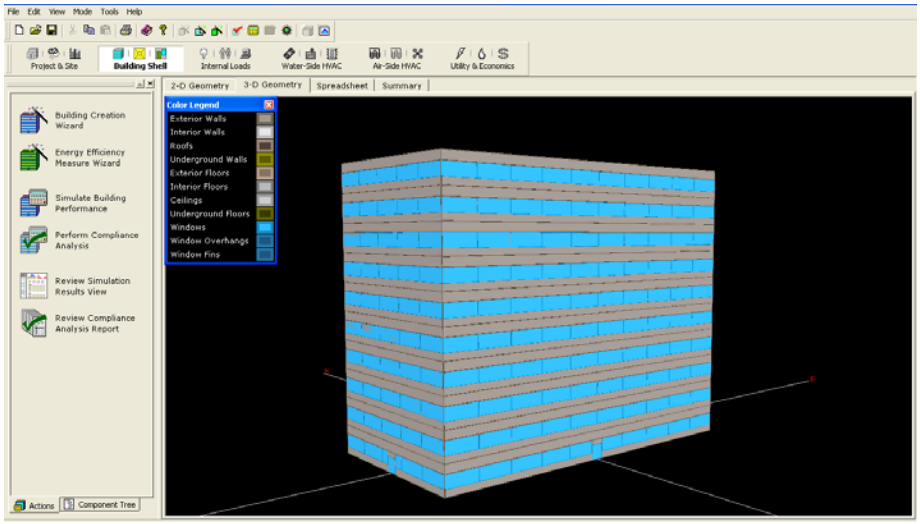

Figure 4.2.1.2 An Office Building Set-Up in eQUEST

Appendix I presents the eQUEST output of annual energy consumption for each façade system. In order to estimate the site energy per façade system with a 40-year service life, the annual energy consumption is multiplied by the number of years of

service life (40 years) and divided by the number of façade units that covers the building (300 units). The resulting energy consumption of each façade system for the FU is shown in Table 4.2.1.4. In order to quantify the total energy consumption, natural gas (Btu) and electricity (kWh) are converted into the same energy unit (MJ) by using conversion factors of 1 MBtu = 1055 MJ and 1 kWh = 3.6 MJ. By this calculation, a TCFS consumes approximately 400,000 MJ and an uncoated GCWS consumes 470,000 MJ, indicating that the TCFS consumes 18% less energy than the uncoated GCWS during the 40-year service life of a building. A coated GCWS, however, consumes 24% less energy than the uncoated GCWS. The baseline of the LCA study is to compare the TCFS (uncoated) and GCWS (uncoated). The additional analysis of coated GCWS is added to understand the effect of high performance coating on the use phase energy. Table 4.2.1.3 shows the total site energy consumed during the 40-year service life of the model building.

Table 4.2.1.3 Site Energy Consumed by End Uses of TCFS and GCWS Per FU

Energy type	End uses	TCFS	Uncoated GCWS	Coated GCWS
Natural gas	Heating (1,000,000 Btu)	189	224	148
Electricity	Cooling (1,000 kWh)	20	30	21
	Lighting (1,000 kWh)	33	32	32

Energy Type	Energy Use (MJ)	TCFS	Uncoated GCWS	Coated GCWS
Natural gas	Heating (MJ)	198,903	236,714	155,929
Electricity	Cooling (MJ	73,916	110,053	77,705
	Lighting (MJ)	122,554	118,888	120,067
Total (MJ)		395,373	465,655	353,701

In order to calculate the primary energy required to provide the calculated site energy, the primary conversion factor of 1:3.72 for electricity and 1:1.15 for natural gas based on the SimaPro 7.1 database is multiplied to each of the identified site energy values. For example, 3.72 MJ of primary energy is required to supply 1 MJ of site energy used for cooling and lighting (electricity), whereas 1.15 MJ of primary energy is needed to supply 1 MJ of the site energy from space heating (natural gas). As a result, the total primary energy of a TCFS and an uncoated GCWS is approximately 960,000 MJ and 1,113,000 MJ respectively, indicating that the primary energy of a TCFS is 15% less than that of an uncoated GCWS. A coated GCWS (915,000 MJ) consumes 18% less primary

energy than that of an uncoated GCWS (1, 1130,000 MJ). Table 4.2.1.4 and Figure 4.2.1.3 compare the differences in primary energy use for a TCFS and a GCWS.

Table 4.2.1.4 Primary Energy Consumption of TCFS and GCWS Per FU

Energy Type	End Uses	TCFS	Uncoated GCWS	Coated GCWS
Natural gas	Heating (MJ)	228,738	272,221	179,318
Electricity	Cooling (MJ	274,968	409,396	289,062
	Lighting (MJ)	455,900	442,265	446,651
Total (MJ)		959,606	1,123,882	915,032

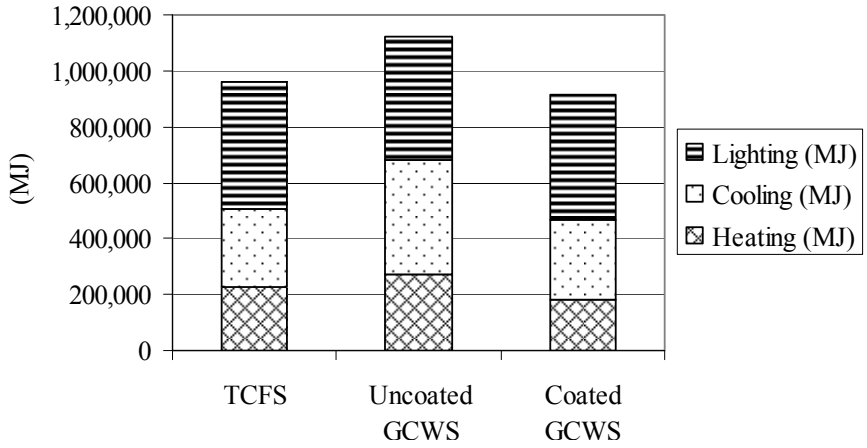

Figure 4.2.1.3 Use Phase Energy of TCFS and GCWS Per FU

4.2.1.3 Post-Use Phase

Incineration or recycling materials at the end of a product's life cycle provides energy or material recovery, and in this regard, the energy consumption is indicated as a negative value. Landfilling, on the other hand, requires life cycle energy to process waste treatment and therefore, is expressed as a positive value. For the disposal scenario of a TCFS and GCWS, it is assumed that both TCFS and GCWS are landfilled. By considering the landfill scenario as a baseline LCA, the sensitivity analysis using recycling scenario can provide more meaningful result to make a recommendation for the end of product management. As Table 4.2.1.5 indicates, a TCFS consumes 1,700 MJ and a GCWS requires 2,700 MJ, and major energy is attributed to the transportation for both systems. Energy required for landfilling the TCFS and GCWS panels is obtained from the SimaPro 7.1 database.

Table 4.2.1.5 Post-Use Energy Consumption of TCFS and GCWS per FU

Façade System	End of Life Scenario	Required Energy (MJ/kg)	Total Post-Use Energy (MJ/FU)
TCFS	TCFS Landfilled	0.007	8
	Transportation (4 trips at 50 km)	3	1,736
	Total		1,744
GCWS	GCWS Landfilled	0.007	15
	Transportation (2 trips at 50 km)	3	2,696
	Total		2,711

4.2.1.4 Total Life Cycle Energy Comparison

A comparison between the life cycle energy input of a TCFS and GCWS is presented in Table 4.2.1.6 and Figure 4.2.1.4. The total life cycle energy of a TCFS (1,110,000 MJ) consumes 7% less energy than that of an uncoated GCWS (1,200,000 MJ) over a 40-year service life. A coated GCWS (989,000 MJ) consumes 18% less energy than an uncoated GCWS (1,200,000 MJ) for the same period. For a TCFS, energy consumption during the pre-use phase accounts for 13% of the system's total life cycle energy, while the energy consumed during the use phase is responsible for 87%. The energy in the pre-use phase of an uncoated GCWS accounts for 6% of the system's total life cycle energy while the use phase's energy (primary energy) accounts for approximately 94%. The post-use phase for both a TCFS and GCWS consumes least energy as energy required energy for landfilling is minimal.

Table 4.2.1.6 Total Life Cycle Energy Input of TCFS and GCWS Per FU

	TCFS	Uncoated GCWS	Coated GCWS
Pre-Use (MJ)	147,919 (13%)	71,178 (6%)	71,178 (7%)
Use (MJ)	959,606 (87%)	1,123,882 (94%)	915,032 (93%)
Post-Use (MJ)	1,744 (0.16%)	2,711 (0.24%)	2,711 (0.28%)
Total (MJ)	1,109,269 (100%)	1,197,771 (100%)	988,921 (100%)

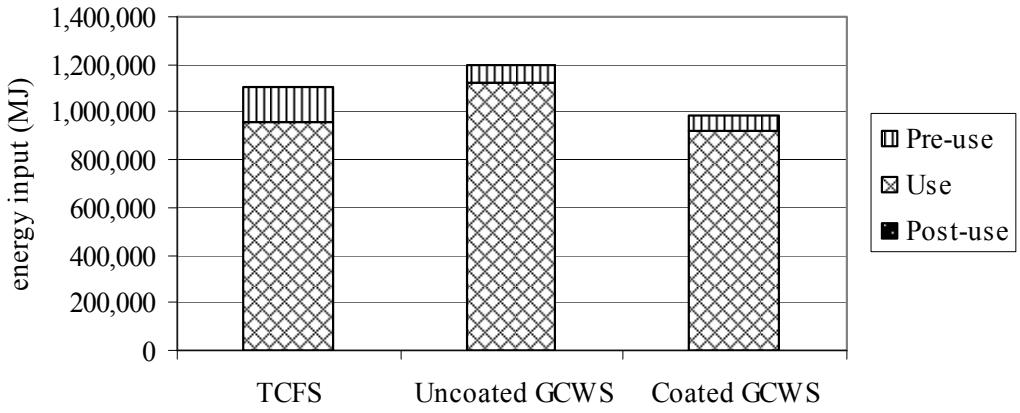

Figure 4.2.1.4 Total Life Cycle Energy Input of TCFS and GCWS Per FU

4.2.3 Environmental Emissions

The greenhouse gas (GHG) emissions that are released during the life cycle stages of a TCFS and GCWS are examined. The primary GHGs inventoried in this section are Carbon Dioxide (CO2), Methane (CH4), Tetrafluoromethane (CF4), and Hexafluoroethane (C2F6), all of which contribute to global warming. The results of the analysis show that a TCFS (77,000 kg) creates 10,000 kg less CO2 than an uncoated GCWS (87,000 kg). A coated GCWS (72,000 kg) releases 15,000 kg less CO2 than an uncoated GCWS (87,000 kg) and 10,000 kg less than a TCFS. During the pre-use phase, the TCFS generates approximately 7,600 kg of CO2, which is 1.7 times that of a GCWS (4,500 kg of CO2). In the pre-use phase of a TCFS, manufacturing the PMMA (6,300 kg of CO2) accounts for 83% of the system's total CO2 emissions while transportation (500 kg) contributes 7%. For a GCWS, the major activities causing CO2 emissions during the pre-use phase are manufacturing glass (2,000 kg) and aluminum (1,700 kg) and transportation (800 kg). A small amount of CF4 and C2F6 is also found in the pre-use phases of both the TCFS and GCWS due to the production of aluminum. For the use phase, the CO2 emissions of a TCFS (70,000 kg) are 15% less than that of an uncoated GCWS (82,000 kg). For the post-use phase, both TCFS (17 kg) and GCWS (27 kg) has very little CO2 emission mainly from the transportation. In sum, the pre-use phase of a TCFS and GCWS contributes 10% and 5% of the total CO2 emissions respectively. The use phase is the dominant phase for CO2 emissions for both a TCFS and an uncoated GCWS, accounting for 90% and 95% of their total CO2 emissions. The CO2 emissions

during the post-use phase for both a TCFS and GCWS are relatively insignificant when landfilled end of life cycle management is considered. Table 4.2.3.1 and Figure 4.2.3.1 show the GHG emissions of each façade system throughout their life cycles.

Table 4.2.3.1 Pollutant Emissions of TCFS and GCWS Per FU

	TCFS				Uncoated GCWS				Coated GCWS			
	CO2 (kg)	CH4 (kg)	CF4 (kg)	C2F6 (kg)	CO2 (kg)	CH4 (kg)	CF4 (kg)	C2F6 (kg)	CO2 (kg)	CH4 (kg)	CF4 (kg)	C2F6 (kg)
Pre-Use	7.64E+03 (10%)	2.51 E+01	1.99E-02	2.32E-03	4.54E+03 (5%)	9.90E+00	6.24E-02	7.28E-03	4.54E+03 (6%)	9.90E +00	6.24E-02	7.28E-03
Use	6.97E+04 (90%)	1.31E +03	0.00E +00	0.00E +00	8.15E+04 (95%)	1.52E+03	0.00E+00	0.00E+00	6.77E+04 (94%)	1.31E +03	0.00E +00	0.00E +00
Post-Use	1.70E+01 (0.02%)	2.08E-02	1.53E-08	1.70E-09	2.65E+01 (0.03%)	3.23E-02	2.37E-08	2.64E-09	2.65E+01 (0.04%)	3.23E-02	2.37E-08	2.64E-09
Total	7.74E+04 (100%)	1.34E +03	1.99E-02	2.32E-03	8.61E+04 (100%)	1.53E+03	6.24E-02	7.28E-03	7.23E+04 (100%)	1.32E +03	6.24E-02	7.28E-03

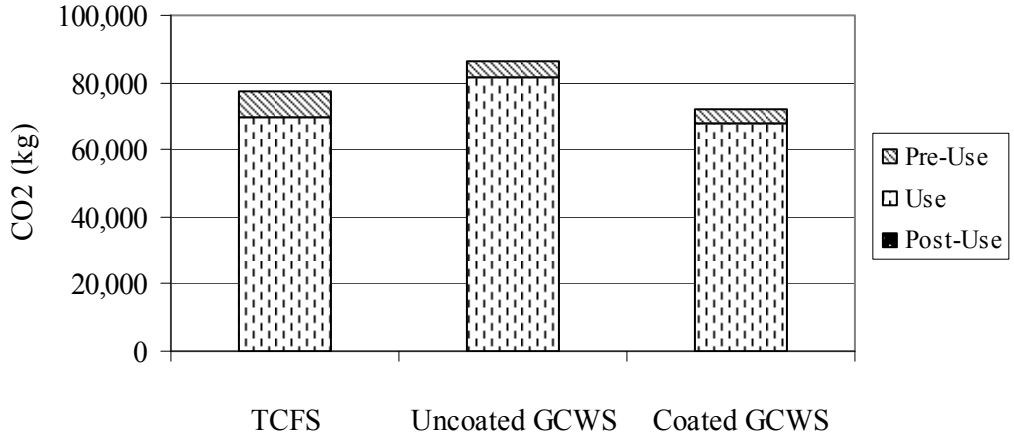

Figure 4.2.3.1 CO2 Emissions of TCFS and GCWS Per FU

4.3 Life Cycle Impact Assessment (LCIA)

Global warming potential (GWP) uses CO2 as the reference gas and each GWP is converted into the equivalent weight (kg) of CO2 accordingly to Intergovernmental Panel on Climate Change (IPCC) 2007. For example, 1 kg of Methane (CH4) creates the same GWP as 21 kg of CO2. Table 4.3.1 shows the global warming potential and the characterization factor of each GHG substance.

Table 4.3.1 Global Warming Potential for 100-Year Time Horizon

Industrial Designation	Chemical Formula	Global Warming Potential for 100-year Time Horizon
Carbon dioxide	CO2	1 kg CO2 equivalent
Methane	CH4	21 kg CO2 equivalent
PFC-14	CF4	6,500 kg CO2 equivalent
PFC-116	C2F6	9,200 kg CO2 equivalent

From "IPCC Technical Paper on 4AR," by Intergovernmental Panel on Climate Change, 2007, p. 212.

The results of this analysis show that, although a TCFS creates approximately 1.5 times the GWP of a GCWS in the pre-use phase, the total life cycle GWP of a TCFS (108,000 kg CO2 equivalent) is 11% less than that of an uncoated GCWS (122,000 kg CO2 equivalent). The total GWP of a coated GCWS (103,000 kg CO2 equivalent) is 19,000 kg less than that of the uncoated GCWS, which is mainly due to a lower amount of CO2 emissions during its use phase. The use phase of a TCFS accounts for 92% of the GWP from its total life cycle, followed by the pre-use phase (8%) and post-use phase (<1%). The use phase of the uncoated GCWS accounts for 95% of the total GWP, followed by the pre-use phase (5%) and the post-use phase (<1%). In both façade systems, the use phase generates the greatest environmental impact per functional unit, and the post-use phase has little impact on GWP generation. Table 4.3.2 and Figure 4.3.1 illustrates the GWP of each façade system over a 40-year service life.

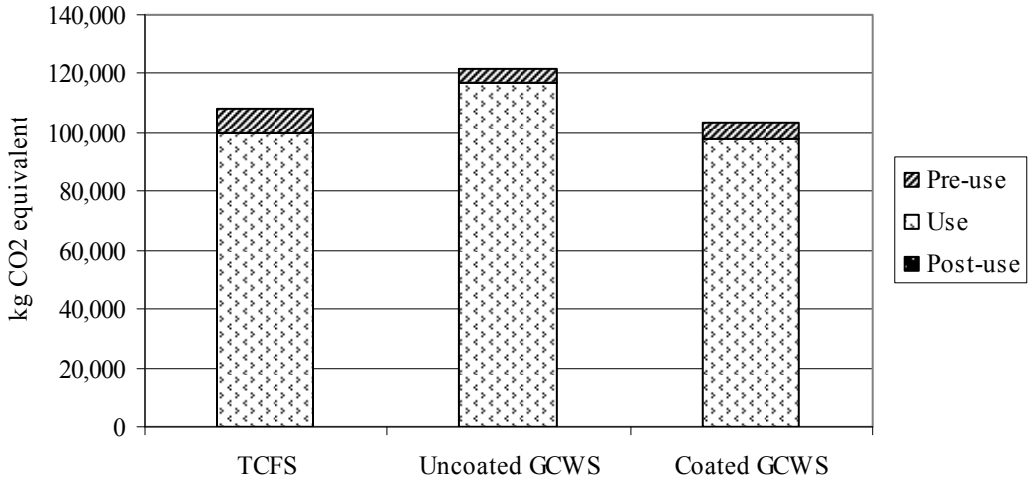

Figure 4.3.1 Global Warming Potential of TCFS and GCWS Per FU

Table 4.3.2 Global Warming Potential of TCFS and GCWS Per FU

TCFS	Pre-use	Use	Post-use	Total
CO2 (= 1 kg CO2 equiv.)	7.64E+03	6.97E+04	2.08E-02	
CH4 (= 21 kg CO2 equiv.)	5.27E+02	3.01E+04	4.37E-01	
CF4 (= 6500 kg CO2 equiv.)	1.29E+02	0.00E+00	9.95E-05	
C2F6 (= 9200 kg CO2 equiv.)	2.13E+01	0.00E+00	1.56E-05	
Total kg CO2 equivalent	8,320	99,790	0.46	108,110

Uncoated GCWS	Pre-use	Use	Post-use	Total
CO2 (= 1 kg CO2 equiv.)	4.54E+03	8.15E+04	2.65E+01	
CH4 (= 23 kg CO2 equiv.)	2.08E+02	3.50E+04	6.78E-01	
CF4 (= 5700 kg CO2 equiv.)	4.06E+02	0.00E+00	1.54E-04	
C2F6 (= 11900 kg CO2 equiv.)	6.70E+01	0.00E+00	2.43E-05	
Total kg CO2 equivalent	5,220	116,580	30	121,830

Coated GCWS	Pre-use	Use	Post-use	Total
CO2 (= 1 kg CO2 equiv.)	4.54E+03	6.77E+04	27	
CH4 (= 23 kg CO2 equiv.)	2.08E+02	3.01E+04	6.78E-01	
CF4 (= 5700 kg CO2 equiv.)	4.06E+02	0.00E+00	1.54E-04	
C2F6 (= 11900 kg CO2 equiv.)	6.70E+01	0.00E+00	2.43E-05	
Total kg CO2 equivalent	5,220	97,820	30	103,070

4.4 Sensitivity Analysis

The sensitivity analysis in this section focuses on identifying potential improvements that can be made to a TCFS and GCWS in order to reduce their life cycle environmental impacts. For this purpose, improved durability and recycling scenarios for a TCFS and GCWS are explored, which is followed by a detailed sensitivity analysis. Table 4.4.1 summarizes the new assumption of the functional unit for the sensitivity analysis.

Table 4.4.1 Key Factors for Sensitivity Analysis

	Pre-Use Phase: Improved Durability		Post-Use Phase: Recycling	
	TCFS panel	GCWS panel	TCFS panel	GCWS panel
Baseline LCA	10 years	20 years	Landfilling	Landfilling
Sensitivity LCA	20years	40 years	Recycling	Recycling

4.4.1 Pre-use Phase: Improved Life Expectancy

The energy input and pollutant output during the pre-use phase of a façade system is directly related to the system's durability and weight. The LCA in the previous section indicated that the pre-use phase of a TCFS is responsible for 13% of the total life cycle energy and 9% of the total GWP emissions over a 40-year building service life. The first sensitivity analysis in this section regards enhancing the durability of both a TCFS and GCWS. While the life spans of a TCFS and GCWS were projected in the LCA study to be 10 years and 20 years respectively, the sensitivity analysis in this section uses the expected maximum service life of 20 years and 40 years. This means that, CGWS would not need to be replaced and a TCFS panel would require two replacements to meet the 40-year service life of a building.

The sensitivity analysis results show that a TCFS still consumes more energy and produces more CO2 emissions compared to a GCWS. However, with improved durability, the 20-year life span of a TCFS (72,000 MJ) reduces the original pre-use energy (148,000 MJ) by approximately 50%, which is mainly due to the decreased use of PMMA. The 40-year life span of a GCWS (50,000 MJ) reduces the original pre-use energy (71,000 MJ) by approximately 32% due to the reduction in glass use. The projected figures of the improved TCFS and GCWS during their pre-use phase result in GWP reductions by 50% (4,100 kg CO2 equivalent) and 30% (1,500 kg CO2 equivalent) respectively. Table 4.4.1.1 and Figure 4.4.1.1 show the sensitivity analysis results associated with the pre-use phase, taking into consideration the actual and improved maximum life spans.

Table 4.4.1.1 Sensitivity Analysis Results for Pre-Use Phase

Pre-Use Phase	Baseline LCA		Sensitivity Analysis	
	TCFS 10 years	GCWS 20 years	TCFS 20 years	GCWS 40 years
Pre-Use Energy (MJ)	147,920	71,180	73,960	50,210
Pre-Use GWP (kg CO2 equivalent)	8,320	5,220	4,160	3,750

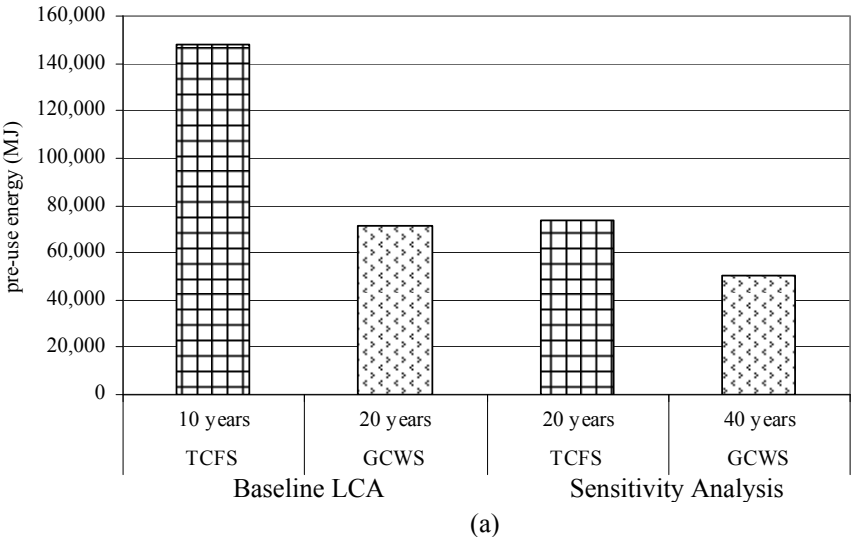

(a)

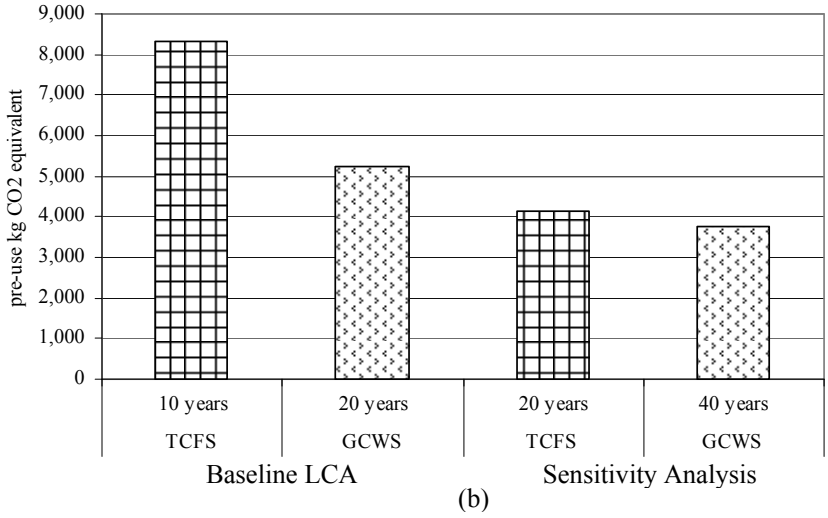

(b)

Figure 4.4.1.1 Sensitivity Analysis Results for Pre-Use Phase:
Pre-Use Energy Consumption (a) and CO2 Equivalent (b)

4.4.2 Post-Use Phase: Recycling as an Alternative to Incineration

Sensitivity analysis focuses on recycling at the end-of-product life for both TCFS and GCWS in order to assess the environmental benefits over landfilling (in the baseline LCA). The results indicate that recycling a TCFS reduces both energy input (-26,900 MJ) and the GWP (-940 kg CO2 equivalent) compared to landfilling. Major energy and GWP reduction of recycling the TCFS resulted from the recycling the PMMA panel (-45 MJ/kg). The energy saved through recycling the aluminum (-104 MJ/kg) significantly impacts the amount of energy recovery and GWP releases for a GCWS. Table 4.4.2.1 and

Figure 4.4.2.1 shows the environmental profiles of different disposal scenarios for each façade system.

Table 4.4.2.1 Sensitivity Analysis Results for Post-Use Phase

Post-Use Phase	Baseline LCA		Sensitivity Analysis	
	TCFS Panel Landfilled	GCWS Landfilled	TCFS Recycled	GCWS Recycled
Post-Use Energy (MJ)	1,740	2,710	-26,900	-19,800
Post-Use GWP (kg CO2 equivalent)	0.46	30	-943	-2,200

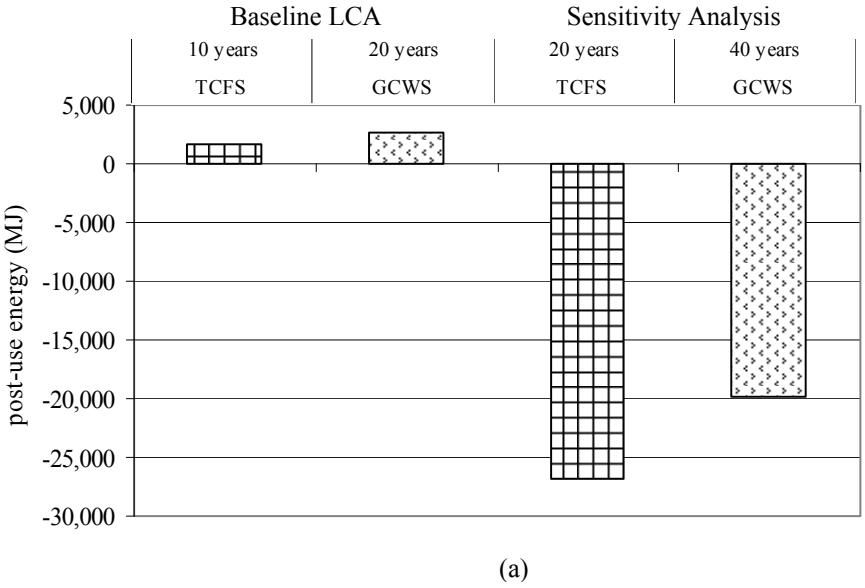

(a)

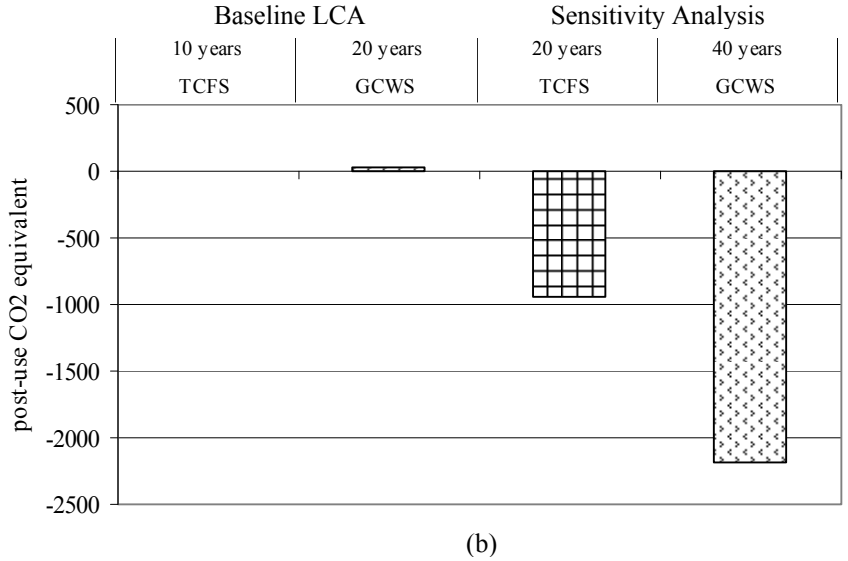

(b)

Figure 4.4.2.1 Sensitivity Analysis Results for Post-Use Phase: Post-Use Energy Consumption (a) and CO2 Equivalent (b)

4.5 LCA Conclusions

A comparative LCA was performed in order to understand the environmental profile of a TCFS relative to that of a GCWS by assessing energy input and global warming potential (GWP) over a 40-year service life of a building. Environmental aspects were analyzed in the pre-use, use, and post-use phases of each façade system's life cycle. For the baseline LCA study, the life span of a TCFS and a GCWS was estimated to be 10 years and 20 years respectively, and the façade area to be covered by the façade system was assumed to be 4.3 m by 4.6 m. The pre-use phase examined the environmental impacts associated with raw material extraction, material processing, and transportation. The use phase inventoried the environmental impacts related to the building's operation–heating, cooling, and lighting–over a 40-year operational period. Building energy simulation using eQUEST was carried out to determine the annual energy consumption of a building, and the energy performance values of each façade system were used as input parameters. The post-use phase focused on environmental impacts associated with a system's end-of-life management and the environmental impacts from landfilling both the TCFS and GCWS were investigated as a baseline LCA study. Inventory data of each façade system were obtained from the SimaPro 7.1 database.

The LCA results showed that a TCFS provided better environmental performance than an uncoated GCWS by consuming 7% less energy and 11% less GWP over a building's 40-year service life. The most significant energy input and environmental emissions occurred during the use phase for both a TCFS and GCWS, where a TCFS consumed approximately 960,000 MJ and an uncoated GCWS consumed approximately 112,000 MJ. A GCWS with high performance low-e coating provided 17% energy reduction compared to a GCWS without low-e coating during the 40 years use phase. However, further validation on the energy performance values of the glazing systems should be carried out as they are highly sensitive to the overall environmental performance. The pre-use phase was the second largest phase in terms of energy consumption and GWP for both a TCFS and GCWS. Production of PMMA (135 MJ/kg; 7 kg CO2 equivalent/kg) and an aluminum frame (169 MJ/kg; 13 kg CO2 equivalent/kg) played dominant roles in increasing the environmental impacts during the pre-use phase. Landfilling the TCFS and GCWS at the post-use phase represented a relatively small

fraction (<1%) of their total life cycle energy and GWP. The environmental impacts associated with the transportation of both the TCFS and GCWS have a minimal impact on the environment relative to the total life cycle energy and GWP.

A sensitivity analysis was carried out to understand how critical uncertain parameters influence overall environmental impacts. New assumptions about the functional unit were made with respect to product durability and recycling the TCFS and GCWS at the end-of-life disposal scenario. The sensitivity analysis showed that a TCFS (1,000,0000 MJ) uses 150,000 MJ (13%) less life cycle energy compared to an uncoated GCWS (1,150,000 MJ). A coated GCWS (950,000 MJ) consumes 230,000 MJ (18%) less life cycle energy than an uncoated GCWS (1,180,000 MJ). Similarly, the sensitivity analysis also revealed that the TCFS (103,000 kg CO2 equivalent) releases 19,000 kg CO2 equivalent (13%) less emissions compared to an uncoated GCWS (122,000 kg CO2 equivalent). The coated GCWS (990,000 kg CO2 equivalent) exhibits 23,000 kg CO2 equivalent (16%) less than that of the uncoated GCWS. Extending the life span and recycling at the post-use phase helps to reduce energy and GWP emissions for the both TCFS and GCWS. The extended durability of materials is more sensitive to the TCFS. Recycling at the end of product's life influenced the total life cycle energy and GWP by less than 1%. For both the baseline LCA and the sensitivity analysis, the use phase of a TCFS and GCWS remains the principal phase for energy consumption and CO2 emissions over a 40-year service life, and the TCFS impacts the environment less than the uncoated GCWS. Table 4.5.1 and Figure 4.5.1 provide quantitative comparisons of energy input and GWP of the baseline LCA and sensitivity analysis for each façade system.

Table 4.5.1 LCA and Sensitivity Analysis Comparisions

Energy (MJ)	TCFS		Uncoated GCWS		Coated GCWS	
	LCA	Sensitivity[1]	LCA	Sensitivity[1]	LCA	Sensitivity[1]
Pre-Use Energy	148,000	74,000	71,200	50,200	71,200	50,200
Use Energy	959,600	959,600	1,123,900	1,123,900	915,000	915,000
Post-Use Energy	1,740	-26,900	2,710	-19,800	2,710	-19,800
Total Energy (MJ)	1,109,340	1,006,700	1,197,810	1,154,300	988,910	945,400

GWP (kg CO2 equivalent)	TCFS		Uncoated GCWS		Coated GCWS	
	LCA	Sensitivity[1]	LCA	Sensitivity[1]	LCA	Sensitivity[1]
Pre-Use GWP	8,320	4,160	5,220	3,750	5,220	3,750
Use GWP	99,790	99,790	116,580	116,580	97,820	97,820
Post-Use GWP	0.46	-940	30	-2,200	30	-2,200
Total GWP (kg CO2 equivalent)	108,110	103,010	121,830	118,130	103,070	99,370

Tables below show % distribution of each analysis by life cycle stage: for example, for the LCA of the TCFS, pre-use, use, and post-use energy account for 13%, 87%, and 0.16% of the total life cycle energy.

	TCFS		Uncoated GCWS		Coated GCWS	
Energy (MJ)	LCA	Sensitivity[1]	LCA	Sensitivity[1]	LCA	Sensitivity[1]
Pre-Use Energy	13%	7%	6%	4%	7%	5%
Use Energy	87%	95%	94%	97%	93%	97%
Post-Use Energy	0.16%	-3%	0.23%	-2%	0.27%	-2%
Total energy (MJ)	100%	100%	100%	100%	100%	100%

Improved durability and recycling of the TCFS save energy by 10%. Durability is an important factor for the TCFS.

	TCFS		Uncoated GCWS		Coated GCWS	
Energy (MJ)	LCA	Sensitivity[1]	LCA	Sensitivity[1]	LCA	Sensitivity[1]
Pre-Use Energy	-	-100%	-	-42%	-	-42%
Use Energy	-		-		-	
Post-Use Energy	-	-106%	-	-114%	-	-114%
Total Energy (MJ)	-	-10%	-	-4%	-	-5%

Total energy use of the TCFS in the baseline LCA is 93% of that of the uncoated GCWS and for the sensitivity analysis, the total energy of the TCFS accounts for 87% of the uncoated GCWS.

	TCFS		Uncoated GCWS		Coated GCWS	
Energy (MJ)	LCA	Sensitivity[1]	LCA	Sensitivity[1]	LCA	Sensitivity[1]
Pre-use energy	208%	147%	-	-	-	-
Use energy	85%	85%	-	-	81%	81%
Post-use energy	64%	136%	-	-	-	-
Total energy (MJ)	93%	87%	-	-	83%	82%

Note: Sensitivity[1] analysis focuses on improved durability and recycling at the end of product life cycle.

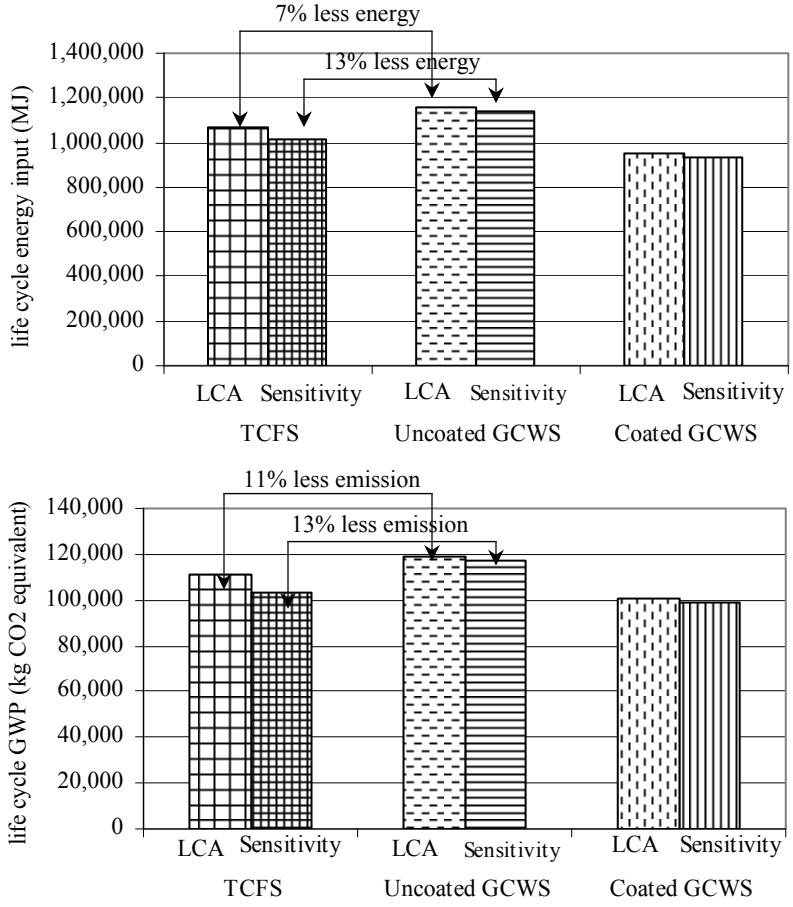

Figure 4.5.1 LCA and Sensitivity Analysis Comparisons

Following recommendations can be made based on the baseline LCA and sensitivity analysis. Materials with low energy and greater durability are recommended at the initial design phase of a façade system, and the greater improvement was realized in the TCFS. Improving energy performance values (U-factor, SHGC, and VLT) of a glazing system is strongly recommended, and further validation process on the performance values should be carried out as they are highly sensitive to the life cycle energy and environmental impact.

Although the environmental impact of the post-use phase is relatively insignificant, recycling materials is recommended over landfilling or incineration in order to recover energy and avoid pollutant emissions resulted from the incineration process. Minimizing the travel distance and material weight helps reduce the negative environmental impacts associated with the transportation process. Table 4.5.2 summarizes the key findings of the LCA study.

Table 4.5.2 Summarized Comparisons of LCA and Sensitivity Analysis

	Processes	Key Findings
Pre-Use	Raw Material Extraction Material Processing Transportation	• Material production of a façade system accounts for 6% (TCFS) ~ 12% (GCWS) of the total life cycle energy and 5% (TCFS) ~ 7 % (GCWS) of the total GWP. • The PMMA (TCFS) and aluminum (GCWS) are the major energy consumers during the pre-use phase. • Transportation of the GCWS is responsible for ~ 15% of the pre-use phase energy; Transportation of the TCFS contributes to little environmental impact.
Use	Operation	• The use phase of a façade system accounts for 87% (TCFS) ~ 94% (GCWS) of the total life cycle energy and 90% (TCFS) ~ 93% (GCWS) of the total GWP. • A coated GCWS results in 19% less energy and GWP than that of an uncoated GCWS.
Post-Use	Recycling/Incineration Transportation	• Recycling or incineration at the end of the product's life reclaims 2% ~ 3% of the total life energy. • Energy input and pollutant emissions for landfilling are minimal. • Environmental impacts associated with transportation are minimal.
Comparison of a TCFS and a GCWS		• A TCFS has ~10% less life cycle energy and GWP compared to an uncoated GCWS. • The improved durability and recycling materials at the end of life cycle enhanced the overall environmental performance, but the use-phase still plays a dominant role in environmental profile; A TCFS with improved durability and recycling at the end-of-product life is 13% less life cycle energy and GWP compared to an uncoated GCWS with improved durability and recycling at the end. • A coated GCWS is 18% less energy and GWP compared to an uncoated GCWS. • Environmental impacts associated with the transportation are insignificant for the total life cycle perspective.

Chapter 5

Conclusions and Future Work

5.1 Structural Conclusions

5.1.1 Problem Statement

The high demand for transparency in contemporary buildings has caused a need for improved structural strength and safety performance in glazing materials. Glass has been a common glazing material for centuries, but its brittleness and catastrophic impact behaviors are still challenging structural attributes. The heavier weight of glass and the need for intermediate mullions in a glass facade impose additional weight to a primary structure. In order to address these shortcomings, a transparent composite façade system (TCFS) was designed as an alternative to a glass wall. The TCFS is a composite panel system made out of a polymer skin and biofiber composite core. The primary objective of this study was to explore the structural characteristics of a TCFS by measuring its structural performance comparing it to that of a glass façade system. The structural performance metrics in this study were characterized by strength, stiffness and impact safety performance.

5.1.2 Summary of Research Activities

Previous studies related to composite panel systems were reviewed in Section 2.1 in order to understand the structural principles and inherent benefits of a composite panel system for use in building applications. Two hybrid glass products consisting of glass skins and cavity-integrated shading devices were reviewed with respect to materials, structural span capability, thermal values and embodied energy. The purpose of product surveys was to understand the unique performance and design features of a TCFS. In Section 2.2, a feasibility study of polymers and biofiber composites designed for outdoor

use was carried out, and the performance of each material was discussed and compared with both glass and glass fiber reinforced composites. A theoretical framework to measure the structural performance of a composite panel under static and impact loading conditions was discussed in Section 2.3. Simple bending theories incorporating a transformed section method and the effective thickness for a composite panel were reviewed. ANSI Z97.1 was referenced to set up an experimental work plan to carry out pendulum impact tests and to understand the safety requirements and classifications of glazing materials.

In Section 3.1, the structural design criteria (i.e., strength and stiffness) of a TCFS were established in accordance with the International Building Code. A new testing frame was designed, fabricated and installed at the University of Michigan to carry out both the static and impact tests (Section 3.2). The primary objective of the static testing was to measure the bending stiffness and stress of a TCFS panel and compare the measurements with the theoretical predictions in order to provide a simple design equation that can be used to estimate a bending stress and displacement during the initial design stage of a TCFS. The static testing of TCFS and glass panels consisted of two-edge support and four-edge support tests, and the test results were compared with simple bending theories, as discussed in Section 2.3 (Section 3.3). A finite element (FE) analysis of a TCFS under static loads was performed and validated by comparing the analysis' outcome to the experimental results.

After the static test was performed, pendulum impact tests were conducted, the results of which were discussed in Section 3.4. The objective of the impact testing was to determine the safety classification, understand post-breakage behaviors and propose recommendations to enhance the impact resistance of a TCFS. Before testing the TCFS, the impact test frame was calibrated using glass specimens. The TCFS and glass panels were each instrumented with a displacement transducer and strain gauges to record time history structural responses. A high speed camera was set up to record global impact behaviors of each specimen during the impact test. The impact results of a TCFS were then compared with those of the glass panels.

5.1.2 Structure Conclusions and Recommendations

Previous studies of a composite panel system in Section 2.1 concluded that composite panels made of a strong, stiff skin material bonded to various types of lightweight core material offer high stiffness- and strength-to-weight ratios, as well as greater impact resistance. The majority of the studies focused on defining simplified design methods (either simple equations or numerical simulation methods), which were validated against test results to provide time efficient, accurate tools that could be used during the initial design stage of a composite panel. It was observed from the product survey that the shading device-integrated insulated glass unit (IGU) is required to meet an ASTM 1300 standard like a typical IGU, and it provides a dynamic solar control ability to improve building energy consumption. Its embodied energy was greatly affected by the material type of the mass input of the shading device. The feasibility study in Section 2.2 revealed that the polymer skin provided lighter in weight, higher impact resistance, lower thermal conductivity, greater optical clarity and increased design flexibility compared to glass, and the biofiber composites core had adequate mechanical properties. Polymers and biofiber composites, however, are prone to weathering effects under UV and moisture, and therefore, it is recommended that protective coatings are applied to enhance the long-term durability and vapor migration of the polymers and biofiber composites. PCs and PMMAs meet the flammability requirements of the International Building Code, but it is recommended that future research is carried out to evaluate the overall fire performance of the polymer skins and the biofiber composite core of a TCFS. The coefficient of thermal expansion of polymers is greater than typical building materials, and therefore, special attention to the joint details of a TCFS is required to allow for its thermal movement. In Section 2.3, the review of simple beam and plate theories concluded that the simple bending theory for the composite panel require a transformed section method and effective thickness calculation because the simple bending theory only applies to a homogeneous section made of isotropic material.

The strength and stiffness criteria of a TCFS were established according to the International Building Code and the specifications of a TCFS met these structural requirements (Section 3.1). The lateral displacement of a TCFS under wind loads was

limited to 19 mm in order to provide a rigid connection between the edge of the panel and the metal spacer. The allowable stress of the TCFS was defined according to Baker's weighted factor, which is based on the yield stress divided by a safety factor of two. A 10-story office building was used as a study model to determine the wind load according to IBC 2003 and to define the actual displacement and bending stress of a TCFS. As a result, a 151 mm thick TCFS section (5 mm PMMA skin + 141 mm cardboard core + 5 mm PMMA skin) provided an acceptable deflection and stress level under the design load based on a 4.1 m floor-to-floor height. As discussed in Section 3.2, a maximum impact design load was verified based on the static testing results of a TCFS that measured the load-displacement behavior. Hand calculation and FEM analysis concluded that the newly installed test frame met the strength and stiffness requirements necessary to conduct impact tests.

The two-edge supported simple beam test indicated that the measurements of a TCFS were in agreement with the values calculated by using the simple beam theory (Section 3.3). However, the four-edge supported static test showed disagreement between the measurements and the theoretical predictions: the simple plate theory predicted a stiffer panel than was actually measured in the TCFS panel. This is due to the fact that the simple plate theory did not account for the shear lag effect present in a TCFS. The open cell core of a TCFS reduces the torsional stiffness, which creates higher flexural stresses at the skin where the core web meets. It is also speculated that microscopic joint failures during the bending test may have occurred between the PMMA skin and cardboard core, resulting in undermining a full composite action. To account for this, a modified simple plate theory was proposed by incorporating adjustments to the simple plate equations. This equation, however, is only applicable to composite panels that have similar aspect ratios, sizes and core geometries to the studied TCFS panel. Therefore, another major recommendation stemming from this study is to carry out an extensive experimental investigation on a four-edge supported TCFS to provide a reliable plate theory that deals with applications with various core types and panel sizes. The main advantage of FEM is that it provides a visual representation of the shear lag effect and help structural optimization of core geometries.

As discussed in Section 3.4, in place of impact testing, a thorough review of the ANSI Z97.1 specifications was conducted, and the calibration process of the impact testing frame was performed using the glass samples before executing the impact test of the TCFS specimen. The breakage mode of the glass samples confirmed that the newly developed testing frame conformed to the ANSI Z97.1 requirement. It was observed that the laminate glass sheet did not develop a hole larger than the size specified when the impact pendulum was dropped from a height of 457 mm, and therefore, it conformed to the Class B safety classification of ANSI Z97.1. The tempered glass panel (6 mm thick) was able to withstand the initial drop of 457 mm without failure, but it failed at the 2nd impact at a lower drop height. The fully tempered glass also complied with the Class B safety classification according to broken particles weight requirement of ANSI Z97.1. Under the impact test of the TCFS specimen at the drop height of 457 mm, the PMMA skin developed circular and diagonal fractures on both the front and rear skins near the point of impact. The cardboard core underwent shear and material failure. Debonding occurred at the epoxy joints, but the broken PMMA skins were still in contact with the cardboard core. It was observed from the time history and displacement measurements that the TCFS panel absorbed less impact energy than did the glass panels, but it is postulated that the TCFS provides greater residual strength after impact. The Charpy impact test was conducted to verify whether the PMMA skin maintained a certain impact resistance after exposure to weathering conditions. The Charpy test confirmed that the PMMA conformed to the safety glazing requirements of the ANSI Z97.1 standard. Therefore, it is concluded that the TCFS conforms to the Class B requirements of the safety glazing criteria of ANSI Z97.1. Some speculations and recommendations can be made from the impact tests regarding the scope and safety criteria of the ANSI Z97.1 standard. Based on the results of the impact test, the initial impact was found to reduce the structural properties of the fully tempered glass. The results suggest that the ANSI Z97.1 standard should stipulate that a specimen must be subjected to a second or even third impact in order to measure the residual strength, and credit would be given to a tested panel that could withstand additional impact. By doing this, human injury could potentially be minimized by guaranteeing the impact strength and improving the residual strength of the glazing material.

5.1.4 Study Limitations and Future Work

The simplified plate equation for the four-edge supported TCFS discussed in section 3.3 is specific to the current studies, and therefore it is recommended that further experiments be carried out concerning the flexural stiffness in relation to various core typologies, core cell sizes and panel sizes. A series of adjustment factors in modified simple plate equations can be established, which accounts for the shear lag effects and torsional stiffness of the composite sections of a TCFS.

Since section 3.4 focused on defining the safety classification of a TCFS panel that was restrained at four edges, a large scale impact test including joint details is recommended in order to investigate post-breakage modes at the interface between the panels and to establish a solid understanding of the impact performance of a two-edge supported TCFS. Further, additional impact testing at the 1219 mm-drop height is recommended to better understand the impact behaviors of a TCFS and to make recommendations on the material thickness, core size, core geometry and panel size of a TCFS.

Further studies on fabrication methods for a TCFS are recommended in order to enhance the panels' structural integrity and quality during the fabrication process. For this study, a laser cutter and CNC router were used to fabricate the skin and core components. However, an automated method for product assembly and application of the different adhesives could alter the static and impact performance of a TCFS.

5.2 LCA Conclusions

5.2.1 Problem Statement

Buildings are responsible for 40% of the energy consumption and 39% of the CO2 emissions in the US, and typical glazed facades play key roles in building energy loss due to their lower thermal performance. High performance glass such as low-e coated or heat reflective glass offers better thermal performance, preventing undesired heat loss or gain during a building operation phase. However, the coatings used on these types of glass may not be as effective in certain climate zones, and create a glare problem for adjacent buildings. A TCFS provides a sustainable alternative to high performance glass because the biofiber composite core acts as a shading device while the airspace

between the polymer skins provides adequate insulation. The material selection criteria of the skin and core of a TCFS are also more sustainable because they are recyclable and renewable. A life cycle assessment (LCA) method was selected as a sustainability measuring tool because it examines the environmental impacts associated with all of the life cycle stages of a product. The environmental performance of a façade system in this study was characterized by the energy consumption and CO2 emissions produced by a TCFS through all stages of its life.

5.2.2 Summary of Research Activities

The theoretical framework of an LCA in accordance with ISO 14040 was reviewed and its application to a window system was discussed in section 2.4. In Chapter 4, a comparative life cycle assessment (LCA) technique was employed to measure the environmental impacts of two façade systems—a transparent composite façade system (TCFS) versus a glass curtain wall system (GCWS)—with respect to energy use and greenhouse gas emissions over the model building's 40-year service life.

The studied boundary of the façade system was divided into three stages (pre-use, use and post-use), and an LCA inventory was taken for each stage. The pre-use phase inventory included measuring the energy input and pollutant emissions associated with raw material extraction and processing, material production and transportation. The use phase measured the operational energy and pollutant emissions associated with heating, cooling, and lighting a building over its 40-year service life. The post-use phase focused on assessing the energy input and emissions attributed to the product's end-of-life management and transportation.

The functional unit of the TCFS was assumed to be a 10 year service life for a façade area that is 4.9 m wide by 4.1 m high whereas, for a GCWS with the same façade area, the life span was assumed to be 20 years. The details of each façade system that were developed to meet the structural design criteria established in Section 3.1 were used to calculate the mass input (kg) required per functional unit. As with the previous studies, 10-story office building located in Detroit, MI was used as the study's model. The distance between product suppliers and the building site was assumed to be 1,600 km, and the distance between the building site and the landfill was assumed to be 50 km. Life

cycle inventory data was obtained from the SimaPro 7.1 database, and eQUEST, a building energy simulation tool, was used to quantify the annual energy usage of the model building. A coated GCWS (high performance low-e coating) was also included in the simulation study in order to better understand the energy saved from the low-e coating.

5.2.3 LCA Conclusions and Recommendation

The baseline LCA study revealed that the total life cycle energy of the TCFS was estimated to be 93% of that of the uncoated GCWS, and the total emission of kg CO2 equivalent for the TCFS was determined to be 89% of the GCWS. The pre-use phase of the TCFS accounted for twice the embodied energy of the GCWS because of the energy-intensiveness of producing PMMA. The energy consumption was highest during the use phase for both the TCFS and GCWS; it consumed 87% and 95% respectively of their total life cycle energy. For the post-use phase, the resulting energy and greenhouse gas emissions associated with landfilling were insignificant (<1%). The environmental impacts associated with transportation was also estimated to be minimal (<1%).

A sensitivity analysis focusing on product durability and recycling disposal scenarios improved the overall life cycle performance of the TCFS by 5% and the uncoated GCWS by 3%. The energy saved from the high performance low-e coating resulted in approximately a 17% reduction in the total life cycle energy. The results indicated that the total life cycle energy of the TCFS was 87% of that of the uncoated GCWS, and the emissions of the TCFS were 87% of the total emissions of the uncoated GCWS.

In warm climate zones, the life cycle energy of a TCFS is speculated to be significantly lower than the uncoated GCWS because the TCFS is able to block intense sunlight due to the shading properties of the biofiber composite core. If the core geometry of the TCFS is reconfigured so that the opening of the core cell is closed off while still admitting an adequate amount of daylighting, its use-phase energy consumption is postulated be comparable to that of a high performance low-e coated GCWS. Although at present a low-e coating on a polymer surface is not available in the market, a low-e

coated TCFS would greatly enhance both the U-factor and SGHC, resulting in reducing costs and saving energy.

The major recommendations for further research are to carry out a parametric study of a TCFS to determine the optimum core geometries for different climate zones and building orientations. It is a well-known principle of glazing systems that, for cold climate zones, the U-factor should be minimized while the SHGC and VLT should be optimized. For a warm climate, on the other hand, reducing the SHGC of a TCFS is more critical than enhancing its U-factor. When selecting building materials, durability should be a priority in order to avoid energy consumption associated with fabricating, transporting and installing replacements. Environmental impacts can be further reduced by using materials with low embodied energy that incorporate energy efficient fabrication processes and technologies. Using lightweight materials requires smaller primary structural members, resulting in cost savings and reduced energy consumption. Minimizing the travel distance can also lessen the negative impacts on the environment, and improving the efficiency of the grid electricity generation lowers the carbon intensity associated with the power generation.

5.2.4 Study Limitations and Future Work

It has been shown that SHGC dominates a building's energy consumption in warm climates and U-factor plays a key role in cold climates. Considering this, the performance values of a TCFS will vary depending on its sectional and material attributes. A parametric study would address these variations by determining the effects of design parameters (i.e., core cell size, typology) on a building's energy performance in different climates. The parametric study would also be of great value to designers for the purpose of providing a climate-responsive design guideline and a wide range of core typologies that could optimize building energy performance.

The building energy performance presented in this research was based on a single SHGC value of a TCFS which was numerically computed as per NFRC 200, and therefore, the building energy usage calculated in this study may change when a dynamic SHGC is used. In order to measure the dynamic SHGC, further experimental studies are

essential to define the range of SHGC throughout a day, a year and in climates with unique characteristics (i.e., different seasons and different sun angles).

Future LCA studies should include the environmental impacts associated with the assembly fabrication, installation, maintenance, replacement, and dismantling of a TCFS in an effort to allow for a holistic environmental assessment. Since the environmental performance of a façade system is highly dependant on building types, orientations, and site locations, additional LCAs as a function of the aforementioned parameters of building type (e.g. a residential building, office building), façade orientation, and a different climate zone, could be performed in order to recommend climate-responsive design guidelines for TCFS panels used in different applications.

A life cycle cost analysis should be calculated to ensure that a TCFS is economically as viable as a GCWS. This study will likely involve extensive cost data collection for raw material, material manufacturing, product fabrication, transportation and installation. These data would likely be gathered through contacting relevant parties directly and through published literature. For the use and post-use phases, the economic study should be relatively explicit because the cost collection will be based mainly on operational, disposal, environmental, and transportation costs.

APPENDICES

Appendix A Material Properties

Table A Material Properties of Polymers and Glass

		Transparent recyclable materials				
		Thermoplastic				**Glass**
		Polycarbonate PC	**Polyesters PET**	**Polypropylene PP**	**Polymethylmethacrylate PMMA**	
Mechanical Properties						
Density (ρ)	Mg/m^3	1.14-1.21	1-1.40	0.89-0.92	1.16-1.22	2.44-2.5
E-modulus (E)	GPa	2.21-2.44	0.3-0.41	0.9-1.55	2.24-3.8	68-72
Poison's Ratio (ν)	dimensionless	0.38-0.42	0.34	0.43	0.37-0.43	0.2
Yield Strength (σ_y)	MPa	58.6 - 70.0	1.30 - 72.2	20.7-37.2	45.0 - 86.0	31-35
Ultimate Strength (σ_{ult})	MPa	65.0 - 72.4	9.70 - 53.0	17.2 - 31.0	30.3 - 100	31-35
Elongation at yield	%	6.00 - 50.0	20.0 - 50.0	5.00 - 37.0	-	0
Elongation at break	%	10.0 - 125	50.0 - 900	10.0 - 600	3.50 - 40.0	0
Thermal Properties						
Thermal Conductivity	W/m-K	0.19-0.22	0.15-0.30	0.11-0.17	0.08-0.25	0.7-1.3
Specific heat capacity	J/kg-K	1535-1634	1160-1587	21870-1956	1485-1606	850-950
Coeff. of thermal exp.	10^-6/K	120.1-136.8	99-180	122-180	72-162	9-9.5
Melting point	C	220-225	150 - 223	138 - 164	130-157	800-1730
Service Temp.	C	-40-120	-30-130	85.2	-50-100	-270-250
Environmental Attributes						
Energy content	MJ/Kg	120-130	89-95	76-84	97-105	20-25
Recycle potential		High	High	High	High	High
Other Attributes Compared to Other Polymers						
UV resistant		No	No	No	Yes	Yes
Impact resistant		Yes	No	Yes	No	No
Fatigue resistant		No	No	No	No	Yes
Flame resistant		No	No	No	No	Yes
Wear resistant		No	No	No	No	Yes
Resilient		Yes	Yes	Yes	No	No
Cost	$/kg	3.8-4.0	1.25-2.5	0.9-1.0	1.7-2.45	0.68-1

From "Materials and Design" by Ashby, M. and Johnson, K., 2005; www.matweb.com

Appendix B Characteristics of Polymers and Glass

Table B Characteristics of Polymers and Glass

	Pros	Cons
PC	Easy to bond and connect Easy to manufacture curved forms High creep resistant High impact resistant High service temperature Recyclable Lightweight	High processing temperature Expensive Low heat/flame resistant Low UV resistant Low weatherability Susceptible to moisture absorption Low abrasion resistant
PET	Tough and rigid Ease of manufacturing Recyclable Lightweight	Low resistant to acids and bases Low heat/flame resistant Low solvent resistant
PMMA	Easy to bond and connect Easy to manufacture curved forms High UV resistant Recyclable Lightweight	Brittle Low weatherability Low heat/flame resistance Susceptible to moisture absorption
PP	Ease of manufacturing Low coefficient of friction High moisture resistant High fatigue resistant High abrasion resistant High service temperature High chemical resistant High flexural strength High impact r Recyclable Lightweight	Low UV resistant Low weatherability Low heat/flame resistance Low bond ability Low solvent resistant
Glass	UV resistant Recyclable Low embodied energy High service temperature High heat resistant	Heavy weight High heat conductivity Brittle Expensive to manufacture curved sheet

From “Industrial plastics,” by E. Lokensgard, 2004.

Appendix C Biocomposites vs. Synthetic Fiber Composites

Table C Characteristics of Biocomposites Synthetic Fiber Composites

	Biocomposites		**Synthetic fiber composites**	
	Fiber	Matrix	Fiber	Matrix
Material	▪ Flax ▪ Jute ▪ Hemp ▪ Straws ▪ Sisal ▪ Leaf fiber ▪ Grass fiber ▪ Kenaf	▪ Bio-based thermoplastic from renewable resources o Cellulose plastic o Starch plastic o Poly lactic acid o Poly hydroxyl alkanoate ▪ Bio-based thermoset plastic from renewable and petroleum resources o Bio-based polyurethane o Bio-based epoxy o Sorona	▪ Glass fiber ▪ Carbon fiber	▪ Thermoplastics o Polypropylene o Thermoplastic polyester o Nylon o Polycarbonate ▪ Thermoset resins o Polyester o Epoxy o Phenolic o Polyurethane o Melamine
Advantages	▪ Low cost ▪ Low density ▪ High specific strength ▪ High specific modulus ▪ Excellent tensile and flexural properties ▪ Good acoustic and thermal insulation ▪ Low embodied energy ▪ Enhanced energy recovery ▪ Low CO2 emissions ▪ Biodegradable	▪ Enhanced energy recovery ▪ Low CO2 emissions ▪ Biodegradability	▪ Low cost ▪ High specific strength ▪ High specific modulus ▪ High moisture resistance ▪ Chemical resistance ▪ Resistance to bacteria growth	▪ Versatile ▪ Low cost
Disadvantages	▪ Susceptible to moisture absorption ▪ Susceptible to microbial attack ▪ Surface treatment required to achieve good matrix adhesion	▪ Susceptible to moisture absorption ▪ Susceptible to microbial attack	▪ Uneven deformation under unidirectional reinforcement ▪ Unsafe ▪ Unhealthy	▪ High pollutant emission ▪ Use of non-renewable resources

From "Natural fibers, biopolymers, and biocomposites," by Mohanty, A., Misra, M., & Drzal, L (Eds.), 2005; "Bio-based polymers and composites'" by Wool and Sun, 2005.

Appendix D Wind Load Calculation in accordance with ASCE 7-02

Velocity pressure (q_z) is calculated using the following equation and parameters given in ASCE 7-02, thus resulting in 0.904 kPa.

$$q_z = 0.00256\, K_z\, K_{zt}\, K_d\, V^2\, I \qquad \text{(Equation D-1)}$$

Where,

q_z = velocity pressure at height, z (assuming 40 m), as given in Eq. 6-15, p. 31

K_z = velocity pressure exposure coefficient evaluated at 40 m, 1.08 as given in Table 6-3, p. 75

K_{zt} = topographic factor, 1 as given in Figure 6-4, p. 47-48

K_d = wind directionality factor. 0.85 as given in Table 6-4, p.76

V= basic wind speed in Michigan, 145 km/hr

I = importance factor, 1 as given in Table 6-1, p.73

The design pressure for components and cladding is calculated using the following equation and parameters given in ASCE 7-02.

$$p = q\,(GCp) - qi\,(GCpi) \qquad \text{(Equation D-2)}$$

Where,

p = pressure on component for building with h > 18.3 m. as given in Eq. 6-23, p. 33.

q = q_z for windward wall calculated at height z above the ground, 0.904 kPa as calculated above.

q_i = q_z value at mean roof height, h, for leeward wall, side walls, and roof.

GC_{pi} = internal pressure coefficient. ±0.18 as given in Fig. 6-5, p.49.

GC_p = external pressure coefficient as given in Fig. 6-17, p. 67.

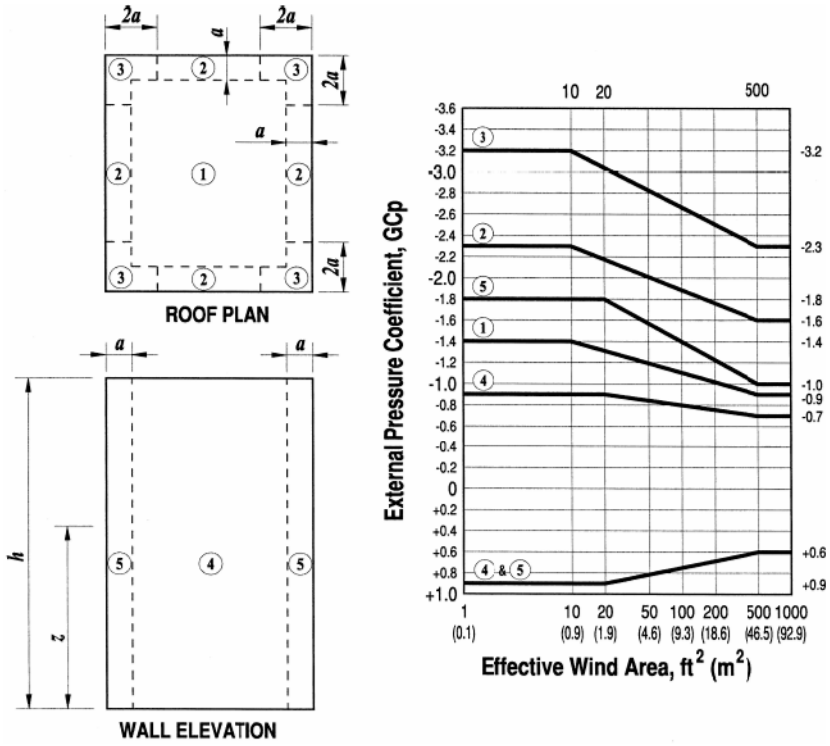

Figure D-1 External Pressure Coefficient, G Cp

Source: ASCE7-02, Fig. 6-17, page 67

Table D-1 External Pressure Coefficient (G Cp) from the Figure Above

Wall component	Effective facade area	Typical zone (Zone 4)		Corner zone (Zone 5)	
		GC_p	$-GC_p$	GC_p	$-GC_p$
Mullion	19.3^2	0.68	-0.75	0.68	-1.22
Panel	19.3^2	0.68	-0.75	0.68	-1.22

Therefore, resulting design wind load in typical and corner zone becomes -0.848 kPa and -1.256 kPa respectively.

Figure D-2 Final Design Wind Load

z (m)	Façade pressure (kPa)			
	Zone 4		Zone 5	
	Windward	Leeward	Windward	Leeward
40	0.775	0.840	0.775	1.256

Appendix E Joint Shear Testing

The joint between PMMA and cardboard was tested under tensile force in order to verify the shear strength and shear modulus of the adhesive of two-part epoxy. The PMMA was routed with 5 mm wide x 2 mm deep groove cut to improve the bonding connection with the cardboard. Figure E-1 illustrates the testing set-up and specimen information.

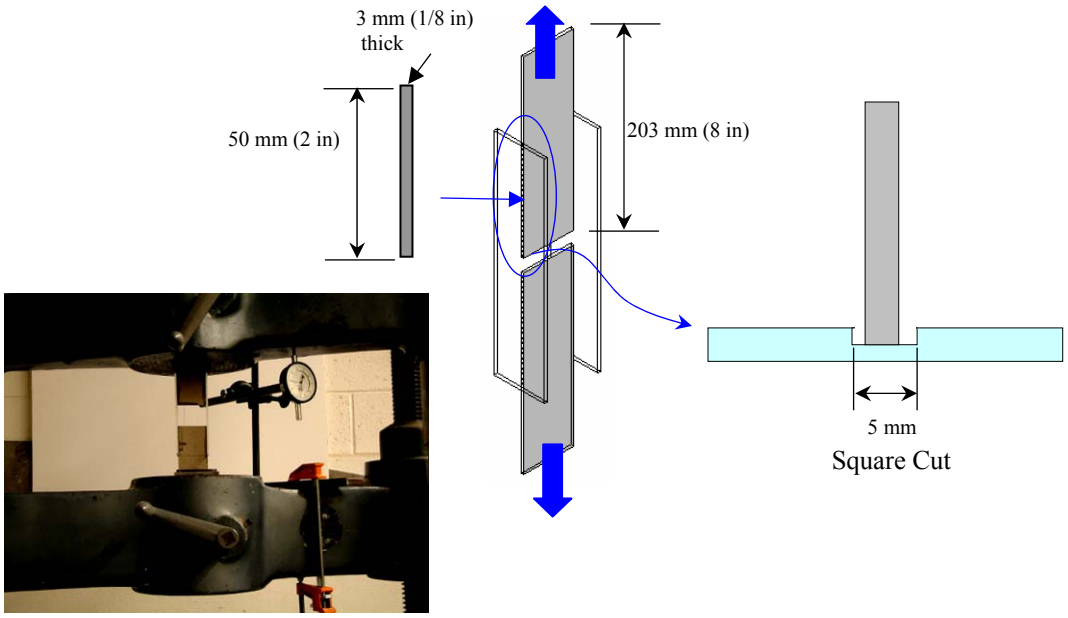

Figure E-1 Testing Set-Up and Specimen

After the specimen was clamped inside the testing machine, the shear load was applied in 445 N increments, and the specimen failed at around 3114 N. The maximum shear strength was calculated based on the load at failure divided by the area of joint connection, and the shear modulus was computed as maximum stress divided by the final deflection. The measured shear strength was around 9.65 MPa with the shear modulus of 213.7 MPa, as noted in Figure E-2.

Table E-1 Experimental Measurement of Load vs. Strain

Deflection (mm)	Increment (mm)	Load (N)	Strain (%)	Shear Stress (MPa)
0	0	0	0	0.00
0.762	0.762	44500	0.75	1.38
1.6764	0.9144	89000	1.65	2.76
2.5146	0.8382	133500	2.48	4.14
2.921	0.4064	178000	2.88	5.52
3.556	0.635	222500	3.5	6.89
4.064	0.508	267000	4	8.27
4.572	0.508	311500	4.5	9.65

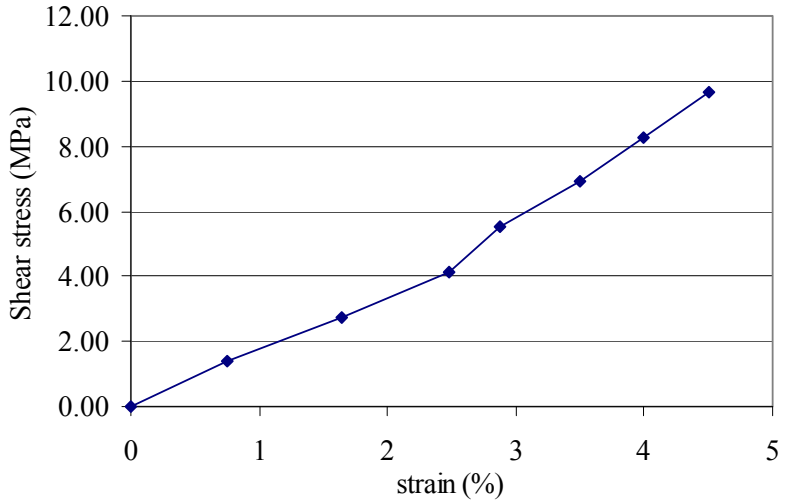

Figure E-2 Shear Stress vs. Strain Curve

After a tensile test was conducted, a peel-off test was performed to confirm the peel-off strength under the twist loading. Clear peel-off along the groove cut was found at the joint area, and material failure of the cardboard occurred, as shown in Figure E-3.

Figure E-3 Material Failure at the Cardboard (left) After Shear Test and the Joint Failure (right) after Peel-Off test

Appendix F LRFD for Testing Frame Members

1. Flexural member in accordance with load resistance factor design (LRFD)

A. Vertical frame of the specimen holder: bending and torsional-buckling moment check

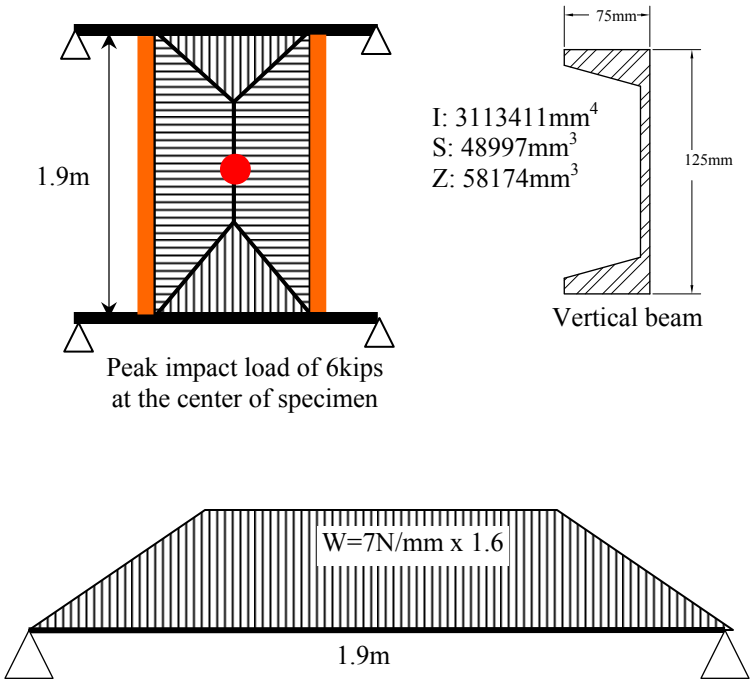

A.1 Yielding

Nominal flexural strength (M_n) = $M_p = F_y Z_x$ = 22.24 kN-mm

Design flexural strength = $M_n \times \Omega_f$ = 20.14 kN-mm > 8.09 kN-mm (Pass)

Where, F_y = specified minimum yield stress (248MPa),

Zx = plastic section modulus about the x-axis (58174 mm^3),

Ω_f = resistance factor of 0.90 (LRFD).

A.2 Lateral-Torsional Buckling

Lateral-torsional buckling does not apply due to $L_b = L_p$ as per ASCI (ASCI: p. 16.1-47). Where, L_b =distance between braces, and L_p = limiting laterally unbraced length for limit state of yielding.

A.3 Result: There is no risk of yielding or buckling of the steel channel under the design load. Expected deflection would be 2.794 mm using simple beam theory.

B. Horizontal frame of the specimen holder– bending and buckling moment check

The single leg angle needs to check with respect to the yielding, lateral-torsional and leg local buckling. Critical moment describes as follows.

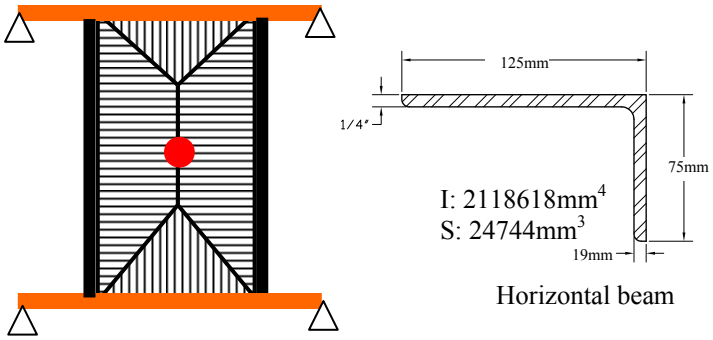

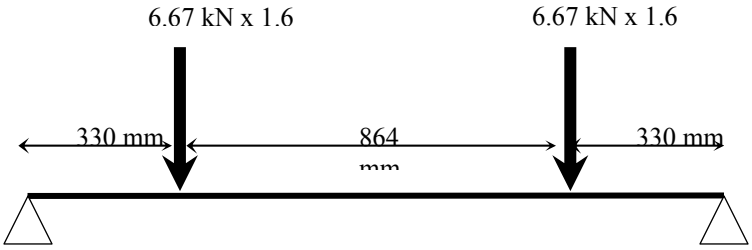

B.1 Yielding

Nominal flexural strength (M_n) = 1.5M_y = 8.33 kN-mm

Design flexural strength = M_n x Ω_f = 7.50 kN-mm > 5.46 kN-mm (Pass)

Where, M_y = 5.55 kN-mm, and Ω_f = resistance factor of 0.90 (LRFD).

B.2 Lateral-Torsional Buckling

Lateral-torsional buckling moment of the unequal-leg angles can be calculated using the following equation.

$$Me = \frac{4.9EI_zC_b}{L^2}\left(\sqrt{\beta_w^2 + 0.052\left(\frac{Lt}{r_z}\right)^2} + \beta_w\right) = 14.53kN - mm \ < 5.46\text{kN-mm (Pass)}$$

Where

C_b= lateral-torsional buckling modification factor as per AISC (= 1),

L = laterally unbraced length (= 864 mm),

I_z = minor principal axis moment of inertia (= 586886 mm^4),

r_z = radius of gyration for the minor principal axis (= 0.853),

t = angle leg thickness (= 6 mm),

β_w = sectional property for unequal leg angles as per AISC (= -2.99)

B.3 Leg Local Buckling

For the compact section, leg local buckling does not apply as per AISC.

B.4 Result: The steel angle of the vertical specimen holder is not subjected to yield or local buckling under the design load. Expected deflection is 2mm.

2. Compressive member in accordance with load resistance factor design (LRFD)

C. Diagonal angle – compressive strength for buckling of members

Slenderness ratio (KL/r) = 2565 mm/1.51 = 66.88

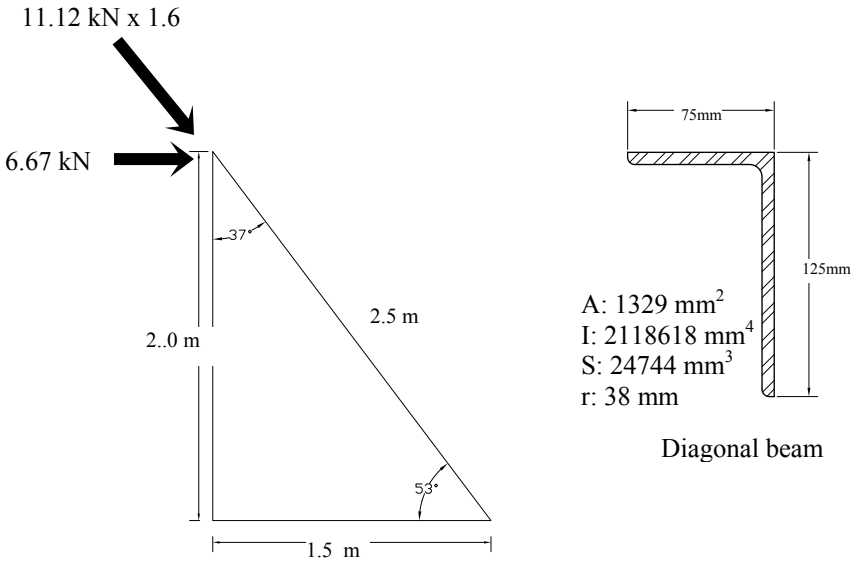

C.1 Compressive strength for flexural buckling of members

The nominal compressive strength (P_n) = $F_{cr}A_g$ = 77.0 kN

The design compressive strength = P_n x Ω_c = 69.4 kN > 17.8 kips (Pass)

When, $\frac{KL}{r} \leq 4.71\sqrt{\frac{E}{F_y}} = 66.88 \leq 133.68 \rightarrow F_{cr} = \left[0.658^{\frac{F_y}{F_e}}\right] F_y = 122.7$ MPa

Where, $F_e = \frac{\pi^2 E}{\left(\frac{KL}{r}\right)^2} = 319.2$ MPa

and Ω_c= resistance factor of 0.90 (LRFD)

C.2 Result: There is no risk of buckling at the unequal leg angle under the actual load.

Appendix G Charpy Impact Testing Report Provided By Bodycote Testing Group

Bodycote

TESTING GROUP
www.bodycote.com
www.mtusa.bodycote.com

30004061

University of Michigan

Charpy Impact Resistance of Acrylic and Polycarbonate

Date: 18th April 2007

Prepared By:

Ahamed Shabeer, Ph.D
Polymer Scientist
ashabeer@bodycoteusa.com

Prepared For:
Kyoung-Hee Kim
University of Michigan
1853 Lake Lila Drive
#9C3
Ann Arbor, MI 48105
(347) 738-1390 x

Reviewed By:

Hosein Shahnazi
Laboratory Manager
hshahnazi@bodycoteusa.com
Bodycote Testing Group
http://www.mtusa.bodycote.com/

Bodycote Testing Group
1975 North Ruby Street • Melrose Park • Illinois • 60160 • USA • Tel: +1 (708) 236-5360 • Fax: +1 (708) 236-5363

INDEX

REPORT

APPENDIX

Bodycote Testing Group
1975 North Ruby Street • Melrose Park • Illinois • 60160 • USA • Tel: +1 (708) 236-5360 • Fax: +1 (708) 236-5363

Introduction

University of Michigan requested Bodycote Testing Group perform non-standarized charpy impact testing on acrylics and polycarbonates (weathered and unweathered). University of Michigan sent six sample groups with three specimens each. University of Michigan also sent two acrylic calibration samples for initial measurements. The sample identification as per University of Michigan and Bodycote Testing group is provided in Table1. This report summarizes the charpy impact test on acrylics and polycarbonate samples.

Testing

Charpy Impact Test

The unnotched charpy impact strength was measured for the samples as per the instructions given by the University of Michigan. The specimen was tested with flat side with the compression side (marked on the specimens) subjected to the impact load. The impact testing was done on a Testing Machines, Inc. Impact Tester with a 5 ft. lb Charpy Impact Hammer. Specimens were conditioned at 23°C, 50% RH for 40 hours prior to testing. The reported values are an average of all tested specimens. The impact property average and standard deviation values are reported in Table 2. The individual data appears in the Appendix to this report. As per the requirement of the client, photographs of the test setup before testing and the broken specimen after testing for two specimens were provided in the report.

Bodycote Testing Group
1975 North Ruby Street • Melrose Park • Illinois • 60160 • USA • Tel: +1 (708) 236-5360 • Fax: +1 (708) 236-5363

Table 1. Specimen Identification

S.no	University of Michigan ID	Bodycote ID
1	Calibration Sample 1	30004061-A1
2	Calibration Sample 1	30004061-A2
3	1-(UN_PC_GP1)	30004061-A3
4	2-(UN_PC_GP2)	30004061-A4
5	3-(UN_PC_GP3)	30004061-A5
6	4-(PC_GP1)	30004061-A6
7	5-(PC_GP2)	30004061-A7
8	6-(PC_GP3)	30004061-A8
9	7-(UN_PC_AR1)	30004061-A9
10	8-(UN_PC_AR2)	30004061-A10
11	9-(UN_PC_AR3)	30004061-A11
12	10-(PC_AR1)	30004061-A12
13	11-(PC_AR2)	30004061-A13
14	12-(PC_AR3)	30004061-A14
15	13-(UN_PMMA1)	30004061-A15
16	14-(UN_PMMA4)	30004061-A16
17	15-(UN_PMMA5)	30004061-A17
18	16-(PMMA1)	30004061-A18
19	17-(PMMA4)	30004061-A19
20	18-(PMMA5)	30004061-A20

Bodycote Testing Group
1975 North Ruby Street • Melrose Park • Illinois • 60160 • USA • Tel: +1 (708) 236-5360 • Fax: +1 (708) 236-5363

Table 2. Unnotched Charpy Impact Test

Sample	Specimen	Average Impact Resistance (ft-lbf/in of width)
Calibration Sample	30004061-A1	5.24
	30004061-A2	5.28
	Average	5.260±0.02828
(UN_PC_GP)	30004061-A3	7.313
	30004061-A4	7.510
	30004061-A5	7.482
	Average	7.435±0.1065
(PC_GP)	30004061-A6	6.619
	30004061-A7	6.628
	30004061-A8	6.539
	Average	6.595±0.04899
(UN_PC_AR)	30004061-A9	7.021
	30004061-A10	7.139
	30004061-A11	7.173
	Average	7.111±0.0797
(PC_AR)	30004061-A12	7.026
	30004061-A13	6.925
	30004061-A14	7.101
	Average	7.017±0.0883
(UN_PMMA)	30004061-A15	1.136
	30004061-A16	1.160
	30004061-A17	1.134
	Average	1.143±0.0144
(PMMA)	30004061-A18	0.746
	30004061-A19	0.738
	30004061-A20	0.797
	Average	0.760±0.0320

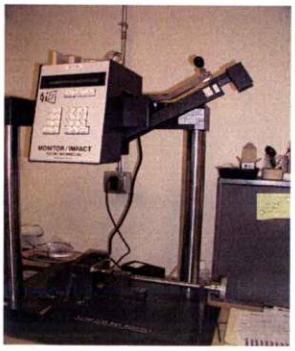

Figure 1. Charpy Impact Test set up

Bodycote Testing Group
1975 North Ruby Street • Melrose Park • Illinois • 60160 • USA • Tel: +1 (708) 236-5360 • Fax: +1 (708) 236-5363

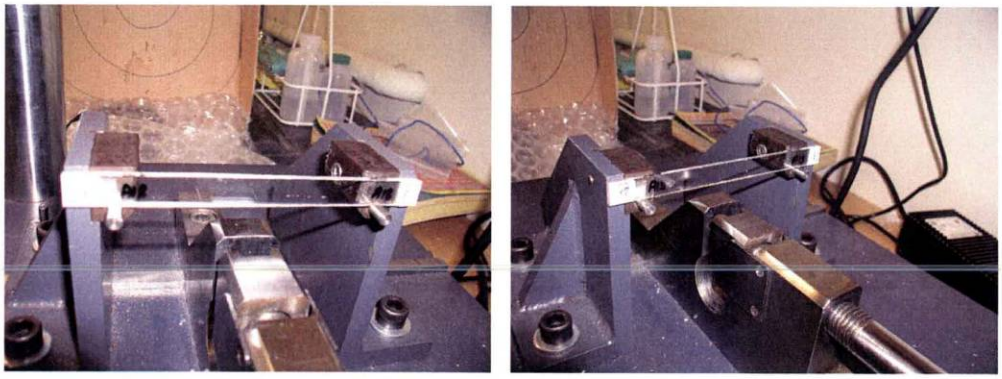

Figure 2. Specimen 16 (PMMA1) and 17(PMMA4) before testing

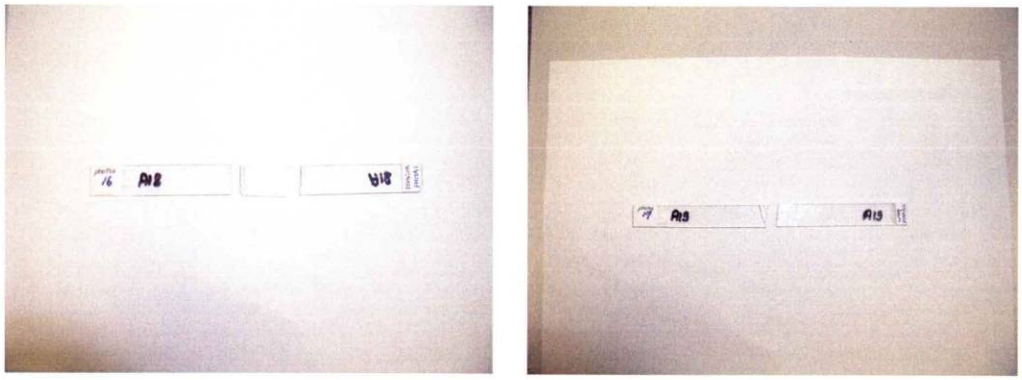

Figure 3. Specimen 16 (PMMA1) and 17(PMMA4) after testing

Bodycote Testing Group
1975 North Ruby Street • Melrose Park • Illinois • 60160 • USA • Tel: +1 (708) 236-5360 • Fax: +1 (708) 236-5363

APPENDIX

Bodycote Testing Group
1975 North Ruby Street • Melrose Park • Illinois • 60160 • USA • Tel: +1 (708) 236-5360 • Fax: +1 (708) 236-5363

Bodycote

TESTING GROUP
www.bodycote.com
www.mtusa.bodycote.com

30004061
University of Michigan
Bodycote Testing Group Melrose Park, IL 60160
4/18/2007
Test Temp.: 74^{0}F,50% RH

University of Michigan ID	Bodycote Specimen ID	Depth (in)	Width (in)	Span (in)	Breakage	Impact Resistance (ft-lbf/in of Width)
Calibration Sample 1	30004061-A1	0.1134	0.494	3.987	Complete	5.240
Calibration Sample 1	30004061-A2	0.1130	0.495	3.987	Complete	5.280
1-(UN_PC_GP1)	30004061-A3	0.1170	0.521	2.394	Non Break	7.313
2-(UN_PC_GP2)	30004061-A4	0.1179	0.522	2.394	Non Break	7.510
3-(UN_PC_GP3)	30004061-A5	0.1184	0.525	2.394	Non Break	7.482
4-(PC_GP1)	30004061-A6	0.1100	0.512	2.394	Non Break	6.619
5-(PC_GP2)	30004061-A7	0.1117	0.498	2.394	Non Break	6.628
6-(PC_GP3)	30004061-A8	0.1113	0.503	2.394	Non Break	6.539
7-(UN_PC_AR1)	30004061-A9	0.1165	0.512	2.394	Non Break	7.021
8-(UN_PC_AR2)	30004061-A10	0.1162	0.512	2.394	Non Break	7.139
9-(UN_PC_AR3)	30004061-A11	0.1165	0.510	2.394	Non Break	7.173
10-(PC_AR1)	30004061-A12	0.1155	0.511	2.394	Non Break	7.026
11-(PC_AR2)	30004061-A13	0.1152	0.513	2.394	Non Break	6.925
12-(PC_AR3)	30004061-A14	0.1156	0.514	2.394	Non Break	7.101
13-(UN_PMMA1)	30004061-A15	0.1120	0.512	3.987	Complete	1.136
14-(UN_PMMA4)	30004061-A16	0.1131	0.492	3.987	Complete	1.160
15-(UN_PMMA5)	30004061-A17	0.1134	0.490	3.987	Complete	1.134
16-(PMMA1)	30004061-A18	0.1131	0.500	3.987	Complete	0.746
17-(PMMA4)	30004061-A19	0.1128	0.495	3.987	Complete	0.738
18-(PMMA5)	30004061-A20	0.1131	0.495	3.987	Complete	0.797

Tested by : Dr.Ahamed Shabeer
Signature :
Reviewed by:

Bodycote Testing Group
1975 North Ruby Street • Melrose Park • Illinois • 60160 • USA • Tel: +1 (708) 236-5360 • Fax: +1 (708) 236-5363

Bodycote

TESTING GROUP
www.bodycote.com
www.mtusa.bodycote.com

30004061
University of Michigan
Bodycote Testing Group Melrose Park, IL 60160
4/18/2007
Test Temp.: 74^{0}F,50% RH

University of Michigan ID	Bodycote Specimen ID ID	Depth (in)	Width (in)	Span (in)	Breakage	Impact Resistance (ft-lbf/in of Width)
Calibration Sample 1	30004061-A1	0.1134	0.494	3.987	Complete	5.240
Calibration Sample 1	30004061-A2	0.1130	0.495	3.987	Complete	5.280
1-(UN_PC_GP1)	30004061-A3	0.1170	0.521	2.394	Non Break	7.313
2-(UN_PC_GP2)	30004061-A4	0.1179	0.522	2.394	Non Break	7.510
3-(UN_PC_GP3)	30004061-A5	0.1184	0.525	2.394	Non Break	7.482
4-(PC_GP1)	30004061-A6	0.1100	0.512	2.394	Non Break	6.619
5-(PC_GP2)	30004061-A7	0.1117	0.498	2.394	Non Break	6.628
6-(PC_GP3)	30004061-A8	0.1113	0.503	2.394	Non Break	6.539
7-(UN_PC_AR1)	30004061-A9	0.1165	0.512	2.394	Non Break	7.021
8-(UN_PC_AR2)	30004061-A10	0.1162	0.512	2.394	Non Break	7.139
9-(UN_PC_AR3)	30004061-A11	0.1165	0.510	2.394	Non Break	7.173
10-(PC_AR1)	30004061-A12	0.1155	0.511	2.394	Non Break	7.026
11-(PC_AR2)	30004061-A13	0.1152	0.513	2.394	Non Break	6.925
12-(PC_AR3)	30004061-A14	0.1156	0.514	2.394	Non Break	7.101
13-(UN_PMMA1)	30004061-A15	0.1120	0.512	3.987	Complete	1.136
14-(UN_PMMA4)	30004061-A16	0.1131	0.492	3.987	Complete	1.160
15-(UN_PMMA5)	30004061-A17	0.1134	0.490	3.987	Complete	1.134
16-(PMMA1)	30004061-A18	0.1131	0.500	3.987	Complete	0.746
17-(PMMA4)	30004061-A19	0.1128	0.495	3.987	Complete	0.738
18-(PMMA5)	30004061-A20	0.1131	0.495	3.987	Complete	0.797
19- (PMMA2)	30004061-A21	0.1131	0.509	2.394	Complete	0.316
20-(PMMA3)	30004061-A22	0.1132	0.511	2.394	Complete	0.394
21-(UN_PMMA2)	30004061-A23	0.1124	0.511	2.394	Complete	0.549
22-(UN_PMMA3)	30004061-A24	0.1120	0.513	2.394	Complete	0.503

Tested by : Dr.Ahamed Shabeer
Signature : _____
Reviewed by :_____

Bodycote Testing Group
1975 North Ruby Street • Melrose Park • Illinois • 60160 • USA • Tel: +1 (708) 236-5360 • Fax: +1 (708) 236-5363

Table H Energy Use and Environmental Emission per 1kg Material, Transportation, Energy Generation, and 1kg Recycling or Incineration

Substance	Compartment	Unit	PMMA sheet 1 kg	Cardboard 1 kg	Epoxy 1 kg	Coated glass 1 kg	Uncoated glass 1kg
Coal, 18MJ per kg, in ground	Energy resource	kg	4.97E-01	1.36E-02	0.00E+00	1.71E-01	1.60E-01
Gas, natural, 36.6 MJ per m3, in ground	Energy resource	m3	2.25E+00	1.21E-02	5.78E-01	2.41E-01	2.29E-01
Gas, petroleum, 35 MJ per m3, in ground	Energy resource	kg	0.00E+00	0.00E+00	0.00E+00	1.84E-03	1.72E-03
Oil, crude, 42.6 MJ per kg, in ground	Energy resource	kg	1.01E+00	2.12E-01	5.05E+00	2.68E-02	2.51E-02
CO2	Air	kg	6.85E+00	7.09E-01	1.10E+00	9.96E-01	9.68E-01
CH4 (=23kg CO2 equiv.)	Air	kg	2.44E-02	8.92E-04	0.00E+00	2.38E-03	2.32E-03
CF4(=5700kg CO2 equiv.)	Air	kg	0.00E+00	0.00E+00	0.00E+00	1.83E-07	1.69E-07
C2F6 (=11900kg CO2 equiv)	Air	kg	0.00E+00	0.00E+00	0.00E+00	2.04E-08	1.88E-08
Coal	Energy	MJ	8.95E+00	3.95E-01	0.00E+00	4.95E+00	4.63E+00
Natural gas	Energy	MJ	8.25E+01	4.23E-01	2.02E+01	8.44E+00	8.00E+00
Crude oil	Energy	MJ	4.32E+01	9.03E+00	2.15E+02	1.14E+00	1.07E+00
Total primary energy	Energy	MJ	1.35E+02	9.85E+00	2.35E+02	1.45E+01	1.37E+01

Table H Energy Use and Environmental Emission per 1kg Material, Transportation, Energy Generation, and 1kg Recycling or Incineration (continued)

Substance	Al, 15% recycled	Construction steel	EPDM gasket	Silicone	Truck 16t	Electricity	NG
	1 kg	1kg	1kg	1kg	1 tkm	1kWh	1 MJ
Coal, 18MJ per kg, in ground	2.20E+00	8.64E-01	5.68E-01	1.66E-01	8.80E-04	2.04E-01	3.30E-04
Gas, natural, 36.6 MJ per m3, in ground	3.91E-01	1.74E-02	6.22E-02	4.90E-01	3.34E-03	2.79E-04	3.09E-02
Gas, petroleum, 35 MJ per m3, in ground	0.00E+00	0.00E+00	6.50E-02	0.00E+00	0.00E+00	0.00E+00	0.00E+00
Oil, crude, 42.6 MJ per kg, in ground	1.10E+00	9.37E-02	1.60E+00	5.20E-01	6.91E-02	9.83E-04	2.92E-04
CO2	8.13E+00	9.00E-01	2.96E+00	1.16E+00	2.28E-01	2.98E-01	5.58E-02
CH4 (= 23kg CO2 equiv.)	1.50E-02	1.63E-04	9.94E-03	7.85E-03	2.77E-04	6.49E-03	1.60E-04
CF4 (= 5700kg CO2 equiv.)	2.78E-04	1.69E-09	8.28E-08	0.00E+00	0.00E+00	0.00E+00	0.00E+00
C2F6 (= 11900kg CO2 equiv)	3.09E-05	2.11E-10	9.20E-08	0.00E+00	0.00E+00	0.00E+00	0.00E+00
Coal	6.37E+01	2.51E+01	1.65E+01	4.81E+00	2.55E-02	5.91E+00	9.57E-03
Natural gas	1.37E+01	6.09E-01	2.18E+00	1.72E+01	1.17E-01	9.76E-03	1.08E+00
Crude oil	4.70E+01	3.99E+00	7.04E+01	2.22E+01	2.94E+00	4.19E-02	1.24E-02
Total primary energy	1.24E+02	2.97E+01	8.91E+01	4.41E+01	3.09E+00	5.96E+00	1.10E+00

Table H Energy Use and Environmental Emission per 1kg Material, Transportation, Energy Generation, and 1kg Recycling or Incineration (continued)

Substance	Plastic. Incineration 1kg	Cardboard incineration 1kg	Plastic recycling 1kg	Cardboard recycling 1kg	Glass recycling 1kg	Steel recycling 1kg	Aluminum recycling 1kg
Coal, 18MJ per kg, in ground	1.08E-02	9.26E-04	4.93E-01	1.52E-02	-4.06E-02	-3.54E-01	-2.62E+00
Gas, natural, 36.6 MJ per m3, in ground	3.79E-03	2.52E-03	-9.43E-01	2.64E-01	1.09E-01	-9.22E-03	-4.06E-01
Gas, petroleum, 35 MJ per m3, in ground	3.90E-04	0	0.00E+00	0.00E+00	0	0	0.00E+00
Oil, crude, 42.6 MJ per kg, in ground	5.70E-03	3.51E-03	-5.68E-01	-3.99E-02	-1.55E-01	-2.31E-02	-1.20E+00
CO2	2.54E+00	1.61E-02	-3.37E-01	-5.55E-01	-3.76E-01	-7.94E-01	-9.33E+00
CH4 (= 23kg CO2 equiv.)	1.11E-04	3.60E-05	8.28E-05	1.31E-03	-4.44E-06	-1.99E-03	-1.57E-02
CF4 (= 5700kg CO2 equiv.)	2.95E-09	9.30E-05	0.00E+00	-6.88E-09	0.00E+00	-7.93E-09	-2.52E-04
C2F6 (= 11900kg CO2 equiv)	3.28E-10	3.00E-08	0.00E+00	-7.64E-10	0.00E+00	-8.81E-10	-2.80E-05
Coal	3.14E-01	2.69E-02	1.43E+01	4.40E-01	-1.18E+00	-1.03E+01	-7.61E+01
Natural gas	1.33E-01	8.82E-02	-3.30E+01	9.24E+00	3.82E+00	-3.23E-01	-1.42E+01
Crude oil	2.43E-01	1.50E-01	-2.42E+01	-1.70E+00	-6.60E+00	-9.84E-01	-5.11E+01
Total primary energy	6.89E-01	2.65E-01	-4.29E+01	7.98E+00	-3.97E+00	-1.16E+01	-1.41E+02

Appendix I Energy Performance Value Verification Process

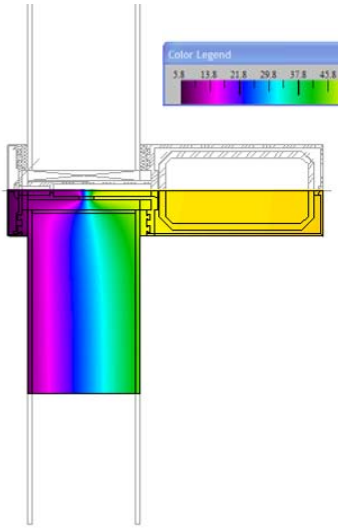

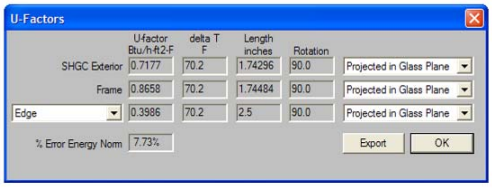

U-factor at the head of a TCFS: 4.88 W/m^2-K
U-factor at the edge of a TCFS: 2.27 W/m^2-K

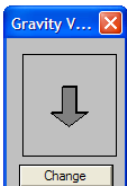

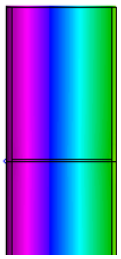

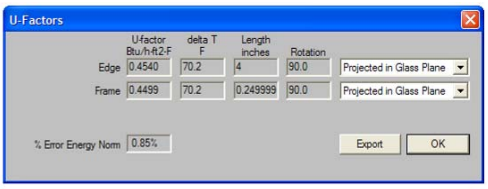

U-factor at the core of TCFS: 2.55 W/m^2-K

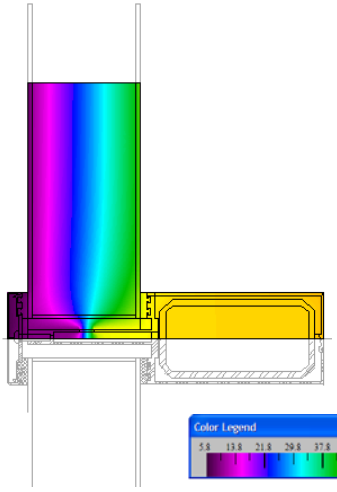

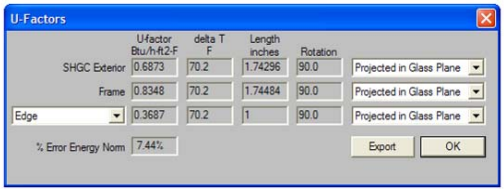

U-factor at the sill of TCFS: 3.86 W/m^2-K
U-factor at the edge of TCFS: 2.1 W/m^2-K

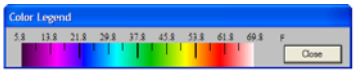

Figure I-1 TCFS Sectional Details:
U-factor Verification Using THERM 5 in accordance with NFRC 100

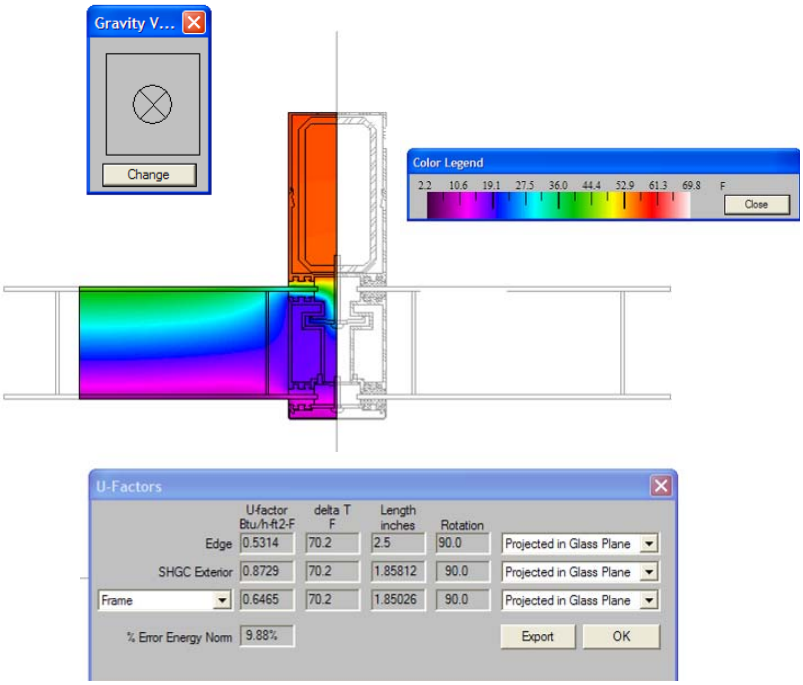

U-factor at the jamb of TCFS: 3.7 W/m^2-K
U-factor at the edge of TCFS: 3.0 W/m^2-K

Figure I-2 TCFS Plan Details:
U-factor Verification Using THERM 5 in accordance with NFRC 100

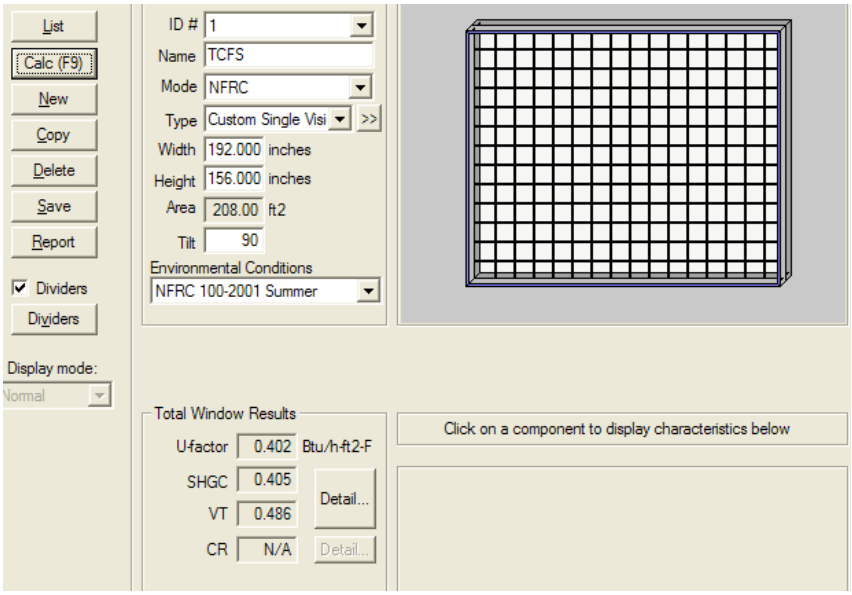

Figure H-3 SHGC and VLT Verification using WINDOW 5
in accordance with NFRC 200

Table I-1 Energy Performance Values of TCFS and GCWS

	U-factor (W/m^2-K)	SHGC	VLT
TCFS	2.589	0.302	0.305
Uncoated GCWS	2.986	0.615	0.656
Coated GCWS	1.862	0.313	0.484

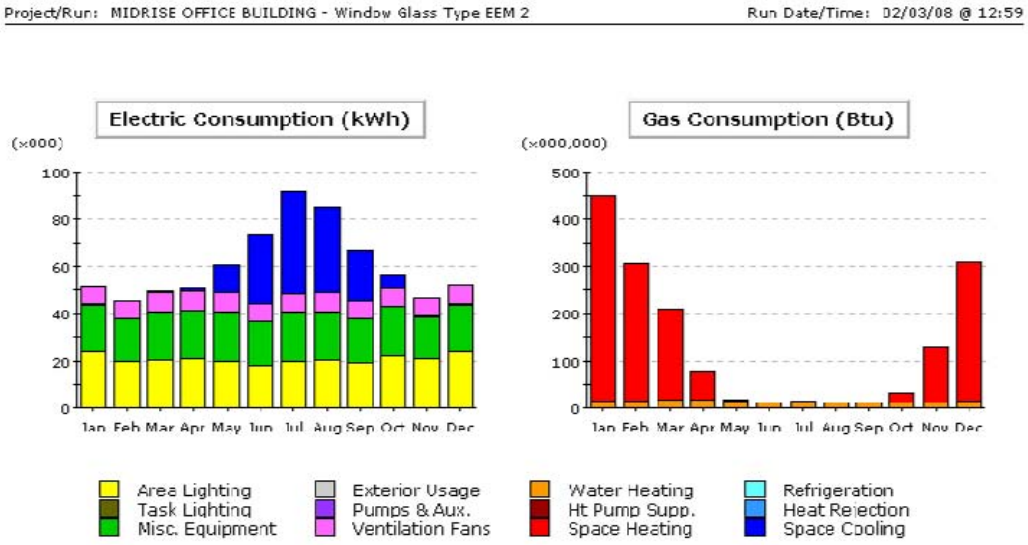

Electric Consumption (kWh x000)

	Jan	Feb	Mar	Apr	May	Jun	Jul	Aug	Sep	Oct	Nov	Dec	Total
Space Cool	-	-	0.88	1.79	11.66	29.04	43.54	36.29	21.52	3.11	-	-	149.83
Heat Reject.	-	-	-	-	-	-	-	-	-	-	-	-	-
Refrigeration	-	-	-	-	-	-	-	-	-	-	-	-	-
Space Heat	-	-	-	-	-	-	-	-	-	-	-	-	-
HP Supp.	-	-	-	-	-	-	-	-	-	-	-	-	-
Hot Water	-	-	-	-	-	-	-	-	-	-	-	-	-
Vent. Fans	7.70	6.97	7.70	8.07	8.07	7.33	8.07	8.07	7.33	8.07	6.97	7.70	92.04
Pumps & Aux.	0.54	0.49	0.47	0.31	0.02	-	-	-	0.01	0.10	0.37	0.49	2.81
Ext. Usage	-	-	-	-	-	-	-	-	-	-	-	-	-
Misc. Equip.	19.89	17.99	19.89	20.59	20.67	19.00	20.68	20.67	19.00	20.67	18.20	19.89	237.15
Task Lights	-	-	-	-	-	-	-	-	-	-	-	-	-
Area Lights	23.55	19.69	20.56	20.65	19.96	17.90	19.73	20.11	19.08	22.24	20.95	23.99	248.42
Total	51.69	45.14	49.51	51.40	60.38	73.28	92.02	85.14	66.93	56.19	46.48	52.07	730.24

Gas Consumption (Btu x000,000)

	Jan	Feb	Mar	Apr	May	Jun	Jul	Aug	Sep	Oct	Nov	Dec	Total
Space Cool	-	-	-	-	-	-	-	-	-	-	-	-	-
Heat Reject.	-	-	-	-	-	-	-	-	-	-	-	-	-
Refrigeration	-	-	-	-	-	-	-	-	-	-	-	-	-
Space Heat	433.6	289.9	194.5	62.9	3.2	-	-	-	0.5	17.9	116.6	294.9	1,414.0
HP Supp.	-	-	-	-	-	-	-	-	-	-	-	-	-
Hot Water	15.6	14.6	16.2	16.5	15.3	12.9	13.1	12.5	11.4	13.0	12.3	14.6	167.9
Vent. Fans	-	-	-	-	-	-	-	-	-	-	-	-	-
Pumps & Aux.	-	-	-	-	-	-	-	-	-	-	-	-	-
Ext. Usage	-	-	-	-	-	-	-	-	-	-	-	-	-
Misc. Equip.	-	-	-	-	-	-	-	-	-	-	-	-	-
Task Lights	-	-	-	-	-	-	-	-	-	-	-	-	-
Area Lights	-	-	-	-	-	-	-	-	-	-	-	-	-
Total	449.3	304.5	210.7	79.4	18.5	12.9	13.1	12.5	11.9	30.9	128.9	309.5	1,581.9

eQUEST 3.60.5200 Monthly Energy Consumption by Enduse Page 1

Figure I-4 eQUEST Output of TCFS

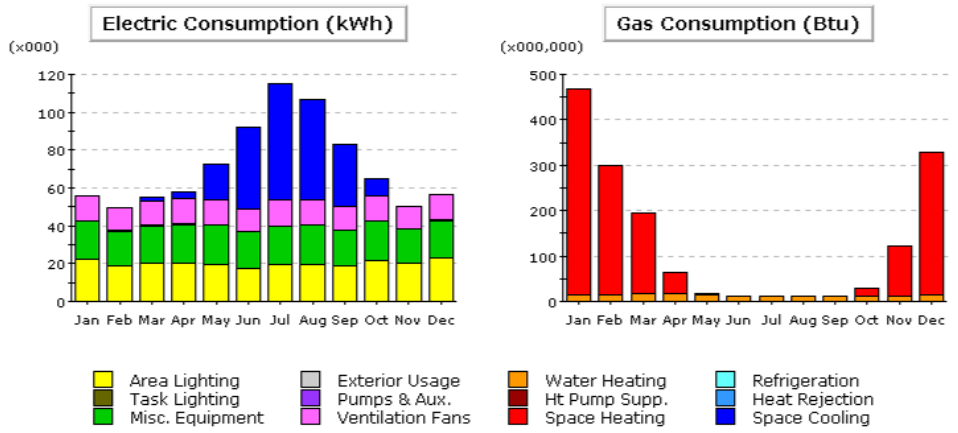

Electric Consumption (kWh x000)

	Jan	Feb	Mar	Apr	May	Jun	Jul	Aug	Sep	Oct	Nov	Dec	Total
Space Cool	-	-	1.88	3.31	18.64	43.09	61.58	52.64	32.77	9.17	-	-	223.08
Heat Reject.	-	-	-	-	-	-	-	-	-	-	-	-	-
Refrigeration	-	-	-	-	-	-	-	-	-	-	-	-	-
Space Heat	-	-	-	-	-	-	-	-	-	-	-	-	-
HP Supp.	-	-	-	-	-	-	-	-	-	-	-	-	-
Hot Water	-	-	-	-	-	-	-	-	-	-	-	-	-
Vent. Fans	13.01	11.77	13.01	13.63	13.63	12.39	13.63	13.63	12.39	13.63	11.77	13.01	155.50
Pumps & Aux.	0.54	0.49	0.47	0.31	0.02	-	-	-	0.01	0.10	0.37	0.49	2.81
Ext. Usage	-	-	-	-	-	-	-	-	-	-	-	-	-
Misc. Equip.	19.89	17.99	19.89	20.59	20.67	19.00	20.68	20.67	19.00	20.67	18.20	19.89	237.15
Task Lights	-	-	-	-	-	-	-	-	-	-	-	-	-
Area Lights	22.35	18.97	19.99	20.13	19.55	17.68	19.40	19.75	18.71	21.58	19.99	22.90	240.99
Total	55.79	49.22	55.24	57.96	72.52	92.16	115.30	106.70	82.88	65.15	50.33	56.29	859.53

Gas Consumption (Btu x000,000)

	Jan	Feb	Mar	Apr	May	Jun	Jul	Aug	Sep	Oct	Nov	Dec	Total
Space Cool	-	-	-	-	-	-	-	-	-	-	-	-	-
Heat Reject.	-	-	-	-	-	-	-	-	-	-	-	-	-
Refrigeration	-	-	-	-	-	-	-	-	-	-	-	-	-
Space Heat	452.0	285.7	178.2	46.1	2.0	-	-	-	0.7	16.8	109.3	313.7	1,404.5
HP Supp.	-	-	-	-	-	-	-	-	-	-	-	-	-
Hot Water	15.6	14.6	16.2	16.5	15.3	12.9	13.1	12.4	11.4	13.0	12.3	14.6	167.8
Vent. Fans	-	-	-	-	-	-	-	-	-	-	-	-	-
Pumps & Aux.	-	-	-	-	-	-	-	-	-	-	-	-	-
Ext. Usage	-	-	-	-	-	-	-	-	-	-	-	-	-
Misc. Equip.	-	-	-	-	-	-	-	-	-	-	-	-	-
Task Lights	-	-	-	-	-	-	-	-	-	-	-	-	-
Area Lights	-	-	-	-	-	-	-	-	-	-	-	-	-
Total	467.6	300.3	194.4	62.5	17.3	12.9	13.1	12.4	12.0	29.8	121.6	328.3	1,572.3

Figure I-5 eQUEST Output of Uncoated GCWS:
(6 mm clear glass + 12 mm air space + 6 mm clear glass)

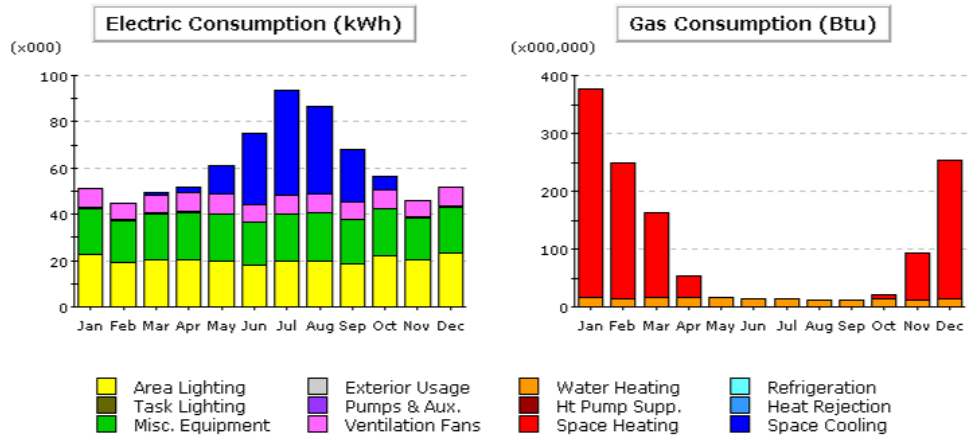

Electric Consumption (kWh x000)

	Jan	Feb	Mar	Apr	May	Jun	Jul	Aug	Sep	Oct	Nov	Dec	Total
Space Cool	-	-	1.04	2.02	12.43	30.55	45.09	37.82	22.79	5.76	-	-	157.51
Heat Reject.	-	-	-	-	-	-	-	-	-	-	-	-	-
Refrigeration	-	-	-	-	-	-	-	-	-	-	-	-	-
Space Heat	-	-	-	-	-	-	-	-	-	-	-	-	-
HP Supp.	-	-	-	-	-	-	-	-	-	-	-	-	-
Hot Water	-	-	-	-	-	-	-	-	-	-	-	-	-
Vent. Fans	7.85	7.10	7.85	8.22	8.22	7.48	8.22	8.22	7.48	8.22	7.10	7.85	93.81
Pumps & Aux.	0.54	0.49	0.47	0.31	0.02	-	-	-	0.01	0.10	0.37	0.49	2.81
Ext. Usage	-	-	-	-	-	-	-	-	-	-	-	-	-
Misc. Equip.	19.89	17.99	19.89	20.59	20.67	19.00	20.68	20.67	19.00	20.67	18.20	19.89	237.15
Task Lights	-	-	-	-	-	-	-	-	-	-	-	-	-
Area Lights	22.74	19.20	20.16	20.32	19.70	17.74	19.51	19.88	18.83	21.82	20.31	23.27	243.48
Total	51.02	44.78	49.41	51.47	61.06	74.76	93.51	86.60	68.10	56.58	45.98	51.50	734.76

Gas Consumption (Btu x000,000)

	Jan	Feb	Mar	Apr	May	Jun	Jul	Aug	Sep	Oct	Nov	Dec	Total
Space Cool	-	-	-	-	-	-	-	-	-	-	-	-	-
Heat Reject.	-	-	-	-	-	-	-	-	-	-	-	-	-
Refrigeration	-	-	-	-	-	-	-	-	-	-	-	-	-
Space Heat	361.8	233.3	147.5	36.4	1.2	-	-	-	0.1	8.9	81.1	238.1	1,108.5
HP Supp.	-	-	-	-	-	-	-	-	-	-	-	-	-
Hot Water	15.6	14.6	16.2	16.5	15.3	12.9	13.1	12.5	11.4	13.0	12.3	14.6	167.8
Vent. Fans	-	-	-	-	-	-	-	-	-	-	-	-	-
Pumps & Aux.	-	-	-	-	-	-	-	-	-	-	-	-	-
Ext. Usage	-	-	-	-	-	-	-	-	-	-	-	-	-
Misc. Equip.	-	-	-	-	-	-	-	-	-	-	-	-	-
Task Lights	-	-	-	-	-	-	-	-	-	-	-	-	-
Area Lights	-	-	-	-	-	-	-	-	-	-	-	-	-
Total	377.4	247.9	163.7	52.9	16.5	12.9	13.1	12.5	11.4	21.9	93.3	252.7	1,276.3

Figure I-6 eQUEST Output of Coated GCWS:
(6 mm clear glass with VRE1559 + 12 mm air space + 6 mm clear glass)

BIBLIOGRAPHY

Abeysundra, U., Babel, S., Gheewala, S. & Sharp, A. (2007). Environmental, economic and social analysis of materials for doors and windows in Sri Lanka, Building and Environment, 42, 2141-2149.

American Architectural Manufacturers Association (AAMA). (1996). *Maximum allowable deflection of framing systems for building cladding components at design wind loads (AAMA TIR-A11-1996).* Illinois; AAMA.

American Institute of Steel Construction. (2006). *Steel construction manual (13th ed.).* Chicago: American Institute of Steel Construction, Inc.

American National Standard. (2004). *ANSI Z97.1-04: American national standard for safety glazing materials used in buildings – safety performance specifications and methods of test*. New York: ANSI.

American Society of Civil Engineers (ASCE). (2002). *Minimum design loads for buildings and other structures (ASCE 7-02)*. VA: Structural Engineering Institute.

American Society of Heating, Refrigerating and Air-conditioning Engineers, Inc. (1997). *ASHRAE handbook - fundamentals (I-P ed.).* Atlanta: ASHRAE, Inc.

American Society for Testing and Materials. (2006). *ASTM D228-06: Standard test method for linear thermal expansion of solid materials with a push-rod dilatometer*. Philadelphia: ASTM.

American Society for Testing and Materials. (1998). *ASTM D570-98: Standard test method for water absorption of plastics*. Philadelphia: ASTM.

American Society for Testing and Materials. (2003). *ASTM D635-03: Standard test method for rate of burning and/or extent and time of burning of plastics in a horizontal position*. Philadelphia: ASTM.

American Society for Testing and Materials. (1999). *ASTM D1044-99: Standard test method for resistance of transparent plastics to surface abrasion*. Philadelphia: ASTM.

American Society for Testing and Materials. (2004). *ASTM D 2843-04 Standard Test Method for Density of Smoke from the Burning or Decomposition of Plastics*. Philadelphia: ASTM.

American Society for Testing and Materials. (2001). *ASTM D2990-01: Standard test method for tensile, compressive, and flexural creep and creep-rupture of plastics.* Philadelphia: ASTM.

American Society for Testing and Materials. (2000). *ASTM D3273-00: Standard test method for resistance to growth of mold on the surface of interior coatings in an environmental chamber*. Philadelphia: ASTM.

American Society for Testing and Materials. (1995*). ASTM D 3274-95: Standard Test Method for Evaluating Degree of Surface Disfigurement of Paint Films by Microbial (Fungal or Algal) Growth or Soil and Dirt Accumulation*. Philadelphia: ASTM.

American Society for Testing and Materials. (2003). *ASTM D3801-03: Standard test method for comparative burning characteristics of solid plastics in a vertical position*. Philadelphia: ASTM.

American Society for Testing and Materials. (2006). *ASTM D6110-06: Standard test Methods for determining the Charpy impact resistance of notched specimens of plastics.* Philadelphia: ASTM.

American Society for Testing and Materials. (2007). *ASTM E 84-07: Standard Test Method for Surface Burning Characteristics of Building Materials.* Philadelphia: ASTM.

American Society for Testing and Materials. (2000). *ASTM E96-00: Standard test method for water vapor transmission of materials*. Philadelphia: ASTM.

Ashby, M., & Johnson, K. (2005). *Materials and design*. London: Elsevier.

Baillie, C. (Ed.). (2004). *Green composites: Polymer composites and the environment*. Abington, Cambridge: Woodhead Publishing.

Bayer Sheet Europe. (2004), Technical information: Makrolon and Vivak environmental aspects. June 2005, from http://www.proplastik.eu/File/lati/Environmental%20Aspects.pdf?PHPSESSID=71ef8d3caae1e34e9fa6e028a362271f.

Bentley. (2007). STAAD.Pro (Version 2007) [Computer software]. Exton, PA: Bentley.

Benayoune, A., Aziz, A., Samad, A., Trikha, D.N., Abdullah Abang Ali, A., Ashrabov, A.A. (2006). Structural behaviour of eccentrically loaded precast sandwich panels, Construction and Building Materials, 20(9), 713-724.

Bitzer, Tom. (1997). *Honeycomb technology: Materials, design, manufacturing, applications, and testing*. New York: Chapman & Hall.

Carmody, J., Selkowitz, S., Lee, E., Arasteh, D., & Willmert, T. (2004). *Window systems for high-performance buildings*. New York: Norton.

Chen, T.Y., Burnett, J., & Chau, C.K. (2001). Analysis of embodied energy use in the residential building of Hong Kong. Journal of Energy, 26, 323-340.

Chong, Ken P., & Hartsock, John A. (1993). Structural analysis and design of sandwich panels with cold-formed steel facings, Thin-Walled Structures, 16(1-4), 199-218.

Citherlet, S., Di Guglielmo, F., & Gay, J. (2000). Window and advanced glazing systems life cycle assessment, Energy and Buildings, 32, 225-234.

Corbie`re-Nicollier, T.B., Lundquist, L., Leterrier, Y., Ma°nson, J.-A.E., & Jolliet, Y.O. (2001). Life cycle assessment of biofibres replacing glass fibres as reinforcement in plastics. Journal of Resources, Conservation, and Recycling, 33, 267-287.

Datta, G. (2001). Effect of fixed horizontal louver shading devices on thermal performance of building by TRNSYS simulation. Journal of Renewable Energy, 21, 497 – 507.

Davies, J.M. (Ed.). (2001). *Lightweight composite construction.* Boston: Wiley-Blackwell.

Department of Energy (DOE). (2007). *2007 Buildings energy data book*. February 2007, from http://buildingsdatabook.eren.doe.gov/.

Dong, J., Sun, Q., & J-Y, W. (2004). Basic study of corn protein, zein, as a biomaterial in tissue engineering, surface morphology and biocompatibility. Journal of Biomaterials, 25, 4691-4697.

Energy Information Administration. (1995). *Measuring energy efficiency in the United States' economy: A beginning*. October 1995, from http://tonto.eia.doe.gov/ftproot/consumption/0555952.pdf.

Energy Information Administration. (2007). *International energy outlook*. Retrieved May 2007, from www.eia.doe.gov/oiaf/ieo/index.html.

Foss, R. (1999). Safety glass testing: Human head impactor simulation by dynamic transient analysis. Proceedings of 7th glass processing days. 1, 444-450.

Franklin Associates and Prairie Village. (1998). *Characterization of building-related construction and demolition debris in the United States (EPA530-R-99-034).* Retrieved June 1998, from http://www.epa.gov/epaoswer/hazwaste/sqg/c&d-rpt.pdf.

Gennadios A. (Ed.). 2002. *Protein-based films and coatings*. Boca Raton, FL: CRC press.

Gentle, C. R., & Lacey, M. R. (1999). Design of a novel insulated construction material Materials & Design, 20(6), 311-315.

Gere, J. (2006). *Mechanics of materials (6th ed.).* Ontario: Thomson.

GE Plastics. (n.d.). *Oxygen and water permeability.* from http://kbam.geampod.com/KBAM/Reflection/Assets/10620.pdf.

Glass Association of North America (GANA). (2004). *Glazing manual*. Kansas; GANA.

Graedel, T. E. (1998). *Streamlined life-cycle assessment*. Englewood Cliffs, NJ: Prentice Hall.

Institute of Structural Engineers. (1999). *Structural use of glass in buildings*. London: SETO.

International Code Council. (2003) *International building code*. New York: American Institute of Architects.

Joshi, S.V., Drzal, L.T., Mohanty, A.K., & Arora, S. (2003). Are natural fiber composites environmentally superior to glass fiber reinforced composites?. Journal of Composites, Part A (35), 371-376.

Harrison, J. (2000). *Seasonally selective passive solar shading system*. United States Patent Number 6,105,318, from http://www.uspto.gov/patft/index.html.

Hayes, R. and Bonadies, A.M. (2007). A new hard coats for automotive plastics. Finishing Today, 83(12), 24-27.

Hough, R. (1980) Sandwich panels from recycled drink cans—A structural appraisal. Building and Environment, 15(1), 57-61.

Huberman, N., Pearlmutter, D. (2008). A life-cycle energy analysis of building materials in the Negev desert. Journal of Energy and Buildings, 40, 837-848.

Hylton, D.C. (2000). *Understanding plastics testing*. Cincinnati: Hanser.

International Organization of Standards. (2006). *ISO 14040:2006 environmental management – life cycle assessment – principle and frame work.* Ireland: National Standard Authority of Ireland.

Jacob, L. (2001). A critical review of impact testing and classification of safety glass for use in buildings. Proceedings of 9th glass processing days. 1, 268-273.

Jaillon L., Poon, C.S., & Chian, Y.H. (in press). Quantifying the waste reduction potential of using prefabrication in building construction in Hong Kong. Journal of Waste Management.

Joshi, S. V., Drzal, L. T., Mohanty, A. K., Arora, S. (2003). Are natural fiber composites environmentally superior to glass reinforced composites?. Science and Technology, 63, 1377–1385.

Katsamberis, D., Browall, K., Iacovangelo, C., Neumann, M., & Morgner, H. (1997). Highly durable coatings for automotive polycarbonate glazing. Journal of Progress in Organic Coatings, 34, 130-134.

Kuenzi, E.W. (1961). *Structural sandwich design criteria*. US Forest Products Laboratory Report No. 2161, Madison: Forest Products Laboratory.

Lawrence Berkeley National Laboratory. (2001). Window (Version 5.2) [Computer software]. Berkeley, CA: LBNL.

Lawrence Berkeley National Laboratory. (2006). THERM (Version 5.2) [Computer software]. Berkeley, CA: LBNL.

Lawrence Berkeley National Laboratory. (2001). eQUEST (Version 3.6) [Computer software]. Berkeley, CA: LBNL.

Limmatvapirat, S., Limmatvapirat, C., Luangtana-anan M., Nunthanid, J., Oguchi, T., Tozuka, Y., et al. (2004). Modification of physicochemical and mechanical properties of shellac by partial hydrolysis. International Journal of Pharmaceutics, 278, 41-49.

Lokensgard, E. (2004). *Industrial plastics*. Clifton Park: Thomson Learning.
Loughran, P. (2003). *Falling glass: Problems and solutions in contemporary architecture*. Basel, Switzerland: Birkhauser.

Lívio Boni, T., & Almeida S. (2008). Laterally supported sandwich panels subjected to large deflections—Part 1: Test apparatus design and experimental results Thin-Walled Structures, 46(4), 413-422.

Margolis, J. (2006). *Engineering plastics handbook*. New York: McGraw – Hill.

McGuire, R.G., & Hagenmaier R.D. (1996). Shellac coatings for grapefruits that favor biological control of penicillium digitatumby candida oleophila. Biological Control, 7, 100-106.

Mohanty, A., Misra, M., & Drzal, L (Eds.). (2005). *Natural fibers, biopolymers, and biocomposites*. Boca Raton, FL: CRC press.

National Fenestration Rating Council, Inc. (2004). *NFRC 100-2004: Procedure for determining fenestration product U-factors*. MD: National Fenestration Rating Council. http: nfrc.org.

National Fenestration Rating Council, Inc. (2004). *NFRC 201-2004: Procedure for interim standard test method for measuring the solar heat gain coefficient of fenestration systems using calorimetry hot box methods.* MD: National Fenestration Rating Council. from http: nfrc.org.

Office of Solid Wastes and Emergency Response. (2003). *Municipal solid waste in the United States: 2001 facts and figures*, EPA530-R-03-011, from http://www.epa.gov/epaoswer/non-hw/muncpl/pubs/msw2001.pdf.

Oketani, Y., Kikuta, M., & Aratani, S.(2001). Investigation of repeatability and reproducibility of the shot bag impactor. Proceedings of 9th glass processing days, 1, 676-681. from www.glassfiles.com.

Papaefthimiou, S., Syrrakou, E., & Yianoulis, P. (2006). Energy performance assessment of an electrochromic window, Thin Solid Films, 502, 257-264.

Pappu, A., Saxena, M., & Asolekar, S.R. (2006). Solid wastes generation in India and their recycling potential in building materials. Journal of Building and Environment, 42, 2311-2320.

Pokharel, N., & Mahendran, M. (2003) Experimental investigation and design of sandwich panels subject to local buckling effects, Journal of Constructional Steel Research, 59(12), 1533-1552.

Pollack, H. (1967). *Applied physics*. Englewood cliffs, New Jersey:Prentice-Hall, Inc.

Rathbun, H.J., Zok, F.W., & Evans, A.G. (2005). Strength optimization of metallic sandwich panels subject to bending, International Journal of Solids and Structures, 42(26), 6643-6661.

Robbins, D.H. (1976). Comparative testing of anthropomorphic dummy and a standardized impactor for glazing materials. UM-HSRI document number 35897, MI: University of Michigan Highway Safety Research Institute.

Rosato, D.V., Schott, N.R., and Rosato M.G. (Eds.). (2001). *Plastics Engineering Manufacturing and Data Handbook.* Norwell, MA: Kluwer Academia Publishers.

Ryntz, R., Bauer, D.R., Fraser, K., & Glogovsky, T. (2001). *Plastics and coatings: durability, stabilization, testing.* Cincinnati: Hanser Gardner Publications.

Scheuer, C., Keoleian, G., & Reppe, P. (2003). Life cycle energy and environmental performance of a new university building: modeling challenges and design implications. Energy and Buildings, 35, 1049-1064.

Schmauder, T., Nauenburg, K-D., Kruse, K., & Ickes, G. (2006). Hard coatings by plasma CVD on polycarbonate for automotive and optical applications. Thin Solid Films, 502, 270-274.

Selkowitz, S. (2008). Fenestration solution for zero energy buildings. Presented at the Building Enclosure Science and Technology (BEST) conference, Minneapolis, MN, from http://www.aia.org/SiteObjects/files/BEST_Selkowitz_6_2008.pdf.

Shah, V. (2007). Handbook of Plastics Testing and Failure Analysis. NJ: Wiley.

Sutherland, R.J.M. (2008). Materials and structural techniques. The Structural Engineer, 86(14), 118-123.

The Institute of Structural Engineers. (1999). *Structural use of glass in buildings*. London: SETO.

Thormark, C. (2006). The effect of material choice on the total energy need and recycling potential of a building, Building and Environment, 41, 1019-1026.

Toakely, A. R. (1977). Stresses and safety levels for glass liable to human impact. Building and Environment, 12, 87-95.

Trinnaman, J. & Clarke, A. (2004). *2004 Survey of energy resources*. London: Elsevier.

Troitzsch, J. (2004). *Plastics flammability handbook.* Cincinnati: Hanser.

Valdevit, L., Wei, Z., Mercer, C., Zok, F.W., & Evans, A.G. Structural performance of near-optimal sandwich panels with corrugated cores, International Journal of Solids and Structures, 43(16), 4888-4905.

Wypych, G. (Ed.). (1999). *Weathering of plastics: Testing to Mirror Real Life Performance (Plastics & Elastomers)*. Norwich, NY: Plastics Design Library.

Wool, R., & Sun, S. (2005). *Bio-based polymers and composites.* San Diego: Elsevier Academic Press.

Xu S., Jayaraman K., Morin C., & Pecqueux N. (2008). Life cycle assessment of wood-fiber-reincored polypropylene composites. Journal of material processing technology, 198, 168-177.

Yasantha Abeysundraa, U.G, Babela, S., Gheewalab, S., & Sharpa, A. (2007). Environmental, economic and social analysis of materials for doors and windows in Sri Lanka. Building Environment, 42, 2141-2149.

Young, H., & Freedman, R. (2000). *Sears and Zemansky's University physics (10th ed.).* San Francisco: Addison-Wesley.

Young, W., & Budynas, R. (2002). *Roark's formulas for stress and strain (7th ed.).* New York: McGraw-Hill Companies, Inc.

Weir, G. & Muneer, T. (1998). Energy and environmental impact analysis of double-glazed windows, Energy Conversion and Management, 39, 243-256.

Product data downloaded from online:

Cyro. (1998). Acrylite AR technical data. Retrieved 1998, from
http://cyro.com/NR/rdonlyres/516E2495-C963-4337-814F-EF0C9F9C7388/0/1970ACRYLITEARTechData.pdf

Cyro. (2001). Acrylite FF technical data. Retrieved 2001, from
http://cyro.com/NR/rdonlyres/3728C0E9-BE9A-4C19-932F-586C2937EC12/0/1121DFFPhysicalProperties.pdf

Sheffield plastics inc. (2008). Makrolon GP product data. Retrieved 2008, from
http://www.sheffieldplastics.com/web_docs/PDS004_GP.pdf

Sheffield plastics inc. (2003). Makrolon AR product data. Retrieved 2003, from
http://www.sheffieldplastics.com/web_docs/PDS001_AR.pdf
Retrieved October 3, 2000, from http://www.commerce.state.wi.us/SBdocs/SB-CommercialBuildingsXProductEvaluations200426-l.pdf

Bayer. (2003). Makrolon AR technical data. Retried 2003, from
http://www.sheffieldplastics.com/web_docs/7955AR_DS.pdf

Material Property Data. (n.d.), from
http://www.matweb.com/Search/MaterialGroupSearch.aspx?GroupID=282

GE Plastics. (1997). Lexan MR10 product data. Retrieved January, 1997, from
http://www.southernsteelwindows.co.nz/images/MR10%20Data%20Sheet.pdf

GE Plastics. (1997). Polymers for great outdoors. Retrieved August, 1997, from
http://kbam.geampod.com/KBAM/Reflection/Assets/8700.pdf

Altuglas. (2000). Tuffak XL weatherable polycarbonate sheet. Retrieved from June, 2000, from http://www.plexiglas.com/literature/pdf/95.pdf

Bayer. (2003). Flame inhibiting product data. Retried March, 2003, from
http://www.professionalplastics.com/professionalplastics/content/FI5000.pdf

PaneliteLLC. (n.d.) Panelite brochure, from
http://www.e-panelite.com/downloads/PANELITE_BROCHURE.pdf

Altuglas product brochure, from www.altuglas.com/literature/pdf